GASTROINTESTINAL ORGANOID STRUCTURE AND TRANSPORT

by

Barkan Sidar

A dissertation submitted in partial fulfillment
of the requirements for the degree

of

Doctor of Philosophy

in

Chemical Engineering

MONTANA STATE UNIVERSITY
Bozeman, Montana

April 2019

DEDICATION

To my mother and family who have given me unconditional love and support.

ACKNOWLEDGEMENTS

Firstly, I would like to express my sincere gratitude to my advisor Professor. J. N. Wilking for the support and assistance he provided through my Ph.D. study and related research. I would give him most of the credit for his tireless efforts to inspire and guide me through the research to become a better scientist and all the help I received for writing this dissertation.

Besides my advisor, I would like to thank the rest of my dissertation committee; Professors D. Bimczok, S. T. Walk, P. Stewart, J. J. Heys for their insightful comments, encouragement, efforts, and support to widen my research from various perspectives. I would like to acknowledge that the research I have conducted through my Ph.D. dissertation would not be possible without the collaboration of Professors D. Bimczok and S. T. Walk.

Specifically, I would like to thank Professors J. J Heys, R. Gerlach and rest of the Chemical and Biological Engineering faculty for having me as a teaching assistant that I consider the origin of my eager to become a scientist. I appreciate the efforts of Betsey Pitts for teaching me imaging and analysis techniques and the research community at the Center for Biofilm Engineering for having me.

I thank my colleagues Andy Sebrell and Brittany Jenkins along with my lab mates for stimulating discussions, help throughout the research and all the fun we had in the labs.

Finally, I would like to thank my family and friends for supporting me, and I feel like the luckiest person for having you.

FUNDING ACKNOWLEDGEMENTS

Funding for this dissertation was mainly provided by the National Science Foundation, DMR-1455247 (JW), the National Institutes of Health grants K01 DK097144 (DB); R03 DK107960 (DB), Gates Foundation OPP1108199 (SW).

TABLE OF CONTENTS

TABLE OF CONTENTS CONTINUED

TABLE OF CONTENTS CONTINUED

TABLE OF CONTENTS CONTINUED

LIST OF TABLES

LIST OF FIGURES

Figure Page

LIST OF FIGURES CONTINUED

Figure Page

LIST OF FIGURES CONTINUED

Figure Page

ABSTRACT

Organoids are three-dimensional (3D) self-assembled, mammalian tissue cultures derived from stem cells that differentiate to contain multiple cell types. These cells spatially organize within the 3D structure and are capable of recapitulating the structure and function of a particular organ. Organoids offer a variety of existing and potential applications in medicine and biotechnology, including drug formulation testing, regenerative medicine, and microbiome research. Despite their value, knowledge of how organoid structure impacts dynamics, mechanics, and transport is lacking. This is particularly true for gastrointestinal organoids, which are composed of a monolayer-thick epithelial sheet wrapped into a closed sphere. The primary goals of this dissertation are to understand the impact of gastrointestinal organoid structure on organoid function, develop a millifluidic chip platform to improve their viability and reliability as a model system and to explore their uses as model co-culture systems. To achieve this, we use a combination of time-lapse microscopy, image analysis, modeling, and fluidics fabrication techniques to develop an understanding of organoid growth and development in addition to expanding current uses as model systems. Our observations revealed that human gastric organoid growth was associated with cyclic rupture of the epithelial shell, rotational movement around their axes within the Matrigel matrix and luminal fusion by adjacent organoids. Furthermore, the rupture events are an indirect result of osmotic swelling carried out by the diffusion of water due to osmolyte concentration regulation by the epithelial shell. To overcome the advection limitation due to the topologically closed spherical structure of the organoids, we developed a millifluidic device called the Gut Organoid Flow Chip (GOFlowChip). This represents the first demonstration of established liquid flow through the luminal space of a gastrointestinal organoid. Given that organoids show great potential as model systems, established co-culture system consisting of dendritic cells (DC) with infected human gastric organoids shows the gastric epithelium actively recruits DCs for immunosurveillance with increased recruitment upon active Helicobacter pylori infection. Finally, investigation on CD103 attachment protein in gastric DCs revealed that CD103 engages in DC-epithelial cell interactions upon contact with epithelial E-cadherin but is not a significant driver of DC adhesion to gastrointestinal epithelia.

INTRODUCTION

Organoids are three-dimensional (3D) self-assembled, mammalian tissue cultures derived from stem cells that differentiate to contain multiple cell types. These cells are spatially organized within the 3D structure and are capable of recapitulating the function of a particular organ (1, 2). Organoids offer a variety of existing and potential applications in medicine and biotechnology, including drug formulation testing, regenerative medicine and microbiome research (1-5). Despite their value, knowledge of how organoid structure impacts organoid dynamics, mechanics, and transport is lacking. This is particularly true for gastrointestinal organoids, which are composed of a monolayer-thick epithelial sheet wrapped into a closed spherical shape. *The primary goals of the dissertation research described here are to understand the impact of gastrointestinal organoid structure on organoid function and develop a millifluidic chip platform to improve their viability and reliability as a model system.* To achieve this, we use a combination of time-lapse microscopy, image analysis, modeling, and fluidics fabrication techniques to develop an understanding of organoid growth and development in addition to expanding current uses as model systems.

Organoid research originated in the field of developmental biology with the study of how cells organize within tissues. In 1907, H. V. Wilson demonstrated that a sponge, which had been disassociated into its constituent cells, could re-organize into a viable organism (6). The search for mechanisms of biological organization progressed slowly over the next 50 years until the field began to focus on animal embryos. In 1960, Weiss and Taylor discovered inductive signaling, the process by which cell fate is determined

by the release of signaling molecules from neighboring cells. This was discovered by observing the dissociation and re-aggregation of tissues gathered from chicken embryos (7), and led to the discovery of various signaling molecules called growth factors which control cellular differentiation. In the following year, long-term *in vitro* culture and differentiation of embryonal carcinoma cells was reported; this extended the time over which experiments could be conducted (8).

Despite the critical discoveries made in the early 20th century, knowledge regarding the mechanisms responsible for driving the cellular organization and generating specific spatial distributions of cells in tissue was still lacking. In 1964, Malcolm Steinberg proposed the "differential adhesion" hypothesis, which later proved to be predictive for the cellular organization in tissues (9). His hypothesis suggested that the differential strength of cell-cell interactions allowed for rearrangement and that cells would rearrange to minimize the free energy associated with these interactions. As a result, more adhesive cells could be found located near the core of cell aggregates, and less adhesive cells could be found surrounding them. Steinberg's hypothesis provided a physical explanation for cell organization in addition to the chemical factors found previously.

Different cell types within a tissue arise from the differentiation of what are known as stem cells (10). While there are many types of stem cells, three types are most relevant to organoid research history: embryonic pluripotent stem cells, which can give rise to any type of specialized cell, adult stem cells, which are already specialized to a form a specific tissue and thus have limited differentiation capability, and adult stem cells

that are re-programmed from adult cells to form “induced” pluripotent stem cells. Stem cell research originated in the early 1960s from the work of McCulloch and Till, but for two decades the use of stem cells was limited to *in vivo* experiments. In 1981, researchers isolated pluripotent stem cells from mouse embryos (11, 12) and established *in vitro* culture methods. This was followed by the demonstration that the extracellular matrix (ECM) material overexpressed by tumor cells could enable breast epithelia to organize into complex 3D structures such as ducts and ductules (13). Until the discovery of what is now referred to as “Matrigel," collagen gel substrate was used for 3D cultures but was not compatible with all cell types (14). By contrast, Matrigel has similarities in composition to the ECM found around the tissues in the embryonic stage of development which may also be why it can be used to culture many cell types including stem cells and tissue explants (15).

While organoid research through the 1990s was limited to animal embryonic and adult stem cells, which were partially differentiated, interest in organoids significantly increased when, in 1998, researchers established human embryonic stem cell (hESC) isolation and culturing (16), and, in 2007, human induced pluripotent stem cell isolation and culturing (17). These advances provided researchers with undifferentiated, pluripotent human stem cells in abundance. In the following years, protocols for growing various types of organoids from adult and pluripotent stem cells emerged rapidly. In 2008, Sasai and his group reported the formation of three-dimensional cerebral cortex organoids from pluripotent stem cells (18) then, in 2009, Hans Clever’s group generated human gut organoids from adult stem cells (19). In 2011, James Wells’s group

established a protocol to grow human gut organoids from human induced pluripotent stem cells (hiPSCs) (20). To date, cerebral (21), gastric (22, 23), colonic(24-26), intestinal (19, 20), lingual (27), thymic (28), thyroid (29), testicular (30), hepatic (31), pancreatic (32), epithelial (19), kidney (33-35), lung (36), cardiac (37), retinal (38) and gastruloic (39-42) organoids have been generated.

Organoids offer immense potential in biotechnology as they resemble organs both structurally and functionally and are grown *in vitro*. As knowledge of organoid cultures increases, they will likely replace conventional animal models and cell culture systems (5). For example, organoids can maintain their genetic and physiological characteristics over multiple generations (43, 44). This allows genetic manipulations to correct diseases in a tissue type through CRISPR/Cas9 (45-48). Organoids also tend to exhibit improved structures and functionalities over traditional cultures. For example, epithelial cell lines such as Caco-2 or T84 cells exhibit an order of magnitude larger transepithelial electrical resistance values than native human small intestine (49-51); thus, they are non-ideal for a variety of biomedical studies. By contrast, human gut organoids exhibit more physiologically-relevant transepithelial electrical resistance values. Organoid research and applications can also be expanded into organogenesis to gain a better understanding of how organs develop while investigating the physical and chemical factors associated with them (1, 52).

Gastrointestinal organoids representing the stomach, small intestine, and colon are widely used in microbiome research, regenerative medicine, and drug formulation testing. These organoids share the same structure: a monolayer thick epithelial sheet

wrapped into a closed spherical shape. The epithelial sheet represents the inner lining of the gut, and the individual cells composing the sheet are polarized, with an apical side facing inward toward what would ordinarily be the lumen of the gut, and a basolateral side facing outward toward what would ordinarily be the basement membrane. Within the epithelium, stem cells differentiate into cells representative of a particular region of the gastrointestinal tract. For example, a human gastric organoid (HGO) contains parietal cells that excrete gastric acid, foveolar cells that excrete mucus, and the secretory cells including chief cells and enteroendocrine cells. A human intestinal organoid (HIO) contains goblet, Paneth, and endocrine cells.

At Montana State University, we have partnered with two research labs focused on two different types of gastrointestinal organoids: HGOs and HIOs. Professor Diane Bimczok's lab works with HGOs derived from tissue biopsy samples. The Bimczok lab's research is focused on using HGOs as model systems for *Helicobacter pylori* infection and dendritic cell interactions to investigate the immune response. Professor Seth Walk's lab is working with hiPSC derived human intestinal organoids (HIOs) in collaboration with Professor Jason Spence at the University of Michigan. The Walk lab is investigating microbiome colonization in the small intestine and microbiome-epithelial tissue interactions using HIOs.

While HIOs and HGOs form topologically-closed, spherical structures, HIOs can grow approximately an order of magnitude larger in size than HGOs and thus are more accessible to geometrical manipulation than HGOs. This size difference may be due to differences in the type of stem cells used to initiate the culture, which result in HIOs

having a mesenchymal cell layer on top of epithelial monolayer, providing additional rigidity to the structure. By contrast, HGOs are more dynamic than HIOs and exhibit unexpected phenomena when observed with time-lapse microscopy. The enclosed structure of organoids allows them to be used for injection experiments where the injected material could be a pathogen, a symbiotic bacterium native to the microbiome of the tissue or a drug. However, the enclosed structure also prevents advection, thus limiting nutrient availability and leading to the buildup of waste in the lumen.

In the following text, our approaches to providing a physical basis to understand the outcomes of structural transport limitation and potential solutions are discussed in detail. The primary dissertation work revolves around Chapter 3 covering a series of experiments that establish a mathematical model for rupture events and Chapter 4 includes the design and optimization of a lab-on-a-chip platform to contain an organoid while providing continuous intraluminal flow. Furthermore, Chapter 2 covers confocal time-lapse and end-point imaging to analyze organoid growth behavior. Chapters 5 and 6 cover novel model systems through co-culture studies involving dendritic cell immunosurveillance mechanisms.

In Chapter 2, we describe time-lapse confocal microscopy observations of HGO's exhibiting a variety of remarkable and unexpected behaviors such as cyclic rupture, axial rotation, basolateral pseudopodia formation, and luminal fusion. Organoids seem to overcome the structural transport limitation by cyclic rupturing events which are investigated extensively in our studies. Live imaging analysis revealed that spheroid growth was associated with cyclic rupture of the epithelial shell at a frequency of 0.32 ±

0.1/day, which led to the release of luminal contents. Spheroid rupture usually resulted in an initial collapse, followed by spontaneous re-formation of the spheres. Moreover, spheroids frequently rotated around their axes within the Matrigel matrix, possibly propelled by basolateral pseudopodia-like formations of the epithelial cells. Additionally, adjacent spheroids occasionally underwent luminal fusion, as visualized by injection of individual spheroids with FITC-dextran (40 kDa). Consequently, our analysis revealed unexpected dynamics in human gastric spheroids that challenge our current view of cultured epithelia as static entities, which may need to be considered when performing spheroid infection experiments.

In Chapter 3, we present the closed spherical structure limiting material transport resulting in human gastric organoids undergoing extraordinary periodic rupture events during which luminal contents are ejected. Here, we report that human gastric organoids undergoing intermittent rupture are slightly pressurized due to an osmotic pressure difference across the epithelial shell. However, there is no strong dependence of the probability of rupture based on pressure; instead, rupture occurs when cells are expelled from the shell. Various osmotic stress conditions showed that moderate osmotic perturbations ($\leq$ 50 mOsm) caused HGOs to shrink and swell proportionally rather quickly mediated by diffusion of water. In contrast, natural osmotic swelling can be observed in hours and even in days. Thus, the rupture events are an indirect result of osmotic swelling carried out by the diffusion of water due to osmolyte concentration regulation by the epithelial shell. This is consistent with the suppressed rupture events through drug treatment that is inhibiting proton pumps. Overall, we show that a simple

pressure balance provides a framework for understanding rupture events and for mitigating these events in future experiments.

In Chapter 4, we describe technology we developed to overcome the transport limitations imposed by the topologically-closed epithelium. To achieve this, we designed and fabricated a millifluidic device we call the Gut Organoid Flow Chip (GOFlowChip), which we use to "port" HIOs and establish steady-state liquid flow through the lumen. To demonstrate the utility of the device, we establish the separate luminal and extraluminal flow for multiple days and use luminal flow to remove accumulated waste. This represents the first demonstration of established liquid flow through the luminal space of a gastrointestinal organoid. Flow cytometry results show that HIO cell viability is unaffected by long-term porting and luminal flow. We expect the GOFlowChip will enable a wide variety of experiments including real-time, long-term control over luminal contents and continuous luminal sampling.

In Chapter 5, we describe the development and evaluation of a novel co-culture model by using HGOs derived from primary human cells enabling functional studies of the interactions between the gastric epithelium, gastric dendritic cells (DCs) and luminal *H. pylori* bacteria, which is a significant risk factor for peptic ulcer disease and gastric cancer. Bacteria were microinjected into HGOs and co-cultures were established by adding human monocyte-derived DCs (MoDCs). Later, co-culture samples were analyzed for DC recruitment and antigen uptake by confocal microscopy. We hypothesize that DC interactions with the gastric epithelium position gastric DCs for uptake of luminal *H. pylori* and promote DC responses to epithelial-derived mediators. With this model, we

demonstrated that human DCs show chemotactic activity in the presence of epithelial-derived factors and form close interactions with the epithelium.

In Chapter 6, we describe the further confocal microscopy investigation of smaller components of the organoid model co-culture systems such as dendritic cells. In the gastrointestinal epithelia, mucosal immunosurveillance is believed to be increased by Dendritic cell (DC) expression of CD103. Given gastric DCs express only low levels of surface CD103, the hypothesis based on promotion DC-epithelial cell adhesion to epithelial cell-expressed E-cadherin by redistributing the intracellular pools of CD103 in human gastric DCs to the cell surface has been tested. Among the various methods used for testing the hypothesis we used confocal microscopy to capture CD103 presence in endosomal compartments, where CD103 partially co-localized with transport and signaling proteins clathrin, early endosome antigen-1 and Rab11, indicating CD103 undergoes endosomal trafficking like b1 integrins. In conclusion, CD103 does not mediate the DC adhesion to gastrointestinal epithelia, though it engages in DC-epithelial cell interactions.

LITERATURE CITED

1. Lancaster MA & Knoblich JA (2014) Organogenesis in a dish: Modeling development and disease using organoid technologies. *Science* 345(6194).

2. Davies J & Lawrence M (2018) *Organs and Organoids* (Academic Press Imprint, Elsevier Science & Technology Books, San Diego, Oxford).

3. Willyard C (2015) The boom in mini stomachs, brains, breasts, kidneys and more. *Nature* 523(7562):520-522.

4. Akkerman N & Defize LHK (2017) Dawn of the organoid era: 3D tissue and organ cultures revolutionize the study of development, disease, and regeneration. *Bioessays* 39(4).

5. Takahashi T (2019) Organoids for Drug Discovery and Personalized Medicine. *Annu Rev Pharmacol* 59:447-462.

6. Wilson HV (1907) A new method by which sponges may be artificially reared. *Science* 25:912-915.

7. Weiss P & Taylor AC (1960) Reconstitution of Complete Organs from Single-Cell Suspensions of Chick Embryos in Advanced Stages of Differentiation. *P Natl Acad Sci USA* 46(9):1177-1185.

8. Pierce GB & Verney EL (1961) An in Vitro and in Vivo Study of Differentiation in Teratocarcinomas. *Cancer* 14(5):1017-&.

9. Steinberg MS (1964) The Problem of Adhesive Selectivity in Cellular Interactions. *Cellular Membranes In Development*, ed Locke M (Academic Press, New York), pp 321-366.

10. Reya T, Morrison SJ, Clarke MF, & Weissman IL (2001) Stem cells, cancer, and cancer stem cells. *Nature* 414(6859):105-111.

11. Evans M (1981) Origin of Mouse Embryonal Carcinoma-Cells and the Possibility of Their Direct Isolation into Tissue-Culture. *J Reprod Fertil* 62(2):625-&.

12. Martin GR (1981) Isolation of a Pluripotent Cell-Line from Early Mouse Embryos Cultured in Medium Conditioned by Teratocarcinoma Stem-Cells. *P Natl Acad Sci-Biol* 78(12):7634-7638.

13. Li ML, *et al.* (1987) Influence of a Reconstituted Basement-Membrane and Its Components on Casein Gene-Expression and Secretion in Mouse Mammary Epithelial-Cells. *P Natl Acad Sci USA* 84(1):136-140.

14. Kleinman HK, Klebe RJ, & Martin GR (1981) Role of Collagenous Matrices in the Adhesion and Growth of Cells. *J Cell Biol* 88(3):473-485.

15. Benton G, George J, Kleinman HK, & Arnaoutova IP (2009) Advancing Science and Technology Via 3D Culture on Basement Membrane Matrix. *J Cell Physiol* 221(1):18-25.

16. Thomson JA, *et al.* (1998) Embryonic stem cell lines derived from human blastocysts. *Science* 282(5391):1145-1147.

17. Yu JY, *et al.* (2007) Induced pluripotent stem cell lines derived from human somatic cells. *Science* 318(5858):1917-1920.

18. Eiraku M, *et al.* (2008) Self-Organized Formation of Polarized Cortical Tissues from ESCs and Its Active Manipulation by Extrinsic Signals. *Cell Stem Cell* 3(5):519-532.

19. Sato T, *et al.* (2009) Single Lgr5 stem cells build crypt-villus structures in vitro without a mesenchymal niche. *Nature* 459(7244):262-U147.

20. Spence JR, *et al.* (2011) Directed differentiation of human pluripotent stem cells into intestinal tissue in vitro. *Nature* 470(7332):105-109.

21. Lancaster MA, *et al.* (2013) Cerebral organoids model human brain development and microcephaly. *Nature* 501(7467):373-+.

22. McCracken KW, *et al.* (2014) Modelling human development and disease in pluripotent stem-cell-derived gastric organoids. *Nature* 516(7531):400-+.

23. Barker N, *et al.* (2010) Lgr5(+ve) Stem Cells Drive Self-Renewal in the Stomach and Build Long-Lived Gastric Units In Vitro. *Cell Stem Cell* 6(1):25-36.

24. Sato T, *et al.* (2011) Long-term Expansion of Epithelial Organoids From Human Colon, Adenoma, Adenocarcinoma, and Barrett's Epithelium. *Gastroenterology* 141(5):1762-1772.

25. Gardiner BS, Joldes GR, Wong KKL, Tan CW, & Smith DW (2016) Controlling seepage in discrete particle simulations of biological systems. *Comput Method Biomec* 19(11):1160-1170.

26. Yip HYK, Tan CW, Hirokawa Y, & Burgess AW (2018) Colon organoid formation and cryptogenesis are stimulated by growth factors secreted from myofibroblasts. *Plos One* 13(6).

27. Hisha H, *et al.* (2013) Establishment of a Novel Lingual Organoid Culture System: Generation of Organoids Having Mature Keratinized Epithelium from Adult Epithelial Stem Cells. *Sci Rep-Uk* 3.

28. Bredenkamp N, *et al.* (2014) An organized and functional thymus generated from FOXN1-reprogrammed fibroblasts. *Nat Cell Biol* 16(9):902-908.

29. Martin A, Barbesino G, & Davies TF (1999) T-cell receptors and autoimmune thyroid disease--signposts for T-cell-antigen driven diseases. *Int Rev Immunol* 18(1-2):111-140.

30. Baert Y, *et al.* (2017) Primary Human Testicular Cells Self-Organize into Organoids with Testicular Properties. *Stem Cell Rep* 8(1):30-38.

31. Huch M, *et al.* (2015) Long-Term Culture of Genome-Stable Bipotent Stem Cells from Adult Human Liver. *Cell* 160(1-2):299-312.

32. Huch M, *et al.* (2013) Unlimited in vitro expansion of adult bi-potent pancreas progenitors through the Lgr5/R-spondin axis. *Embo J* 32(20):2708-2721.

33. Unbekandt M & Davies JA (2010) Dissociation of embryonic kidneys followed by reaggregation allows the formation of renal tissues. *Kidney Int* 77(5):407-416.

34. Takasato M, *et al.* (2015) Kidney organoids from human iPS cells contain multiple lineages and model human nephrogenesis. *Nature* 526(7574):564-U238.

35. Morizane R, *et al.* (2015) Nephron organoids derived from human pluripotent stem cells model kidney development and injury. *Nat Biotechnol* 33(11):1193-U1127.

36. Lee JH, *et al.* (2014) Lung Stem Cell Differentiation in Mice Directed by Endothelial Cells via a BMP4-NFATc1-Thrombospondin-1 Axis. *Cell* 156(3):440-455.

37. Lee EJ, Kim DE, Azeloglu EU, & Costa KD (2008) Engineered cardiac organoid chambers: Toward a functional biological model ventricle. *Tissue Eng Pt A* 14(2):215-225.

38. Wiley LA, *et al.* (2016) cGMP production of patient-specific iPSCs and photoreceptor precursor cells to treat retinal degenerative blindness. *Sci Rep-Uk* 6.

39. van den Brink SC, *et al.* (2014) Symmetry breaking, germ layer specification and axial organisation in aggregates of mouse embryonic stem cells. *Development* 141(22):4231-4242.

40. Turner DA, Baillie-Johnson P, & Arias AM (2016) Organoids and the genetically encoded self-assembly of embryonic stem cells. *Bioessays* 38(2):181-191.

41. Turner DA, *et al.* (2017) Anteroposterior polarity and elongation in the absence of extra-embryonic tissues and of spatially localised signalling in gastruloids: mammalian embryonic organoids. *Development* 144(21):3894-3906.

42. Beccari L, *et al.* (2018) Multi-axial self-organization properties of mouse embryonic stem cells into gastruloids. *Nature* 562(7726):272-+.

43. DiMarco RL, *et al.* (2014) Engineering of three-dimensional microenvironments to promote contractile behavior in primary intestinal organoids. *Integr Biol-Uk* 6(2):127-142.

44. Grabinger T, *et al.* (2014) Ex vivo culture of intestinal crypt organoids as a model system for assessing cell death induction in intestinal epithelial cells and enteropathy. *Cell Death Dis* 5.

45. Doudna JA & Charpentier E (2014) The new frontier of genome engineering with CRISPR-Cas9. *Science* 346(6213):1077-+.

46. Schwank G & Clevers H (2016) CRISPR/Cas9-Mediated Genome Editing of Mouse Small Intestinal Organoids. *Methods Mol Biol* 1422:3-11.

47. Driehuis E & Clevers H (2017) CRISPR/Cas 9 genome editing and its applications in organoids. *Am J Physiol-Gastr L* 312(3):G257-G265.

48. Drost J, *et al.* (2017) Use of CRISPR-modified human stem cell organoids to study the origin of mutational signatures in cancer. *Science* 358(6360):234-+.

49. Maloy KJ & Powrie F (2011) Intestinal homeostasis and its breakdown in inflammatory bowel disease. *Nature* 474(7351):298-306.

50. van Breemen RB & Li Y (2005) Caco-2 cell permeability assays to measure drug absorption. *Expert Opin Drug Metab Toxicol* 1(2):175-185.

51. Sjoberg A, *et al.* (2013) Comprehensive study on regional human intestinal permeability and prediction of fraction absorbed of drugs using the Ussing chamber technique. *Eur J Pharm Sci* 48(1-2):166-180.

52. Dahl-Jensen S & Grapin-Botton A (2017) The physics of organoids: a biophysical approach to understanding organogenesis. *Development* 144(6):946-951.

CHAPTER 2

LIVE IMAGING ANALYSIS OF HUMAN GASTRIC EPITHELIAL SPHEROIDS REVEALS SPONTANEOUS RUPTURE, ROTATION, AND FUSION EVENTS

Contribution of Authors and Co-Authors

Manuscript in Chapter 2

Author: Thomas A. Sebrell

Contributions: Performed the experiments, analyzed the data, wrote the manuscript.

Author: Barkan Sidar

Contributions: Performed the experiments.

Co-Author: Rachel Burns

Contributions: Performed the experiments, analyzed the data.

Co-Author: Royce A. Wilkinson

Contributions: Performed the experiments.

Co-Author: Blake Wiedenheft

Contributions: Planned and oversaw the experiments.

Co-Author: Paul J. Taylor

Contributions: Developed microinjection equipment and protocols.

Co-Author: Brian A. Perrino

Contributions: Provided human gastric tissue samples.

Co-Author: Linda C. Samuelson

Contributions: Planned and oversaw the experiments.

Co-Author: James N. Wilking

Contributions: Planned and oversaw the experiments.

Co-Author: Diane Bimczok

Contributions: Planned and oversaw the experiments, analyzed the data, wrote the manuscript.

Manuscript Information

T. Andrew Sebrell, Barkan Sidar, Rachel Bruns, Royce A. Wilkinson, Blake Wiedenheft,

Paul J. Taylor, Brian A. Perrino, Linda C. Samuelson, James N. Wilking, Diane Bimczok

Cell and Tissue Research

Status of Manuscript:
____ Prepared for submission to a peer-reviewed journal
____ Officially submitted to a peer-reviewed journal
____ Accepted by a peer-reviewed journal
__X_ Published in a peer-reviewed journal

DOI: 10.1007/s00441-017-2726-5

Published by Springer Berlin Heidelberg
In Volume 371, Issue 2, 293-307 (2018)

Correspondence: Diane Bimczok, diane.bimczok@montana.edu, Address: 960 Technology Blvd., Bozeman, MT, 59717, USA; Phone: 406-994-4928, Fax: 406-994-3953.

Conflict of Interest Statement: Dr. Paul Taylor has a potential conflict of interest, since he is the owner of GeneSearch, Inc., Bozeman, MT, which manufactures the EmbryoCradle microinjector that was used in this study. None of the other authors declare a conflict of interest.

ABSTRACT

Three-dimensional cultures of primary epithelial cells including organoids, enteroids and epithelial spheroids have become increasingly popular for studies of gastrointestinal development, mucosal immunology and epithelial infection. However, little is known about the behavior of these complex cultures in their three-dimensional culture matrix. Therefore, we performed extended time-lapse imaging analysis (up to 4 days) of human gastric epithelial spheroids generated from adult tissue samples in order to visualize the dynamics of the spheroids in detail. Human gastric epithelial spheroids cultured in our laboratory grew to an average diameter of 443.9 ± 34.6 μm after 12 days, with the largest spheroids reaching diameters of > 1,000 μm. Live imaging analysis revealed that spheroid growth was associated with cyclic rupture of the epithelial shell at a frequency of 0.32 ± 0.1/day, which led to the release of luminal contents. Spheroid rupture usually resulted in an initial collapse, followed by spontaneous re-formation of the spheres. Moreover, spheroids frequently rotated around their axes within the Matrigel matrix, possibly propelled by basolateral pseudopodia-like formations of the epithelial cells. Interestingly, adjacent spheroids occasionally underwent luminal fusion, as visualized by injection of individual spheroids with FITC-dextran (40 kDa). In summary, our analysis revealed unexpected dynamics in human gastric spheroids that challenge our current view of cultured epithelia as static entities and that may need to be considered when performing spheroid infection experiments.

INTRODUCTION

In recent years, epithelial organoids have become increasingly popular as a new and powerful tool to study gastrointestinal development and disease (1-3). Since the initial description of epithelial organoids derived from murine intestine (4, 5), organoid culture systems have been adapted to multiple epithelial organ systems and species (6, 7). For the first time, primary gastrointestinal epithelial cells from various species can now be propagated for extended periods of time by culturing the cells in a 3-dimensional collagen matrix and by supplementing Wnt3a, noggin, R-spondin to support maintenance of the stem cell compartment. Importantly, the utilization of adult stem cells enables the generation of primary epithelial cell lines from patient tissues with the potential of performing translational studies and patient-specific analyses (8, 9). The availability of established protocols for primary epithelial cell cultures has led to exponential growth in publications using these methods over the last five years, with the number of "organoid" publications per year increasing from <10 in 2007 to ≥450 in 2016. Thus, various forms of organoid cultures are starting to replace more traditional epithelial culture methods that involve the use of transformed cell lines derived from gastrointestinal tumors.

However, little is known about the behavior of these complex living spheres in their three-dimensional matrix, beyond diametrical expansion due to cell proliferation. Several publications on gastrointestinal organoids or spheroids include video supplements showing growth over time (10-13). Some of these videos challenge our concept of epithelial organoids as static entities that undergo diametrical growth, though the dynamic behaviors observed were not evaluated in detail.

In our study, we have established primary gastric epithelial cell lines from 13 healthy human adults. These lines were maintained as spheroids following the protocol published by Miyoshi and Stappenbeck (14), which has been used by multiple groups to culture organoids from intestinal (7, 15-17) and gastric sites (9, 18-20). With these cultures, we have performed live imaging analysis for up to 4 days. Under the culture conditions used, rupture events occurred cyclically in the majority of the cultures imaged and were associated with the release of luminal material and subsequent healing of the majority of spheroids. In addition, we also observed spheroids that rotated in the Matrigel, and spheroids that fused with other spheroids. These observations indicate that human gastric spheroid cultures are surprisingly dynamic, at least under the specific culture conditions used here. Notably, epithelial barrier function of the spheroids may temporarily be compromised because of relatively common spontaneous rupture events that are not visible using routine monitoring techniques.

MATERIALS AND METHODS

Human Gastric Epithelial Spheroid Culture

Thirteen gastric tissue specimens from sleeve gastrectomy surgeries were obtained with Institutional Review Board (IRB) approval by the National Disease Research Interchange (NDRI; Philadelphia, PA) or by Dr. Kent Sasse (Sasse Surgical Associates, Reno, NV). Donor characteristics are listed in **Table 1**. Information on pathological alteration of the tissues were provided by the NDRI. Gastric glands were isolated as described previously (Bimczok 2013 and 2015). Briefly, we dissected the

gastric mucosa off the muscle layer, cut the mucosa into <1mm pieces, which were placed into RPMI-1640 medium supplemented with 0.5 U/mL collagenase type IV, 0.2 mg/mL DNAse (Sigma-Aldrich, St. Louis, MO), 0.3% BSA, 250 µg/mL amphotericin B (Fisher Scientific, Fair Lawn, NJ), 100 U/mL penicillin/streptomycin, 2 mM L-glutamine, 1 mM HEPES (GE Healthcare Life Sciences, Logan UT) and 50 µg/mL Gentamycin (IBI Scientific, Peosta, IL). The tissue was incubated at 200 rpm in a 37ºC water bath for 1 h. The tube was then vortexed for 30 s to release glands from the tissue. To establish gastric spheroid cultures, the glands and remaining tissue pieces were centrifuged at 200 x *g*, 4ºC for 5 min. The pellet was resuspended in 30 mL ice-cold DPBS (Hyclone GE Healthcare Life Sciences, Logan UT) and vortexed again for 30 s. Tissue pieces were allowed to settle to the bottom of the tube, and gastric glands in the supernatant were transferred to a new 50 mL tube, pelleted and transferred to Matrigel (Corning, Bedford, MA). Glands suspended in Matrigel were pipetted into a pre-warmed 24-well plate. Gastric spheroid cultures were maintained following the protocol of Miyoshi and Stappenbeck (14), with minor modifications as described by Gifford et al. (19). After polymerization, Matrigel was overlaid with 500 µL of L-WRN medium composed of Advanced DMEM/F12 (Gibco by Life Technologies, Grand Island, NY) supplemented with 10mM HEPES, 1% Pen/Strep, 50% L-WRN conditioned medium, 10 µM Rock-inhibitor Y-27632 (Tocris Biosciences, Bristol, UK), Amphotericin B, Gentamycin, L-Glutamine, 10 µM TGF-β inhibitor SB-431542 (Tocris), 10% FBS (Rocky Mountain Bio, Missoula, MT) and 50 % of cell culture supernatant from L-WRN cells, which constitutively secrete murine Wnt3a, noggin and R-spondin 3 (21). L-WRN

cells were kindly provided by Dr. T. Stappenbeck, Washington University, St. Louis. The final concentration of Wnt3a in the culture media was 6.2 ± 0.2 μg/mL as determined by testing 3 individual supernatants from L-WRN cells with the TopFlash assay (22), using the Firefly Luciferase Assay Kit 2.0 (Biotium, Fremont, CA) and recombinant murine Wnt3a (Peprotech, Rocky Hill, NJ) as a standard. Formed spheroids were maintained in a 37ºC, 5% CO_2 incubator, with fresh medium added every 2 – 3 days, and were passaged by trypsinization and re-plating at 1 : 4 every 5 - 7 days. The conditions used in this study allowed the continuous culture of human gastric spheroids for at least 50 passages (approximately 11 months), without apparent changes in growth, morphology or viability.

Immunohistochemistry and Immunofluorescence Analysis

For paraffin-embedded sections, Matrigel plugs containing spheroids were fixed in 10% neutral buffered formalin (Richard Allen Scientific, Kalamazoo, MI). Paraffin embedded sections were prepared on a Sakura Tissue-Tek VIP1000 tissue processor and embedding center and sectioned at 5 μm on a Leica 2035 rotary microtome. Sections were stained with hematoxlin-eosin (HE) reagent (Richard Allen Scientific). For whole mount staining, gastric epithelial spheroids grown on 8-well chamber slides were fixed for 30 min at 4ºC in Cytofix (BD Biosciences, San Diego, CA). Samples were blocked in PBS containing 10% FBS (Rocky Mountain Bio, Missoula, MT), 0.2% Triton X-100, 0.1% BSA and 0.05% Tween-20 (Fisher Scientific) and were incubated with primary antibody overnight at 4ºC. The following primary antibodies were used: mouse anti-human cytokeratin, clone CAM5.2 (BD Biosciences, San Jose, CA; recognizes Moll's

cytokeratin peptide #8 and #7) and mouse anti-human E-Cadherin, clone 67A4 (BioLegend, San Diego, CA). Wells were washed with DPBS, and isotype-specific Alexa488-labeled secondary antibody (SouthernBiotech, Birmingham, AL) was added for 2 h at room temperature. After a final wash step, samples were covered with ProLong Gold with DAPI (Fisher Scientific).

Quantitative RT-PCR

Total RNA was isolated from epithelial spheroids and human gastric tissue samples using the Direct-zol RNA MiniPrep Kit (ZymoResearch, Irvine, CA). Complementary DNA was generated using reverse transcription performed from 1 μg RNA using the iScript cDNA Synthesis Kit (Bio-Rad Laboratories, Hercules, CA). qPCR was performed using iTaq Universal SYBR Green Supermix (Bio-Rad) on a Roche LightCyler96 (Roche, Basel, Switzerland). PCR primers sequences used are listed in Supplemental Table 1. PCR data were analyzed using the $2^{-\Delta\Delta CT}$ method, with gastric spheroid gene expression normalized to *GAPDH* and gene expression in human gastric biopsy tissue.

Growth Measurements and Counting

To determine spheroid size, cultures were imaged by phase contrast microscopy, and spheroid diameters were measured on composite images of entire culture wells. To obtain cell counts, spheroid cultures were incubated with 0.25% Trypsin EDTA solution (EMD Millipore, Billerica, MA) at 37ºC for 5 – 7 min and mixed with a pipet tip until a

single cell suspension was obtained. Cells were then counted on a hemocytometer or on a flow cytometer using reference cells (23).

Generation of EGFP- and mCherry-expressing Spheroids by Lentiviral Transduction

To produce lentiviral particles, HEK293 cells were plated at 40% confluency in DMEM/10% fetal calf serum/penicillin/streptomycin the day before transfection. One hour before transfection, the media was replaced with pre-warmed OptiMEM (Gibco, Grand Island, NY). Cells were co-transfected with pCMV-VSV-G (a gift from Bob Weinberg; Addgene plasmid # 8454, Stewart, *et al.* (24)), psPAX2 (a gift from Didier Trono; Addgene plasmid # 12260), and either pLJM1-EGFP (a gift from David Sabatini; Addgene plasmid # 19319, Sancak, *et al.* (25)) or pLV-mCherry (a gift from Pantelis Tsoulfas; Addgene plasmid # 36084) using Lipofectamine 3000 (ThermoFisher) according to the manufacturer's instructions. Six hours after transfection, the OptiMEM was removed and replaced with DMEM/10% fetal calf serum/1% BSA. The supernatant containing the lentivirus was harvested 48 h and 60 h post-transfection. The combined (48 h & 60 h) samples were centrifuged for 10 min at 1000 × *g* at 4°C, filtered through a low-protein binding 0.45 µm filter, and concentrated by ultracentrifugation (80,000 × *g* at 4°C for 2 h). The virus was resuspended by overnight incubation at 4°C in DMEM/10% FCS/1% BSA, aliquoted and stored at -80°C.

To perform lentiviral transduction of gastric spheroids, the spheroids were harvested and trypsinized to obtain a single cell suspension. Cells were suspended in spheroid L-WRN media prepared with 10 µM ROCK Inhibitor Y-27632 (Tocris Biosciences) and hexadimethrine bromide (Sigma-Aldrich). Cells were incubated with 30

μL of lentivirus in 250 μL L-WRN media and incubated at 37ºC, 5% CO_2. After 6 hours, suspensions were transferred to Eppendorf tubes and centrifuged at 500 × *g* for 5 min. Epithelial cells were transferred to Matrigel and plated into a warmed 24-well plate for further culture and were maintained in the presence of puromycin (Sigma) for EGFP. Spheroids with high EGFP or mCherry expression were derived from FACS-purified single cell suspensions.

Microinjection of Gastric Spheroids with FITC-Dextran

A Fisher stereomicroscope fitted with a Genesearch Embryo Cradle (Genesearch, Bozeman, MT) and a 2 μL syringe (Hamilton Co., Reno, NV) was used for microinjection. Injection needles with beveled tips were pulled from glass capillaries to a size of 21-23 μm. For the injection, 10 days plated spheroids in 35mm MatTek dishes were injected with 0.2 μL of 25 μM FITC-Dextran 4 kDa (Sigma-Aldrich, St. Louis, MO). Spheroids were left in the Matrigel Matrix for injection.

Microscopic Analysis

Epiflourescence and phase contrast images were acquired using a Life Technologies EVOS FL Auto system equipped with an onstage incubator. Live confocal imaging analysis was performed on an inverted Leica SP5 Confocal Scanning Laser Microscope with 405, 488, 561 and 633 nm laser excitation lines and a heated stage with an environmental control chamber. Fluorescence, phase contrast and backscattered light images were collected at 10 min intervals over 17 to 112 h using a 10 x objective. Backscattered laser light images were obtained by adjusting the wavelength range of the

imaging detector to capture the excitation laser wavelength. This technique allows the visualization of interfaces between materials of different densities.

For transmission electron microscopy analysis (26), epithelial spheroid cultures were fixed overnight with 3% glutaraldehyde in 0.05 M potassium sodium phosphate buffer, pH 7.2, followed by postfixation in 2% osmium tetroxide for 4 h. Samples were dehydrated using an ethanol series (50 to 100%) and propylene oxide. After dehydration, epithelial spheroids were gradually infiltrated with Spurr's resin and baked overnight at 70°C. 60 to 90 nm ultrathin sections were cut with a Diatome diamond knife on a Reichert OM-U2 ultramicrotome, floated onto 300-mesh copper grids, and stained with uranyl acetate and Reynold's lead citrate. All sections were viewed with a LEO 912AB TEM and photographed with a Proscan 2,048- by 2,048-pixel charge-coupled-device camera.

RESULTS

Phenotypic Analysis of Human Gastric Epithelial Spheroids

To confirm the identity and differentiation stage of our gastric epithelial spheroid lines maintained using the protocol of Miyoshi and Stappenbeck (14), we first performed phenotypic analyses using light microscopy, qRT-PCR and transmission electron microscopy (TEM). As anticipated, the epithelial cells formed spheroids with columnar to cuboidal epithelium and expressed epithelial cytokeratin and E-cadherin (**Fig. 1a-c**). Quantitative RT-PCR analysis of the gastric spheroids confirmed expression of genes specific for all five major gastric epithelial cell subsets, i.e., parietal cells (*ATP4B*), chief

cells (pepsinogen C, *PGC*), surface mucus cells (*MUC5ac*), mucus neck cells (*MUC6*), and enteroendocrine cells (chromogranin A, *CHGA*, **Fig. 1d**). Notably, gene expression for the enteroendocrine marker *CHGA* was very low. Moreover, gene expression levels of all five genes analyzed were decreased compared to the levels detected in the gastric biopsy specimens that were used as positive controls for PCR normalization.

Ultrastructural analysis by TEM revealed that the gastric spheroids contained several morphologically distinct cell types (**Fig. 2**). The predominant cell type was a secretory-type cell with large electron-dense vesicles in the apical portion of the cell (**Fig. 2a and 2a′**), comparable to a mucus pit cell (27, 28). Cells with electron-lucent vesicles near their luminal surface were also present (**Fig. 2a and 2a′′**), similar to mucus neck cells. Some cells had large amounts of rough ER and mitochondria, consistent with active protein synthesis as typically found in chief cells (**Fig. 2b**) (27). Moreover, we also detected cells with large intracellular canaliculi with projecting microvilli, similar to those described for parietal cells (**Fig. 2c**) (29). We did not detect any cells with basal vesicles typical for enteroendocrine cells. Consistent with the general morphology of the gastrointestinal epithelium, spheroid cells had basal nuclei, short apical microvilli (**Fig. 2d, and d′**) and distinct apical junctional complexes (**Fig. 2e**). We also observed extensive formation of interdigitating lateral processes (**Fig. 2d and f**), as shown by Necchi, Manca, Ricci and Solcia (30) for human gastric mucosa. Overall, gastric spheroids show typical features of the human gastric epithelium, but do not appear to be fully differentiated.

Growth Dynamics of Human Gastric Epithelial Spheroids

Next, we analyzed spheroid growth dynamics, size distribution and cellularity of the spheroids (**Fig. 3**). Spheroids expanded in size over a period of around 10 days and then plateaued, with a median diameter of 398 μm (average 443.9 ± 34.6 μm) after 12 days of culture (**Fig. 3a-a‴, b**). Spheroids within one culture well varied significantly in size (**Fig. 3c**). To determine the size distribution of gastric spheroids within a culture, spheroids from 4 different lines were grown until the largest ones reached a size of > 600 μm. Cultures were then imaged, and spheroid diameters measured on composite digital images of culture wells (**Fig. 3d**). Size distribution was remarkably consistent between individual spheroid lines and followed a right-skewed bell curve, with 73 ± 8 % of spheroids only reaching diameters of ≤ 300 μm. A small subset of spheroids (0.4 ± 0.4%) reached diameters of ≥ 800 μm after 7 to 10 days of culture.

Using composite images of entire culture wells, digital image measurements and manual cell counting of single cell suspensions derived from the spheroids, we determined the average relationship between spheroid size and cell numbers in our cultures (**Fig. 3e**), with *n* being equivalent to the numbers of cells that can be recovered from a spheroid of a defined radius (in μm):

$$n = (0.00395 \pm 0.0007)\ \frac{1}{\mu m}\ 4\,\pi\,r$$

These cell counts correspond to radius of 20 μm per single epithelial cell. Similar results were obtained using FACS-based cell counting with reference cells (23). The number of cells per spheroid can be used to assess the recovery of DNA, RNA and protein from

cultures with organoids of certain sizes and to calculate the multiplicity of infection for pathogen microinjection experiments.

Spontaneous Rupture and Healing Events of Human Gastric Organoids

Based on published and anecdotal reports of organoid rupture events (11-13), we performed live imaging analysis of six distinct human gastric spheroid lines, with 9 – 83 spheroids per line imaged over 17 to 112 h. As shown in **Fig. 4a-a′′′′** and **Suppl. Movie 1**, spheroids frequently oscillated in diameter, consistent with rupture and healing processes. We observed an average of 0.32 ± 0.1 ruptures per spheroid per 24 h period (**Fig. 4b**), with significant variations between the three lines that were analyzed ($P \leq 0.01$). Within a given 24 h time period, some spheroids did not rupture at all, whereas some spheroids ruptured more than once. Overall, 43 ± 10 % of spheroids in each line analyzed showed rupture events. We did not observe any significant difference in rupture frequency between low passage (<10) and high passage (>10) spheroids (**Fig. 4c**). Interestingly, there was a trend for an increased rupture frequency in larger epithelial spheroids (**Fig. 4d**).

Imaging of EGFP-expressing epithelial spheroids with a combination of fluorescence confocal imaging, backscatter confocal imaging (31) and bright field imaging revealed that rupture events were focal and were associated with the release of material with increased scattering properties – possibly mucus and cell debris – from the spheroid lumen (**Fig. 5a-c′′′′ and Suppl. Movie 2**). To visualize loss of material from the spheroid lumen, we performed live imaging on gastric epithelial spheroids that were microinjected with 4 kDa FITC dextran. As shown in **Fig. 5d-e′′′′**, injected FITC

dextran remained in the spheroid lumen for >12 h, indicating that the epithelial barrier of the spheroids was intact. Upon rupture, the FITC dextran completely disappeared from the spheroid lumen (**Fig. 5d-e‴ and Suppl. Movie 3**). Notably, epithelial thickness was low prior to rupture events and increased immediately following a rupture event. In summary, our data show that spontaneous spheroid rupture is a common event and involves release of luminal material.

Human Gastric Spheroids Rotate within the Matrigel Matrix

Surprisingly, our live imaging analysis also revealed that, even in the absence of rupture events, spheroid interactions with the Matrigel matrix were not static. In particular, spheroids frequently rotated around an axis, with an average of 53.6 ± 11.4% of spheroids in all cultures analyzed displaying rotational movement within the matrix (**Fig. 6a-a⁗, b** and **Suppl. Movie 4**). This behavior was predominantly observed in smaller spheroids (< 100 μm in diameter, data not shown), but showed large variation between individual spheroid lines and individual cultures. Again, there was no significant difference between low passage (≤ p 10) or high passage (>10) spheroids. To further investigate the dynamic interactions between the spheroids and the Matrigel, we performed backscatter light imaging (**Fig. 6c-c″** and **Suppl. Movie 5**). This backscatter light analysis revealed that spheroid epithelia form temporary, pseudopod-like basolateral projections that may enable movement of the spheroids within the Matrigel capsule.

Adjacent Spheroids may Undergo Membrane Fusion

Live imaging analysis also revealed that, in some cases, two adjacent spheroids fused to form one larger spheroid (**Fig. 7**). These events were rare, but seen in three out of five different lines analyzed between passages 4 and 18 (**Fig. 7a-a′′′′, b**). To confirm that the observed events represented true luminal fusions, spheroids that had been injected with FITC-dextran (4 kDa) were monitored by live confocal imaging. As shown in **Fig. 7c-d′′′** and **Supplemental Movie 6**, spheroid fusion resulted in the transfer of green fluorescent FITC-dextran from the lumen of one injected spheroid to a non-injected spheroid. These observations indicate that spheroid fusions lead to the formation of a common luminal compartment.

DISCUSSION

In this study, we used live imaging to demonstrate that human gastric epithelial spheroids – or gastrospheres (32) – cultured under the conditions described (see methods) display several dynamic behaviors that may be overlooked when performing end-point analyses and that may impact experimental results. Specifically, spheroids spontaneously ruptured and sometimes fused, and spheroids frequently rotated in the Matrigel matrix. Notably, there were significant differences in the behavior of distinct gastric spheroid lines, and in the behavior of individual spheroid lines analyzed after a different number of passages.

Spontaneous rupture was a relatively common event, with >40 % of spheroids imaged showing rupture events. Videos included in several previous publications on

murine intestinal organoids and human gastric organoids also showed organoid ruptures, although these events were not addressed directly (11-13), which suggests that spontaneous ruptures are not specific to the specific culture conditions used here. In our study, we quantified rupture events and demonstrated that ruptures occurred in all gastric spheroid lines analyzed in our laboratory. We also showed that ruptures were preceded by thinning of the epithelium, suggesting that the luminal pressure of the spheroids increased over time. There was a trend for larger spheroids to rupture more frequently, but the reasons for this increased rupture behavior is unclear. Since the gastric epithelium normally lines a tubular structure rather than a closed sphere, mechanisms that prevent rupture are not likely to exist. Notably, our observation that spheroids rupture on a regular basis could theoretically impact the outcome of experiments, if injected microorganisms or other luminally secreted substances were to be released into the Matrigel and unexpectedly interacted with the basolateral side of the epithelium.

Gastric spheroids generally underwent additional growth following rupture, indicating efficient and rapid epithelial restitution. As previously described (14, 33), isolated glands spontaneously form spheres within several hours, which represents another example of epithelial healing behavior. Moreover, we observed that adjacent spheroids occasionally fused, which may also represent a healing mechanism. The ability of organoids to contribute to epithelial healing has been previously demonstrated. In a recent study by Engevik et al. (34), gastric organoids were transplanted into the gastric submucosa of mice following chemical induction of gastric ulcers. These transplanted organoids significantly improved gastric wound healing, demonstrating that gastric

organoids efficiently regenerate defective epithelia (34). Similarly, colonic organoids improved the healing of epithelial defects in the murine colon (35). Such wound healing behavior of gastrointestinal epithelia involves chemotactic migration of epithelial cells and epithelial flattening and lateral lamellipodia extension that lead to rapid closure of epithelial gaps independent of cell proliferation (36-38). In addition, the efficient reformation of spheroids after rupture and the fusion of closely adjacent spheroids was possibly enhanced by the high medium concentrations of Wnt, which promotes gastrointestinal epithelial wound healing (39).

Notably, gastrointestinal epithelial cells are highly dynamic *in vivo,* with a high epithelial cell turnover rate and efficient closure of gaps caused by apoptotic cell extrusion (40, 41). Gastric surface mucus cells migrate from the isthmus, where stem cells are located, to the surface mucosa within 1 – 3 days (42-44). Intestinal epithelial cells move as a much as 5 – 10 μm/hr from the base of the crypts towards the tips of the villi, and apical junctional complexes have to be constantly re-organized to close gaps left by epithelial cells that undergo apoptosis (37). This constant reformation of intracellular junctions due to epithelial cell turnover may have played a role the formation of cell-cell junctions in the observed fusions of intact spheroids.

It remains unclear whether the formation of dynamic pseudopods observed on the basolateral side of human gastric spheroids was a normal process or specific to our culture conditions. Basal pseudopodia or lamellipodia that may promote epithelial cell movement have been identified in normal intestinal epithelium, but they occur at low frequencies (41). In contrast, basal pseudopodia play a major role in epithelial

carcinogenesis, where pseudopodia can contribute to invasion and matrix degradation by expanding tumors (45). Basal pseudopod-like processes in the small intestine also appear to be more frequent during early development (46) and on certain types of enteroendocrine cells, where they are thought to allow directed secretion of hormones (47). In our spheroid cultures, increased basal pseudopod formation might be associated with the low differentiation stage of the cells or might have been provoked by the specific characteristics of the Matrigel matrix, which differs from normal basement membrane and extracellular matrix in composition and structure (48). Since pseudopodia are generally associated with cellular movement, these processes may have enabled spheroid movement including the observed rotation and fusion events within the Matrigel shell.

Our detailed analysis of gastric spheroid growth under previously published culture conditions (14, 18-20) revealed several additional interesting properties of this model system. Thus, although some spheroids grew to a size of >1,000 μm in diameter, the percentage of these large spheroids was <0.5%, while the majority of spheroids remained in the 100 – 300 μm diameter size range after 7 – 10 days in culture. Also, we never observed spheroids that grew larger than 1,300 μm. Interestingly, TEM analysis of the cultures revealed extensive formation of lateral interdigitating folds, as also observed in some gastric tissue specimens in previous studies (30). Structurally similar lateral folds have been detected in the gall bladder and other epithelial tissues with increased ion transport capacity and have been implicated in contributing to water retention (49, 50).

Notably, we did not alter the composition of the culture media during the experiments in order to induce gastric epithelial cell differentiation, and our spheroids did

not develop gland-like invaginations. Differentiation of primary gastric epithelial cell cultures has previously been achieved by withdrawal of Wnt and noggin (6) or Notch inhibition (9, 18, 51). Since we detected expression of genes specific for all five major epithelial cell subsets, and the TEM analysis revealed structures very similar to the intracellular canaliculi that are considered typical for gastric parietal cells, we consider the epithelial cells in our cultures partially differentiated. It remains unknown whether the behaviors and growth dynamics described here similarly occur under culture conditions different from the ones used in our study. Ruptures and organoid movement in the Matrigel have been shown for a number of different epithelial and culture protocols (11-13), but the frequency of these events had not previously been evaluated. Several different protocols have been used to generate and maintain gastric organoids (10, 11, 33, 52, 53), and variations in media composition were shown to affect organoid morphology, differentiation and growth. Future studies will evaluate whether altering culture conditions or adding drugs to affect gastric secretion, e.g. omeprazole, cimetidine or naproxen, may prevent dynamic events such as ruptures that may be undesirable for certain experimental applications.

Overall, our study revealed several interesting features of 3-D gastric spheroids, including spontaneous ruptures, fusions and rotation events. Interestingly, human gastric epithelial spheroid lines derived from different human donors and spheroids analyzed after a different number of passages showed marked, sometimes significant, differences in many of the parameters analyzed. Consequently, for future studies using human spheroids, gastroids and other organoid culture systems, a general consensus within the

scientific community on quality control parameters of organoids would be beneficial, so that data obtained in different laboratories with different cell lines can be compared.

ACKNOWLEDGEMENTS

Funding for our study was provided by the National Institutes of Health grants K01 DK097144 (DB); R03 DK107960 (DB), the National Science Foundation, DMR-1455247 (JW), and the Montana University System Research Initiative 51040-MUSRI2015-03 (DB). We greatly appreciate support from the National Institutes of Health IDeA Program grant GM110732, an equipment grant from the M.J. Murdock Charitable Trust, and the Montana State University Agricultural Experimental Station for the Flow Cytometry Core Facility at Montana State University. Funding for shared facilities used in this work was also provided by the NSF under award number CBET-1039785. GeneSearch, Inc. development of the GeneSearch Embryo Cradle was funded by an SBIR grant from ORIP/NIH 5R44OD012083 (PJT). We would also like to thank Dr. K. Sasse (Sasse Surgical Associates, Reno, NV) for collecting human gastric tissue samples, Dr. T. Stappenbeck (Washington University, St. Louis) for sharing the L-WRN cell line with us, and Dr. Seth Walk for helpful discussions.

Table 2.1

Organoid lines and donor characteristics used in this study.

Organoid line	Tissue	Donor (age/sex)	Pathology	Experiments
hu001	Gastric body	45/F	polypoid fundic nodules	Imaging, FACS
hu002	Gastric body	49/F	moderate gastritis	Imaging, FACS
hu003	Gastric body	45/F	mild gastritis	FACS
hu004	Gastric body	52/F	mild chronic inflammation	Imaging, FACS
hu005	Gastric body	38/F	no alterations observed	FACS
hu006	Gastric antrum	42/F	not available	Imaging, FACS
hu007	Gastric body	26/F	not available	FACS
hu008	Gastric body	35/F	no alterations observed	Imaging, FACS
hu009	Gastric body	31/F	no alterations observed	FACS
hu010	Gastric body	43/F	mild gastritis	FACS
hu011	Gastric body	52/M	no alterations observed	qRT-PCR
hu013	Gastric body	57/M	not available	qRT-PCR
hu014	Gastric body	57/M	no alterations observed	qRT-PCR

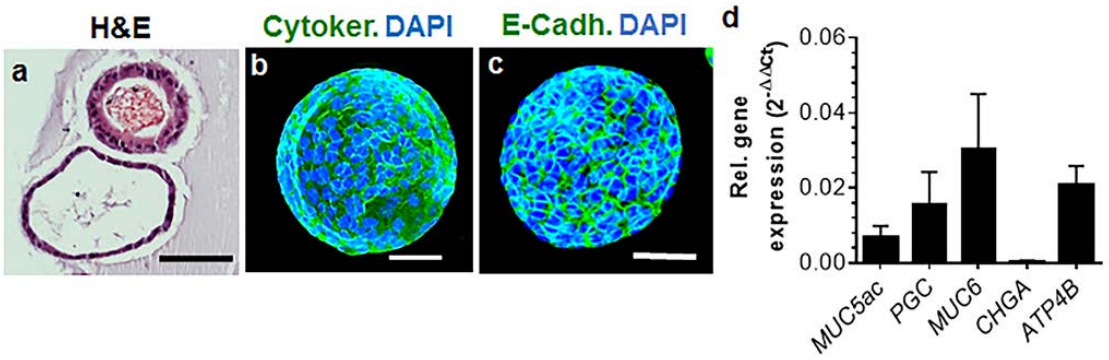

Figure 2.1. Microscopic analysis and gene expression analysis of human gastric epithelial spheroids. (a) Spheroids were fixed, paraffin-embedded, and sections stained with hematoxylin-eosin. Bar = 50 µm. (b,c) E-Cadherin (FITC) and cytokeratin (FITC) whole-mount immunofluorescence staining of human gastric spheroids; nuclei were labelled with DAPI. Bar = 50 µm. (d) Quantitative RT-PCR analysis of gastric spheroids (n=3; hu011, hu013 and hu014). Samples were analyzed for expression of *MUC5A* (mucous neck cells), *PGC* (pepsinogen C; chief cells), *MUC6* (surface mucus cells), *CHGA* (chromogranin A, enteroendocrine cells) and *ATP4B* (Potassium-transporting ATPase subunit beta, parietal cells). Data were analyzed by the $2^{-\Delta\Delta CT}$ method, with *GAPDH* used as a housekeeping gene and cDNA from human gastric biopsies (geometric mean of n=3) used for normalization.

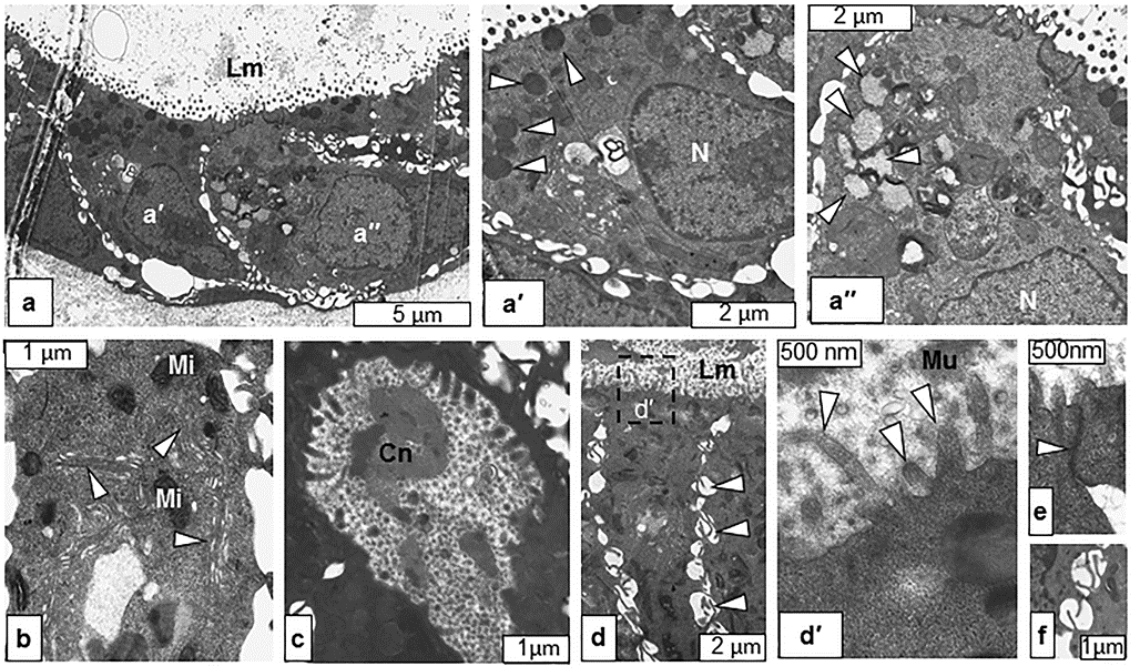

Figure 2.2. Transmission electron microscopy of human gastric epithelial spheroids. (a) Cross-section of a gastric spheroid shows a simple cuboidal to columnar microvillated epithelium with vacuolated secretory cells and basal nuclei. Lm, lumen; bar, 5 µm. (a′) Epithelial cell from (a) with large, electron-dense vacuoles (arrowheads). N, nucleus; bar, 2 µm. (a″) Epithelial cell from (a) with large, electron-lucent vacuoles (arrowheads). N, nucleus; bar, 2 µm. (b) Epithelial cell with copious amounts of rough endoplasmic reticulum (arrowheads) and multiple large mitochondria (Mi). Bar, 1 µm. (c) Large microvillated intracellular canaliculus (Cn) in a gastric epithelial cell. Bar, 1 µm. (d) Columnar epithelial cells with luminal microvilli and lateral interdigitating intercellular leaflets (arrowheads). Bar, 2 µm. (d′) Enlarged image from (d, dashed box) shows luminal microvilli (arrowheads) and mucus (Mu); bar 500 nm. (e) Luminal-junctional complex (arrowhead) between two epithelial cells; bar, 500 nm. (f) Lateral interdigitating intercellular leaflets, bar 1 µm.

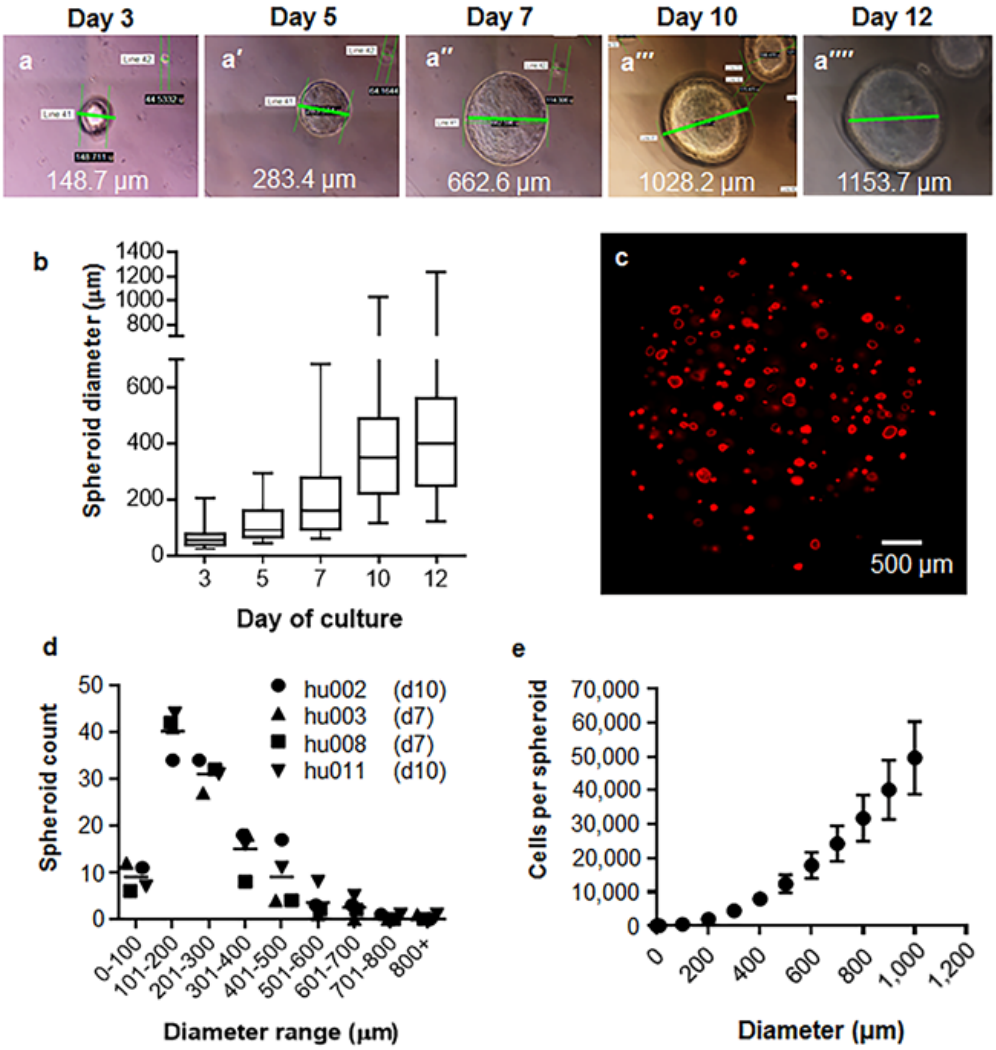

Figure 2.3. Gastric epithelial spheroid growth. (a - a′′′′) Representative phase contrast images of one gastric epithelial spheroid imaged repeatedly between day 3 and 12 after plating (line hu001, p17). (b) Diameters of 65 randomly selected spheroids in one representative well (line hu001, p17) were measured repeatedly on days 3, 5, 7, 10 and 12 after plating. Box delineates 1st and 3rd quartile and median, whiskers show minimum and maximum size. (c) Composite image of a representative culture well containing mCherry-expressing human gastric spheroids. Bar = 500 µm. (d) Size distribution of gastric epithelial spheroids in one representative well each from 4 different lines, imaged on day 7 or 10 after seeding (see label). Graph shows mean (line) and individual values for the 4 spheroid lines. (e) Relationship between spheroid diameter and cell count was determined by measuring all spheroids within one well followed by disruption of the spheroids using trypsin-EDTA and hemocytometer cell counting. Averages ± SEM calculated from 3 independent cultures are shown.

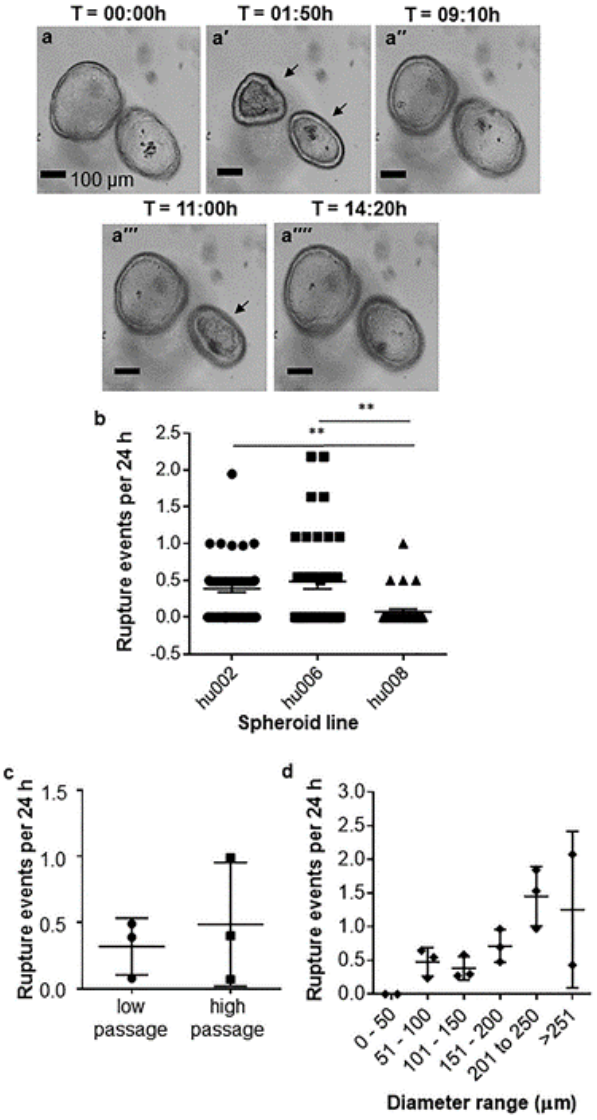

Figure 2.4. Spontaneous spheroid rupture and healing. (a - a‴) Representative image series from a 22 h time course experiment shows epithelial spheroid expansion and rupture (indicated by arrows), followed by re-forming and continued expansion over time. Phase contrast images, bar = 100 µm. (b) Frequency of rupture events in 3 different gastric epithelial spheroid lines analyzed at passage ≤10. Graph shows average number of rupture events per 24 h period for individual spheroids (n=33-59) and mean ± SD of each line. ** indicates statistically significant difference at $P \leq 0.01$. (c) Average rupture frequency per 24 h in low passage number cultures (p≤ 10; hu002, n=59; hu006, n=38; hu008, n=33) and high passage number cultures (p >11, hu001, n=9; hu004, n=9; hu006, n=45); individual values, mean ± SD; n.s. – not significant. (d) Relationship between rupture frequency and size. Spheroid lines hu001 (n=33 spheroids), hu002 (n=53) and hu006 (n=31) were analyzed.

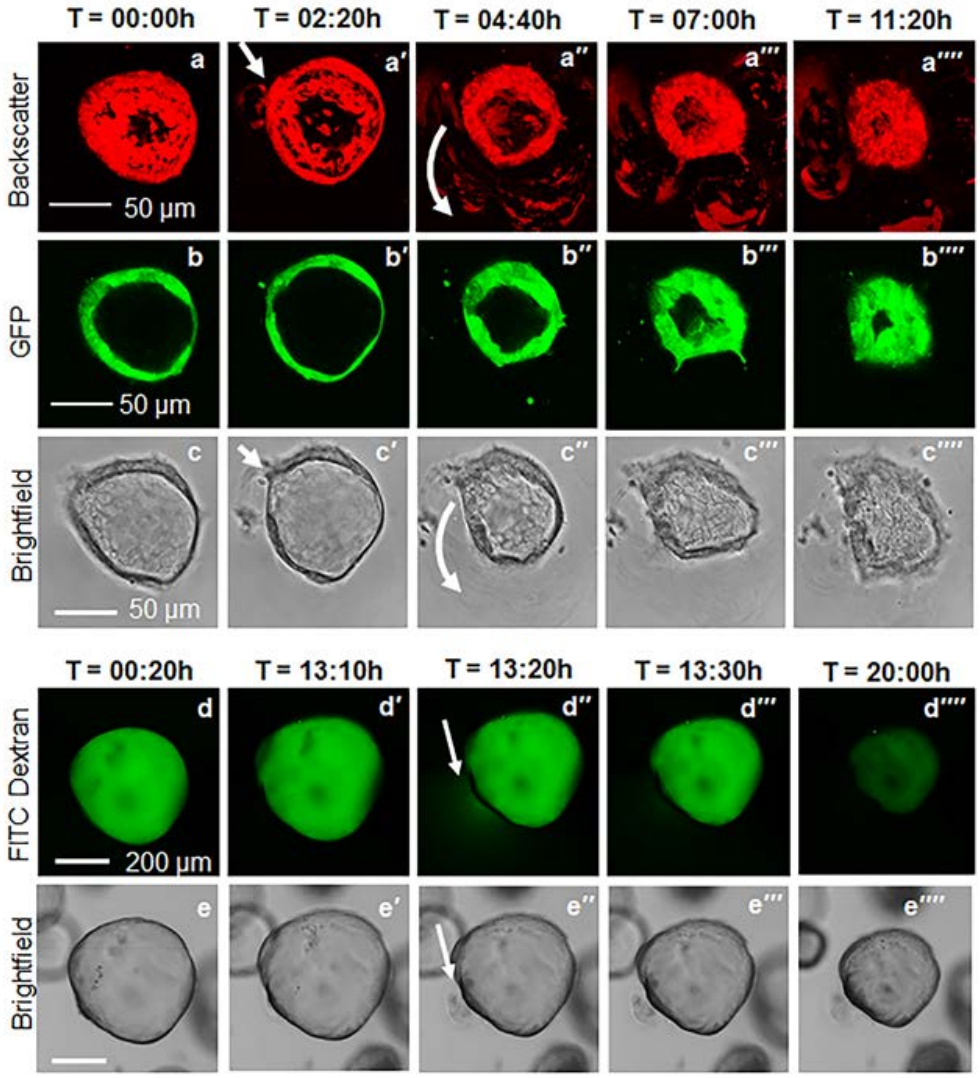

Figure 2.5. Release of luminal contents from ruptured gastric epithelial spheroids. (a - c‴′) Confocal and backscatter light image series from a 14 h time course analysis shows rupture, release of optically dense material (a - a‴′) from the inside of the GFP-expressing spheroid (b - b‴′), and thickening of the epithelial layer upon healing. (c - c‴′) Brightfield images. Bar = 50 µm. (d - e‴′) Release of injected 4 kDa FITC-Dextran (d - d‴′) from an mCherry-expressing gastric spheroid (e - e‴′) upon rupture. Images show disappearance of green FITC-Dextran signal after rupture at 13:20 h. Bar = 200 µm.

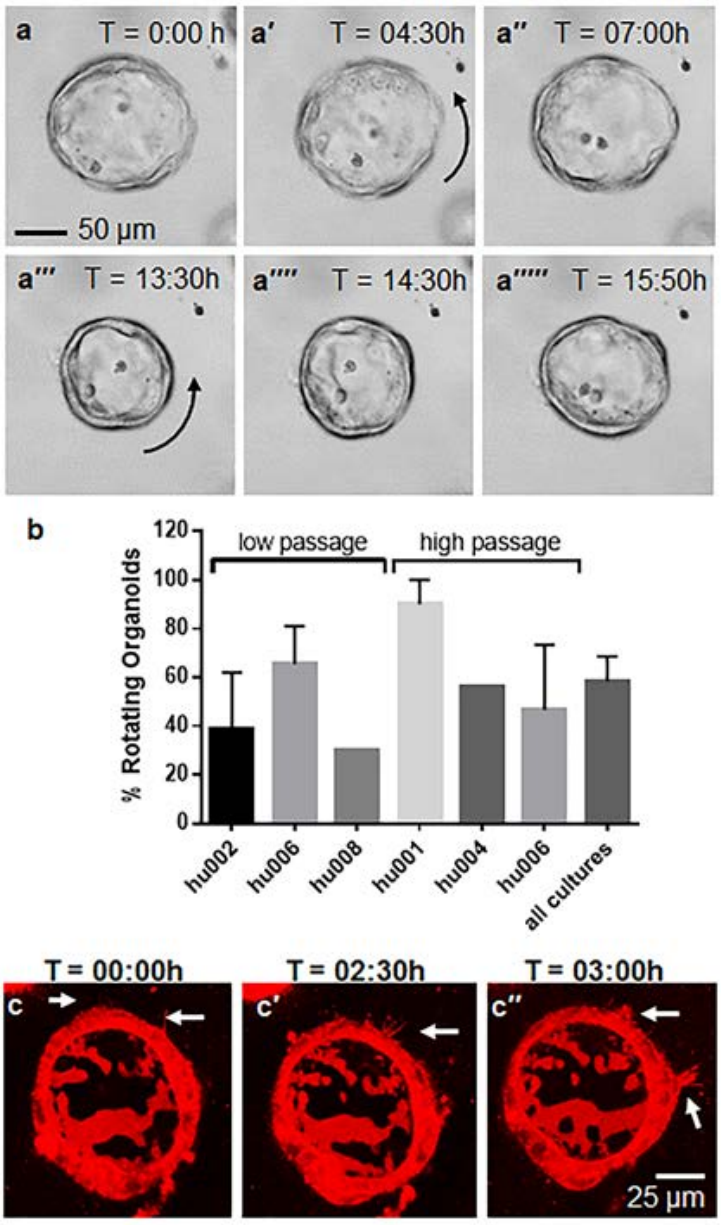

Figure 2.6. Gastric epithelial spheroids rotate within the Matrigel. Spheroids commonly rotate around their axis within the Matrigel matrix. (a - a⁗) Representative image series of a small single spheroid observed rotating counter-clockwise as indicated by the arrows over a time course of 16 h. (b) Percentage of low passage (hu002, p8-10, n=59; hu006, p7-10, n=38; hu008, p4, n=33) and high passage gastric spheroids (hu001, p44-45, n=9; hu004, p18, n=9; hu006, p11-16, n=45) observed for 46 ±1 h that showed rotation. Bars show mean ± SEM of individual cultures (n = 1 to 3 per line). The percentage of rotating epithelial spheroids did not differ significantly between individual lines. (c - c″) Backscatter light imaging reveals basolateral formation of pseudopod-like extensions. Arrows point out pseudopods. Bar = 25 µm.

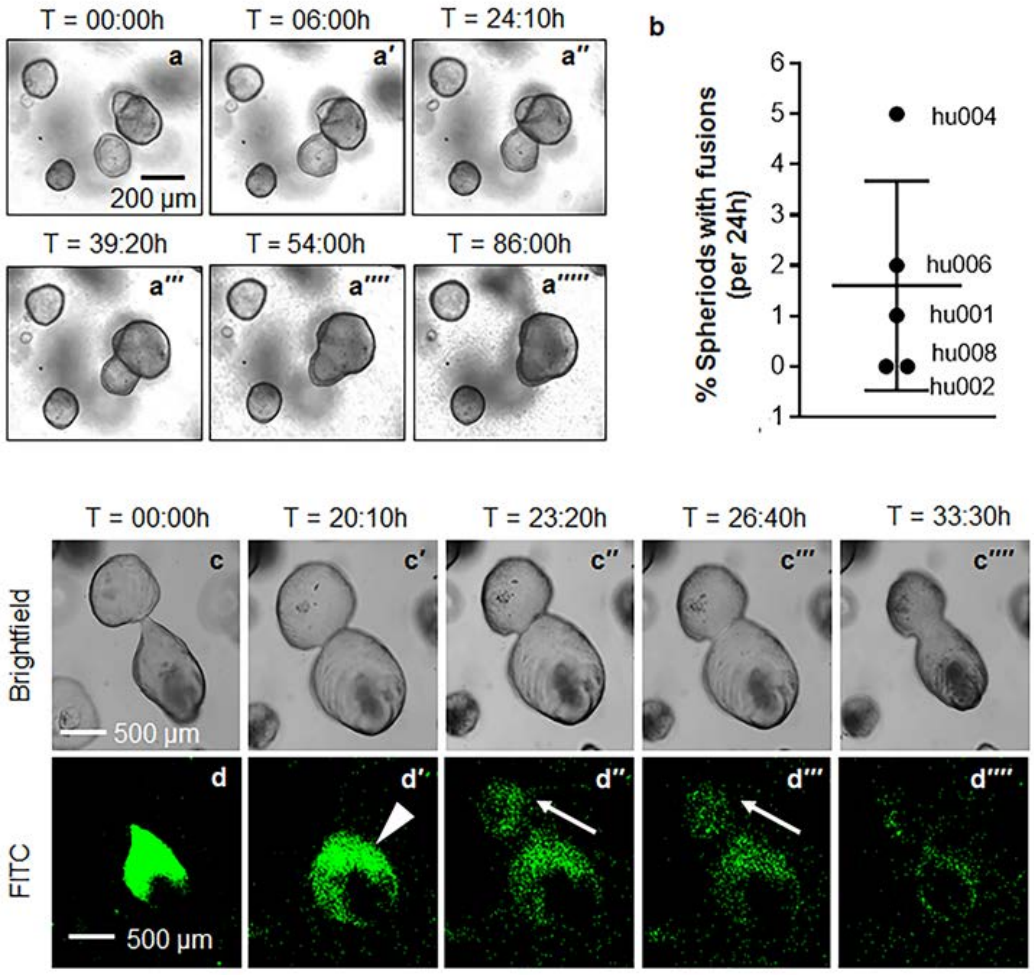

Figure 2.7. Gastric epithelial spheroid fusion events. (a - a⁗′) Phase contrast image series of two human gastric spheroids undergoing fusion. Spheroid line hu004. Scale bar = 200 µm. (b) Percentage of spheroids with observed fusion events in 5 different human gastric spheroid lines (hu001, p10, n=149; hu002, p8-10, n=59; hu004, p18, n=9; hu006, p7-16, n=83; and hu008, p4, n=33), normalized to a 24 h observation period. (c - d‴) 4 kDa FITC-Dextran injected into one gastric spheroid (arrowhead) is transferred to an adjacent spheroid upon membrane fusion (arrow). Brightfield (c - c⁗′) and green fluorescent images (d - d‴). Spheroid line hu006. Scale bar = 500 µm.

SUPPLEMENTAL INFORMATION

Supplemental table 1

Primer sequences and melting temperatures (Tm) for quantitative RT-PCR analysis of gastric spheroids and tissues.

Gene	5' Forward	5' Reverse	Tm	Reference
MUC5ac	**CTTCTCAACGTTTGACGGGAAGC**	CTTGATCACCACCACCGTCTG	56ºC	Bartfeld, *et al.* (33)
MUC6	GCCCCGGTATCTTCTCTCGG	ACACCTGCAGGGTGAGTACG	56ºC	Bartfeld, *et al.* (33)
PGC	AGAGCCAGGCCTGCACCAGT	GCCCCTGTGGCCTGCAGAAG	56ºC	Bartfeld, *et al.* (33)
ATP4B	ACCACGTAGAAGGCCACGTA	**TGGAGGAGTTCCAGCGTTAC**	56ºC	McCracken, *et al.* (52)
CHGA	TGACCTCAACGATGCATTTC	CTGTCCTGGCTCTTCTGCTC	57ºC	McCracken, *et al.* (52)
GAPDH	**GGTATCGTGGAAGGACTCATGAC**	**ATGCCAGTGAGCTTCCCGTTCAG**	56ºC	Bartfeld, *et al.* (33)

Supplemental movie 1:

Spontaneous rupture and healing of gastric epithelial spheroids. Phase contrast live imaging over 22 h.

Supplemental movie 2:

Rupture and release of luminal contents in an EGFP-expressing human gastric epithelial spheroid visualized by confocal and backscatter light imaging.

Supplemental movie 3:

Live imaging of a gastric epithelial spheroid microinjected with 4 kDa FITC dextran. At 13.20 h, the spheroid ruptures, and FITC-dextran is released into the Matrigel matrix surrounding the spheroid and slowly disappears from the lumen.

Supplemental movie 4:

Spontaneous rotation of gastric epithelial spheroids in Matrigel visualized by phase contrast live imaging. Note change in rotational direction of the spheroid.

Supplemental movie 5:

Gastric epithelial spheroids form temporary pseudopod-like extensions on the basolateral surface. Backscatter light imaging.

Supplemental movie 6:

Spheroid fusion event. One spheroid was injected with FITC-dextran (4 kDa) to visualize the lumen. Upon fusion of the two adjacent spheroids, FITC-dextran is transferred into to lumen of the second spheroid.

LITERATURE CITED

1. Dedhia PH, Bertaux-Skeirik N, Zavros Y, & Spence JR (2016) Organoid Models of Human Gastrointestinal Development and Disease. *Gastroenterology* 150(5):1098-1112.

2. Hynds RE & Giangreco A (2013) Concise review: the relevance of human stem cell-derived organoid models for epithelial translational medicine. *Stem Cells* 31(3):417-422.

3. Leushacke M & Barker N (2014) Ex vivo culture of the intestinal epithelium: strategies and applications. *Gut* 63(8):1345-1354.

4. Sato T, *et al.* (2009) Single Lgr5 stem cells build crypt-villus structures in vitro without a mesenchymal niche. *Nature* 459(7244):262-U147.

5. Ootani A, *et al.* (2009) Sustained in vitro intestinal epithelial culture within a Wnt-dependent stem cell niche. *Nature medicine* 15(6):701-706.

6. Sato T & Clevers H (2015) SnapShot: Growing organoids from stem cells. *Cell* 161(7):1700-1700 e1701.

7. Powell RH & Behnke MS (2017) WRN conditioned media is sufficient for in vitro propagation of intestinal organoids from large farm and small companion animals. *Biol Open* 6(5):698-705.

8. Dekkers JF, *et al.* (2013) A functional CFTR assay using primary cystic fibrosis intestinal organoids. *Nat Med* 19(7):939-945.

9. VanDussen KL, *et al.* (2015) Development of an enhanced human gastrointestinal epithelial culture system to facilitate patient-based assays. *Gut* 64(6):911-920.

10. Schumacher MA, *et al.* (2015) The use of murine-derived fundic organoids in studies of gastric physiology. *J Physiol* 593(8):1809-1827.

11. Schlaermann P, *et al.* (2016) A novel human gastric primary cell culture system for modelling Helicobacter pylori infection in vitro. *Gut* 65(2):202-213.

12. Mahe MM, *et al.* (2013) Establishment of gastrointestinal epithelial organoids. *Curr Protoc Mouse Biol* 3(4):217-240.

13. Schwank G, Andersson-Rolf A, Koo BK, Sasaki N, & Clevers H (2013) Generation of BAC transgenic epithelial organoids. *PloS one* 8(10):e76871.

14. Miyoshi H & Stappenbeck TS (2013) In vitro expansion and genetic modification of gastrointestinal stem cells in spheroid culture. *Nat Protoc* 8(12):2471-2482.

15. Riehl TE, Santhanam S, Foster L, Ciorba M, & Stenson WF (2015) CD44 and TLR4 mediate hyaluronic acid regulation of Lgr5+ stem cell proliferation, crypt fission, and intestinal growth in postnatal and adult mice. *Am J Physiol Gastrointest Liver Physiol* 309(11):G874-887.

16. Howitt MR, *et al.* (2016) Tuft cells, taste-chemosensory cells, orchestrate parasite type 2 immunity in the gut. *Science* 351(6279):1329-1333.

17. Bradford EM, *et al.* (2017) Epithelial TNF Receptor Signaling Promotes Mucosal Repair in Inflammatory Bowel Disease. *J Immunol* 199(5):1886-1897.

18. Demitrack ES, *et al.* (2017) NOTCH1 and NOTCH2 regulate epithelial cell proliferation in mouse and human gastric corpus. *Am J Physiol Gastrointest Liver Physiol* 312(2):G133-G144.

19. Gifford GB, *et al.* (2017) Notch1 and Notch2 receptors regulate mouse and human gastric antral epithelial cell homoeostasis. *Gut* 66(6):1001-1011.

20. den Hartog G, *et al.* (2016) Regulation of Rac1 and Reactive Oxygen Species Production in Response to Infection of Gastrointestinal Epithelia. *PLoS Pathog* 12(1):e1005382.

21. Miyoshi H, Ajima R, Luo CT, Yamaguchi TP, & Stappenbeck TS (2012) Wnt5a potentiates TGF-beta signaling to promote colonic crypt regeneration after tissue injury. *Science* 338(6103):108-113.

22. van de Wetering M, Oosterwegel M, Dooijes D, & Clevers H (1991) Identification and cloning of TCF-1, a T lymphocyte-specific transcription factor containing a sequence-specific HMG box. *EMBO J* 10(1):123-132.

23. Pechhold K, Pohl T, & Kabelitz D (1994) Rapid quantification of lymphocyte subsets in heterogeneous cell populations by flow cytometry. *Cytometry* 16(2):152-159.

24. Stewart SA, *et al.* (2003) Lentivirus-delivered stable gene silencing by RNAi in primary cells. *RNA* 9(4):493-501.

25. Sancak Y, *et al.* (2008) The Rag GTPases bind raptor and mediate amino acid signaling to mTORC1. *Science* 320(5882):1496-1501.

26. Brumfield SK, *et al.* (2009) Particle assembly and ultrastructural features associated with replication of the lytic archaeal virus sulfolobus turreted icosahedral virus. *J Virol* 83(12):5964-5970.

27. Zeitoun P & Lambling A (1967) Ultrastructure of the gastric mucosa in human hemochromatosis. *Scand J Gastroenterol* 2(3):222-234.

28. Corpron RE (1966) The ultrastructure of the gastric mucosa in normal and hypophysectomized rats. *Am J Anat* 118(1):53-90.

29. Rohrer GV, Scott JR, Joel W, & Wolf S (1965) The fine structure of human gastric parietal cells. *Am J Dig Dis* 10:13-21.

30. Necchi V, Manca R, Ricci V, & Solcia E (2009) Evidence for transepithelial dendritic cells in human H. pylori active gastritis. *Helicobacter.* 14(3):208-222.

31. Mollazade K, Omid M, Tab FA, & Mohtasebi SS (2012) Principles and applications of light backscattering imaging in quality evaluation of agro-food products: a review. *Food Bioprocess Tech* 5(5):1465-1485.

32. Stelzner M, *et al.* (2012) A nomenclature for intestinal in vitro cultures. *Am J Physiol Gastrointest Liver Physiol* 302(12):G1359-1363.

33. Bartfeld S, *et al.* (2015) In vitro expansion of human gastric epithelial stem cells and their responses to bacterial infection. *Gastroenterology* 148(1):126-136.

34. Engevik AC, *et al.* (2016) The development of spasmolytic polypeptide/TFF2-expressing metaplasia (SPEM) during gastric repair is absent in the aged stomach. *Cell Mol Gastroenterol Hepatol* 2(5):605-624.

35. Yui S, *et al.* (2012) Functional engraftment of colon epithelium expanded in vitro from a single adult Lgr5(+) stem cell. *Nature medicine* 18(4):618-623.

36. Smith JM, Johanesen PA, Wendt MK, Binion DG, & Dwinell MB (2005) CXCL12 activation of CXCR4 regulates mucosal host defense through stimulation of epithelial cell migration and promotion of intestinal barrier integrity. *American journal of physiology. Gastrointestinal and liver physiology* 288(2):G316-326.

37. Iizuka M & Konno S (2011) Wound healing of intestinal epithelial cells. *World J Gastroenterol* 17(17):2161-2171.

38. Silen W & Ito S (1985) Mechanisms for rapid re-epithelialization of the gastric mucosal surface. *Annu Rev Physiol* 47:217-229.

39. Miyoshi H (2017) Wnt-expressing cells in the intestines: guides for tissue remodeling. *J Biochem* 161(1):19-25.

40. Williams JM, *et al.* (2015) Epithelial cell shedding and barrier function: a matter of life and death at the small intestinal villus tip. *Vet Pathol* 52(3):445-455.

41. Heath JP (1996) Epithelial cell migration in the intestine. *Cell Biol Int* 20(2):139-146.

42. Creamer B, Shorter RG, & Bamforth J (1961) The turnover and shedding of epithelial cells. I. The turnover in the gastro-intestinal tract. *Gut* 2:110-118.

43. Karam SM, Li Q, & Gordon JI (1997) Gastric epithelial morphogenesis in normal and transgenic mice. *Am J Physiol* 272(5 Pt 1):G1209-1220.

44. Lipkin M (1965) Cell replication in the gastrointestinal tract of man. *Gastroenterology* 48:616-624.

45. McNiven MA (2013) Breaking away: matrix remodeling from the leading edge. *Trends Cell Biol* 23(1):16-21.

46. Burgess DR (1976) Structure of the epithelial - mesenchymal interface during early morphogenesis of the chick duodenum. *Tissue Cell* 8(1):147-158.

47. Bohorquez DV, Chandra R, Samsa LA, Vigna SR, & Liddle RA (2011) Characterization of basal pseudopod-like processes in ileal and colonic PYY cells. *J Mol Histol* 42(1):3-13.

48. Benton G, George J, Kleinman HK, & Arnaoutova IP (2009) Advancing science and technology via 3D culture on basement membrane matrix. *J Cell Physiol* 221(1):18-25.

49. Diamond JM & Tormey JM (1966) Role of long extracellular channels in fluid transport across epithelia. *Nature* 210(5038):817-820.

50. Larsen EH, Willumsen NJ, Mobjerg N, & Sorensen JN (2009) The lateral intercellular space as osmotic coupling compartment in isotonic transport. *Acta Physiol (Oxf)* 195(1):171-186.

51. Demitrack ES, *et al.* (2015) Notch signaling regulates gastric antral LGR5 stem cell function. *EMBO J* 34(20):2522-2536.

52. McCracken KW, *et al.* (2014) Modelling human development and disease in pluripotent stem-cell-derived gastric organoids. *Nature* 516(7531):400-+.

53. Bertaux-Skeirik N, *et al.* (2015) CD44 plays a functional role in Helicobacter pylori-induced epithelial cell proliferation. *PLoS Pathog* 11(2):e1004663.

CHAPTER 3

RUPTURING OF HUMAN GASTRIC ORGANOIDS

Contribution of Authors and Co-Authors

Manuscript in Chapter 3

Author: Barkan Sidar

Contributions: Conceptualized the experiments, developed methodology, performed experiments, analyzed the data, wrote the original manuscript.

Co-Author: Thomas A. Sebrell

Contributions: Developed methodology, performed experiments.

Co-Author: Bengisu Kilic

Contributions: Analyzed the data.

Co-Author: David Brown

Contributions: Analyzed the data.

Co-Author: Mert Aytac

Contributions: Analyzed the data.

Co-Author: Brian A. Perrino

Contributions: Funding acquisition, provided resources.

Co-Author: Linda C. Samuelson

Contributions: Funding acquisition, provided resources.

Co-Author: Henry Fu

Contributions: Analyzed the data, funding acquisition, provided resources.

Co-Author: Diane Bimzcok

Contributions: Conceptualized the and supervised the experiments, developed methodology, funding acquisition, provided resources.

Co-Author: James N. Wilking

Contributions: Conceptualized the and supervised the experiments, developed methodology, wrote the original manuscript, funding acquisition, provided resources.

Manuscript Information

Barkan Sidar, T. Andrew Sebrell, Bengisu Kilic, David Brown, Mert Aytac, Brian A. Perrino, Linda C. Samuelson, Henry Fu, Diane Bimzcok, James N. Wilking

Status of Manuscript:
__X__ Prepared for submission to a peer-reviewed journal
____ Officially submitted to a peer-reviewed journal
____ Accepted by a peer-reviewed journal
____ Published in a peer-reviewed journal

ABSTRACT

Human organoids are three-dimensional, millimeter-scale tissue cultures that recapitulate much of the structure and function of naturally-formed human organs. Organoids contain the critical cell types and some of the spatial organization representative of specific organs; thus, they are widely used for biological research and drug testing. Human gastrointestinal (gut) organoids (HGOs) are comprised of an epithelial sheet wrapped into a closed, spherical shell rather than an open-ended tube like the human gastrointestinal tract. This closed spherical structure allows gut organoids to be used as containers for host-microbe studies, where microbes or other contents are injected into the enclosed lumen; however, this structure also limits material transport. Consequently, HGOs undergo extraordinary periodic rupture events during which luminal contents are ejected. Here, we report that human gastric organoids undergoing intermittent rupture are slightly pressurized due to an osmotic pressure difference across the epithelial shell. However, the probability of rupture is not strongly dependent on pressure; instead, rupture occurs when cells are expelled from the shell. Various osmotic stress conditions showed that moderate osmotic perturbations ($\leq$ 50 mOsm) caused HGOs to shrink and swell proportionally rather quickly due to the diffusion of water. In contrast with the osmotic perturbations applied, organoids swell in their growth media over hours and even days. Thus, the rupture events are an indirect result of osmotic swelling carried out by the diffusion of water due to osmolyte concentration regulation by the epithelial shell, consistent with the suppressed rupture events through drug treatment that inhibits proton pumps. Overall, we show that a simple pressure balance provides a framework for understanding rupture events and for mitigating these events in future experiments.

INTRODUCTION

Human organoids are three-dimensional, millimeter-scale tissue cultures that recapitulate much of the structure and function of naturally-formed human organs like the stomach (1, 2), kidney (3-5), and brain (6). These tissues are distinct from more traditional engineered tissue constructs in that they self-assemble from stem cells, which differentiate when exposed to key growth factors at specific periods during cell growth and development (7-10). Organoids contain the critical cell types and some of the spatial organization representative of particular organs; thus, they are widely used for biological research and drug testing (7, 11-14). For example, gastrointestinal organoids are used for studying host-gut microorganism interactions (15-19), liver organoids are used for the treatment of acute liver failure (20), lung organoids are used studying parasite infections (21), and breast cancer organoids are used for drug screening (22).

Organoids form under *in vitro* conditions that do not adequately reproduce the local environmental conditions in a developing embryo (23). This can result in structural differences that impact organoid behavior and transport and the interpretation of biological studies involving organoids (12, 24). For example, gastrointestinal (gut) organoids are comprised of an epithelial sheet wrapped into a closed, spherical shell rather than an open-ended tube like the human gastrointestinal tract (10, 25). Gut organoids are routinely used as containers for host-microbe studies, where microbes or other contents are injected into the enclosed lumen (15, 26-29), but they undergo striking periodic rupture events during which luminal contents are ejected (25). Our group and others have reported this behavior, but it is not clear what drives these rupture events, or

how these rupture events impact the outcome of organoid experiments. This lack of knowledge hinders experiments and prevents organoids from being used to their full potential.

Here, we report that human gastric organoids undergoing intermittent rupture are slightly pressurized due to an osmotic pressure difference across the epithelial shell. However, the probability of rupture is not strongly dependent on pressure; instead, rupture occurs when cells are expelled from the shell. Various osmotic stress conditions showed that moderate osmotic perturbations ($\leq$ 50 mOsm) caused HGOs to shrink and swell proportionally rather quickly due to the diffusion of water. In contrast with the osmotic perturbations applied, organoids swell in their growth media over hours and even days. Thus, the rupture events are an indirect result of osmotic swelling carried out by the diffusion of water due to osmolyte concentration regulation by the epithelial shell. This is consistent with the suppressed rupture events through drug treatment that inhibits proton pumps. Overall, we show that a simple pressure balance provides a framework for understanding rupture events and for mitigating these events in future experiments.

Background

Gastrointestinal organoids representing the human stomach, small intestine, and colon share the same overall structure: a spherical tissue shell with an inner surface that represents the inner lining of the gut (**Fig. 1a)**. The shell is comprised of a single layer of epithelial cells (**Fig. 1b**) that differentiate into the cells representative of a particular region of the gastrointestinal tract. For example, the epithelium in a mature gastric (stomach) organoid containing parietal cells that excrete gastric acid, foveolar cells that

excrete mucus, and other secretory cells including chief cells and enteroendocrine cells (30). The cells comprising the shell are polarized, with an apical side that faces inward toward the lumen and a basolateral side that faces outward toward what would be the basement membrane (10, 31). Materials such as mucus, acid, and signaling molecules are excreted into the inner space of the organoid, creating an environment that represents the luminal space of the gut (32).

The epithelial shell forms a closed surface, so the movement of material into or out of the organoid is governed by epithelium permeability. The epithelium is composed of individual cells that are bound together by tight junctions, and transport can occur either between cells or through cells. Though regulation of epithelial permeability remains poorly understood (33), most water (34) and nutrients are transported through transcellular pathways (35). Molecules must pass through two lipid membranes, to move from one side of the epithelial shell to the other. Transport across these lipid membranes is mediated by protein channels and carriers (36). Water transport, for example, is mainly allowed by membrane proteins known as aquaporins (34, 37, 38), which permit the free passage of water. Additionally, tight junction proteins called claudins carry out a small amount of water transportation (39). By contrast, ions and nutrients are transported actively though tight junctions that allow small molecule and ion diffusion (40). Thus, the epithelium is a semi-permeable barrier: permeable to water, selectively permeable to ions and molecules, and impermeable to colloidal-scale objects.

RESULTS AND DISCUSSION

To investigate HGO swelling and rupture dynamics, we monitor individual organoids continuously over several days with time-lapse confocal microscopy. We observe that HGOs increase in size, as depicted by the series of microscopy images in **Fig. 2a**. This increase in size is primarily due to an increase in luminal volume (swelling) rather than growth of the epithelial monolayer. This indicates that water is moving across the epithelial shell, from the outside of the organoid to the inside. In seemingly random intervals, the organoid shell undergoes striking rupture, expelling internal contents into the area surrounding the organoid (**Fig. 3a,b**). As luminal contents are expelled, the organoid collapses. This is followed by healing, after which the HGOs swell and the cycle is repeated (**Fig. 2a**).

The expulsion of luminal contents and contraction of the epithelial shell indicates that the inner contents are under pressure and the epithelial shell is under tension. To investigate rupture dynamics, we image multiple organoids to capture a rupture event occurring within the image plane. Results reveal that the hole formed during rupture is circular and grows with time; high-speed imaging of thin liquid films undergoing rupture reveals similar behavior, and this is a clear indication that the shell is under tension (**Fig. 2b**). While thin film rupture occurs in milliseconds, organoid shell rupture occurs over tens of minutes. This is because the shell is viscoelastic and adhered to the surrounding viscoelastic hydrogel. Thus, the timescale of shell rupture and collapse is set by the timescale of viscoelastic relaxation. Imaging also reveals that as the organoid swells (**Fig. 2c**), the epithelial shell thins (**Fig. 2d**), and as the organoid contracts, the shell thickens

rapidly and dramatically. Together, these observations support the hypothesis that the organoid lumen is under pressure.

To determine the source of pressure inside an HGO, we consider the properties of the organoid shell. Epithelial tissue sheets are semi-permeable: freely permeable to water, selectively permeable to ions and small molecules, and impermeable to large molecules and colloids. Aquaporin channels, which allow for water transport are passive, so any controlled flow of water from one side of the shell to the other must be driven by a pressure or concentration gradient. Given the semipermeable nature of the shell, we posit that the source of the pressure is osmotic, arising from a higher concentration of dissolved osmolyte inside the organoid than outside, with $\Delta c = c_{\mathrm{in}} - c_{\mathrm{out}}$ where c_{in} is the intraluminal osmolyte concentration and c_{out} is the extraluminal media concentration. This condition will create an osmotic pressure difference $\Delta\Pi = RT(\Delta c)$, where R is the gas constant, and T is the temperature. At equilibrium, $\Delta\Pi$ must be counterbalanced by an opposing pressure, provided by the elasticity of the epithelial shell. For a spherical, elastic shell of radius a, the pressure difference across the shell is $\Delta P = 2\sigma/a$, where σ is the elastic tension of the shell. Balancing these two pressures provides $2\sigma/a = RT(\Delta c)$. This condition is analogous to an inflated balloon, where the elasticity of the balloon counterbalances the difference in air pressure between the inside and outside of the balloon.

Provided this pressure balance captures the basic physics of HGOs at equilibrium, HGOs should respond to abrupt changes in external osmolality by shrinking or swelling. Rapidly increasing the osmolality of the external media should cause the organoids to

shrink, and rapidly decreasing the osmolality of the external media should cause the organoids to swell. To test this, we systematically vary the osmolality of the external media in increments of 50 mOsm over the range: 150 mOsm – 450 mOsm, corresponding to ±150 mOsm above and below the osmolality of the growth media (≈ 300 mOsm) and monitor HGO response using confocal time-lapse microscopy. External osmolality is increased by the addition of dissolved mannitol and decreased by dilution of the growth media (see Methods). Cursory observations of HGO dynamics before and after osmotic shocking reveal that HGOs undergo dramatic changes in size (see Supplementary Videos 1 and 2).

To quantify changes in HGO size, we perform image analysis on multiple HGOs ($15 \leq n \leq 30$ for each condition) throughout the osmotic shock experiments. The initial volume normalizes the volume V of each HGO, V_0 at the time of osmotic shock ($t = 0$), and the average, normalized volume for each osmolality condition plotted as a function of time. When the external osmolality is decreased, HGOs swell rapidly and approach a saturation value. Moreover, a more significant reduction in osmolality results in increased swelling (**Fig. 4a**). This is consistent with our hypothesis; that is, an HGO initially at equilibrium ($\Delta\Pi_{e,0} = \Delta P$), responds to a drop in the external osmolality by swelling until equilibrium is again met ($\Delta\Pi_{e,t} = \Delta P$). For all dilutions, HGOs reach a plateau value within $t \leq 30$ minutes. Conversely, when the external osmolality is increased, HGOs shrink rapidly, and higher external osmolality results in more shrinking (**Fig. 4b**). This again is consistent with our hypothesis; however, in contrast to HGO swelling, HGO shrinking occurs more slowly, and only the lowest concentration approaches an

equilibrium value over the time scale of our experiments. HGOs subjected to higher concentrations continue to decrease in size beyond $t > 30$ minutes. For both cases, HGO size changes are consistent with liquid flow across a semipermeable membrane driven by an osmotic concentration gradient.

According to our hypothesis, volume changes in response to osmotic perturbation are mediated by the elasticity of the epithelial shell, the extent to which is determined by the magnitude of the elasticity. In the limit where the shell is weak, such that $\Delta\Pi_{e,0} \to 0$, HGO dynamics should just be described by the dilution equation: $c_0 V_0 = c_f V_f$, where c_0, c_f, V_0, and V_f are the initial and final external osmolality, and initial and final HGO volume, respectively, which can be rearranged to the following form: $r_f/r_0 = \left(c_0/c_f\right)^{1/3}$, where r_0, and r_f are the initial and final HGO radii, respectively. This condition provides the low-elasticity limit with which to compare our experimental results. In plotting our data, choice of r_f is straightforward for swelling experiments which reach a plateau; however, for shrinking experiments, all but the lowest osmolality continue to change throughout the experiments, so the choice of r_f is not clear. Thus, we select r_f in increments of Δt = 10 min over the range: 30 min ≤ t ≤ 100 min and plot r_f/r_0 as a function of c_0/c_f in a log-log format for these different time points. Strikingly, we find that for the two osmolyte perturbations closest to physiological (± 50 mOsm), the data falls directly on the dilution equation prediction (**Fig. 5**). This suggests that, at equilibrium, the osmotic pressure difference across the membrane is very low.

Osmotic perturbations further than ± 50 mOsM from physiological osmolality deviate from the dilution equation prediction. For example, HGOs subjected to $c_f \geq 350$

mOsM (corresponding to $c_0/c_f < 0.8$) shrink more than the dilution equation predicts so that r_f/r_0 drops beneath the prediction in **Fig. 5**. No signs of cell death are observed, even over long times after the addition of mannitol ($\Delta t \approx 12$ h; Supplemental Video 3). Instead, we observe cells being expelled from the epithelial shell into the lumen of the HGO. It is known that epithelial sheets can respond to compression by expelling cells and this is consistent with our experimental results. Thus, our initial assumption that mass is conserved within the shell is not valid for HGOs subjected to $c_f \geq 350$ mOsm and should not be expected to follow the dilution equation. HGOs subjected to $c_f \leq 250$ mOsm (corresponding to $c_0/c_f > 1.2$) also deviate from the prediction in that they do not swell as much as the dilution equation would predict, and the deviation increases with decreasing c_f. We hypothesize that this behavior arises due to the elasticity of the shell; that is, as the HGO swells, the epithelium becomes sufficiently deformed (i.e. stretched) that the elasticity of the shell is no longer negligible. Thus, to describe the mechanical response of the epithelial shell a model incorporating strain-dependent shell elasticity is needed.

While it is not clear what triggers epithelial rupture, the presence of an equilibrium osmotic pressure difference across the epithelium counterbalanced by epithelium elasticity suggests that reduced osmotic pressure should result in reduced rupture frequency. To test this hypothesis, we subjected HGO treated with the histamine antagonist cimetidine, which is known to result in reduced secretion of acid into the lumen (41). The analysis of drug-treated and control HGOs time-lapse images ($\Delta t \approx 50$ h) showed that treated HGOs rupture ~40% less compared to the control group which had

roughly 0.3 rupture events per day (**Fig. 6**), consistent with our osmotic pressure hypothesis.

CONCLUSIONS

In conclusion, human gastric organoids undergo periodic rupture events during which luminal contents are ejected. We presented a simple pressure balance to provide a framework for understanding rupture events. Various osmotic stress conditions showed that moderate osmotic perturbations (≤ 50 mOsm) caused HGOs to shrink and swell proportionally rather quickly due to the diffusion of water. Even though the shell elasticity was negligible at smaller perturbations, at very dilute media concentrations, osmotic swelling caused strain-dependent shell elasticity to become a significant factor in the structural integrity of the organoid. In contrast with the osmotic perturbations applied, organoids swell in their growth media over hours and even days. Thus, the rupture events are an indirect result of osmotic swelling carried out by the diffusion of water due to osmolyte concentration regulation by the epithelial shell, consistent with the suppressed rupture events through drug treatment that inhibits proton pumps.

MATERIALS AND METHODS

Organoid Culture

Sleeve gastrectomy surgeries were obtained with Institutional Review Board (IRB) approval by the National Disease Research Interchange (NDRI; Philadelphia, PA) or by Dr. Kent Sasse (Sasse Surgical Associates, Reno, NV). Upon dissection of the

gastric mucosa off muscle layer, the mucosa was cut into <1mm pieces and were placed into RPMI-1640 medium supplemented with 0.5 U/mL collagenase type IV, 0.2 mg/mL DNAse (Sigma-Aldrich, St. Louis, MO), 0.3% BSA, 250 µg/mL amphotericin B (Fisher Scientific, Fair Lawn, NJ), 100 U/mL penicillin/streptomycin, 2 mM L-glutamine, 1 mM HEPES (GE Healthcare Life Sciences, Logan UT) and 50 µg/mL Gentamycin (IBI Scientific, Peosta, IL). Later, the tissue was incubated at 200 rpm in a 37ºC water bath for 1 h. To release glands from the tissue, the tube was vortexed for 30 s. To establish HGO cultures, the glands, and remaining tissue pieces were centrifuged at 200 x g, 4ºC for 5 min. The pellet was resuspended in 30 mL ice-cold DPBS (Hyclone GE Healthcare Life Sciences, Logan UT) and vortexed again for 30 s. Tissue pieces settled to the bottom of the tube, and gastric glands in the supernatant were transferred to a new 50 mL tube, pelleted and transferred to Matrigel (Corning, Bedford, MA). Glands suspended in Matrigel were pipetted into a pre-warmed 24-well plate. HGO cultures were maintained following the protocol of Miyoshi and Stappenbeck (42), with minor modifications as described by Gifford et al. (43). After polymerization, Matrigel was overlaid with 500 µL of L-WRN medium composed of Advanced DMEM/F12 (Gibco by Life Technologies, Grand Island, NY) supplemented with 10mM HEPES, 1% Pen/Strep, 50% L-WRN conditioned medium, 10 µM Rock-inhibitor Y-27632 (Tocris Biosciences, Bristol, UK), Amphotericin B, Gentamycin, L-Glutamine, 10 µM TGF-β inhibitor SB-431542 (Tocris), 10% FBS (Rocky Mountain Bio, Missoula, MT) and 50 % of cell culture supernatant from L-WRN cells, which constitutively secrete murine Wnt3a, noggin and R-spondin 3. Formed HGOs were maintained in a 37ºC, 5% CO2 incubator, with fresh medium added

every 2 – 3 days, and were passaged by trypsinization and re-plating at 1 : 4 every 5 - 7 days.

Imaging and Image Analysis

Imaging was performed using a Leica SP5 confocal scanning laser microscope equipped with LiveCell StageTop Incubator from Pathology Devices capable of maintaining physiological conditions. Brightfield, fluorescence and backscattered light images were collected at regular intervals (Δt = 10 min) throughout 10 h to 100 h. High and low-resolution images were obtained with a 63x water immersion and 10x air objective, respectively. Images were then processed to follow organoid dynamics with respect to time by using integrated morphometry analysis module within MetaMorph image analysis software. Through the module, mean radii measurements collected by using a threshold method for each organoid and calculated volume assuming perfect spherical geometry. Automated the process for each time plane to obtain approximately 1000 organoids providing statistically relevant data. In addition to the automated process, manual measurements and optimizations performed to collect accurate information primarily for the noisy brightfield images where the threshold method was incompatible. Time-lapse videos compiled through IMARIS software for qualitative observations along with image analysis.

Osmotic Shock Experiments

To manipulate the osmolality difference across the epithelial shell, the osmolyte must be impermeable to the epithelial sheet and should not affect the metabolism of the

tissue; hence an osmotic pressure difference can be maintained throughout the experiment. Two candidates for this purpose exist, which are commonly used in similar applications: polyethylene glycol (PEG) and mannitol (40, 44, 45). PEG and mannitol were dissolved in media, and a series of dilutions were prepared to obtain incremental concentrations of the polymer solutions. Organoids that were grown in a 96-well-plate were placed under the microscope in an environmental chamber to provide the natural growth conditions of the organoids. After several hours, the stock media replaced with the media consisting known concentration of polymer. The resulting shrinking effect on organoids was due to the osmotic stress was measured throughout the quantitative imaging analysis tools stated previously. Also, the expected rupture frequency and growth rate decreased with respect to control samples were analyzed by comparing with the model.

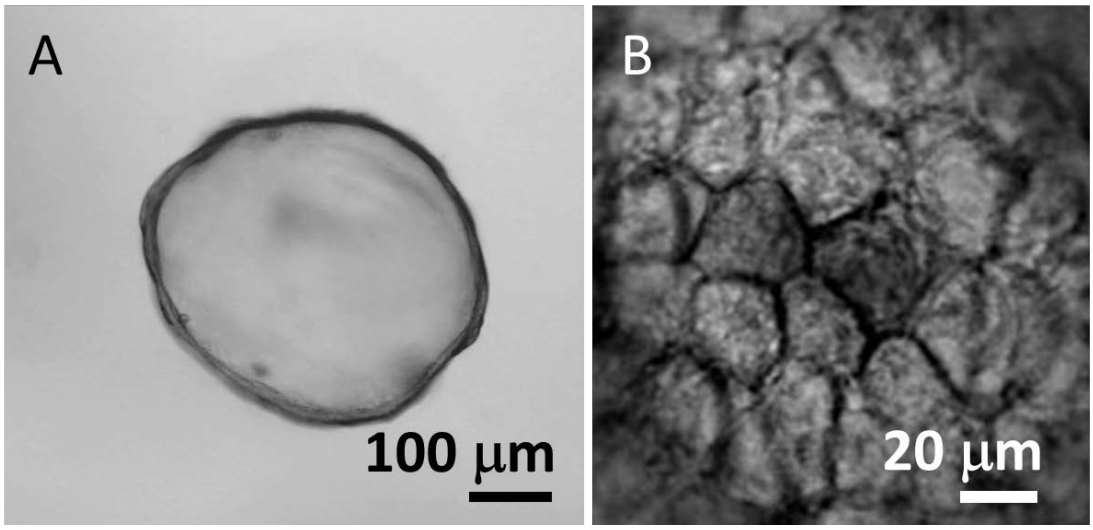

Fig. 3.1. General structure of gastrointestinal organoids. (**A**) Light microscopy image of spherical human gastric organoid (HGO) embedded in the hydrogel and composed of a single cell layer thick of epithelium enclosing an inner luminal space. (**B**) Magnified light microscopy image of the epithelial sheet reveals individual cells bound together by tight junctions.

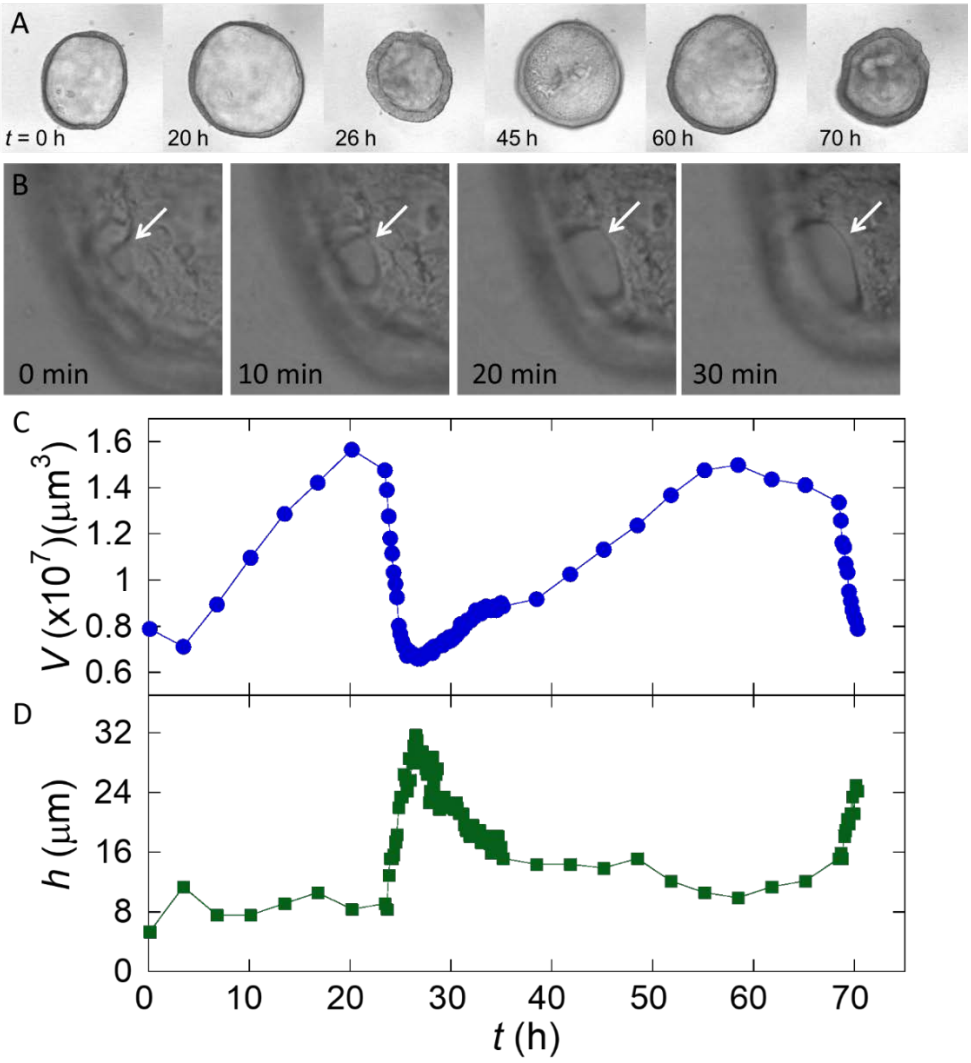

Fig. 3.2. Rupturing of gastric organoids. (**A**) Series of time-lapse microscopy images reveal organoid swelling followed by rupturing, healing, swelling and rupturing. (**B**) Series of high magnification time-lapse microscopy images of a rupture point reveal the rupture site to be a round hole that grows with time. (**C, D**) Volume (C) and shell thickness (D) for the organoid in (A) plotted as a function of time. Rupturing results in a dramatic reduction in organoid volume and thickening of the organoid shell.

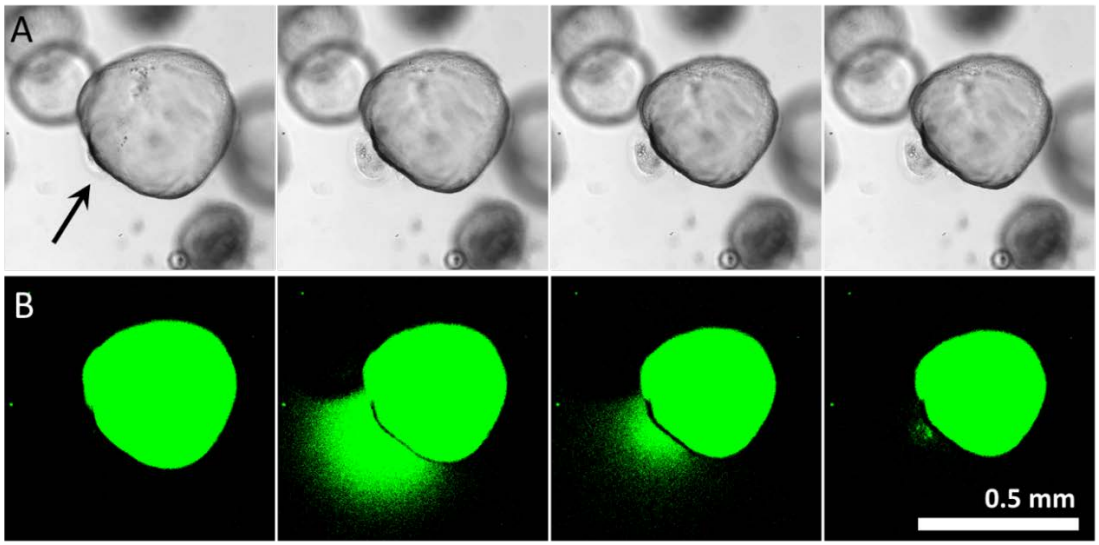

Fig. 3.3. Ejection of luminal contents. Series of time-lapse brightfield (**A**) and fluorescence (**B**) microscopy images reveal that upon rupture luminal contents are ejected into the extraluminal space. Fluorescence signal comes from FITC-Dextran that was previously injected into the HGO.

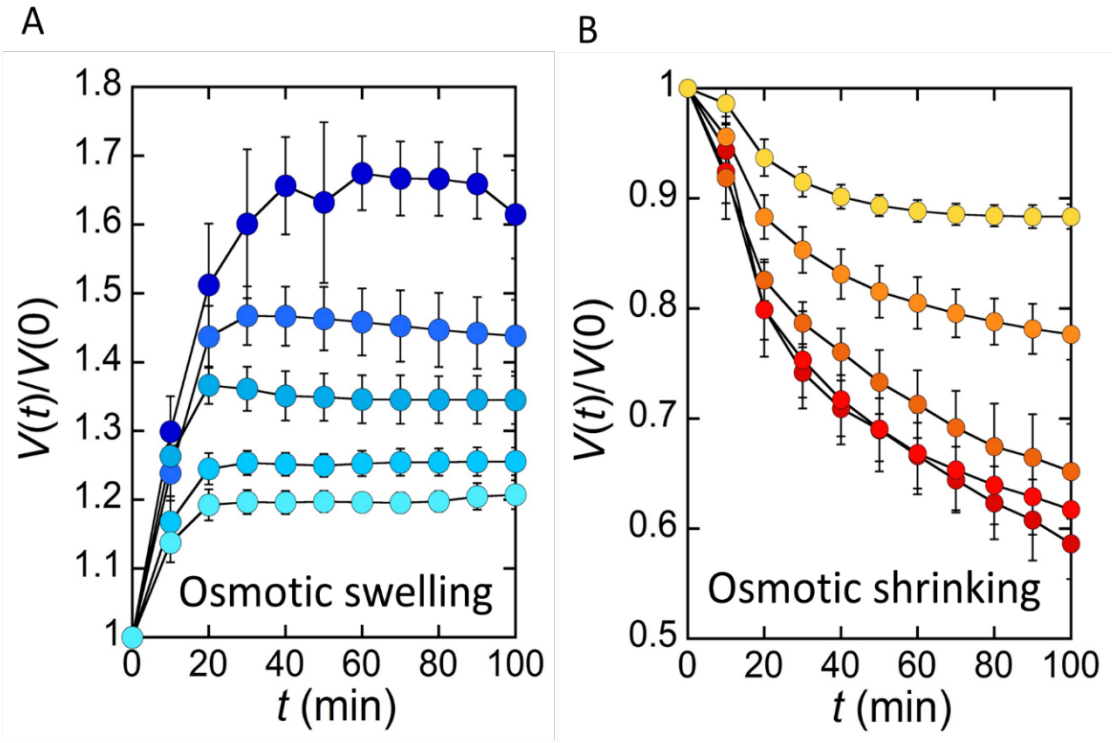

Fig. 3.4. Osmotic shocking of HGOs. (**A**) Average normalized volume increase plotted as a function of time for HGOs subjected to a reduction in external osmolality. From top to bottom: 150 mOsM, 175 mOsM, 200 mOsM, 225 mOsM, and 250 mOsM ($15 < n < 30$). (**B**) Average normalized volume decrease plotted as a function of time for HGOs subjected to an increase in external osmolality. From top to bottom: 350 mOsM, 375 mOsM, 400 mOs, 425 mOsM, and 450 mOsM ($15 < n < 30$).

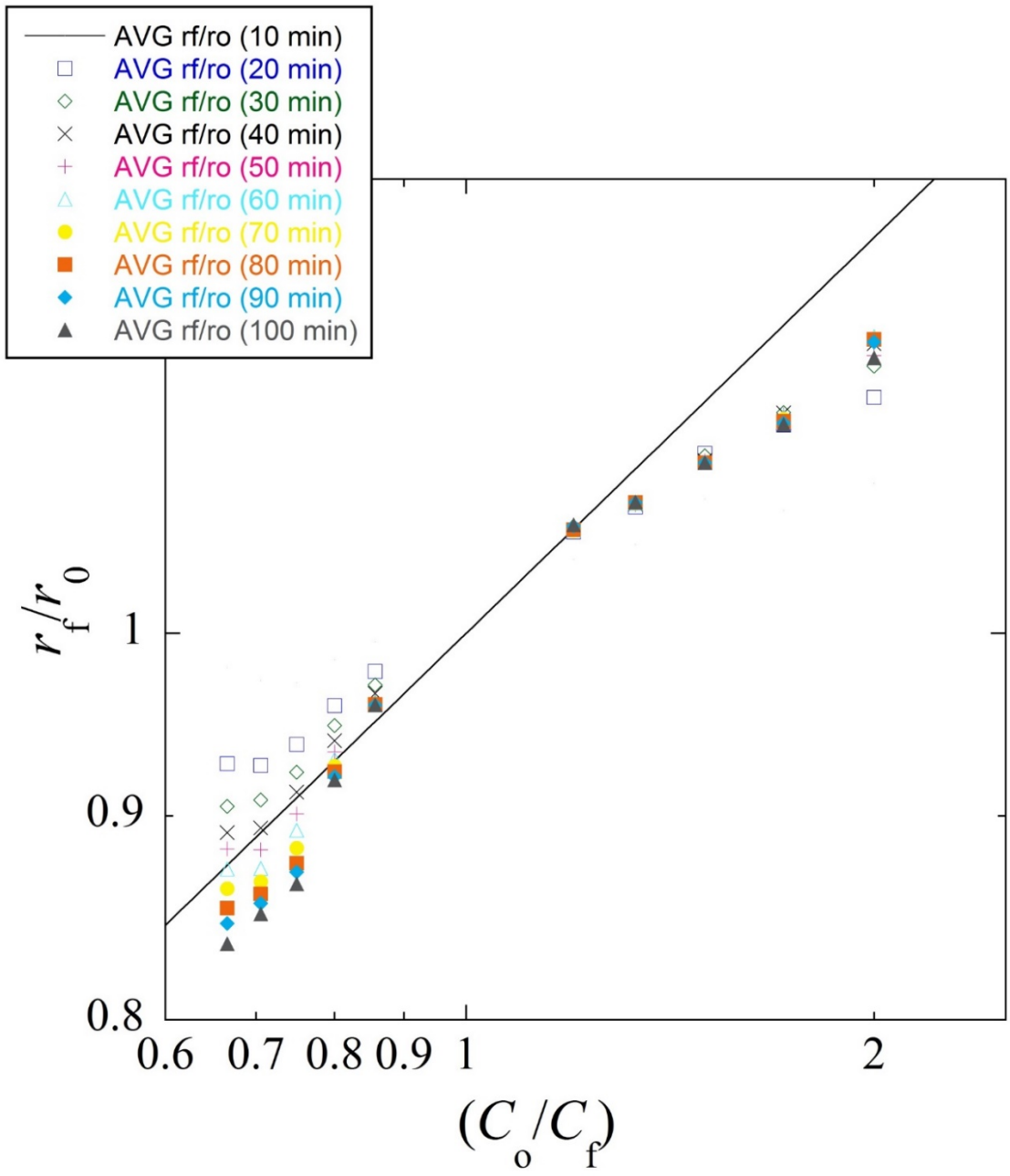

Fig. 3.5. A plot of relative volume change (r_f/r_0) as a function of the inverse of the relative change in concentration $(c_0/c_f)^{-1}$, where r_0, r_f, c_0, and c_f are the initial and final HGO radii, and initial and final external osmolality, respectively. Data was taken from the plot in Fig. 4 with different r_f values corresponding to different time points as shown in the legend. The solid black line corresponds to the dilution equation: $r_f/r_0 = (c_0/c_f)^{1/3}$.

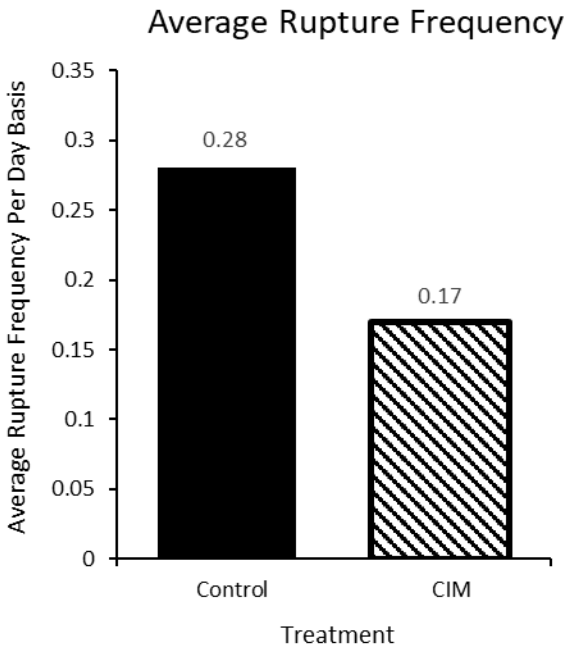

Fig. 3.6. Cimetidine treatment of human gastric organoids. Average rupture frequencies per day basis calculated from 71 and 117 total rupture events observed by drug-treated (n = 146) and control group (n = 144) human gastric organoids respectively over 69 hours.

LITERATURE CITED

1. McCracken KW, *et al.* (2014) Modelling human development and disease in pluripotent stem-cell-derived gastric organoids. *Nature* 516(7531):400-+.
2. Barker N, *et al.* (2010) Lgr5(+ve) Stem Cells Drive Self-Renewal in the Stomach and Build Long-Lived Gastric Units In Vitro. *Cell Stem Cell* 6(1):25-36.
3. Unbekandt M & Davies JA (2010) Dissociation of embryonic kidneys followed by reaggregation allows the formation of renal tissues. *Kidney Int* 77(5):407-416.
4. Takasato M, *et al.* (2015) Kidney organoids from human iPS cells contain multiple lineages and model human nephrogenesis. *Nature* 526(7574):564-U238.
5. Morizane R, *et al.* (2015) Nephron organoids derived from human pluripotent stem cells model kidney development and injury. *Nat Biotechnol* 33(11):1193-U1127.
6. Lancaster MA, *et al.* (2013) Cerebral organoids model human brain development and microcephaly. *Nature* 501(7467):373-+.
7. Takahashi T (2019) Organoids for Drug Discovery and Personalized Medicine. *Annu Rev Pharmacol* 59:447-462.
8. Sato T, *et al.* (2011) Long-term Expansion of Epithelial Organoids From Human Colon, Adenoma, Adenocarcinoma, and Barrett's Epithelium. *Gastroenterology* 141(5):1762-1772.
9. Schweinlin M, *et al.* (2016) Development of an Advanced Primary Human In Vitro Model of the Small Intestine. *Tissue Eng Part C-Me* 22(9):873-883.
10. Spence JR, *et al.* (2011) Directed differentiation of human pluripotent stem cells into intestinal tissue in vitro. *Nature* 470(7332):105-109.
11. Lancaster MA & Knoblich JA (2014) Organogenesis in a dish: Modeling development and disease using organoid technologies. *Science* 345(6194).
12. Akkerman N & Defize LHK (2017) Dawn of the organoid era: 3D tissue and organ cultures revolutionize the study of development, disease, and regeneration. *Bioessays* 39(4).
13. Willyard C (2015) The boom in mini stomachs, brains, breasts, kidneys and more. *Nature* 523(7562):520-522.
14. Davies J & Lawrence M (2018) *Organs and Organoids* (Academic Press Imprint, Elsevier Science & Technology Books, San Diego, Oxford).

15. Sebrell TA, *et al.* (2019) A Novel Gastric Spheroid Co-Culture Model Reveals Chemokine-Dependent Recruitment of Human Dendritic Cells to the Gastric Epithelium. *Cellular and Molecular Gastroenterology and Hepatology*.

16. Martinez-Guryn K, *et al.* (2018) Small Intestine Microbiota Regulate Host Digestive and Absorptive Adaptive Responses to Dietary Lipids. *Cell Host Microbe* 23(4):458-+.

17. Hill DR & Spence JR (2017) Gastrointestinal Organoids: Understanding the Molecular Basis of the Host-Microbe Interface. *Cellular and Molecular Gastroenterology and Hepatology* 3(2):138-149.

18. Nigro G, Rossi R, Commere PH, Jay P, & Sansonetti PJ (2014) The Cytosolic Bacterial Peptidoglycan Sensor Nod2 Affords Stem Cell Protection and Links Microbes to Gut Epithelial Regeneration. *Cell Host Microbe* 15(6):792-798.

19. Lukovac S, *et al.* (2014) Differential Modulation by Akkermansia muciniphila and Faecalibacterium prausnitzii of Host Peripheral Lipid Metabolism and Histone Acetylation in Mouse Gut Organoids. *Mbio* 5(4).

20. Nie YZ, Zheng YW, Ogawa M, Miyagi E, & Taniguchi H (2018) Human liver organoids generated with single donor-derived multiple cells rescue mice from acute liver failure. *Stem Cell Res Ther* 9.

21. Heo I, *et al.* (2018) Modelling Cryptosporidium infection in human small intestinal and lung organoids. *Nat Microbiol* 3(7):814-+.

22. Sachs N, *et al.* (2018) A Living Biobank of Breast Cancer Organoids Captures Disease Heterogeneity. *Cell* 172(1-2):373-+.

23. Mathew B, *et al.* (2019) Mouse ICM Organoids Reveal Three-Dimensional Cell Fate Clustering. *Biophys J* 116(1):127-141.

24. Simunovic M & Brivanlou AH (2017) Embryoids, organoids and gastruloids: new approaches to understanding embryogenesis. *Development* 144(6):976-985.

25. Sebrell TA, *et al.* (2018) Live imaging analysis of human gastric epithelial spheroids reveals spontaneous rupture, rotation and fusion events. *Cell Tissue Res* 371(2):293-307.

26. Hill DR, *et al.* (2017) Bacterial colonization stimulates a complex physiological response in the immature human intestinal epithelium. *Elife* 6.

27. Forbester JL, *et al.* (2015) Interaction of Salmonella enterica Serovar Typhimurium with Intestinal Organoids Derived from Human Induced Pluripotent Stem Cells. *Infect Immun* 83(7):2926-2934.

28. Leslie JL, *et al.* (2015) Persistence and Toxin Production by Clostridium difficile within Human Intestinal Organoids Result in Disruption of Epithelial Paracellular Barrier Function. *Infect Immun* 83(1):138-145.

29. Engevik MA, *et al.* (2015) Human Clostridium difficile infection: altered mucus production and composition. *Am J Physiol-Gastr L* 308(6):G510-G524.

30. Noguchi TK, *et al.* (2015) Generation of stomach tissue from mouse embryonic stem cells. *Nat Cell Biol* 17(8):984-U962.

31. Nakajo A, *et al.* (2016) EHBP1L1 coordinates Rab8 and Bin1 to regulate apical-directed transport in polarized epithelial cells. *J Cell Biol* 212(3):297-306.

32. Barker N, *et al.* (2007) Identification of stem cells in small intestine and colon by marker gene Lgr5. *Nature* 449(7165):1003-U1001.

33. Fung KYY, Fairn GD, & Lee WL (2018) Transcellular vesicular transport in epithelial and endothelial cells: Challenges and opportunities. *Traffic* 19(1):5-18.

34. Reuss L (2009) Water Transport by Epithelia. in *Encyclopedia of Life Sciences* (John Wiley & Sons, Ltd, Chichester).

35. Lodish H BA, Zipursky SL, et al. (2000) *Transport across Epithelia* (W. H. Freeman, New York).

36. Alberts B JA, Lewis J et al. (2002) *Principles of Membrane Transport* (Garland Science, New York) 4th Ed.

37. Day RE, *et al.* (2014) Human aquaporins: Regulators of transcellular water flow. *Bba-Gen Subjects* 1840(5):1492-1506.

38. Ma TH & Verkman AS (1999) Aquaporin water channels in gastrointestinal physiology. *J Physiol-London* 517(2):317-326.

39. Rosenthal R, *et al.* (2010) Claudin-2, a component of the tight junction, forms a paracellular water channel. *J Cell Sci* 123(11):1913-1921.

40. Watson CJ, Rowland M, & Warhurst G (2001) Functional modeling of tight junctions in intestinal cell monolayers using polyethylene glycol oligomers. *Am J Physiol-Cell Ph* 281(2):C388-C397.

41. Clayman CB (1977) Evaluation of cimetidine (tagamet). An antagonist of hydrochloric acid secretion. *JAMA* 238(12):1289-1290.

42. Miyoshi H & Stappenbeck TS (2013) In vitro expansion and genetic modification of gastrointestinal stem cells in spheroid culture. *Nature Protocols* 8(12):2471-2482.

43. Gifford GB, *et al.* (2017) Notch1 and Notch2 receptors regulate mouse and human gastric antral epithelial cell homoeostasis. *Gut* 66(6):1001-1011.

44. Rosenthal R, *et al.* (2010) Claudin-2, a component of the tight junction, forms a paracellular water channel. *J Cell Sci* 123(Pt 11):1913-1921.

45. Sandbichler AM, Egg M, Schwerte T, & Pelster B (2011) Claudin 28b and F-actin are involved in rainbow trout gill pavement cell tight junction remodeling under osmotic stress. *J Exp Biol* 214(9):1473-1487.

CHAPTER 4

FLOW THROUGH HUMAN INTESTINAL ORGANOIDS WITH THE GUT ORGANOID FLOW CHIP (GOFLOWCHIP)

Contribution of Authors and Co-Authors

Manuscript in Chapter 4

Author: Barkan Sidar

Contributions: Conceptualized the experiments, developed methodology, performed investigation, wrote the original manuscript, reviewed and edited the manuscript.

Co-Author: Brittany R. Jenkins

Contributions: Developed methodology, performed investigation, wrote the original manuscript, reviewed and edited the manuscript.

Co-Author: Sha Huang

Contributions: Performed investigation.

Co-Author: Jason R. Spence

Contributions: Conceptualized the and supervised the experiments, developed methodology, reviewed and edited the manuscript, funding acquisition, provided resources.

Co-Author: Seth T. Walk

Contributions: Conceptualized the and supervised the experiments, developed methodology, wrote the original manuscript, reviewed and edited the manuscript, funding acquisition, provided resources.

Co-Author: James N. Wilking

Contributions: Conceptualized the and supervised the experiments, developed methodology, wrote the original manuscript, reviewed and edited the manuscript, funding acquisition, provided resources.

Manuscript Information

Barkan Sidar, Brittany R. Jenkins, Sha Huang, Jason R. Spence, Seth T. Walk, James N. Wilking

Lab on a Chip

Status of Manuscript:
____ Prepared for submission to a peer-reviewed journal
__X_ Officially submitted to a peer-reviewed journal
____ Accepted by a peer-reviewed journal
____ Published in a peer-reviewed journal

Submitted to Royal Society of Chemistry
27 February 2019

Grant Support: This work was supported in part by the Bill & Melinda Gates Foundation, Grant OPP1108199 (S.T.W. and J.R.S.) and the National Science Foundation, DMR-1455247 (J.N.W.).

ABSTRACT

Human intestinal organoids (HIOs) are millimeter-scale models of the human intestinal epithelium and hold tremendous potential for advancing fundamental and applied biomedical research. HIOs resemble the native gut in that they consist of a fluid-filled lumen surrounded by a polarized epithelium and associated mesenchyme; however, their topologically-closed, spherical shape prevents flow through the interior luminal space, making the system less physiological and leading to the buildup of cellular and metabolic waste. These factors ultimately limit experimentation inside the HIOs. Here, we present a millifluidic device called the Gut Organoid Flow Chip (GOFlowChip), which we use to "port" HIOs and establish steady-state liquid flow through the lumen. To demonstrate the utility of the device, we establish separate luminal and extraluminal flow for multiple days and use luminal flow to remove accumulated waste. This represents the first demonstration of established liquid flow through the luminal space of a gastrointestinal organoid. Flow cytometry results show that HIO cell viability is unaffected by long-term porting and luminal flow. We expect the GOFlowChip will enable a wide variety of experiments including real-time, long-term control over luminal contents and continuous luminal sampling.

INTRODUCTION

Human intestinal organoids (HIOs) are millimeter-scale experimental models of the intestinal epithelium(1-3). These tissues are grown in the lab through directed differentiation of human pluripotent stem cells (iPSC)(1) and have become a standard for basic and applied biomedical research(3-13). HIOs are spherical in shape and consist of an inner, liquid-filled space enclosed by a polarized epithelial shell that mimics the cellular complexity of the intestinal epithelium. The shell is comprised of several epithelial lineages, including stem cells, progenitors, and absorptive enterocytes, as well as secretory goblet, enteroendocrine, and Paneth cell precursors(1, 14). These cells are bound to one another through tight junctions and thus provide a physical barrier between the lumen and the outside environment. As in the human gut, the HIO barrier is dynamic and both actively and passively mediates the transport of molecules and water(15-17). Quite remarkably, HIOs exist as topologically-closed, self-contained systems for human gut research.

HIOs are particularly useful for studying interactions between bacteria and human host tissue. For example, the natural microbial colonization of immature intestinal epithelium, such as that in newborn infants, has been modelled by co-culturing microorganisms inside HIOs(3). HIOs also represent a new and unconventional model for understanding enteric dysfunction, which can be caused by pathogenic bacteria and viruses(10-12). To study such interactions, microbes have been injected into the luminal space using a micropipette(3, 10-12). After injection, the epithelial shell rapidly heals, and both HIO and microbes can be cultured together. The topologically-closed surface of

the epithelial shell is beneficial in that it acts to contain the microorganisms, thus allowing for short-term assays. However, the human gut is not a closed system and transport into and out of the intestine is critical to clear human and microbial cellular waste. The lack of liquid advection through the luminal space in HIOs and other gastrointestinal organoids leads to buildup of waste and cellular debris that can eventually lead to “popping” events(18). Thus, enclosed HIOs do not adequately mimic natural luminal flow through the human gut. An engineered system that better reflects *in vivo* conditions with controlled luminal flow would open up new avenues of experimentation involving real-time monitoring of luminal contents and physiologically-relevant shear flow.

Here, we present a multilayer millifluidic device used to establish internal liquid HIO flow in parallel with external flow around the outer surface of the HIO. We call this device the Gut Organoid Flow Chip (GOFlowChip). Internal liquid flow allows for the removal of accumulated waste from the lumen, while the extraluminal flow exchanges nutrients and waste to mimic collection by mesenteric arteries and portal vein transport. Luminal flow through the organoid is provided by tapered glass capillaries, which are used to puncture the HIO and establish flow for periods as long as t = 65 h. Flow around the outside of the organoid is provided by an additional channel cut into the device. The seal which forms at each puncture site is sufficient to maintain separation between the inner and outer contents of the organoid under physiologically relevant flow conditions. This device can be used for a broad range of experimentation and imaging. For example, independent control of luminal and extra-luminal liquid flow will allow for the

introduction of molecules or colloidal-scale objects, such as bacteria, into the luminal space and in close proximity to the epithelial surface. Additionally, fine-scale control of HIO luminal flow will enable continuous sampling of the luminal contents.

Background

HIOs are routinely grown from stem cells into multi-lineage, millimeter-scale, enclosed spheres with an internal lumen (**Fig. 1a**)(1, 2). The spheres are generated and propagated within a bio-compatible hydrogel(19-21), and, during growth, are exposed to growth factors necessary for cellular differentiation and proliferation(13). HIOs are considered fully differentiated once they have reached several millimeters in diameter, which requires six to eight weeks of growth. Functional and physiological assays conducted on HIOs at this stage reveal the presence of brush borders on enterocytes, production of mucin by goblet cells, peptide transport systems, and barrier-forming tight junctions(13, 22). HIOs older than eight weeks become dense with accumulated waste and the epithelial shell can lose mechanical integrity. HIOs can be maintained as long-term cultures for periods longer than a year, but this requires periodically cutting mature spheres into individual pieces(23), which reform into intact, closed spherical organoids(15, 16). Methods for establishing control over luminal and extraluminal transport are clearly needed.

A common approach for establishing well-defined flow control within a tissue culture is to integrate the tissue into a microfluidic or millifluidic device(24-26). This typically involves designing microscale fluid flow together with engineered cell scaffolds to replicate the structure and function of a specific human tissue or organ. For example,

human “organ-on-a-chip” systems that are designed to replicate the kidney(27-30), heart(31-36), lung(37-43), intestine(38, 44-50), liver(42, 45, 49, 51-62), blood vessels(40, 41, 63-65), bone(66-68), marrow(69), nerve(70-75), muscle(76) and cornea(77) have been developed. The exquisite control of liquid flow provided by fluidic devices can be used to deliver minute quantities of chemical or biological material with spatial and temporal precision(25, 26), allows for on-demand monitoring and analysis of nanoliter and picoliter liquid volumes(24), and can be used to maintain chemostasis(26). In contrast to the wide-spread development of “templated” organ-on-chip systems, the integration of preformed organoid cultures into fluidic systems has been limited. Human brain organoids have been successfully produced in a microfluidic chip(78) and liver, cardiac, and vascular organoids have been combined in a single, circulatory microfluidic system to create a “body-on-a-chip” platform(79, 80), and microfluidic channels have been used to template cells from disrupted human gastrointestinal organoids(81, 82); however, intact multicellular 3D gastrointestinal organoids with an enclosed lumen and surrounding epithelium and mesenchyme have not yet been integrated into such devices.

RESULTS AND DISCUSSION

To demonstrate the transport limitations caused by the closed epithelial shell, we follow the accumulation of waste inside the lumen of an HIO over several days using time-lapse light microscopy. Our imaging reveals that colloidal-scale cell debris sloughs off from the inner surface of the HIO and settles to the bottom of the lumen where it remains for multiple days (image series, **Fig. 1a, b**; Supplementary Video 1). As waste

builds, HIOs eventually darken and become optically opaque, as shown by the image in **Fig. 1c**. While the images in Fig. 1 provide a visual depiction of waste accumulation, dissolved molecular-scale waste and metabolites which are not visible also likely accumulate due to the semipermeable nature of the epithelial shell(13, 15-17, 22). Accumulation of waste impacts organoid viability and physiology and limits the time period over which organoids remain viable for experimentation(13).

To establish real-time control over luminal contents, we develop a chip-based fluidic device for establishing luminal liquid flow. Mature HIOs are millimeters in diameter; so, a fabrication method capable of generating a device with millimeter-scale features and channels is needed. To achieve device features at this scale, we use a laser to cut thin acrylic sheets into precise shapes. Our device consists of three layers: a middle layer containing the organoid and a channel for extraluminal flow, and an upper and lower layer which enclose the middle layer (**Fig. 2a**). These layers are then sandwiched together to form a three-dimensional millifluidic device (**Fig. 2b**). Thin, laser-cut silicone rubber sheets are also included between acrylic layers to seal the device and prevent leaking. Holes in the upper acrylic layer allow for the introduction of liquid into and out of the upper (extraluminal) flow channel, and the bottom layer forms the floor of the device. Laser-cut cylindrical side channels with long axes normal to the side walls of the device and perpendicular to the layer plane (**Fig. 2c**) allow for tapered glass capillaries to be inserted into the HIO. Luminal flow is established in one of two ways: using a single double-lumen capillary (**Fig. 2d**, bottom) or two single-lumen capillaries (**Fig. 2d**, top). Laser-cut silicone rubber gaskets are used on the sides as compression seals to prevent

leakage. The modular design of the device allows each layer to be designed independently and the device to be disassembled and reassembled for sterilization and repeated use. The transparency of the acrylic allows for optical imaging of a ported HIO.

To establish flow through an organoid, the lower and middle layers (**Fig. 2a**) are assembled under sterile conditions. An HIO embedded in Matrigel is then placed in the circular well formed by the two layers, and the organoid is punctured on one or two sides by manipulating tapered capillaries using independent three-axis micromanipulators. An HIO before and after puncturing is depicted in **Fig. 3a** and **Fig. 3b**, respectively. Most organoids, when punctured, deflate slightly, but do not immediately collapse. This is due to the fact that the outer surface of the organoid attaches to the surrounding Matrigel through cellular adhesions. Matrigel is viscoelastic with a characteristic relaxation time on the order of tens of minutes, which provides sufficient time to puncture both sides and establish flow. We find that HIOs with diameters between 2 mm and 3 mm are ideal for porting in our device; HIOs with diameters larger than 3 mm typically have a large amount of accumulated waste, which leads to clogging of the outlet capillary, and organoids with diameters smaller than 1 mm are difficult to manipulate with our current setup. While this lower size limit precludes the use of mouse organoids and human organoids derived from primary tissues, which are an order of magnitude smaller in diameter than HIOs derived from iPSCs (18, 23), a smaller version of a GOFlowChip imaged with appropriate optics could be used to port organoids and spheroids with sub-mm scale sizes. After the HIO is punctured, the two upper layers are added to the assembly, and the device is sealed by compression. To drive luminal liquid flow through

the HIO, the outer ends of the glass capillaries are attached through microfluidic tubing to computer-controlled syringe pumps, two of which provide independent control over the infusion and withdrawal of liquid from the organoid. To drive liquid flow through the extraluminal flow channel, ferrules inserted into the top layer of the chip (**Fig. 2a-c**) are connected through microfluidic tubing to other computer-controlled syringe pumps. A detailed description of the loading and assembly protocol, including the most commonly encountered problems, is included in Supplementary Information along with the design files needed to fabricate the device.

A ported HIO will ideally possess the same barrier integrity found in the native gastrointestinal tract. In an unported HIO, barrier integrity is maintained by the epithelial shell via intact cellular tight junctions; however, when the shell is punctured, integrity is contingent on the formation of a seal at the puncture site. To test the seal of a fully ported HIO, we pressurize the HIO by flowing liquid through the left-side capillary, c1 (q_{in} = 5 μL/h) while suppressing liquid outflow through the right-side capillary, c2 (q_{out} = 0). Thus, a seal forms at the puncture site which allows for dramatic inflation without any leakage of liquid even over several hours, as shown by the series of images in **Fig. 4a** (Supplementary Video 2). High resolution imaging suggests that Matrigel plays a role in maintaining this seal by closing around the capillary until the ruptured epithelium regrows and adheres to the capillary. This is not surprising, given that gut organoids are commonly punctured, injected with material, and the capillary removed without observable deflation or ejection of luminal contents(12). We note that the temporary barrier provided by Matrigel differs from that provided by intact epithelium; while

Matrigel suppresses liquid flow and the diffusion of colloidal-scale objects(83), molecules smaller than the mesh size of the gel ($\xi \approx 10$ nm) diffuse through the gel(84). Thus, for experiments where barrier integrity immediately following HIO puncture is critical, the nature of the seal and time needed to ensure complete epithelium healing should be investigated further. To establish luminal flow and verify the integrity of the ported seal, we design a flow sequence that should result in organoid inflation and deflation. The inflation condition is achieved by infusing liquid media through c1, while preventing flow through c2, resulting in a positive net flow of media into the organoid, Δq. Here, $\Delta q = q_{in} - q_{out}$, where q_{in} is the total flow rate into the organoid and q_{out} is the total flow rate out of the organoid. The deflation condition is achieved by withdrawing liquid from c2, while preventing flow through c1, resulting in a negative net flow of liquid ($q_{in} < q_{out}$). We initiate this flow sequence, alternating between the two flow conditions, and observe that the organoid undergoes striking volume changes in response to flow, as depicted by the series of images in **Fig. 4b** and **Fig. 4c** (Supplementary Video 3). To quantify this volume change, we plot the net imposed flow rate as a function of time (**Fig. 3d**, top plot) along with the maximum diameter of the organoid measured along the *y*-axis as a function of time (**Fig. 3d**, bottom plot), and observe that the diameter changes consistently in response to the imposed flow. This represents, to our knowledge, the first demonstration of luminal flow through a topologically-closed gastrointestinal organoid.

For long-term experimentation, the chip must be capable of maintaining luminal flow through an HIO for hours and even days. In preliminary attempts, we find that

establishing flow for this length of time is limited mainly by clogging of the exit capillary. Clogging presents a problem because syringe pumps are flow rate-controlled rather than pressure-controlled and thus insensitive to pressure buildup in the HIO; if blockage of the exit capillary occurs, liquid is driven into the HIO until it ruptures. To mitigate this, we explore a range of exit tip diameters (20 μm $\leq d \leq$ 120 μm) and find that for fully differentiated organoids containing a significant amount of waste, an exit capillary with a tip diameter $d \approx 80$ μm and a flow rate $q_{out} \leq 5$ μL/h is ideal; capillaries with smaller tip diameters tend to clog, and capillaries with larger tip diameters are difficult to puncture HIOs. We also find that during long-term experiments bubbles form in the overflow liquid, which negatively impacts image quality and HIO barrier integrity. Thus, to suppress bubble formation, we pressurize the liquid slightly by constricting the outlet of the overflow liquid (see *Methods*). After significant optimization we regularly establish steady-state flow through HIOs for $t \geq 65$ h using both the single, double-lumen capillary and double, single-lumen capillary porting methods (Supplementary Videos 4 and 5); longer flow experiments could be achieved but we were limited by microscope access in our shared facility. Luminal flow on the order of days will enable a wide variety of future experiments.

Continuous luminal flow could be used to introduce materials to the lumen or remove and sample luminal contents. To demonstrate the value of luminal flow, we port an HIO containing significant accumulated waste and use flow to remove waste. The HIO is ported using capillaries with tip diameters c1 = 40 μm and c2 = 80 μm, steady state flow is established by setting flow into and out of organoid equal ($q_{in} = q_{out} = 5$ μL/h),

and the organoid is imaged for 20 h. During this time, the organoid undergoes significant fluctuations, moving in and out of our objective focus (Supplementary Video 6); however, no leaking, signs of cell death, or loss of barrier integrity are observed. At the 20 h mark, when the microscope is refocused, it is apparent that the HIO has clarified, and that waste is being removed by liquid flow through the exit capillary (**Fig 5a**). The organoid continues to clarify over the next 7 hours as depicted by the series of microscopy images in **Fig 5b-d**. Waste is observed exiting the organoid through c2. Images of the flow profile along c2 reveal the movement of large objects moving from left to right as they are carried by liquid flow, as shown by the series of microscopy images in **Fig 5e** (Supplementary Video 7). To quantify the removal of waste from the HIO, we measure the intensity profile along the center of the capillary as a function of time and plot the data as a kymograph in **Fig. 5f**. In this format, the *y*-axis represents the grayscale pixel intensity along a horizontal line bisecting the images in **Fig. 5e**, and the *x*-axis represents time. Thus, the lines moving from the bottom left to the upper right represent the movement of objects from left to right within c2, and the slope of these lines provides their velocity. The dark line represents the large piece of waste depicted by the image series in **Fig. 5e** with a velocity, $v = 0.276$ mm/s. The green crosses in **Fig. 5e** represent the positions associated with the pixels marked by the green crosses in **Fig. 5f**. This result demonstrates that luminal flow can be used to perform a useful function: the removal of accumulated waste.

Ideally, flow through a ported HIO will mimic flow through the human gut. The topology of a dual-ported HIO, with an inlet and outlet on opposing sides, is identical to

that of the gut, but the dimensions and aspect ratio differ significantly. A dual-ported HIO is a short tube with equal diameter and length ($d \approx$ 3-5 mm); by comparison, the lumen of the human intestine is an order of magnitude wider in diameter ($d \approx$ 2-3 cm), and the length of the human intestine is three orders of magnitude longer ($\ell \approx$ 2-3 m) than an HIO. Because of these differences in size and aspect ratio, matching the volumetric flow rate would result in flow conditions that are unrealistically fast, which could result in the removal of not just waste, but also key molecules that are critical to epithelial health and function. Instead of flow rate, liquid velocity, v appears to be the relevant parameter as it controls the rate at which materials are transported to and from the inner wall of the epithelium, as well as determining the stress exerted by the luminal contents on the inner lining of the gut, which is critical for gut physiology. The average velocity through the human gut is reported to be on the order of 0.4 mm/s(85, 86). For comparison, the average velocity in our pulsatile experiment (**Fig. 3**), where q = 25 μL/min, $d = 2r \approx$ 1.5 mm, is $v = q/\pi r^2 \approx$ 0.24 mm/s. Thus, the luminal flow velocity through our HIOs is comparable to that in the human gut. We note that the shear stress exerted by luminal contents on the inner wall of the gut is also governed by the topography of the gut lining and the rheological properties of the material in the lumen, and the impact of these parameters on HIO physiology warrant further investigation.

Similarly, flow outside a ported HIO should ideally mimic flow around the outside of the human gut. To determine the relevant range for extraluminal flow in our HIO chip, we begin by considering the frequency of media exchange needed to maintain HIOs under standard culture conditions. Cultured HIOs require media replacements of 50

μl per HIO every 48 h, which is approximately equal to 1 μl/h of continuous flow in our chip for a single HIO. In the native human gut, the transport of blood through gut tissue is on the order of 10 μl/h per mg of tissue, which corresponds to continuous flow on the order of 10s of μl/h in our chip for a single HIO (see Methods). For practical purposes, in the experiments described here we use flow rates in the range 50 μl/h ≤ q ≤ 300 μl/h, but to explore the impact of extraluminal flow on HIO physiology, q could be significantly reduced. In the future, additional changes could be made to mimic physiologically-relevant conditions. For example, media composition could be altered such that oxygen-poor, nutrient-rich liquid is delivered to the lumen and oxygen-rich, nutrient-poor liquid is delivered to the basolateral surface. Additionally, the structure of the material around the HIO could be engineering to mimic the complex, layered tissues around the native gut, which govern liquid flow and transport and contain vasculature.

To determine if puncturing the epithelium and subjecting HIOs to long-term luminal and extraluminal flow adversely affects HIO viability, we perform measurements of cell viability using flow cytometry. Ported HIOs subjected to flow for t = 65h are removed from the device, individually dispersed as single cell suspensions, stained with a fluorescent indicator of membrane integrity (intracellular/extracellular amines strained with a Live/Dead cell stain, ThermoFisher Inc.) that differentially labels viable and nonviable cells, and assayed using flow cytometry (see Methods). A histogram of stain fluorescence intensity reveals a bimodal distribution (**Fig. 6a**), representing the fraction of live and dead cells from each HIO. When the data are compared (**Fig. 6c**), we find that the fraction of dead cells in ported HIOs (mean ± SD: 0.1296 ± 0.063, n = 3) was not

statistically different from our two controls: unported HIOs assayed individually (0.1555 ± 0.1115, n = 4) and unported HIOs combined and assayed together (0.177 ± 0.0512, n = 3)(ANOVA: $F_{2,7}$ 0.64, P = 0.55). This critical experiment and positive result support our microscopy observations that HIO viability is not adversely affected by porting and luminal flow. In the future, the impact of flow velocity, luminal content rheology, and nutrient concentration on gene expression, cellular differentiation, and cellular proliferation should be investigated to determine how these parameters impact the distribution of cell types and behaviors in an HIO.

Flow cytometry can also provide a measure of insoluble cellular debris; particles with low intensity forward and side scattering are characteristic of suspended particles with sizes smaller than a cell (**Fig. 6b**). When these data are compared (**Fig. 6d**), we also find that the fraction of scattering events in ported HIOs corresponding to cellular debris (mean ± SD: 0.098 ± 0.01, n = 3) was not statistically different from controls: unported HIOs assayed individually (0.1415 ± 0.07, n = 4) and unported HIOs assayed collectively (0.1133 ± 0.0522, n = 3)(ANOVA: $F_{2,7}$ = 1.42, P = 0.30). While this is somewhat surprising given the dramatic removal of luminal waste depicted in **Fig. 5**, it could be that luminal HIO waste is solubilized during preparation for flow cytometry and no longer scatters light. It is also possible that even though more debris is being removed, the epithelium is producing more waste because it is more active in the ported state. Regardless, waste is being removed by the porting and flow process, which is clearly apparent from microscopy.

We expect that the results presented here will enable a wide variety of experiments. Luminal flow provides a means of introducing materials to the luminal space as well as extracting materials from this space; so, the device will be ideal for experiments exploring the establishment and stability of the microbiome, including the introduction of microbes, monitoring microbial dynamics with fluorescence microscopy, and detecting the presence of detached microbes and dissolved waste products and metabolites in the luminal effluent. In addition, maintained barrier integrity and independent control of luminal and extraluminal liquid streams will allow researchers to explore transport across the epithelial shell. For example, the absorption of nutrients and pharmaceutical compounds through the apical surface of the epithelium could be explored. The functionality of the millifluidic chip presented here could be enhanced through the integration of a variety of soft, PDMS-based microfluidic modules such as flow-focusing drop makers and detection and sorting capabilities(87, 88). While the design presented here could be parallelized to port small numbers of HIOs, the delicate porting process is not amenable to high-throughput testing. Truly massive parallelization would require the development of an automated porting method as well as improvements in HIO culture techniques to generate large numbers of HIOs with monodisperse sizes.

CONCLUSIONS

In conclusion, the fluidic chip presented here represents the first device engineered to establish liquid flow through the lumen of a gastrointestinal organoid. The multilayer chip design allows for straightforward assembly, disassembly, and

sterilization, enabling multiple uses without replacement. Separation of luminal and extraluminal fluid is ensured by the formation of a seal at each epithelial puncture site, which maintains barrier integrity and allows for independent control of the two liquid streams. This approach opens the field for broader application of HIO models in biomedical research. The limits of HIO culturing and experimentation have not been fully explored, but this prototype provides a significant advancement by mimicking a critically important physiologic parameter of the human gut: luminal flow.

EXPERIMENTAL

Device Fabrication

Multilayer devices composed of three distinct layers and silicone rubber gaskets were cut from clear cast acrylic plastic sheets (McMaster Carr; dimensions: 12” x 12”) and silicone rubber sheets (McMaster Carr, Durometer 40A, White; dimensions: 12” x 12”, 1/16” thickness) using an automated laser cutter (Universal). Top and bottom layers were cut from sheets with thicknesses of h = 2.0 mm and h = 1.5 mm, respectively. The middle layer was cut from h = 4.5 mm thick sheets. Layers and gaskets were designed using AutoCAD software and design files are included in the supplementary section. Layers were sealed through gaskets between each layer and compressing the assembled layers using nuts and bolts (McMaster Carr; 316 stainless steel, M3 x 0.3 mm thread, 10 mm length). For the single-lumen, two capillary setup; tapered glass capillaries for puncturing the HIOs were created by pulling thin wall borosilicate glass capillaries (World Precision Instruments TW150-6) using a micropipette puller (Sutter Instruments,

P-97). Capillaries with tip diameters between 40 μm and 80 μm and taper lengths of 4 mm and 3.5 cm were used. For dual-lumen, single capillary setup; septum theta borosilicate glass capillaries (World Precision Instruments TST150-6) were pulled in the same way to obtain a 100 μm tip with 3 mm taper length. Capillaries were mounted to three-axis translational micromanipulators (Quater Research; XYZ 300 ML) with capillary holders designed in Fusion 360 and 3D printed using SLA 3D printer (see design files) for precision control during organoid puncturing.

Liquid Flow

Luminal and extraluminal liquids were introduced to the device by connecting liquid-filled syringes (Hamilton 500μL and BD 10 mL, respectively) fitted with blunt-tip stainless steel dispensing needles (McMaster Carr; luminal flow: 26 gauge and 17; extraluminal flow: 16 gauge) to medical grade polyethylene micro-tubing (Scientific Commodities Inc., PE/9, ID = 1.40 mm, OD = 1.91 mm). For luminal flow, tubing was connected to the non-tapered ends of the glass capillaries. For extraluminal flow, tubing was connected to blunt-tip stainless steel dispensing needles (McMaster Carr, 90° angle, 20 gauge) inserted into holes in the upper layer of the device. Both luminal and extraluminal liquid flow was driven by programmable, computer-controlled New Era NE-1000 syringe pumps for precise delivery and withdrawal of small volumes of liquid. For short-term periodic flow experiments, phosphate-buffered saline (PBS) was used for both luminal and extraluminal flow. For long-term, steady-state flow experiments, HIO growth media was used for both luminal and extraluminal flow. To establish a baseline

for extraluminal flow, we estimate the transport of blood through gut tissue in the native human gut.

We estimate cardiac output to be 5L/min of which 20% is shared between the spleen, liver, stomach, small intestine and large intestine which are approximately 5 kg in total(89-92). This corresponds to approximately 10 μl/h per mg of tissue. The HIOs used in our experiments contain tissue mass on the order of 2-5 mg, so we estimate the baseline for extraluminal flow to be 20-50 μl/h.

Sterilization

The glass transition of the cast acrylic sheets is below our autoclave temperature range ($T \approx$ 121-132 C), so sterilizing the millifluidic device using heat is not feasible. Instead, the device was sterilized by disassembling individual layers and soaking them in pure ethanol for five minutes, followed by rinsing in autoclaved distilled water. After assembly, the device and associated tubing and connectors were again flushed with pure ethanol followed by autoclaved distilled water.

Bubble Suppression

The pressure required to drive liquid flow through a microfluidic device is usually sufficient to suppress air bubble formation in the device; however, this is not the case for millifluidic devices. To suppress bubble formation, we pressurize the liquid by attaching a tapered capillary at the outlet of the overflow channel. We observed that flow rates of 100-150 μl/hr and exit tip diameters of 40-60 μm corresponding to pressure drops of 70-140 Pa were sufficient to suppress bubble formation during multiday flow experiments.

Imaging

Time-lapse video microscopy measurements were performed using a laser scanning confocal microscope (Leica SP5 II) equipped with an environmental control chamber (Life Imaging Services) maintained at 37°C. Fluorescence and brightfield images were collected with 10X air objective (Leica 506505, HC PL Fluotar 10X/0.03) and 1.25 X air objective (Leica 506215, HCX PL Fluotar 1.25X/0.04). Time-lapse measurements were also collected using a stereomicroscope (Leica, M205 FA) equipped with color CMOS video camera (Leica, DFC3000 G). After collection, images were processed and analyzed using IMARIS, MetaMorph and ImageJ image analysis software.

Organoid Culture

Derivation and maintenance of HIOs followed published protocols(1, 23). Briefly, HIOs were embedded in Matrigel (BD Biosciences) and overlaid with Advanced DMEM-F12 medium (Invitrogen, Carlsbad, CA) containing 1X B27 supplement (Invitrogen), 1X GlutaMAX (Life Technologies, Carlsbad, CA), 10 µM Hepes, 10% pen/strep, 100 ng/mL rhNoggin (R&D Systems), 100 ng/mL epidermal growth factor (R&D Systems), and approximately 500 ng/mL R-Spondin1 (RSPO1). RSPO1 was obtained from conditioned media collected from a HEK293 cell line that was stably transfected and zeocin-selected for the RSPO1 expression vector. Media was changed every two to four days, and HIOs were transferred to fresh Matrigel once a week until they reached approximately 2 to 3 mm in diameter for experiments. This size was reached on average 48 days after initial spheroid formation.

Cell Viability and Cellular Debris Assays

Cell viability and cellular debris assays were determined using a LIVE/DEAD Fixable Dead Cell Stain Kit (ThermoFisher) and flow cytometry. Ported HIOs were collected after being subjected to luminal flow for $t \geq 65$ h and preparation of the HIOs for the LIVE/DEAD stain occurred within 1 hour of collection. To disperse HIOs as single-cell suspensions, individual HIOs were washed with PBS, incubated in 0.25% trypsin-EDTA, and subjected to mechanical shear by passing the HIO through a P1000 pipette tip or 21-gauge needle. Cells were then washed in PBS, incubated with fluorescent dye, and fixed with formaldehyde following the manufacturer's instructions. Cell viability, as determined by near-IR fluorescence intensity, was quantified using a LSRFortessa flow cytometer, fluorescence-activated cell sorting (FACS), and FACSDiva Software (BD Biosciences). Gating single cells was based on forward and side-scatter profiles using an isotype control made from a pooled sample of four unported HIOs that were maintained under static cell culture conditions. The percentages of live and dead cells were determined by using the manufacturer's recommended settings and guidelines. After removing doublets and cell clumps from analysis, infrared staining was analyzed to determine the best fit of separation between live cells and dead cells, which are represented by low and high APC-Cy7-A emission intensity, respectively. As an additional control, unported HIOs similar in size and age to the ported HIOs were collected and analyzed individually following the protocol above.

Statistical Analysis

A one-way ANOVA with multiple comparisons was performed to test statistical differences between the means of three groups: unported, pooled HIOs; unported, single HIOs; and ported HIOs.

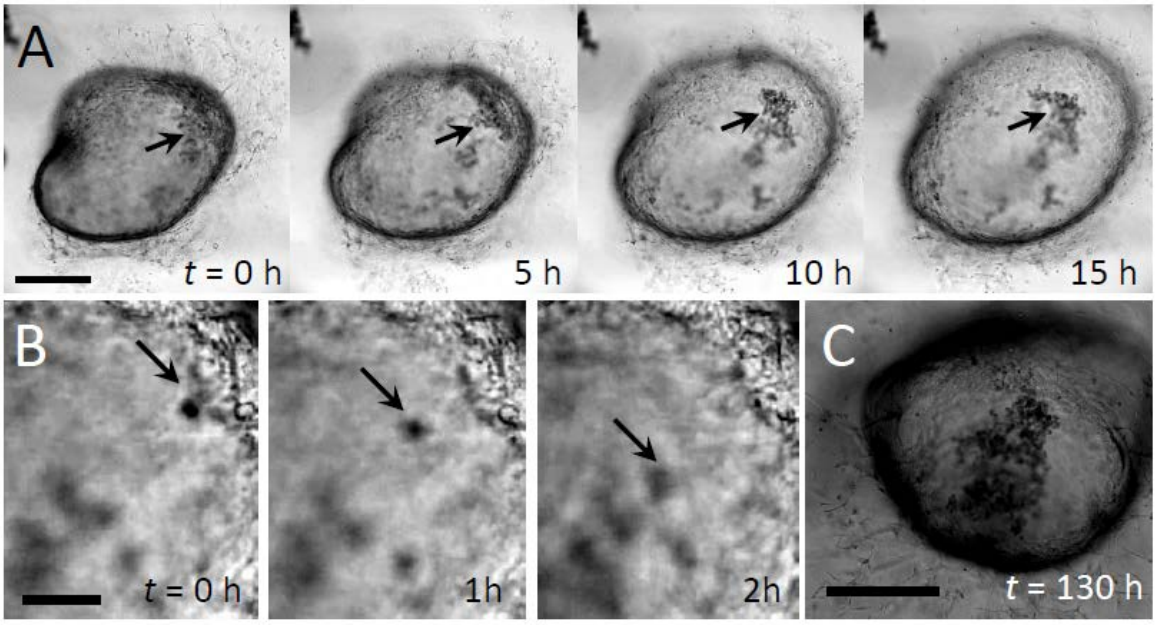

Fig. 4.1. Time-lapse microscopy imaging of a human intestinal organoid (HIO) reveals waste accumulation. (A) Image series. Closed-shell structure formed by an HIO. The epithelial sheet acts as semipermeable membrane, limiting transport between the luminal and extraluminal space. In the early stages of organoid growth, HIOs are optically transparent, but cellular debris accumulates over time (black arrows). Scale bar represents 1 mm. (B) Image series. High magnification time-lapse images of small debris (black arrows) sloughing off the inner surface and settling to the bottom of the interior space. Images are separated by 1 h each. Scale bar represents 0.1 mm. (C) After 130 h, the HIO from (A) has darkened significantly and waste has continued to accumulate in the luminal space.

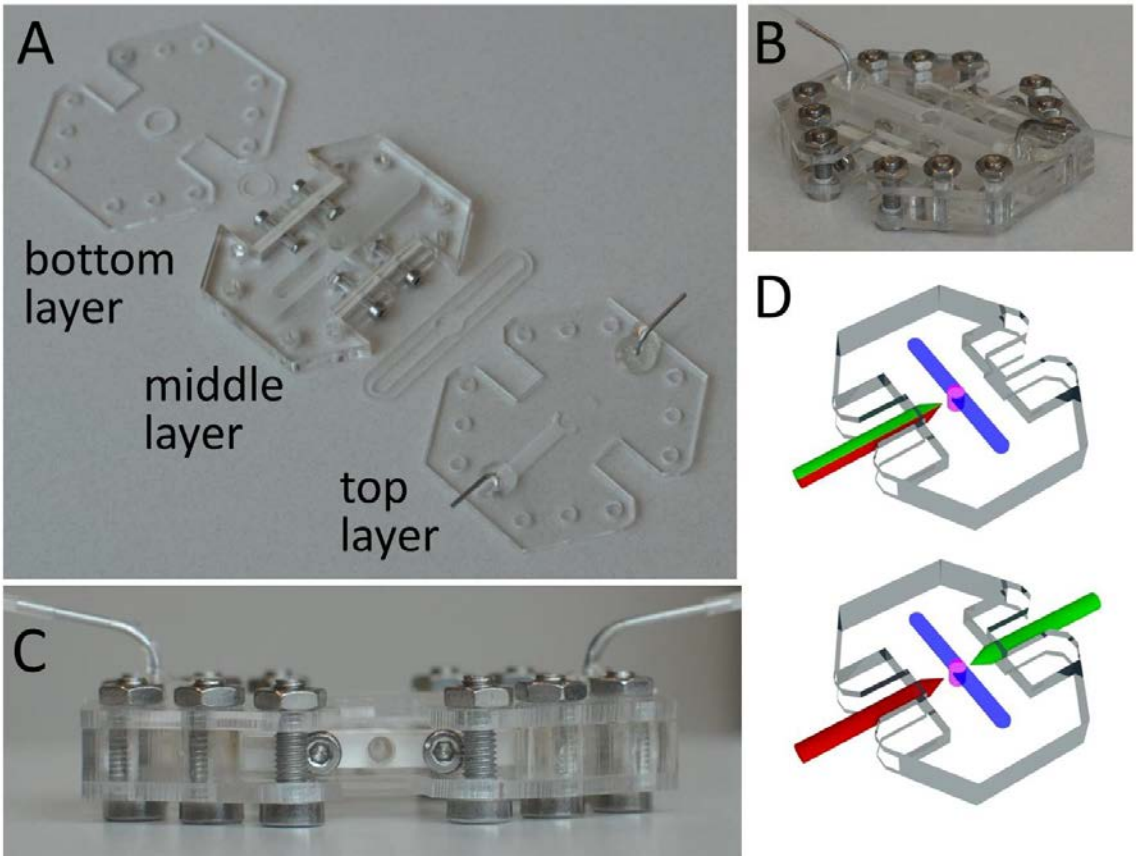

Fig. 4.2. Multilayer millifluidic chip for establishing distinct luminal and extraluminal flow. (A) The device is composed of three layers. The HIO is contained in a central well in the middle layer. Extraluminal flow is guided by an engraved channel in the top layer just above the organoid. The bottom layer encloses the bottom of the device. Arrows indicate laser-cut silicone gaskets. (B) Orthogonal view of the assembled device with fluidics assembled for extraluminal flow but no capillaries yet inserted for HIO porting. (C) Side view of the assembled device with the side port gasket (white) clearly visible. (D) Illustrations highlighting two different configurations for HIO porting. Upper: Porting with a single, double-lumen capillary (green-red). Lower: Porting with two, single-lumen capillaries (red and green).

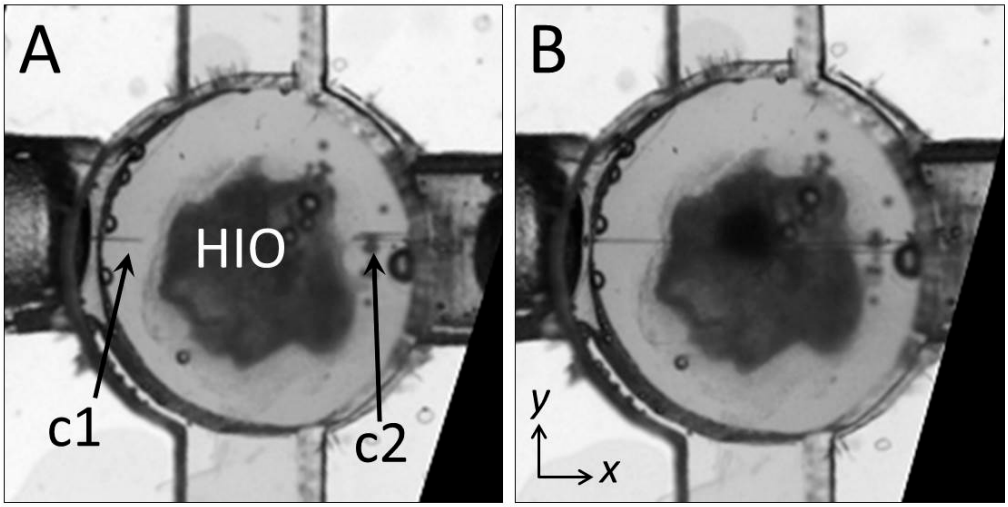

Fig. 4.3. HIO Porting Process. (A) Microscopy image of HIO in an assembled device before puncturing with capillaries (c1, c2). (B) Image of the same HIO after puncturing on either side. The diameter of the circular well in (A) and (B) is 4 mm.

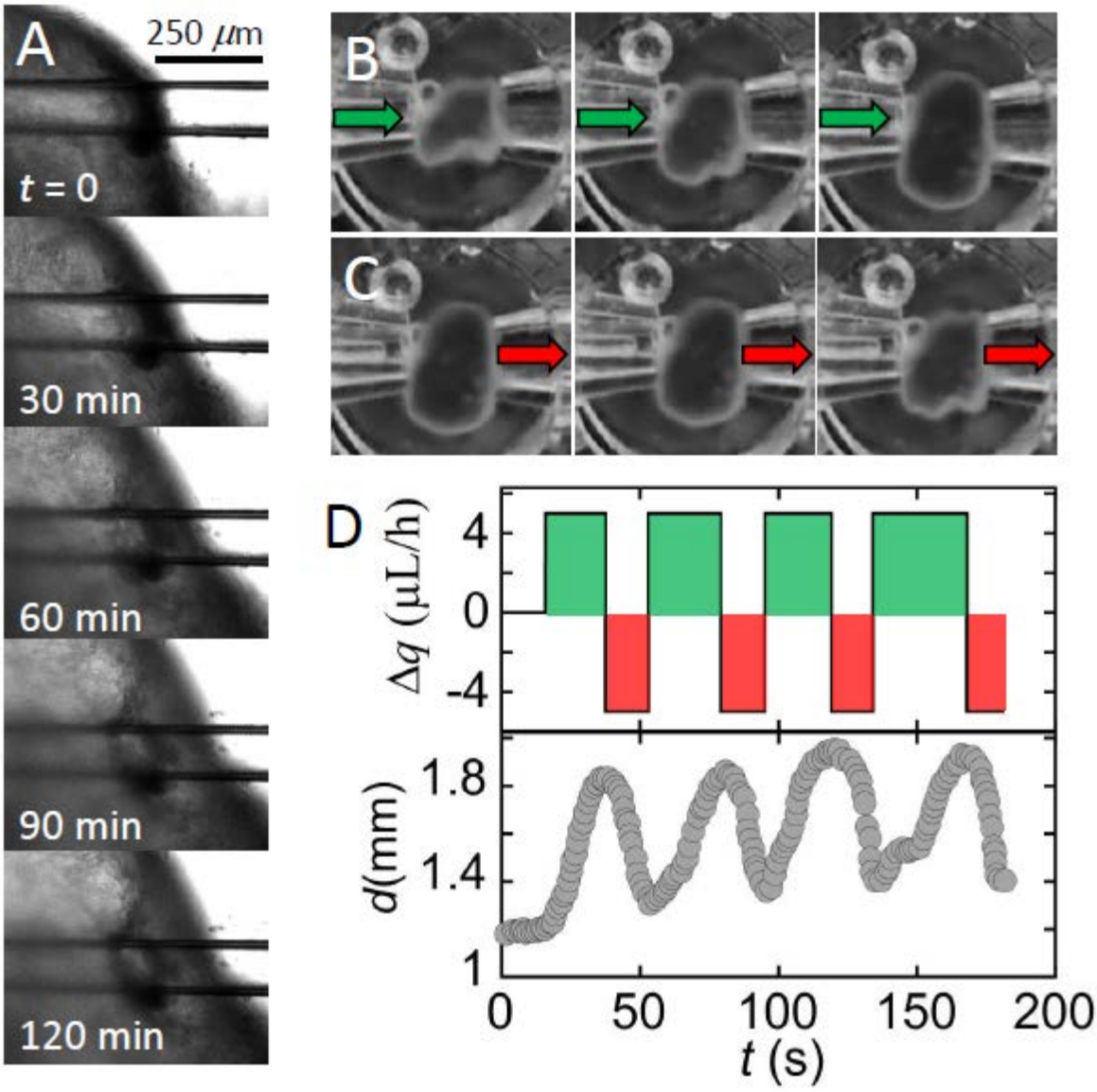

Fig. 4.4. Demonstration of puncture seal and luminal flow. (A) Microscopy image series. An HIO punctured on both sides and subjected to a net influx of liquid (q_{in} = 5 μL/h; q_{out} = 0 μL/h) swells, but no leaking of liquid at the puncture site is detected. (B) Microscopy image series. An HIO punctured on both sides swells as aqueous media is infused from the left capillary (q_{in} = 5 μL/h). No liquid is removed from the HIO through the right capillary (q_{out} = 0 μL/h). Time between images is 20 s. (C) Microscopy image series. The HIO shrinks as media is withdrawn through the right capillary (q_{out} = 5 μL/h; q_{in} = 0 μL/h). Images in each series (B, C) are separated by Δt = 20s. (D) Upper plot. Net flow of media, $\Delta q = q_{in}-q_{out}$, into or out of the HIO is plotted as a function of time. Lower plot. Corresponding change in HIO diameter, d (y-axis) as a function of time in response to infusion and withdrawal.

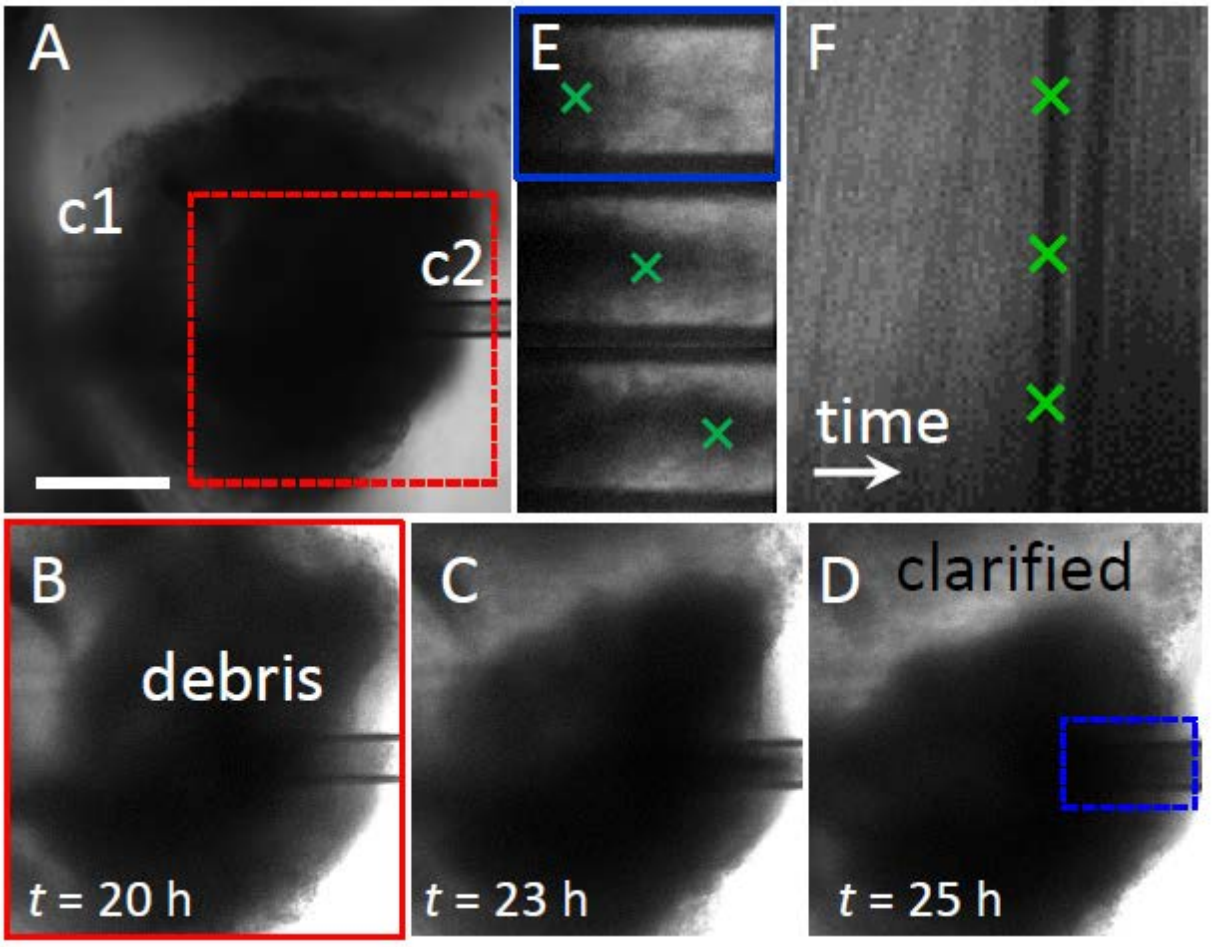

Fig. 4.5. Clearing waste with luminal flow. (A) *Microscopy image series*. Steady state luminal flow is established in an HIO with significant waste accumulation by setting q_{in} = q_{out} = 5 μL/h. Flow is from left to right. After 20 h, the HIO is still viable, and no blebbing or leaking is observed. (B-D) Over time, the HIO becomes more transparent as waste is carried by liquid flow through c2. Images correspond to region in (A), red dashed box. (E) Series of images of c2 depict movement of the waste exiting the organoid from left to right. Images correspond to region in (D), blue dashed box. (F) Kymograph representing the intensity profile along a line in the center of the channel in c2 (*y*-axis) plotted as a function of time (*x*-axis). The dark line indicated by the green crosses represents a large piece of waste moving from left to right along the channel. The slope of the line represents the velocity, v = 4.6 μm/min.

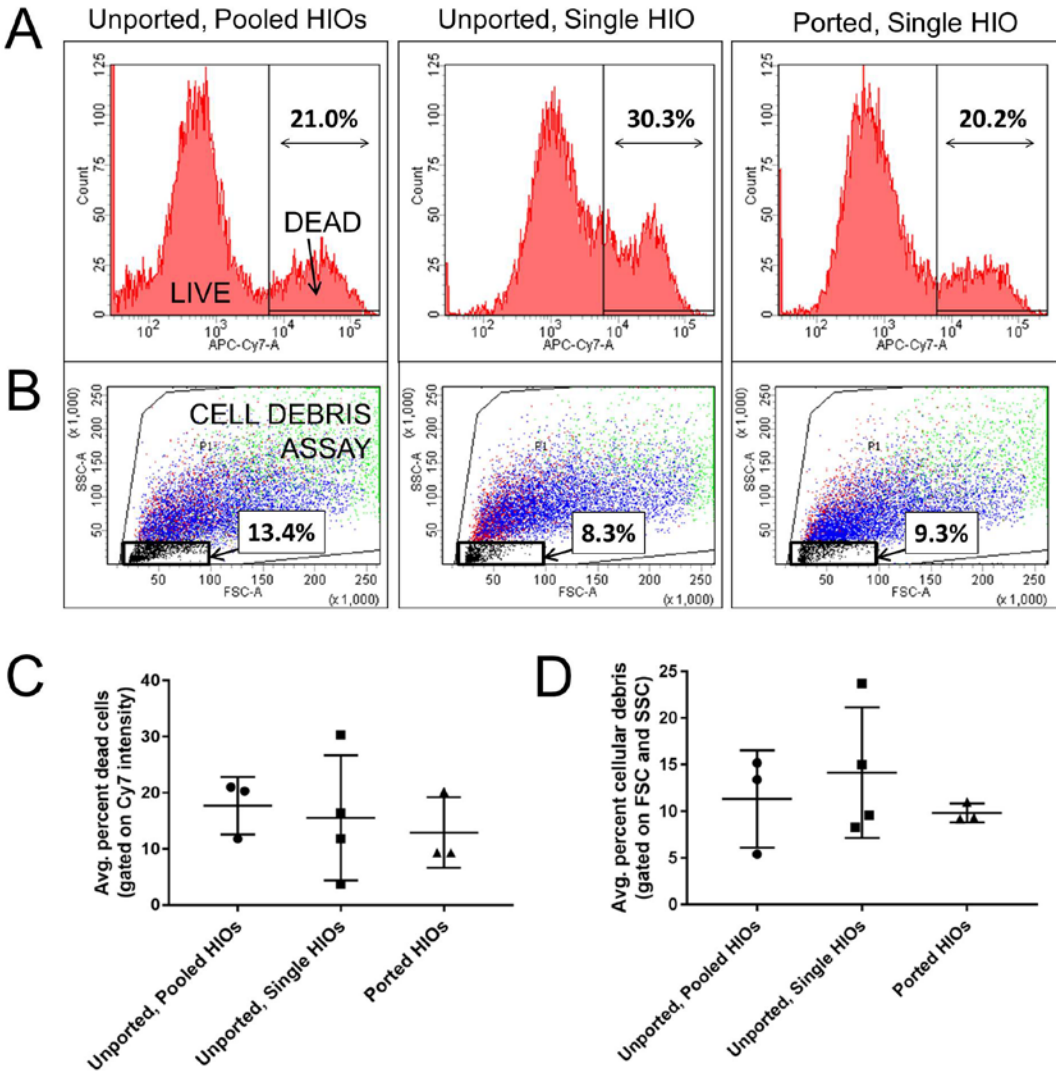

Fig. 4.6. Flow cytometry results show that HIO viability is not adversely affected by porting and luminal flow. (A) Representative flow cytometry histograms of near-IR fluorescence intensity (APC-Cy7-A) from homogenized HIOs reveal two populations of cells: live (low intensity) and dead (high intensity). (B) Forward (FSC) and side (SSC) scattering at low intensities provide a measure of cellular debris as indicated by the black box and percentage values. (C) The average percent of dead cells present in HIOs that were either unported or ported, as determined by the LIVE/DEAD cell staining data represented in (A). (D) The average percent of cell debris present in HIOs that were either unported or ported, as determined by the scattering data represented in (A).

SUPPLEMENTAL INFORMATION

Table of Contents:

1. GOFlowChip Assembly and Loading Protocol

A. Sterilization:

- Individual device pieces including acrylic layers, silicone seals, ferrules, glass capillaries, syringes, microfluidic connectors, and microfluidic tubing are immersed in pure ethanol for at least five minutes.
- After sterilization in ethanol, the pieces are dried in a laminar flow biohazard hood. The following assembly procedure is conducted in the hood to maintain sterility.

B. Assembly:

- Two micromanipulator and four screws are attached loosely to platform base to allow for further adjustments (see SI Fig. 1 below).
- The middle acrylic layer, flow-through gaskets, and gasket cap are assembled. The small diameter gasket must be attached to middle layer followed by the bigger diameter gasket and cap (SI Fig. 2A-C).
- Bottom layer consisting 8 screws is placed on top of the platform with 4 screws (SI Fig. 3A).
- O-ring is inserted in place on the bottom acrylic layer of the device followed by the middle layer with side port assemblies, and the over-flow channel gasket (SI Fig. 3B-E).
- Needle holder(s) is attached to micromanipulator leaving not more than a 1 mm gap between the side port entrance and needle tip (SI Fig. 4).

C. Filling with Liquid:

- The luminal inlet flow syringe (glass, 500 μL, Hamilton) fitted with a Luer lock connection is attached to a three-way connector (Kimble, nylon 3-way stopcock), filled with the appropriate liquid (e.g. media or PBS), then attached to the microfluidic tubing (Scientific Commodities Inc. PE/9, 1.40mm I.D. 1.91mm O.D.), before attaching to the pulled glass inlet capillary (c1). Care is taken throughout the process to remove air bubbles.

- The same process above is repeated for the luminal outlet flow syringe and the extraluminal inlet flow syringe.
- The over-flow outlet can remain partially filled with liquid as this channel will be used to remove air bubbles from the device after porting and before pressurization.

D. HIO Loading:

- To coat the bottom of the HIO well, approximately 10-20 μL of pre-chilled liquid Matrigel previously held in an ice bath is added to the center well and allowed to solidify for several minutes at room temperature. The total volume of the well is 60-100 μL, so the gel should only form a thin layer on the bottom of the well.
- The device, including the central well and side ports, is filled with media to prevent air interfaces or bubbles from forming and remaining in the device after sealing.
- Glass needles mounted on micromanipulators are guided through the side ports but are not forced all the way into the well.
- After removing any bubbles, the HIO is loaded into the center well using a P1000 pipette with a truncated tip.
- Once the HIO is placed in the central well, the top layer is placed on top of the middle layer with a silicone gasket between the two. As the top layer is laid onto the device, the end nearest the overflow channel inlet should be brought into contact with the middle layer first. As the opposite end of the upper layer is brought into contact with the middle layer, air will be forced out through the outlet of the overflow channel.
- Nuts should be rotated onto the screws but care should be taken to avoid over compressing the device before the porting procedure.

E. Preparation for Porting:

- The device is moved to a microscope with an environmental chamber.
- Syringes are loaded into syringe pumps and syringe pumps are pre-programmed.
- Liquid is flushed through overflow channel to ensure the remove of trapped air bubbles. During this step, a small amount of liquid may leak from the side ports as the device is not yet completely sealed.
- A glass capillary (50 μm tip diameter) is attached to the end of the overflow channel outlet tubing to slightly pressurize the device when flow is initiated.

F. HIO Porting:

- The glass inlet capillary (c1), mounted on a micromanipulator, is translated in through the side port until the HIO shell is punctured. Successful puncturing of the shell is readily observable as the shell pops back from being deformed by the capillary.

- The glass outlet capillary (c2) is inserted similarly to c1. c2 is larger in diameter than c1, so greater pressure is required to puncture the HIO shell; however the Matrigel and c1 provide enough support for the larger diameter needle to puncture the organoid without allowing it to be pushed to the wall of the organoid chamber.
- At this point, the nuts are tightened to compress the silicone and seal the device.
- Over flow is initiated by starting the syringe pump.
- The syringe pump driving flow through c1 should be initiated with 1 μL pulsating injections. Swelling of the HIO should be observed to confirm successful porting of the HIO.
- Similarly, the syringe pump withdrawing flow through c2 should be initiated with 1 μL pulsating withdrawals to confirm successful porting of the HIO.
- If porting is confirmed in c1 and c2, luminal flow through is initiated by setting $q1 = q2$.

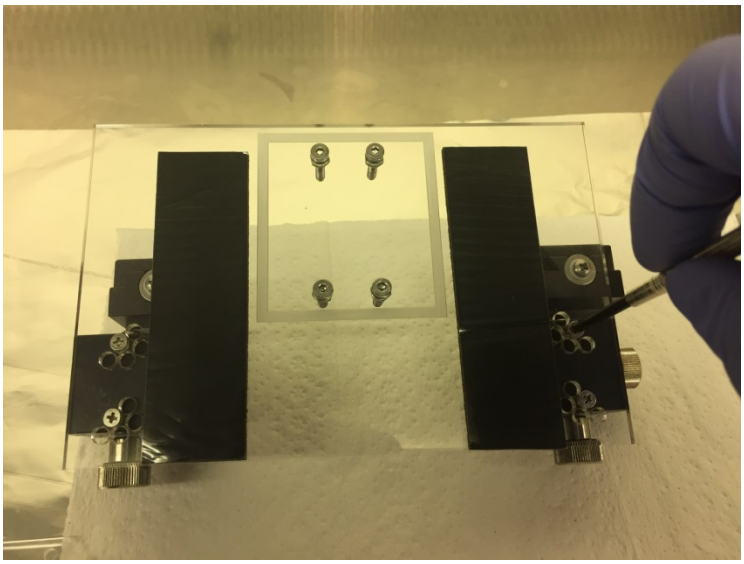

SI Fig. 1: Image of platform base (upside down) with four screws inserted.

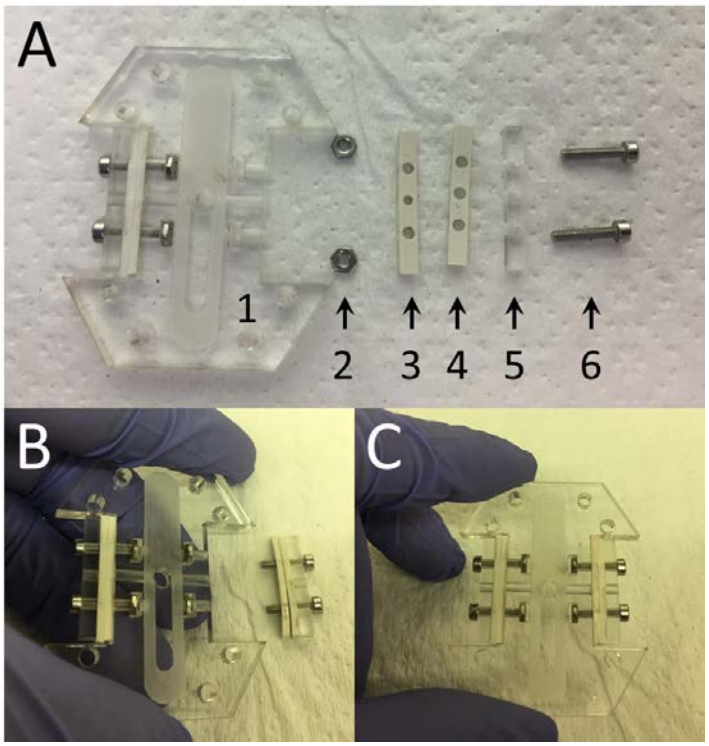

SI Fig. 2: (**A**) Image of parts needed to put together the side port assembly: (1) middle acrylic layer, (2) nuts, (3) inner, small-diameter gasket, (4) outer, larger-diameter gasket, (5) acrylic gasket cap, (6) bolts. The side port assembly on the left has already been assembled. (**B**, **C**) After assembling parts (3-6), the nuts are placed into recessed holds and the assembly is screwed into place.

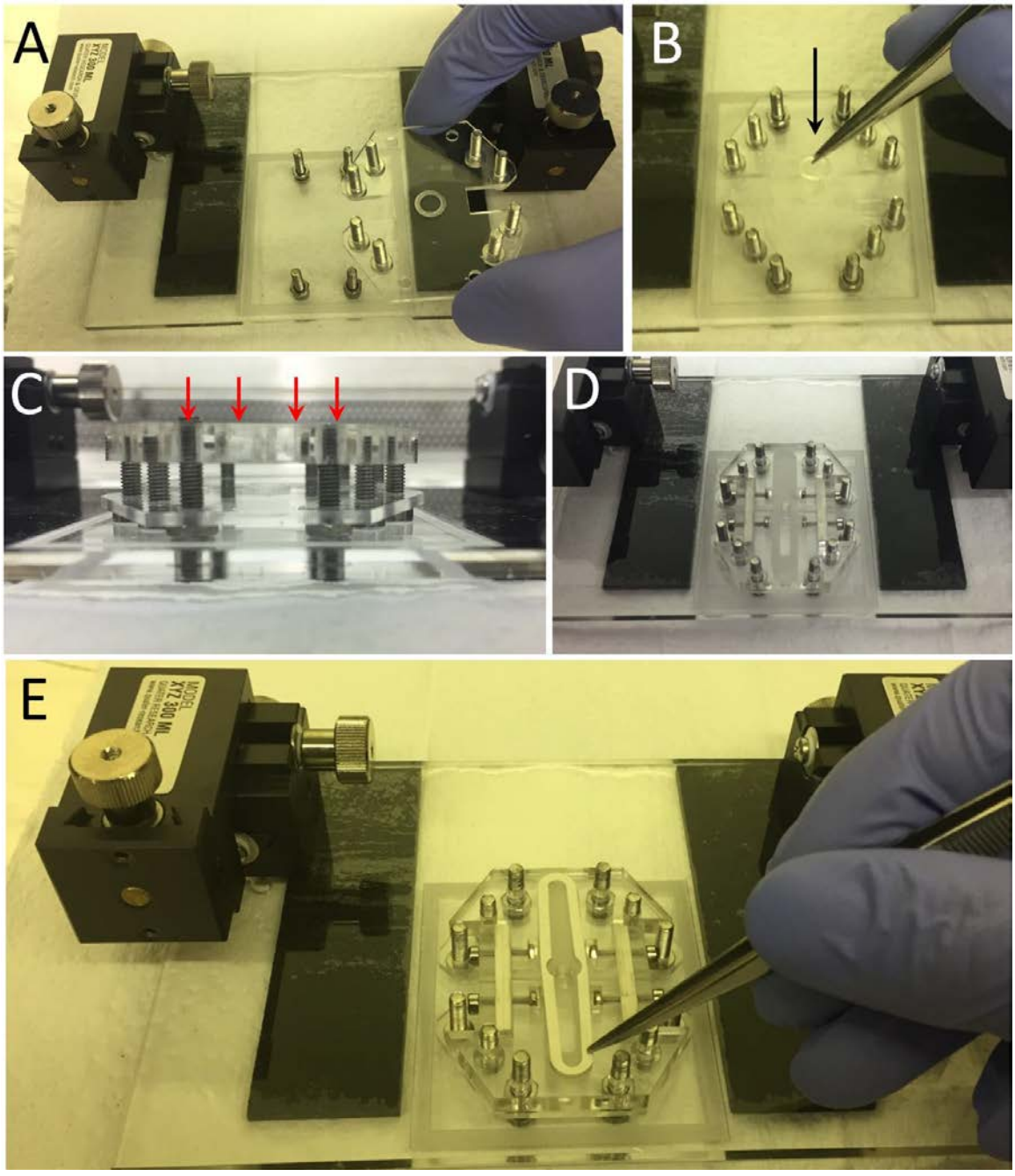

SI Fig. 3: (**A**) Bottom acrylic layer consisting 8 screws is socketed on top of the platform that has 4 screws. (**B**) O-ring (arrow) is inserted into recessed holder on top of bottom acrylic piece. (**C**) Middle acrylic layer with side port assemblies attached is placed on top of the bottom acrylic piece, with the o-ring sandwiched between. Red arrows indicate middle piece is moving down. Device assembly before (**D**) and after (**E**) placement of the over flow gasket into the recessed portion of the layer.

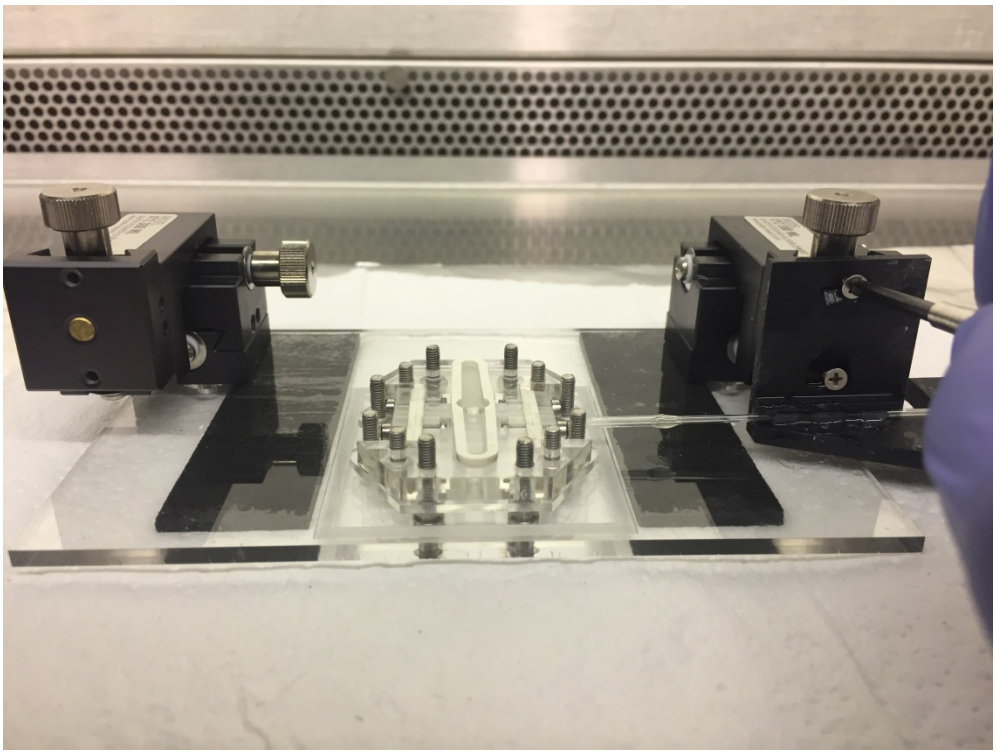

SI Fig. 4: Black 3D-printed needle holder(s) with attached capillary is attached to micromanipulator. The tip of each capillary needle should be approximately 1 mm from the side port entrance. The same process is repeated for the left-hand side.

2. Additional Practical Considerations for Porting and Establishing Luminal Flow

Through extensive optimization and device design iteration, and while attempting to port approximately 50-70 HIOs, we identified the two most common problems associated with porting and flow to be (1) issues encountered during HIO puncture and (2) clogging of the exit capillary during long-term flow. These two problems occur in roughly the same frequency.

Puncturing problems occur for two main reasons. First, poor alignment of the capillary needle with the side port and with the HIO can lead to breaking of the capillary or missing the HIO entirely during attempted puncture. Once an HIO has been placed in the device well and adhered to the Matrigel in the bottom of the well, it is difficult to relocate without damaging the HIO or rupturing the epithelial shell. Second, difficulty in puncturing an HIO can arise due to heterogeneities in the mesenchymal layer on the outside of the HIO; regions with a thicker mesenchymal layer provide greater resistance to puncture. Here, pressure applied to puncture the HIO with the capillary may dislodge the HIO, driving it to the opposite side of the well, and often leading to HIO rupture. These problems could be mitigated by the use of optics with improved perception in the z-axis.

As briefly mentioned in the bulk manuscript, clogging problems occur when luminal waste blocks the lumen of the exit capillary. While we have been able to minimize this effect by using a capillary tip diameter of $d \approx 80$ μm and a flow rate $q_{out} \leq 5$ μL/h, clogging still occurs in approximately 50% of ported HIOs over $t = 65$ h, which means that ported HIOs should be monitored and flow rates adjusted if clogging occurs. In the future, clogging could be minimized in a number of ways: (1) by porting HIOs before substantial amounts of luminal waste accumulate, (2) by introducing enzymes or chemicals to degrade the luminal waste, (3) by replacing syringe pumps with pressure-driven flow regulators that can sense and adjust to pressure buildup.

3. SI Video Descriptions

SI Video 1: Time-lapse microscopy video of an HIO embedded in Matrigel and imaged for 25 hours. Cellular debris accumulates over time and settles to the inner, bottom surface of the HIO due to gravity. Video corresponds to the images series in Figure 1a.

SI Video 2: Time-lapse microscopy video of an HIO swelling due to a net influx of liquid (q_{in} = 5 μL/h; q_{out} = 0 μL/h). No leaking from the puncture site is observed. Video corresponds to the images series in Figure 4a, and the length of the video spans 120 minutes.

SI Video 3: Time-lapse microscopy video of an HIO undergoing striking volume changes in response to oscillations in the net influx of liquid. Video corresponds to the images series in Figure 4b, c and the flow conditions plotted in Figure 4d.

SI Video 4: Time-lapse microscopy video of steady state luminal flow through an HIO for $t \geq 65$ h using both a single, double-lumen capillary device.

SI Video 5: Time-lapse microscopy video of steady state luminal flow through an HIO for $t \geq 65$ h using both a double, single-lumen capillary device.

SI Video 6: Time-lapse microscopy video of waste being swept from the luminal space of an HIO over a time period of approximately 27 hours. At the 20 h mark, the image was refocused revealing the removal of waste from the HIO. Video corresponds to the images series in Figure 5a-d.

SI Video 7: Time-lapse microscopy video of a digitally-zoomed region from Supplementary Video 6 reveals the movement of large objects moving out through the exit capillary as they are carried by liquid flow. Video corresponds the series of microscopy images in Figure 5e, f, and the length of the video spans 152 minutes.

4. SI Flow Cytometry

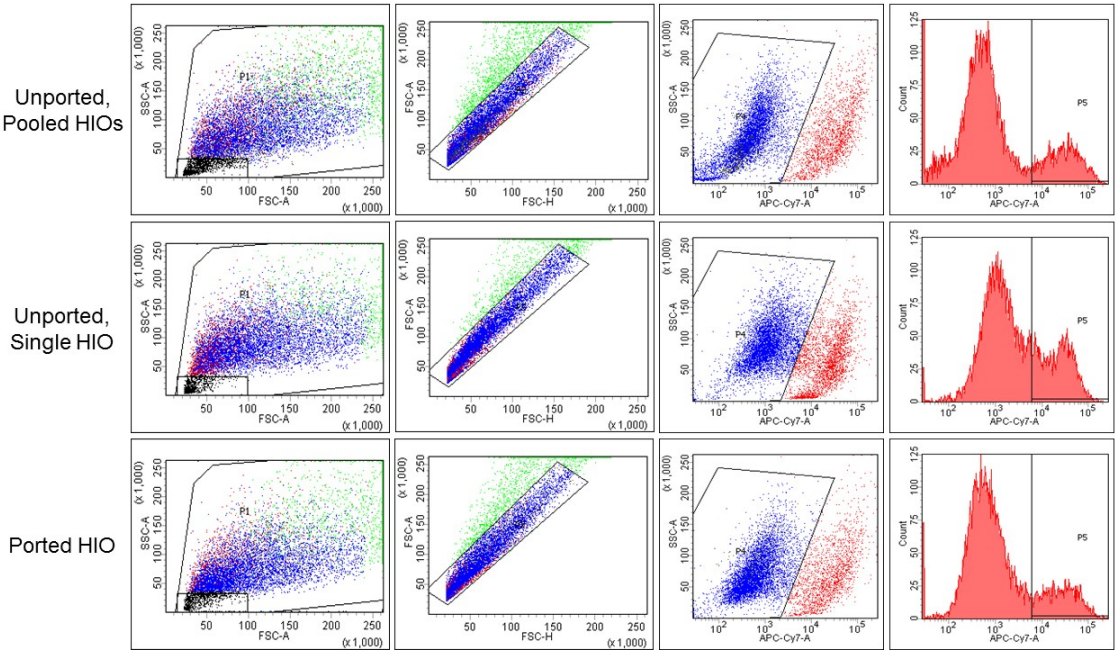

SI Fig. 5. Additional flow cytometry plots to demonstrate gating decisions and live/dead stain analysis. (**Panel 1, left**) Cells are first analyzed and gated based on forward scatter area (FSC-A) and side scatter area (SSC-A) profiles. Cells that have very small FSC-A and SSC-A profiles are considered mostly cell fragments, cell debris, and dead cells that are captured as a sub-population, shown in black on the bottom left. (**Panel 2, mid-left**) FSC-height (FSC-H) and FSC-A are then used to gate around singlets and also to exclude doublets and clumps of cells. (**Panel 3, mid-right**) The intensity of the emitted infrared staining of single cells after excitation is indicated on the x-axis using the APC-Cy7-A setting and plotted against SSC-A. (**Panel 4, right**) A histogram of the counts of single cells across the spectrum of APC-Cy7-A emitted infrared staining. Dead cells were gated based on the manufacturer's guidelines and an overall assessment of the staining profiles of all data. The exact same gating parameters were applied to all datasets.

LITERATURE CITED

1. Spence JR, *et al.* (2011) Directed differentiation of human pluripotent stem cells into intestinal tissue in vitro. *Nature* 470(7332):105-109.

2. Sato T, *et al.* (2011) Long-term Expansion of Epithelial Organoids From Human Colon, Adenoma, Adenocarcinoma, and Barrett's Epithelium. *Gastroenterology* 141(5):1762-1772.

3. Hill DR, *et al.* (2017) Bacterial colonization stimulates a complex physiological response in the immature human intestinal epithelium. *Elife* 6.

4. Finkbeiner SR, *et al.* (2012) Stem Cell-Derived Human Intestinal Organoids as an Infection Model for Rotaviruses. *Mbio* 3(4).

5. Lindemans CA, *et al.* (2015) Interleukin-22 promotes intestinal-stem-cell-mediated epithelial regeneration. *Nature* 528(7583):560-+.

6. Nozaki K, *et al.* (2016) Co-culture with intestinal epithelial organoids allows efficient expansion and motility analysis of intraepithelial lymphocytes. *J Gastroenterol* 51(3):206-213.

7. Wells JM & Spence JR (2014) How to make an intestine. *Development* 141(4):752-760.

8. Aurora M & Spence JR (2016) hPSC-derived lung and intestinal organoids as models of human fetal tissue. *Dev Biol* 420(2):230-238.

9. Dedhia PH, Bertaux-Skeirik N, Zavros Y, & Spence JR (2016) Organoid Models of Human Gastrointestinal Development and Disease. *Gastroenterology* 150(5):1098-1112.

10. Forbester JL, *et al.* (2015) Interaction of Salmonella enterica Serovar Typhimurium with Intestinal Organoids Derived from Human Induced Pluripotent Stem Cells. *Infect Immun* 83(7):2926-2934.

11. Leslie JL, *et al.* (2015) Persistence and Toxin Production by Clostridium difficile within Human Intestinal Organoids Result in Disruption of Epithelial Paracellular Barrier Function. *Infect Immun* 83(1):138-145.

12. Engevik MA, *et al.* (2015) Human Clostridium difficile infection: altered mucus production and composition. *Am J Physiol-Gastr L* 308(6):G510-G524.

13. Sinagoga KL & Wells JM (2015) Generating human intestinal tissues from pluripotent stem cells to study development and disease. *Embo J* 34(9):1149-1163.

14. Finkbeiner Stacy R, *et al.* (2015) Transcriptome-wide Analysis Reveals Hallmarks of Human Intestine Development and Maturation In Vitro and In Vivo. *Stem Cell Reports* 4(6):1140-1155.

15. Buckley A & Turner JR (2018) Cell Biology of Tight Junction Barrier Regulation and Mucosal Disease. *Csh Perspect Biol* 10(1).

16. Hill DR, Huang S, Tsai YH, Spence JR, & Young VB (2017) Real-time Measurement of Epithelial Barrier Permeability in Human Intestinal Organoids. *J Vis Exp* (130).

17. Gray H & Standring S (2008) *Gray's anatomy: the anatomical basis of clinical practice* (Churchill Livingstone).

18. Sebrell TA, *et al.* (2018) Live imaging analysis of human gastric epithelial spheroids reveals spontaneous rupture, rotation and fusion events. *Cell and Tissue Research* 371(2):293-307.

19. Cruz-Acuña R, *et al.* (2017) Synthetic hydrogels for human intestinal organoid generation and colonic wound repair. *Nature Cell Biology* 19:1326.

20. Cruz-Acuña R, *et al.* (2018) PEG-4MAL hydrogels for human organoid generation, culture, and in vivo delivery. *Nature protocols* 13(9):2102-2119.

21. Capeling MM, *et al.* (2019) Nonadhesive Alginate Hydrogels Support Growth of Pluripotent Stem Cell-Derived Intestinal Organoids. *Stem Cell Reports* 12(2):381-394.

22. Zachos NC, *et al.* (2016) Human Enteroids/Colonoids and Intestinal Organoids Functionally Recapitulate Normal Intestinal Physiology and Pathophysiology. *J Biol Chem* 291(8):3759-3766.

23. McCracken KW, Howell JC, Wells JM, & Spence JR (2011) Generating human intestinal tissue from pluripotent stem cells in vitro. *Nature protocols* 6(12):1920-1928.

24. deMello AJ (2006) Control and detection of chemical reactions in microfluidic systems. *Nature* 442(7101):394-402.

25. El-Ali J, Sorger PK, & Jensen KF (2006) Cells on chips. *Nature* 442(7101):403-411.

26. Maschmeyer I, *et al.* (2015) A four-organ-chip for interconnected long-term co-culture of human intestine, liver, skin and kidney equivalents. *Lab Chip* 15(12):2688-2699.

27. Baudoin R, Griscom L, Monge M, Legallais C, & Leclerc E (2007) Development of a renal microchip for in vitro distal tubule models. *Biotechnol Progr* 23(5):1245-1253.

28. Jang KJ, *et al.* (2013) Human kidney proximal tubule-on-a-chip for drug transport and nephrotoxicity assessment. *Integr Biol-Uk* 5(9):1119-1129.

29. Jang KJ & Suh KY (2010) A multi-layer microfluidic device for efficient culture and analysis of renal tubular cells. *Lab Chip* 10(1):36-42.

30. Snouber LC, *et al.* (2012) Analysis of transcriptomic and proteomic profiles demonstrates improved Madin-Darby canine kidney cell function in a renal microfluidic biochip. *Biotechnol Progr* 28(2):474-484.

31. Agarwal A, Goss JA, Cho A, McCain ML, & Parker KK (2013) Microfluidic heart on a chip for higher throughput pharmacological studies. *Lab Chip* 13(18):3599-3608.

32. Cheng W, Klauke N, Sedgwick H, Smith GL, & Cooper JM (2006) Metabolic monitoring of the electrically stimulated single heart cell within a microfluidic platform. *Lab Chip* 6(11):1424-1431.

33. Giridharan GA, *et al.* (2010) Microfluidic Cardiac Cell Culture Model (mu CCCM). *Anal Chem* 82(18):7581-7587.

34. Grosberg A, Alford PW, McCain ML, & Parker KK (2011) Ensembles of engineered cardiac tissues for physiological and pharmacological study: Heart on a chip. *Lab Chip* 11(24):4165-4173.

35. Khanal G, Chung K, Solis-Wever X, Johnson B, & Pappas D (2011) Ischemia/reperfusion injury of primary porcine cardiomyocytes in a low-shear microfluidic culture and analysis device. *Analyst* 136(17):3519-3526.

36. Nguyen MD, *et al.* (2015) Effects of Physiologic Mechanical Stimulation on Embryonic Chick Cardiomyocytes Using a Microfluidic Cardiac Cell Culture Model. *Anal Chem* 87(4):2107-2113.

37. Fritsche CS, *et al.* (2009) Pulmonary tissue engineering using dual-compartment polymer scaffolds with integrated vascular tree. *Int J Artif Organs* 32(10):701-710.

38. Henry OYF, *et al.* (2017) Organs-on-chips with integrated electrodes for trans-epithelial electrical resistance (TEER) measurements of human epithelial barrier function. *Lab Chip* 17(13):2264-2271.

39. Huh D, *et al.* (2007) Acoustically detectable cellular-level lung injury induced by fluid mechanical stresses in microfluidic airway systems. *P Natl Acad Sci USA* 104(48):18886-18891.

40. Huh D, *et al.* (2012) A Human Disease Model of Drug Toxicity-Induced Pulmonary Edema in a Lung-on-a-Chip Microdevice. *Sci Transl Med* 4(159).

41. Huh D, *et al.* (2010) Reconstituting Organ-Level Lung Functions on a Chip. *Science* 328(5986):1662-1668.

42. Sin A, *et al.* (2004) The design and fabrication of three-chamber microscale cell culture analog devices with integrated dissolved oxygen sensors. *Biotechnol Progr* 20(1):338-345.

43. Tavana H, Zamankhan P, Christensen PJ, Grotberg JB, & Takayama S (2011) Epithelium damage and protection during reopening of occluded airways in a physiologic microfluidic pulmonary airway model. *Biomed Microdevices* 13(4):731-742.

44. Shah P, *et al.* (2016) A microfluidics-based in vitro model of the gastrointestinal human–microbe interface. *Nature Communications* 7:11535.

45. Chen WLK, *et al.* (2017) Integrated Gut/Liver Microphysiological Systems Elucidates Inflammatory Inter-Tissue Crosstalk. *Biotechnol Bioeng* 114(11):2648-2659.

46. Esch MB, *et al.* (2012) On chip porous polymer membranes for integration of gastrointestinal tract epithelium with microfluidic 'body-on-a-chip' devices. *Biomed Microdevices* 14(5):895-906.

47. Kim HJ, Huh D, Hamilton G, & Ingber DE (2012) Human gut-on-a-chip inhabited by microbial flora that experiences intestinal peristalsis-like motions and flow. *Lab Chip* 12(12):2165-2174.

48. Kim HJ & Ingber DE (2013) Gut-on-a-Chip microenvironment induces human intestinal cells to undergo villus differentiation. *Integr Biol-Uk* 5(9):1130-1140.

49. Lee DW, Ha SK, Choi I, & Sung JH (2017) 3D gut-liver chip with a PK model for prediction of first-pass metabolism. *Biomed Microdevices* 19(4).

50. Mahler GJ, Esch MB, Glahn RP, & Shuler ML (2009) Characterization of a Gastrointestinal Tract Microscale Cell Culture Analog Used to Predict Drug Toxicity. *Biotechnol Bioeng* 104(1):193-205.

51. Allen JW & Bhatia SN (2003) Formation of steady-state oxygen gradients in vitro - Application to liver zonation. *Biotechnol Bioeng* 82(3):253-262.

52. Carraro A, *et al.* (2008) In vitro analysis of a hepatic device with intrinsic microvascular-based channels. *Biomed Microdevices* 10(6):795-805.

53. Chao P, Maguire T, Novik E, Cheng KC, & Yarmush ML (2009) Evaluation of a microfluidic based cell culture platform with primary human hepatocytes for the prediction of hepatic clearance in human. *Biochem Pharmacol* 78(6):625-632.

54. Cheng S, Prot JM, Leclerc E, & Bois FY (2012) Zonation related function and ubiquitination regulation in human hepatocellular carcinoma cells in dynamic vs. static culture conditions. *Bmc Genomics* 13.

55. Kane BJ, Zinner MJ, Yarmush ML, & Toner M (2006) Liver-specific functional studies in a microfluidic array of primary mammalian hepatocytes. *Anal Chem* 78(13):4291-4298.

56. Lee PJ, Hung PJ, & Lee LP (2007) An artificial liver sinusoid with a microfluidic endothelial-like barrier for primary hepatocyte culture. *Biotechnol Bioeng* 97(5):1340-1346.

57. Legendre A, *et al.* (2013) Metabolic Characterization of Primary Rat Hepatocytes Cultivated in Parallel Microfluidic Biochips. *J Pharm Sci-Us* 102(9):3264-3276.

58. Novik E, Maguire TJ, Chao PY, Cheng KC, & Yarmush ML (2010) A microfluidic hepatic coculture platform for cell-based drug metabolism studies. *Biochem Pharmacol* 79(7):1036-1044.

59. Sivaraman A, *et al.* (2005) A microscale in vitro physiological model of the liver: Predictive screens for drug metabolism and enzyme induction. *Curr Drug Metab* 6(6):569-591.

60. Toh YC, *et al.* (2009) A microfluidic 3D hepatocyte chip for drug toxicity testing. *Lab Chip* 9(14):2026-2035.

61. Viravaidya K & Shuler ML (2004) Incorporation of 3T3-L1 cells to mimic bioaccumulation in a microscale cell culture analog device for toxicity studies. *Biotechnol Progr* 20(2):590-597.

62. Esch MB, *et al.* (2015) Multi-cellular 3D human primary liver cell culture elevates metabolic activity under fluidic flow. *Lab Chip* 15(10):2269-2277.

63. Booth R & Kim H (2012) Characterization of a microfluidic in vitro model of the blood-brain barrier (mu BBB). *Lab Chip* 12(10):1784-1792.

64. Liu MC, *et al.* (2013) Electrofluidic pressure sensor embedded microfluidic device: a study of endothelial cells under hydrostatic pressure and shear stress combinations. *Lab Chip* 13(9):1743-1753.

65. Shin M, *et al.* (2004) Endothelialized networks with a vascular geometry in microfabricated poly(dimethyl siloxane). *Biomed Microdevices* 6(4):269-278.

66. Park SH, *et al.* (2012) Chip-Based Comparison of the Osteogenesis of Human Bone Marrow- and Adipose Tissue-Derived Mesenchymal Stem Cells under Mechanical Stimulation. *Plos One* 7(9).

67. Zhang WT, Lee WY, Siegel DS, Tolias P, & Zilberberg J (2014) Patient-Specific 3D Microfluidic Tissue Model for Multiple Myeloma. *Tissue Eng Part C-Me* 20(8):663-670.

68. Zhang Y, Gazit Z, Pelled G, Gazit D, & Vunjak-Novakovic G (2011) Patterning osteogenesis by inducible gene expression in microfluidic culture systems. *Integr Biol-Uk* 3(1):39-47.

69. Torisawa YS, *et al.* (2014) Bone marrow-on-a-chip replicates hematopoietic niche physiology in vitro. *Nat Methods* 11(6):663-+.

70. Park HS, Liu S, McDonald J, Thakor N, & Yang IH (2013) Neuromuscular Junction in a Microfluidic Device. *Ieee Eng Med Bio*:2833-2835.

71. Shi MJ, *et al.* (2013) Glia co-culture with neurons in microfluidic platforms promotes the formation and stabilization of synaptic contacts. *Lab Chip* 13(15):3008-3021.

72. Tsantoulas C, *et al.* (2013) Probing Functional Properties of Nociceptive Axons Using a Microfluidic Culture System. *Plos One* 8(11).

73. van de Wijdeven R, *et al.* (2018) Structuring a multi-nodal neural network in vitro within a novel design microfluidic chip. *Biomed Microdevices* 20(1).

74. Xiao RR, *et al.* (2013) Simultaneous Generation of Gradients with Gradually Changed Slope in a Microfluidic Device for Quantifying Axon Response. *Anal Chem* 85(16):7842-7850.

75. Ziegler L, Grigoryan S, Yang IH, Thakor NV, & Goldstein RS (2011) Efficient Generation of Schwann Cells from Human Embryonic Stem Cell-Derived Neurospheres. *Stem Cell Rev Rep* 7(2):394-403.

76. Grosberg A, *et al.* (2012) Muscle on a chip: In vitro contractility assays for smooth and striated muscle. *J Pharmacol Tox Met* 65(3):126-135.

77. Puleo CM, Ambrose WM, Takezawa T, Elisseeff J, & Wang TH (2009) Integration and application of vitrified collagen in multilayered microfluidic devices for corneal microtissue culture. *Lab Chip* 9(22):3221-3227.

78. Wang YQ, Wang L, Guo YQ, Zhu YJ, & Qin JH (2018) Engineering stem cell-derived 3D brain organoids in a perfusable organ-on-a-chip system. *Rsc Adv* 8(3):1677-1685.

79. Skardal A, *et al.* (2017) Multi-tissue interactions in an integrated three-tissue organ-on-a-chip platform. *Sci Rep-Uk* 7.

80. Zhang YS, *et al.* (2017) Multisensor-integrated organs-on-chips platform for automated and continual in situ monitoring of organoid behaviors. *P Natl Acad Sci USA* 114(12):E2293-E2302.

81. Schweinlin M, *et al.* (2016) Development of an Advanced Primary Human In Vitro Model of the Small Intestine. *Tissue Eng Part C-Me* 22(9):873-883.

82. Workman MJ, *et al.* (2018) Enhanced Utilization of Induced Pluripotent Stem Cell–Derived Human Intestinal Organoids Using Microengineered Chips. *Cellular and Molecular Gastroenterology and Hepatology* 5(4):669-677.e662.

83. Marshall LE, Koomullil R, Frost AR, & Berry JL (2017) Computational and Experimental Analysis of Fluid Transport Through Three-Dimensional Collagen-Matrigel Hydrogels. *Ann Biomed Eng* 45(4):1027-1038.

84. Miura T & Tanaka R (2009) In vitro Vasculogenesis Models Revisited Measurement of VEGF Diffusion in Matrigel. *Math Model Nat Pheno* 4(4):118-130.

85. Wang YT, *et al.* (2015) Regional gastrointestinal transit and pH studied in 215 healthy volunteers using the wireless motility capsule: influence of age, gender, study country and testing protocol. *Aliment Pharm Ther* 42(6):761-772.

86. Stevens CE & Hume ID (1995) *Comparative physiology of the vertebrate digestive system* (Cambridge University Press, Cambridge ; New York) 2nd Ed pp xvi, 400 p.

87. Meng ZJ, *et al.* (2015) Plug-n-play microfluidic systems from flexible assembly of glass-based flow-control modules. *Lab Chip* 15(8):1869-1878.

88. Girabawe C & Fraden S (2017) An image-driven drop-on-demand system. *Sensor Actuat B-Chem* 238:532-539.

89. Lowrey LG (1911) Prenatal Growth of the Pigs. *The American Journal of Anatomy* 12:131.

90. Chou CC (1983) Contribution of Splanchnic Circulation to Overall Cardiovascular and Metabolic Homeostasis - Introduction. *Fed Proc* 42(6):1656-1657.

91. Baraki YM, Traverso P, Elariny HA, & Fang Y (2010) Preoperative prediction of stomach weight to be removed in laparoscopic sleeve gastrectomy procedure. *Surg Technol Int* 20:167-171.

92. John W. Calvert DJL (2012) Overview of Cardiac Muscle Physiology. *Muscle*, ed Joseph A. Hill ENO (Academic Press), Vol 1, pp 57-66.

CHAPTER 5

A NOVEL GASTRIC SPHEROID CO-CULTURE MODEL REVEALS CHEMOKINE-DEPENDENT RECRUITMENT OF HUMAN DENDRITIC CELLS TO THE GASTRIC EPITHELIUM

Contribution of Authors and Co-Authors

Manuscript in Chapter 5

Author: Thomas A. Sebrell

Contributions: Designed and performed the experiments, analyzed the data, wrote and edited the manuscript.

Author: Marziah Hashimi

Contributions: Designed and performed the experiments, analyzed the data, wrote and edited the manuscript.

Co-Author: Barkan Sidar

Contributions: Designed and performed the experiments

Co-Author: Royce Wilkinson

Contributions: Designed and performed the experiments

Co-Author: Liliya Kirpotina

Contributions: Designed and performed the experiments

Co-Author: Mark T. Quinn

Contributions: Wrote and edited the manuscript, provided funding for the study.

Co-Author: Zeynep Malkoç

Contributions: Analyzed the data.

Co-Author: Paul J. Taylor

Contributions: Designed and provided the EmbryoCradle microinjector, provided funding for the study.

Co-Author: James N. Wilking

Contributions: Supervised the experimental work, provided funding for the study.

Co-Author: Diane Bimczok

Contributions: Designed and performed the experiments, supervised the experimental work, analyzed the data, wrote and edited the manuscript, provided funding for the study.

Manuscript Information

Thomas A. Sebrell, Marziah Hashimi, Barkan Sidar, Royce Wilkinson, Liliya Kirpotina,

Mark T. Quinn, Zeynep Malkoç, Paul J. Taylor, James N. Wilking, Diane Bimczok

Cellular and Molecular Gastroenterology and Hepatology

Status of Manuscript:
____ Prepared for submission to a peer-reviewed journal
____ Officially submitted to a peer-reviewed journal
__X_ Accepted by a peer-reviewed journal
____ Published in a peer-reviewed journal

Accepted for Publication by Elsevier Inc.
20 February 2019

Correspondence: Dr. Diane Bimczok, diane.bimczok@montana.edu, Address: 2155 Analysis Drive, Bozeman, MT, 59717, USA; Phone: 406-994-4928, Fax: 406-994-3953

Disclosures: Dr. Paul Taylor is the owner of GeneSearch, Inc., Bozeman, MT, which manufactures the EmbryoCradle microinjector that was used in this study. None of the other authors declare a conflict of interest. The funding agencies played no role in study design, collection, analysis, or interpretation of data.

Synopsis: Human gastric spheroids recruited DCs to the basolateral surface of the epithelium through a chemokine-dependent mechanism and established tight contacts with the DCs. *H. pylori* infection of the organoids increased DC recruitment and enabled DC phagocytosis of the bacteria.

Grant support: Funding for our study was provided by the National Institutes of Health grants K01 DK097144 (DB); R03 DK107960 (DB), the National Science Foundation, DMR-1455247 (JW), and the Montana University System Research Initiative 51040-MUSRI2015-03 (DB). We greatly appreciate support from the National Institutes of Health IDeA Program grant P30 GM110732 (DB, MQ). GeneSearch, Inc. development of the GeneSearch Embryo Cradle was funded by an SBIR grant from ORIP/NIH R44 OD012083 (PJT).

Abbreviations: CFU, colony-forming unit; DC, dendritic cell; IL-1β, interleukin 1 beta; IRB, Institutional Review Board; MALT, mucosa-associated lymphoid tissue; MNP, mononuclear phagocyte; MoDC, monocyte-derived DC; NDRI, National Disease Research Interchange; PBMC, peripheral blood mononuclear cell; TNF-α, tumor necrosis factor alpha., TSLP, thymic stromal lymphopoietin

ABSTRACT

Background & Aims: Gastric dendritic cells (DCs) control the adaptive response to infection with *Helicobacter pylori*, a major risk factor for peptic ulcer disease and gastric cancer. We hypothesize that DC interactions with the gastric epithelium position gastric DCs for uptake of luminal *H. pylori* and promote DC responses to epithelial-derived mediators. The aim of this study was to determine whether the gastric epithelium actively recruits DCs, using a novel co-culture model of human gastric epithelial spheroids and monocyte-derived DCs.

Methods: Spheroid cultures of primary gastric epithelial cells were infected with *H. pylori* by microinjection. Co cultures were established by adding human monocyte-derived DCs (MoDCs) to the spheroid cultures and were analyzed for DC recruitment and antigen uptake by confocal microscopy. Protein array, gene expression PCR array and chemotaxis assays were used to identify epithelial-derived chemotactic factors that attract DCs. Data from the co-culture model were confirmed using human gastric tissue samples.

Results: Human MoDCs co-cultured with gastric spheroids spontaneously migrated to the gastric epithelium, established tight interactions with the epithelial cells and phagocytosed luminally applied *H. pylori*. DC recruitment was increased upon *H. pylori* infection of the spheroids and involved the activity of multiple chemokines including CXCL1, CXCL16, CXCL17 and CCL20. Enhanced chemokine expression and DC recruitment to the gastric epithelium was also observed in *H. pylori*-infected human gastric tissue samples.

Conclusions: Our results indicate that the gastric epithelium actively recruits DCs for immunosurveillance and pathogen sampling through chemokine-dependent mechanisms, with increased recruitment upon active *H. pylori* infection.

Keywords: Stomach, organoid, mononuclear phagocyte, *in vitro* model

INTRODUCTION

Infection with the gastric pathogen *Helicobacter pylori* is the leading cause of chronic gastritis, peptic ulcer disease, MALT lymphoma and gastric adenocarcinoma worldwide(1, 2). Dendritic cells (DCs) in the human gastric mucosa are thought to be the major antigen-presenting cells that induce protective immune responses to *H. pylori* infection(3). We previously showed that human HLA-DR^{high} gastric mononuclear phagocytes (MNPs) with functional properties of DCs were present directly adjacent to the gastric epithelium or integrated within the gastric epithelium(4). In a mouse model of *Helicobacter* infection, increased numbers of CD11c^{+} DCs migrated to the epithelial layer and extended projections between the gastric epithelial cells(5). These interactions between DCs and the epithelium likely promote sampling of *H. pylori* bacteria from the gastric lumen. Close association with the epithelium also positions the DCs for uptake of *H. pylori* antigen that may have crossed the epithelial barrier into the gastric lamina propria. Furthermore, bi-directional crosstalk between gastric mucosal DCs and epithelial cells contributes to the maintenance of gastric homeostasis, as we have shown(6, 7).

A recent study performed in murine small intestine showed that MNP recruitment to the epithelium at steady state is dependent on CCR6 and is required for luminal antigen access(8). However, the mechanisms that determine how human gastric DCs are recruited and retained by the gastric epithelium are currently unclear. Therefore, we developed an *in vitro* co-culture model of human gastric spheroids and monocyte-derived

DCs (MoDCs) to study the mechanisms of gastric DC – epithelial interactions in primary human cells.

Transwell-based co-culture systems have provided crucial insights into the interactions of the gastrointestinal epithelium with pathogens and immune cells(9-12). In a groundbreaking study by Rescigno et al.(9), DCs were shown to open the tight junctions between epithelial cells, send dendrites outside the epithelium and directly sample bacteria from the luminal side of the colonic epithelium. Co-culture studies also have revealed the importance of TGF-β and thymic stromal lymphopoietin (TSLP) for the homeostatic conditioning of intestinal DCs by the epithelium(10, 12). However, traditional co-culture systems have several drawbacks. First, epithelial monolayers for co-culture studies are generally derived from transformed cell lines such as Caco2 cells that differ in their phenotype and function from primary epithelial cells. Second, epithelial cells in co-culture systems are usually cultured on transwell inserts composed of a synthetic polymer membrane with pores. This membrane presents an artificial barrier that impairs and limits the contact between immune cells and the epithelium. Third, to promote contacts between DCs and the basolateral side of the epithelium, DCs are either placed on the basolateral side of inverted transwells, so that they move towards the epithelium due to gravity(10, 13), or epithelial cells are seeded on top of the DCs(14), also leading to forced interactions.

In two recent studies, researchers have started to utilize organoids as an improved epithelial cell model to investigate epithelial interactions with immune cells(15, 16). Our co-culture model of human gastric epithelial spheroids and MoDCs lead to the

spontaneous establishment of direct interactions between DCs and the basolateral side of the gastric epithelium. Using this model, we showed that DCs added to gastric epithelial spheroid cultures spontaneously migrated towards the epithelium to establish tight contacts. DC migration was dependent on epithelial chemokine secretion and was enhanced in the presence of luminal *H. pylori* infection. Moreover, DCs were able to phagocytose *H. pylori* applied to the spheroid lumen. These functionally relevant findings indicate that our primary cell co-culture model is suitable for studies of gastric infection and epithelial-immune cell interactions and will allow us to advance our understanding of human gastric immunobiology.

RESULTS

Human Dendritic Cells are Recruited to the Epithelium of Gastric Spheroids

In order to perform functional studies of human DC interactions with the gastric epithelium, we generated gastric epithelial spheroids from adult stomach tissue and then established co-cultures with human DCs by adding immature MoDCs to the culture medium surrounding the epithelial spheroids (**Fig. 1A**). Although DCs appeared to accumulate at the border between the tissue culture medium and the spheroid-containing Matrigel plug to some extent (**Fig. 1B**), a considerable number of DCs rapidly entered the Matrigel matrix and associated with the organoids. Live imaging of spheroids and CellTracker™ Green-labeled MoDCs revealed that DCs spontaneously migrated toward the epithelium of the spheroids and accumulated around the basolateral side of the gastric epithelium (**Fig. 1C**). Importantly, particle tracking analysis showed directed migration

of the DCs towards the basolateral side of the epithelial cells (**Fig. 1D**). In fact, some gastric spheroid-associated DCs were detected as early as 10 min after initiation of the experiment (**Fig. 1E**).

MoDCs Establish Direct Contacts with Co-Cultured Astric Epithelial Spheroids

To analyze the interactions between human gastric epithelial spheroids and co-cultured DCs in more detail, we performed high-resolution confocal imaging of co-cultures. DCs were frequently present directly adjacent to the basolateral side of the epithelium (**Fig. 2A-C**). Specifically, MoDCs formed direct contacts with the epithelium and extended long dendrites along the basolateral side of the gastric epithelium (**Fig. 2D-F**). In some instances, dendrites with globular endings were extended between the epithelial cells (**Fig. 2F**). These dendrites were morphologically similar to the transepithelial dendrites formed by DCs in the stomach and intestine *in vivo* and in other co-culture systems(5, 9, 15, 17, 18). Notably, some MoDCs contained mCherry-positive cytoplasmic inclusions (**Fig. 2E**), possibly representing phagocytosed material derived from apoptotic gastric epithelium(7). Interestingly, we also detected DCs that had migrated into the spheroid lumen in 7/159 (4.4%) of spheroids analyzed (data not shown). Overall, these observations indicate that DCs in our co-culture model spontaneously establish interactions with the gastric epithelium.

H. pylori Infection of Guman Gastric Epithelial Spheroids Induced an Increased Recruitment of DCs to the Ggastric Epithelium

To determine the effects of luminal *H. pylori* infection on DC recruitment to the spheroid epithelium, we performed microinjection of gastric spheroids with *H. pylori*.

Successful injections were confirmed by re-plating a small proportion of dissociated spheroids at the end of the experiment. Recovery of significant numbers of viable bacteria was achieved consistently after 48 h, but bacterial numbers varied widely between experiments (**Fig. 3A**). In contrast, *H. pylori* was unable to survive when injected directly into Matrigel, and we also were unable to recover viable bacteria from the media surrounding the injected organoids (not shown). Interestingly, bacterial recovery was lower in cultures where DCs were present than in cultures of infected organoids alone (**Fig. 3A**). Luminal oxygen concentrations in the gastric spheroids were significantly reduced compared to the surrounding Matrigel, possibly supporting growth of the microaerophilic *H. pylori* (**Fig. 3B**). These data are consistent with earlier reports showing that human intestinal organoids have reduced luminal oxygen levels(19).

We next performed confocal imaging analysis of DCs co-cultured with GFP-*H. pylori*-infected or mock-injected gastric spheroids (**Fig. 3D**). DCs were added 2 – 3 h after *H. pylori* infection of the spheroids. After 48 h, a significantly higher number of DCs were detected in close proximity to *H. pylori*-infected spheroids compared to non-infected spheroids (**Fig. 3C, E**). We also compared DC recruitment by gastric spheroids injected with *H. pylori* 60190 to DC recruitment by spheroids injected with the TLR5 agonist *Salmonella* flagellin, which consistently induced spheroid activation as determined based on CXCL8 gene expression (**Fig. 3F**). FITC-dextran was injected as a fluorescent tracer in order to identify injected organoids that remained intact throughout the experiment. TLR stimulation caused a slight, but not significant increase in DC recruitment (**Fig. 3G**). Interestingly, however, infection of the organoids with a CagA-

negative deletion mutant of *H. pylori* 60190(20) did not enhance DC accumulation above baseline (**Fig. 3G**). Intensity analysis of FITC-dextran fluorescence showed no difference between treatments, indicating that the injected substances did not significantly alter epithelial barrier function (data not shown). Overall, these observations suggest that *H. pylori* infection promotes DC recruitment to the gastric epithelium, likely through a mechanism that involves *H. pylori* -dependent release of chemotactic factors by the epithelial cells.

Gastric Epithelial-Derived Chemokines Induce DC Recruitment

To determine the mechanism for DC recruitment to the gastric epithelium, we analyzed supernatants from gastric spheroid cultures in transwell chemotaxis assays. MoDCs were significantly recruited by supernatants from uninfected spheroid supernatants (**Fig. 4A**), consistent with the data obtained by microscopic analysis of the MoDC-gastric spheroid co-cultures. Moreover, *H. pylori* infection of the spheroids significantly increased the chemotactic index of MoDCs towards spheroid culture supernatants (**Fig. 4B**), corroborating the confocal microscopy data shown in Fig. 3. Notably, we did not observe significant chemokinetic activity of MoDCs in response to gastric spheroid supernatants (data not shown). Addition of pertussis toxin (PTX, 10 μg/mL), which blocks G-protein-dependent signaling, significantly reduced DC recruitment by both *H. pylori*-infected and non-infected spheroids, suggesting that DC recruitment is mediated by chemokine-dependent mechanisms (**Fig. 4C**).

To identify the chemokines involved in both steady state and infection-induced recruitment of DCs to the gastric epithelium, we performed a chemokine antibody array

with supernatants from non-infected and *H. pylori* infected gastric spheroids. Using this approach, we detected baseline secretion of CXCL5, CXCL17, CCL20, CXCL8 (IL-8), CXCL16, CXCL1 and midkine (neurite growth-promoting factor 2) ≥2-fold above background levels present in spheroid media, with considerable variations between spheroid lines (**Fig. 4D and Supplemental Table 1**). Spheroid infection with *H. pylori* significantly increased the secretion of CCL20 and consistently upregulated CXCL1 and CXCL8 by the gastric epithelium, whereas CXCL16, CXCL17 and midkine were consistently decreased in the presence of *H. pylori.*

We also analyzed the effect of *H. pylori* infection of human gastric spheroids on chemokine gene expression using an RT^2 Profiler™ RT-PCR gene expression array (**Fig. 4E and Supplemental Table 2**). Overall, gene expression patterns largely matched protein secretion data. CXCL1, CXCL2 and CXCL8 were significantly upregulated after 3 h of *H. pylori* stimulation in three independent experiments ($P \leq 0.05$), confirming the results from previous studies(21, 22) CCL2, CCL20, CXCL3 and CXCL6 were also consistently upregulated ≥2-fold in *H. pylori*-infected spheroids, but the magnitude of upregulation varied widely. No significant downregulation of was observed for any of the genes analyzed.

Having shown that luminal application of wild type *H. pylori* but not of CagA-deficient *H. pylori* or *Salmonella* flagellin induced an accumulation of DC immediately around the organoid (**Fig. 3G**), we next compared the chemotactic activity and the chemokine profile of supernatants recovered from spheroids treated with broth alone, wild type *H. pylori*, CagA-deficient *H. pylori* and flagellin. Similar to our observations

with the co-cultures, wild type *H. pylori* was the most efficient at inducing DC chemotaxis ($P \leq 0.01$), but the CagA-deficient *H. pylori* also induced significant DC migration in the trasnwell assay ($P \leq 0.05$), whereas no significant effects were observed for flagellin application (**Fig. 4F**). Analysis of chemokines in the culture supernatants showed inconsistent changes in the chemokine profiles between the different treatment groups (**Fig. 4G**). Chemokines induced by the CagA-deficient *H. pylori* largely followed the same pattern as those induced by wild type *H. pylori*, with similar CCL20 and CXCL1 release, but significantly lower CXCL8 levels. In contrast, flagellin, caused higher CXCL8 release, but lower CCL20 release compared to wild type *H. pylori*. These observations suggest that a combination of redundantly active chemokines control DC recruitment to the gastric epithelium.

Human MoDCs Show Chemotactic Responses to CXCL1, CXCL16, CXCL17 and CCL20

Having demonstrated that gastric spheroids release factors with chemotactic activity for human DCs and that multiple chemokines, including CXCL5, CXCL17, CCL20, CXCL8, CXCL16, CXCL1, are released basolaterally by gastric spheroids, we tested the ability of human MoDCs to migrate towards these chemokines (**Fig. 5A-F**). In transwell chemotaxis assays, the DCs showed a strong and significant response to CXCL1 and CXCL16 (**Fig. 5E,F**) and a moderate response to CCL20 and CXCL17 (**Fig. 5C,E**). A weak chemotactic response was observed to CXCL5 and CXCL8 (**Fig. 5A,D**). Together with the observations shown in Fig. 4, these data indicate that DC recruitment to the epithelial interface involves the activity of multiple epithelial-derived chemokines

and that *H. pylori* infection of increases the immune cell recruitment to the epithelium by upregulating chemokine expression.

Human *H. pylori* Infection Increases Chemokine Expression and DC Recruitment to the Epithelium

To confirm the relevance of our *in vitro* data, we analyzed chemokine gene expression and epithelial DC recruitment in gastric tissues from *H. pylori*-infected and non-infected donors. Gene expression profiling data overall were consistent with protein and gene expression data obtained from gastric spheroids (**Fig. 6A**). CCL20, CXCL1, CXCL5 and CXCL8 were significantly upregulated ($P \leq 0.05$) in *H. pylori*-infected gastric body with and without atrophy and in *H. pylori*-infected gastric antrum without atrophy, and CCL20 and CXCL8 expression remained significantly increased in atrophic gastric antrum. We also detected significantly upregulated expression of several other chemokines such as CCL18 and CXCL10, predominantly in non-atrophic samples from gastric body. In contrast, *H. pylori* infection did not alter gene expression of CXCL17 and CXCL16 in any of the groups.

We next analyzed whether human *H. pylori* infection increases DC recruitment to the gastric epithelium *in situ*. As previously shown, DCs in the gastric mucosa frequently interact with the epithelium (**Fig. 6B**). Importantly, the number of both lamina propria DCs in direct contact with the gastric epithelium and the number of intraepithelial DCs was significantly increased in *H. pylori*-infected samples (**Fig. 6C,D**; $P=0.04$ and $P=0.01$, respectively).

Co-culture of MoDCs with *H. pylori*-Infected Gastric Epithelial Spheroids Results in DC Uptake of *H. pylori*

To determine whether DC-epithelial interactions in gastric spheroid-DC co-cultures enable the DCs to sample *H. pylori* antigens, we used high resolution confocal imaging. A significant percentage of MoDCs in *H. pylori*-infected co-cultures (1.8 ± 0.6%) contained GFP-positive material consistent with phagocytic uptake of *H. pylori* ($P \leq 0.05$), whereas green fluorescent material was generally absent from DCs in co-cultures that were not infected with GFP-*H. pylori* (**Fig. 7A-D**). Interestingly, 5.3 ± 1.3% of DCs in spheroid co-cultures contained CellTracker-labelled material of presumed epithelial origin (**Fig. 7E**), as shown in Fig. 2E. The proportion of these cells was significantly decreased upon *H. pylori* infection ($P \leq 0.05$). Overall, these results suggest that MoDCs co-cultured with gastric spheroids perform relevant phagocytic functions, as shown for mononuclear phagocytes in gastric tissues(7, 23).

DISCUSSION

The immunological mechanisms specific to the human stomach as a unique mucosal environment remain poorly understood. Specifically, it is unclear how antigen-presenting cells are recruited to and interact with the gastric epithelium in order to access *H. pylori* antigens. To address this knowledge gap, we have developed and evaluated a novel organotypic co-culture model based on primary human cells that enables functional studies of the interactions between the gastric epithelium, DCs and luminal *H. pylori* bacteria. With this model, we demonstrate that human DCs show chemotactic activity for epithelial-derived factors and form tight interactions with the epithelium.

Importantly, *H. pylori* infection of the gastric epithelium increased epithelial chemokine expression and DC recruitment to the epithelial interface, both in our co-culture model and in *H. pylori*-infected human subjects.

Crosstalk between MNP populations and epithelial cells at mucosal sites is important for immunosurveillance and mucosal imprinting of the MNPs by epithelial-derived factors (6, 24, 25). In our model, MoDCs co-cultured with gastric epithelial spheroids spontaneously migrated towards the gastric epithelium and established direct contacts with the epithelial cells. To establish contacts with the epithelium, the MoDCs actively penetrated the Matrigel within less than 30 min. DCs have been previously shown to migrate through Matrigel by using matrix metalloproteinases that degrade extracellular matrix components(26, 27). Once DCs have migrated towards the gastric epithelium, our co-cultures closely resembled the human gastric mucosa, where MNPs are present immediately beneath the epithelial cell layer and sometimes integrated into the epithelium(4, 7, 17). Moreover, the MoDCs extended dendrites in between epithelial cells that were morphologically similar to those previously reported to be involved in antigen uptake by MNPs in the small intestine(18, 28) and the stomach(5, 17). Possibly, the dendrites seen in our model enabled the observed phagocytosis of GFP-*H. pylori* bacteria in our study.

Notably, DCs were recruited to the epithelium in the absence of inflammation or infection, likely representing steady-state recruitment. Due to the short life span of mucosal DCs, constant DC recruitment is necessary to replace dying cells in order to maintain epithelial immunosurveillance(29). A similar steady state recruitment of DCs to

the epithelium was recently shown in the murine intestine(8). Importantly, we also showed that DC recruitment to the epithelial interface was increased upon *H. pylori* infection, both in our co-culture model and in gastric biopsies obtained from human donors. Our study thus confirms and extends previous reports that *H. pylori* infection induces gastric epithelial chemokine expression and significantly promotes MNP recruitment(4, 5, 30, 31). In the gastric mucosa, murine *Helicobacter* infection resulted in elevated numbers of $CD11c^{+}$ and $CD68^{+}$ cells(5, 30, 31), and we have previously detected increased numbers of HLA-DR^{high} MNPs upon human *H. pylori* infection(4). Here, we specifically demonstrated that increased numbers of gastric DCs interacted with the epithelial layer upon *H. pylori* infection. These increased interactions may have important functional implications for continuous luminal antigen sampling and for positioning DCs for antigen uptake when the epithelial barrier is compromised during *H. pylori* infection. Indeed, DCs co-cultured with *H. pylori*-infected spheroids showed evidence of *H. pylori* phagocytosis, again resembling the behavior of DCs in *H. pylori*-infected gastric mucosa, where *H. pylori* phagocytosis by gastric DCs was recently observed in a mouse model(23).

Interestingly, significantly higher numbers of DCs accumulated at the epithelium of spheroids infected with wild type *H. pylori* compared to CagA-deficient *H. pylori*. CagA is a major virulence factor of *H. pylori* that is injected into host cells through a type 4 secretion system and that activates a number of pro-inflammatory host signaling pathways including NF-κB, leading to enhanced chemokine secretion(32, 33). However, we did not see any clear differences in chemotactic activity of DCs towards supernatants

from spheroids infected with wild type versus CagA-deficient *H. pylori*. Although CXCL8 secretion by spheroids infected with CagA-deficient *H. pylori* was lower than that induced by wild type bacteria, confirming earlier studies(34), other chemokines with stronger chemotactic activity for DCs were unchanged or upregulated. Thus, the mechanism for the lack of DC recruitment in spheroid co-cultures infected with CagA-deficient *H. pylori* remains elusive. Mustapha et al. previously investigated *H. pylori*-dependent chemokine release using primary gastric epithelial cells and showed that disruption of the CagA T4SS significantly decreased chemokine gene expression after 3 h, but not after 24 h(35). Early differences in chemokine secretion may have contributed to altered DC recruitment towards infected spheroids, since co-cultures were established 2 – 3 h after injection, but these differences may have disappeared after 48 h, when spheroid supernatants were collected.

Using a combination of chemokine analysis in gastric spheroid supernatants, gene expression profiling of gastric spheroids, DC chemotaxis assays and gene expression analysis of human gastric tissues, we identified a number of chemokines that likely contribute to DC recruitment to the gastric epithelium under steady state conditions and during *H. pylori* infection. *CCL20* was identified as a chemokine that attracted DC and that was expressed by the gastric epithelium both at steady state and at increased levels upon *H. pylori* infection. *CCL20* has previously been shown to regulate steady-state DC recruitment to the epithelium in the murine small intestine(8). However, whether *CCL20* promotes recruitment of human DCs has been a matter of debate(36, 37). Here, we demonstrate that certain concentrations of *CCL20* did significantly promote DC

recruitment and may therefore contribute to both steady state and infection-induced DC recruitment in the stomach. Likewise, CXCL1 was secreted at high levels by the gastric epithelium at steady state, was upregulated during *H. pylori* infection at the protein and the RNA level and had significant chemotactic activity on human MoDCs. Thus, CXCL1 likely plays an important role in DC recruitment to the gastric epithelium. CXCL8 is a signature chemokine that activates CXCR2 for neutrophil recruitment and that is known to be upregulated upon gastric *H. pylori* infection(38, 39). We showed that CXCL8 was secreted at high levels by non-infected gastric spheroids, was upregulated upon *H. pylori* infection in a CagA-dependent manner and that CXCL8 also acts on DCs. Interestingly, we also demonstrated that gastric epithelial cells release significant amounts of CXCL5, CXCL16 and CXCL17, and that human DCs display chemotactic responses to both chemokines. However, *H. pylori* infection increased neither CXCL16 nor CXCL17, suggesting that CXCL16 and 17 play a role in steady state DC recruitment. Previous studies had demonstrated that activated DCs express CXCL16(40), but whether human DCs express the CXCL16 receptor CXCR6 and are responsive to CXCL16 has not yet been investigated. Likewise, how DCs respond to CXCL17 is currently unknown, since the receptor for this orphan chemokine has not yet been identified(41).

Taken together these observations suggest that steady state migration of DCs to the gastric epithelium involves CXCL1, 5, 8, 16, 17 and CCL20, whereas increased DC recruitment upon *H. pylori* infection is mostly driven by CXCL1, CCL20 and possibly CXCL8. Notably, it is unknown whether gastric DCs show chemotactic responses to the same chemokines as the MoDCs used in this study, and we were unable to perform

chemotaxis experiments with human gastric DCs, due to limited cell availability. However, we found that chemokine expression by gastric spheroids matched gene expression profiles detected in biopsies of *H. pylori*-infected human subjects, and DC recruitment to the epithelium was likewise increased both in our *in vitro* model and *in vivo*. These observations indicate that the results obtained with the spheroid-MoDC co-cultures were biologically relevant.

Notably, our model system is the first that utilizes organoid cultures of primary human gastric epithelial cells together with human DCs cells to study gastric immunobiology. A recent study by Noel et al.(15) used epithelial monolayers derived from human enteroids and showed that co-cultured macrophages enhanced epithelial barrier function. We have previously co-cultured human blood monocytes on the luminal surface of short term primary gastric epithelial cell cultures to demonstrate that human MNPs are conditioned by retinoic acid (RA) released by the gastric epithelium(6). However, unlike RA, most epithelial surface proteins and soluble mediators are expressed in a polar manner(15), so that DCs need to be added to the basolateral side of the epithelium to replicate the physiological orientation of the tissue. Most previous studies have utilized transwell systems, where epithelial cells are seeded on top of a porous membrane and DCs are added to the bottom compartment, to achieve the correct spatial relationship between epithelium and immune cells(9-13, 15, 42-44). Organoids, including epithelial spheroids and other 3-dimensional long-term culture systems of primary epithelial cells, have a closed lumen and a fully accessible basolateral side on the outside. Thus, our model allows spontaneous interactions between DCs that are added to

the cultures and the basolateral surface of the gastric epithelium in the absence of filter membranes. In a similar model, Nozaki et al. recently co-cultured murine intraepithelial lymphocytes (IELs) with small intestinal organoids and showed that dynamic interactions between IELs and the epithelium supported prolonged maintenance of the IELs in culture(16). Overall, our co-culture system has the advantages of using primary human gastric epithelial cells, allowing direct access of immune cells to the basolateral side of the epithelium, and supporting active *H. pylori* infection over several days and is therefore suitable for studying gastric epithelial cell – DC crosstalk *in vitro*. Moreover, we anticipate that the DC-epithelial cell co-culture model described here can be easily adapted for studying other mucosal sites, immune cells and pathogens.

We recognize that our new co-culture system still has certain limitations. Spheroids and organoids may occasionally rupture, releasing luminal material including infectious agents and apoptotic epithelial cell material and mucus in an uncontrolled manner(45). We addressed this issue by injecting FITC-dextran as a tracer into the spheroids. FITC dextran is rapidly released from the spheroid lumen upon rupture, as we have shown(45). Therefore, organoids that remained intact throughout the experiment could be identified based on the presence of the tracer. However, we still cannot rule out the presence of some *H. pylori* bacteria outside the gastric spheroids due to leakage during microinjection. One other limitation of any organoid culture system is that, unless cells are re-seeded on a transwell insert, it is impossible to determine epithelial cell numbers, and thus multiplicity of infection, with a high degree of accuracy, due to differences in size and shape of the organoids. Moreover, bacterial delivery into the

lumen of gastric spheroids by microinjection remains difficult to automate. In spite of these challenges, our co-culture system yielded reproducible and statistically significant results. Specifically, our experiments using gastric spheroid-MoDC co-cultures have demonstrated that the gastric epithelium promotes accelerated recruitment of DCs to the epithelial cell interface upon *H. pylori* infection through a chemokine-dependent mechanism.

METHODS

Human Blood and Tissue Samples

Blood samples for isolation of monocytes were obtained with local Institutional Review Board (IRB) approval from our healthy adult donor pool at Montana State University by a trained phlebotomist. Healthy human gastric tissue samples for the generation of spheroid lines were obtained with IRB approval as surgical resection material from sleeve gastrectomies from the National Disease Research Interchange (NDRI; Philadelphia, PA).

Gastric Epithelial Spheroid Cultures

Gastric epithelial spheroids were derived from human gastric glands and cultured in the presence of Wnt3a, noggin and R-spondin, as previously described(45). Lentiviral transduction was used to generate mCherry-expressing spheroid lines(45).

Monocyte-Derived Dendritic Cells (MoDCs)

$CD14^+$ monocytes were isolated from peripheral blood mononuclear cells using anti-human CD14 MACS beads (Miltenyi Biotec 130-050-201, Cologne, Germany), as previously described(46). All monocyte preparations were analyzed for activation based on cluster formation and spontaneous TNF-α release, and pre-activated cells were excluded from our experiments. Monocytes were then cultured in RPMI1640 medium supplemented with 10% human AB serum (Corning 35060CI, Manassas, VA), 100 U/L penicillin, 100 μg/L streptomycin (Gibco 15140-122), 50 μg/mL gentamycin (IBI Scientific IB2030, Peosta, IA), 5 mM Hepes (SH3023710), and 2 mM L-glutamine (SH30034.1) (both Hyclone, Logan, UT), 25 ng/mL rhGM-CSF (215-GM-050) and 7 ng/mL rhIL-4 (204-IL-050) (both R&D systems, Minneapolis, MN). After 5 – 6 days in culture, DCs were harvested by vigorous pipetting.

Gastric Epithelial Spheroid – DC Co-Cultures

In order to perform fluorescence imaging, co-cultures were set up using mCherry-expressing spheroid cultures and MoDCs stained with CellTracker™ Green (C7025) or CellTracker™ DeepRed (C34565) (both ThermoFisher Scientific, Waltham, MA). To establish DC – spheroid co-cultures, spheroid culture medium was replaced with antibiotic-free DC culture medium (RPMI1640 with 10% human AB serum). For each 35 mm MatTek culture plate containing approximately 80 spheroids, we then added 5 x 10^5 immature MoDCs directly to the medium overlaying the spheroids in the Matrigel.

Chemokine Detection

To analyze chemokine secretion by gastric spheroids, supernatants were collected from 24 well plates 48 h after medium change. Supernatants were then analyzed using the Proteome Profiler Human Chemokine Array Kit (ARY017; R&D Systems, Minneapolis, MN), which detects 31 different chemokines with specific monoclonal antibodies. Arrays were imaged on a FluorChem R System (Proteinsimple, San Jose, CA), and relative pixel densities of duplicate spots were measured using ImageJ software. Relative chemokine expression was calculated by normalizing results from spheroid supernatants to results obtained with spheroid growth medium alone.

Chemotaxis Assays

The chemotactic activity of MoDCs to spheroid supernatants and recombinant chemokines was in a measured in a transwell migration assay using the 96 well ChemoTX system with 5μm polycarbonate membrane (Neuro Probe, Inc., Gaithersburg, MD, 106-5). 1-2 x 10^5 MoDCs were incubated in triplicate for 4 h at 37, and viable migrated cells were counted using a CellTiter-Glo® Luminescent Cell Viability Assay (Promega, Madison, WI, G7570). Migration toward the following recombinant human chemokines was assessed: CXCL1 (300-11), CXCL5 (300-22), CXCL16 (300-55), CCL20 (300-29A, all from PeproTech, Rocky Hill, NJ); CXCL8 (208-IL, R&D Systems); CXCL17 (NBPS-35133, Novus Biologicals, Littleton, CO). The chemotactic index for recombinant chemokines was calculated by dividing the number of migrated cells for the experimental condition by the number of migrated cells in medium alone. Data from gastric spheroid supernatants were additionally normalized to the number of

epithelial cells present in the cultures, as determined by cell counting at the end of the experiment.

H. pylori Infection and TLR Agonist Treatment of Gastric Epithelial Spheroids

To establish *H. pylori* infection of the spheroids, we plated *H. pylori* strain 60190 wild type, a CagA-deficient mutant of strain 60190(47) (kind gifts from Dr. G. Perez-Perez) or the GFP-expressing strain M6 (kind gift from Dr. John Y. Kao) under microaerophilic conditions on Brucella agar, 5% horse blood (Becton Dickinson 221261) for 3 – 4 days. Spheroids for injection experiments were seeded on 35 mm MatTek dishes for 8 – 12 days, with the Matrigel applied as a thin streak to facilitate injection of multiple spheroids. Prior to injections, gastric epithelial spheroids were overlaid with antibiotic-free medium (3 media changes) for 3 days to prevent bacterial death. We selected spheroids with a diameter of 200 – 800 μm and used a GeneSearch Embryo Cradle micromanipulator (GeneSearch Inc., Bozeman, MT) and a 2 μL syringe (Hamilton Co., Reno, NV) for microinjection. Injection needles with beveled tips were pulled from glass capillaries to a tip size of 21-23 μm. We injected 20 – 80 organoids per culture with 0.2 μL of *H. pylori* suspension (2×10^5 bacteria) in Brucella broth, corresponding to a multiplicity of infection of 10 – 50, or with 1 μg/mL of *Salmonella* flagellin. Control spheroids were injected with Brucella broth alone. In some experiments, 0.2 μL of 25 μM 4 kDa FITC–dextran (Sigma-Aldrich, 46944, St. Louis, MO, USA) was added to the injection media as a fluorescent tracer. Successful *H. pylori* infection was confirmed by re-culturing bacteria recovered from trypsinized organoids on Brucella agar plates and performing colony counts. MoDCs were added to *H. pylori*-

infected spheroids after 2 – 3 h. To evaluate gastric epithelial cell responses to TLR agonist treatment, spheroids were-re-plated on collagen-coated 24-well plates (Biocoat, 08-772-71, Corning, Tewksbury, MA). Established monolayers were stimulated for 6 h with the Human TLR1-9 agonist kit containing the following: TLR1/2 Agonist: Pam3CSK4, TLR2 Agonist: HKLM, TLR3 Agonist: Poly(I:C), TLR3 Agonist: Poly(I:C)-LMW, TLR4 Agonist: LPS *E.coli* K12, TLR5 Agonist: Flagellin *S. typhimurium*, TLR6/2 Agonist: FSL1, TLR7 Agonist: Imiquimod, TLR8 Agonist: ssRNA40/LyoVec, TLR9 Agonist: ODN2006 (InVivoGen, tlrl-kit1hw, SanDiego, CA) and then were analyzed for *IL-8/CXCL8* gene expression using qRT-PCR, as previously described(48).

Oxygen Concentrations in Gastric Spheroids

Mock-injected spheroids were compared to spheroids infected with *H. pylori* bacteria for 3 h. Oxygen concentration profiles in the organoids were measured with an OX-25 Clark-type oxygen microelectrode with a 25 μm sensor tip diameter (Unisense A/S, Aarhus, Denmark). The microelectrode was connected to a Unisense microsensor multimeter and millivolt data was logged onto a laptop computer with Sensor Trace Pro software (Unisense). A motor-controlled micromanipulator (Unisense model MM33) was used to move the oxygen electrode during profile measurements. A two-point calibration was performed for O_2 sensors using buffer sparged with air and medium sparged with pure N_2(g) for at least 30 minutes. A Leica S80 APO stereomicroscope was used to visualize the microsensor tip and confirm placement on the organoid surface prior to profiling.

RT^2 Profiler™ PCR Array

To analyze the expression of chemokines, chemokine receptors and other related genes, we used the Human Chemokines & Receptors RT^2 Profiler™ PCR array (PAHS-022Z, Qiagen, Valencia, CA), following the manufacturer's instructions. RNA from *H. pylori*-infected (strain 60190) or control cultures was isolated using the Direct-zol Mini-RNA prep kit (Zymo Research R2052, Irvine, CA), and 0.15 – 0.5 μg of RNA was converted into cDNA. Arrays were run on a Lightcycler 96 (Roche, Penzberg, Germany) and were analyzed using the Qiagen Data Analysis Center online tool (www.qiagen.com), with a Ct cutoff of 35 and Beta-2-microglobulin and Ribosomal Protein Lateral Stalk Subunit P0 (RPLP0) used as housekeeping genes.

Immunofluorescence Analysis of Tissue Sections

Cryosections or a paraffin-embedded gastric tissue microarray(7) (kind gift from Dr. Paul Harris, Pontifical Catholic University of Chile, Santiago, Chile) prepared from human gastric tissue were labelled with anti-HLA-DR (cryosections: L243, BD 340689; tissue array: LN-3, Abcam ab166777) to stain DCs and with anti-cytokeratin-FITC (cryosections: CAM5.2, BD 347653; tissue array: C11, Cell Signaling Technology 4545) to stain epithelial cells, as previously described(4, 7). Cell nuclei were stained with DAPI. Samples were imaged on a Nikon Eclipse T2000-U fluorescent microscope equipped with a CoolSnap ES digital camera and NIS Elements BR2.30. ImageJ V1.48(49) was used to measure epithelial cell length and count DCs that were in direct contact with the epithelium.

Microscopy and Image Analysis

Epifluorescence and phase contrast images were acquired on a Nikon Eclipse T2000-U fluorescent microscope equipped with a CoolSnap ES digital camera and NIS Elements BR2.30 software or on a Life Technologies EVOS FL Auto system equipped with an onstage incubator. For confocal image analysis, we fixed the co-cultures with Cytofix Reagent (BD Biosciences 554655). Samples were imaged on an inverted Leica SP5 Confocal Scanning Laser Microscope (Leica, Wetzlar, Germany) with 405, 488, 561 and 633 nm laser excitation lines using a 20x objective or a 63x water immersion objective with Immersol (W 2010, Zeiss, Oberkochen, Germany). We recorded Z-stacks of 2 - 11 randomly selected organoids with intact morphology for each experiment and experimental condition. To quantitate MoDC recruitment to the epithelial interface, we used ImageJ version 1.48V(49), with the LOCI plugin to allow access to Leica .lif files. For analysis of DC recruitment, area and circumference of the spheroid were measured, and pixels positive for the DC dye CellTracker™ DeepRed (pseudocolored blue) were counted automatically on thresholded images. DCs that were within 75 μm of the basolateral side of the epithelium were considered epithelial cell-associated DCs. To determine MoDC uptake of *H. pylori* bacteria or epithelial cell-derived material, DCs with fluorescent inclusions were manually counted on individual confocal slices using the Cell Counter plugin, and the total number of DCs in an image stack was determined by counting the cells on a maximum Z-projection of the image stack.

Live Imaging Analysis and Particle Tracking

Live imaging was performed using a Life Technologies EVOS FL Auto system equipped with an onstage incubator. Fluorescence and phase contrast images were collected at 10 min intervals over 48 h using a 10x objective. The migration of cells toward gastric spheroids was analyzed using the Particle Tracking feature in Imaris version 8.4 (Bitplane, Zurich, Switzerland).

Gene Expression Analysis of Gastric Biopsies

Gene expression of relevant chemokines in gastric antral and corpus biopsies of non-*H. pylori* infected patients and *H. pylori*-infected patients with and without gastric atrophy (n=3 each) was analyzed using the Gene Expression Omnibus reference series GSE27411, data set records GDS5411 (body) and GDS 5338 (antrum)(50).

Data and Statistical Analysis

All authors had access to the data and have reviewed and approved the final manuscript. Data were analyzed using GraphPad Prism 7.02. Results are presented as mean ± SD. Differences between values were analyzed for statistical significance by the two-tailed Student's t-test, one- or two-way ANOVA or Kruskall-Wallis test with appropriate post hoc tests. Differences were considered significant at $P<0.05$.

ACKNOWLEDGEMENTS

Funding for our study was provided by the National Institutes of Health grants K01 DK097144 (DB); R03 DK107960 (DB), the IDeA Program grant GM110732 (DB, MQ), the National Science Foundation, DMR-1455247 (JW), and the Montana University System Research Initiative 51040-MUSRI2015-03 (DB, MQ). GeneSearch, Inc. development of the GeneSearch Embryo Cradle was funded by an SBIR grant from ORIP/NIH 5R44OD012083 (PJT). We would like to thank Dr. Ellen Lauchnor, MSU Department of Biological Engineering, for performing oxygen measurements in the spheroids, Dr. Paul Harris, Pontifical Catholic University of Chile, Santiago, Chile, for providing human gastric tissue microarrays, and Thea Sherwood for helping with MoDC preparation.

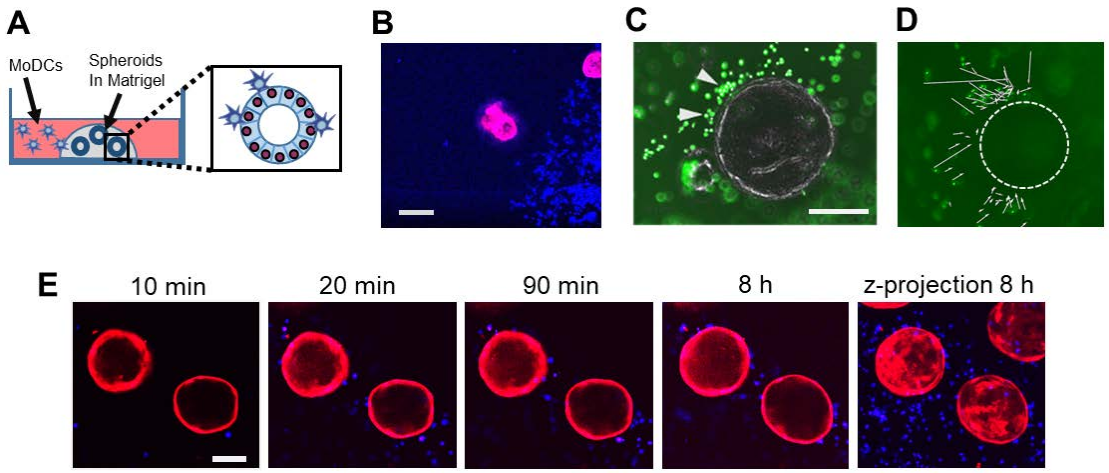

Figure 5.1. MoDCs spontaneously migrate to the basolateral side of the gastric epithelium upon co-culture with gastric spheroids. (A) Graphical representation of the DC-epithelial spheroid co-culture model. (B) Fluorescent confocal image of the bottom of a representative culture plate shows the Matrigel border with accumulated cells. CellTracker™ DeepRed-labeled DCs: blue; mCherry-expressing spheroids: red; bar: 200 µm. (C) Representative gastric spheroid with surrounding CellTracker™ Green-labeled MoDCs. Merge of phase contrast image and green fluorescent image. Arrowheads indicate accumulated MoDCs. Bar: 200 µm. (D) Particle tracking analysis of time lapse images shows DC tracks directed towards the spheroid. Dotted line indicates position of the spheroid. Images were acquired on an EVOS FL Auto system with a 10 x objective and are representative of 4 independent experiments. (E) Time lapse confocal imaging of mCherry-expressing gastric spheroids and CellTracker™ DeepRed-labeled MoDCs (blue) shows rapid recruitment of MoDCs to the spheroids. Single images obtained at different time points after initiation of the co-culture and a Z-stack projection of 50 slices obtained after 8 hours (right panel, step size 10 µm). Bar = 100 µm. All data are representative of 4 or more independent experiments performed with different spheroid lines and DC preparations.

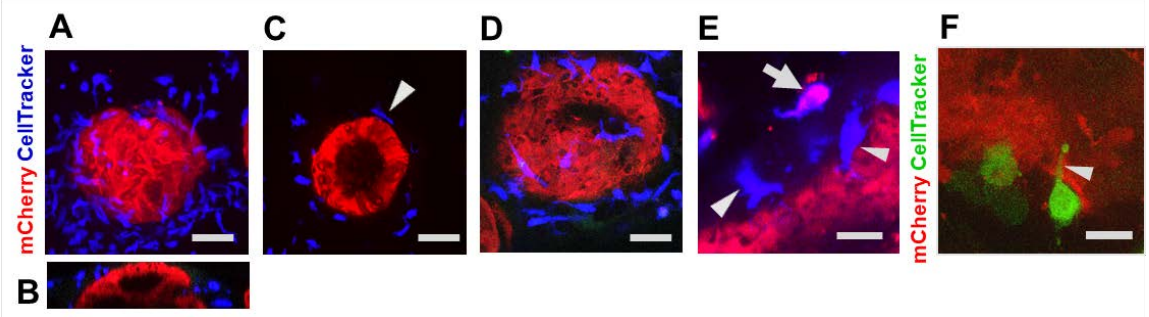

Figure 5.2. MoDCs directly associate with the epithelium of co-cultured gastric spheroids. CellTracker™-labeled MoDCs were added to cultures of mCherry expressing gastric spheroids. After 48 h, cultures were fixed and imaged on a Leica SP5 Confocal Scanning Laser Microscope using a 63x water immersion objective. (A-C) CellTracker™ DeepRed-labeled MoDCs (blue) that have migrated to the basolateral side of a gastric epithelial spheroid (red); bar: 50 µm. (A) XY image, maximum Z projection of 57 individual images, step size 1 µm. (B) XZ projection of the same spheroid. (C) Single XY slice shows physical association between a DC (arrowhead) and the spheroid. (D) Z-projection of 6 adjacent slices shows extensive dendrite formation on the surface of a gastric spheroid. (E) High resolution image showing CellTracker™ DeepRed-labeled MoDCs (blue) in direct contact with gastric epithelial cells (arrowheads) and one MoDC with internalized $mCherry^{+}$ gastric epithelial cell material (pink in merged image; arrow). Single XY slice, bar: 20 µm. (F) CellTracker™ Green-labeled MoDC (green) extending a dendrite (arrowhead) into the epithelial layer (red). XY image, Z projection of 4 adjacent slices; bar: 20 µm. All data are representative of 4 or more independent experiments performed with different spheroid lines and DC preparations.

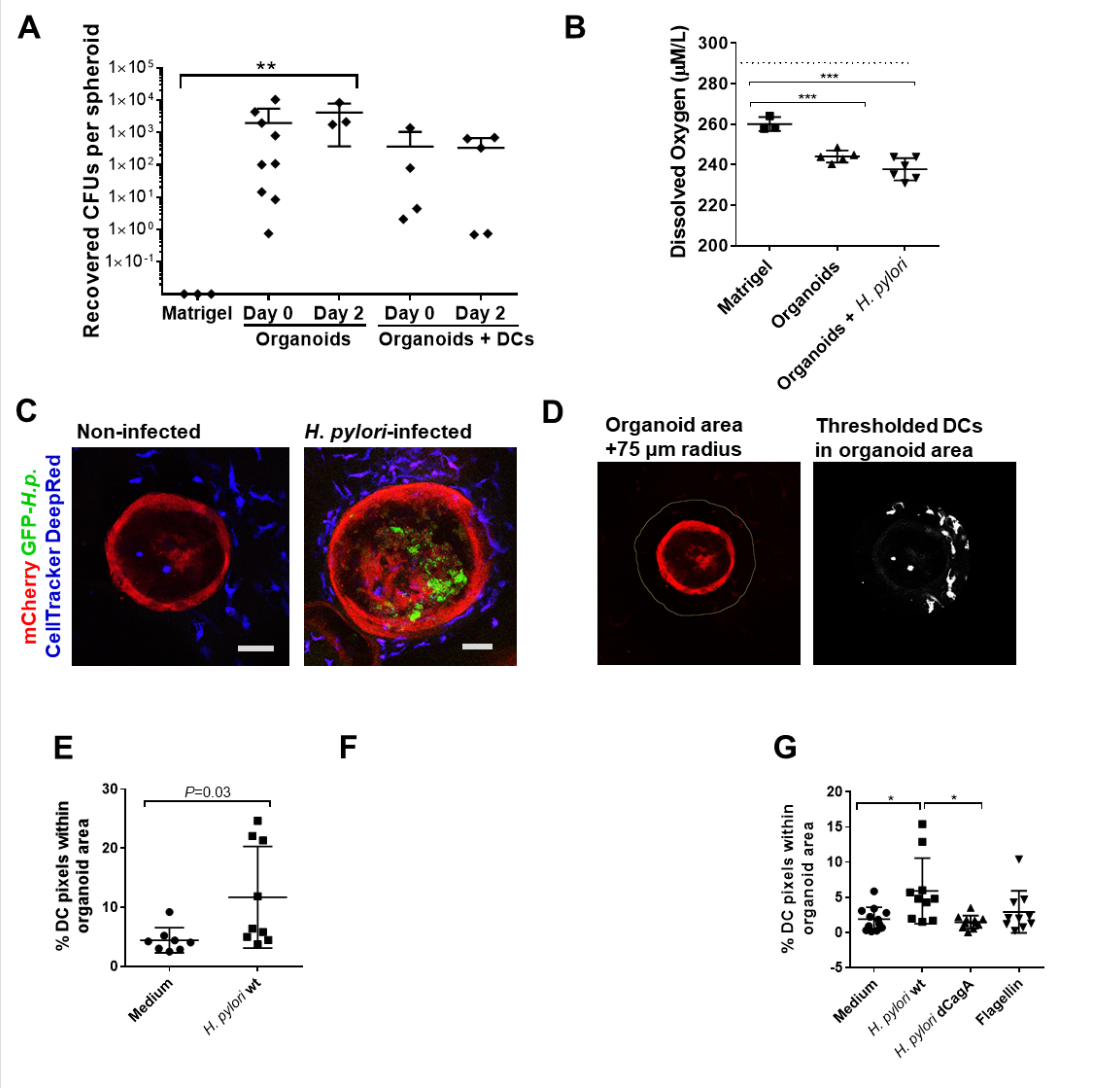

Figure 5.3. *H. pylori* infection of human gastric epithelial spheroids leads to increased DC recruitment. (A) Bacterial recovery from Matrigel alone or from *H. pylori*-infected gastric spheroids (20 – 50/culture) with or without co-cultured MoDCs present. Spheroid cultures were disrupted by trypsinization within the first 3 h after *H. pylori* infection or 48 h later, and cells were plated for CFU counts. N= 3-9. Mean ± SD and individual values are shown; $^{**}P \leq 0.01$, Kruskall-Wallis test with Dunn's multiple comparisons. (B) Microsensor analysis of luminal oxygen concentrations measured in gastric spheroids (n=5 or 6 organoids, mean ± SD). $^{***}P \leq 0.001$, one-way ANOVA with Dunnett's multiple comparisons. Dotted line indicate concentration of oxygen in buffer. (C) Representative confocal images (single optical sections) of a non-infected and a GFP-*H. pylori* (green)-infected, mCherry-expressing gastric spheroid (red) co-cultured with CellTracker™-labeled MoDCs (blue) for 48 h and then analyzed by confocal imaging. Bar = 50 µm. (D) Image analysis approach for organoid co-cultures. Organoid area was

defined as the area within a 75 μm radius of the spheroid, and DC area was measured digitally on an auto-thresholded image. (E) Digital image analysis of 8 non-infected and 9 spheroid co-cultures infected with GFP-*H. pylori* from 3 independent experiments. Individual data points mean ± SD are shown. Significance between groups was analyzed by unpaired Student's *t* test. (F) Gastric epithelial spheroids were re-plated as monolayers and treated with *H. pylori* 60190 wt ($5x10^7$/well) or a panel of TLR agonists (see methods) for 6 h. Gene expression of *CXCL8* was determined by TaqMan quantitative RT-PCR. Individual values (symbols) and mean ± SD (bar and error bars) from 3 independent experiments are shown. $*P \leq 0.05$; Kruskall-Wallis Test with Dunnett's multiple comparisons. (G) Gastric spheroids were microinjected with FITC-dextran alone (MW 4 kDa, tracer) or with FITC-dextran containing *H. pylori* 60190 wild type, *H. pylori* 60190 ΔCagA, or *Salmonella* Flagellin (1 μg/mL). Spheroids that remained intact throughout the experiment, as determined by retention of FITC-dextran in the lumen, were analyzed for DC recruitment after 48 h. Pooled data from 2 independent experiments were analyzed by Kruskall-Wallis test with Dunn's multiple comparisons; $*P \leq 0.05$. All co-cultures were imaged on a Leica SP5 Confocal Scanning Laser Microscope using a 20x objective, and imaging data were analyzed using ImageJ software.

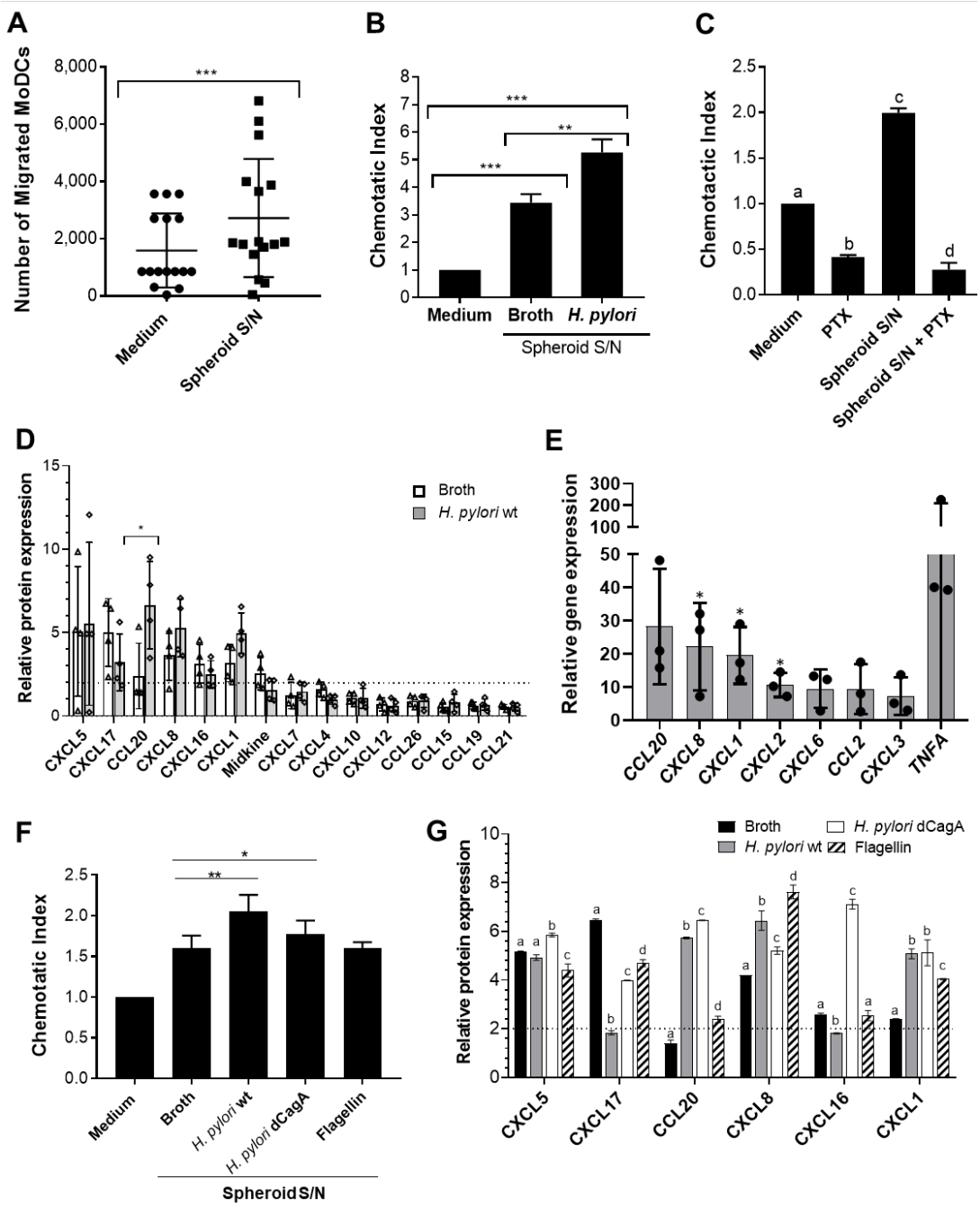

Figure 5.4. *H. pylori* infection increases human gastric epithelial cell chemokine expression, leading to enhanced DC recruitment. (A) Culture supernatants collected over 48 h from established spheroid cultures were tested for their ability to attract MoDCs (2 x 10^5/well) in a transwell chemotaxis assay. Individual data points from 16 independent experiments performed in triplicate, mean± SD, ***$P \leq 0.001$, paired Student's *t* test. (B)

Culture supernatants collected from gastric spheroids with or without *H. pylori* infection 48 h after microinjection of the spheroids were analyzed in transwell chemotaxis assays with MoDCs (1 x 10^5/well). Mean ± SD of triplicate wells, one representative experiment out of four is shown. ANOVA with Tukey's multiple comparisons test; $^{**}P \leq 0.01$; $^{***}P \leq 0.001$. (C) MoDC chemotaxis to medium alone or gastric spheroid supernatants in the presence of absence of pertussis toxin (PTX, 10 μg/mL) was analyzed. Mean ± SD of triplicate wells, one representative experiment out of three is shown. ANOVA with Tukey's multiple comparisons test; different letters signify statistically significant differences ($P \leq 0.05$). (D) Supernatants collected from spheroid cultures with and without *H. pylori* infection (48 h) were analyzed for the presence of chemokines using a chemokine array. Pooled data from 4 independent experiments. $^{*}P \leq 0.05$, Student's *t* test. (E) Relative gene expression of select chemokine and cytokine genes in *H. pylori*-infected compared to non-infected spheroids. Mean ± SD of 3 independent infection experiments. Only genes that showed consistent >2-fold upregulation in all 3 experiments are shown. $^{*}P \leq 0.05$, Student's *t* test. (F) Culture supernatants were collected after 48 h from gastric spheroids microinjected with broth alone, *H. pylori* wild type (wt), *H. pylori* ΔCagA, or *Salmonella* flagellin. Supernatants were analyzed in transwell chemotaxis assays with MoDCs. One representative of 3 experiments, mean ± SD of triplicate wells, ANOVA with Tukey's multiple comparisons test; $^{*}P \leq 0.05$, $^{**}P \leq 0.01$. (G) Supernatants from spheroid cultures with different treatments were analyzed for the presence of chemokines by chemokine array. One representative of 2 experiments. Different letters signify statistically significant differences in chemokine concentration ($P \leq 0.05$).

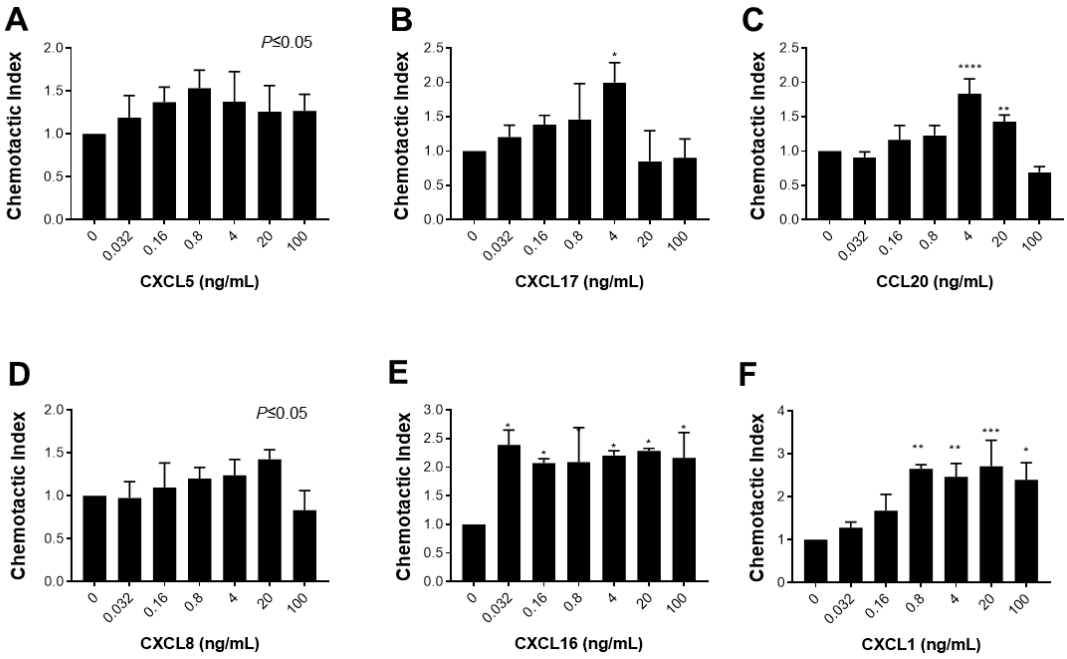

Figure 5.5. MoDCs show chemotactic activity to multiple chemokines that are release by the gastric epithelium. Chemotactic activity of MoDCs towards various concentrations of (A) CXCL5; (B) CXCL17; (C) CCL20; (D) CXCL8; (E) CXCL16 and (F) CXCL1 was analyzed in transwell chemotaxis assays. Representative results of 3 or more experiments each are shown. Mean ± SD of triplicate wells, analyzed by one-way ANOVA. Tukey's post hoc test was used to determine differences between individual chemokine concentrations and control, **P*≤0.05; ***P*≤0.01; ****P*≤0.001; *****P*≤0.0001.

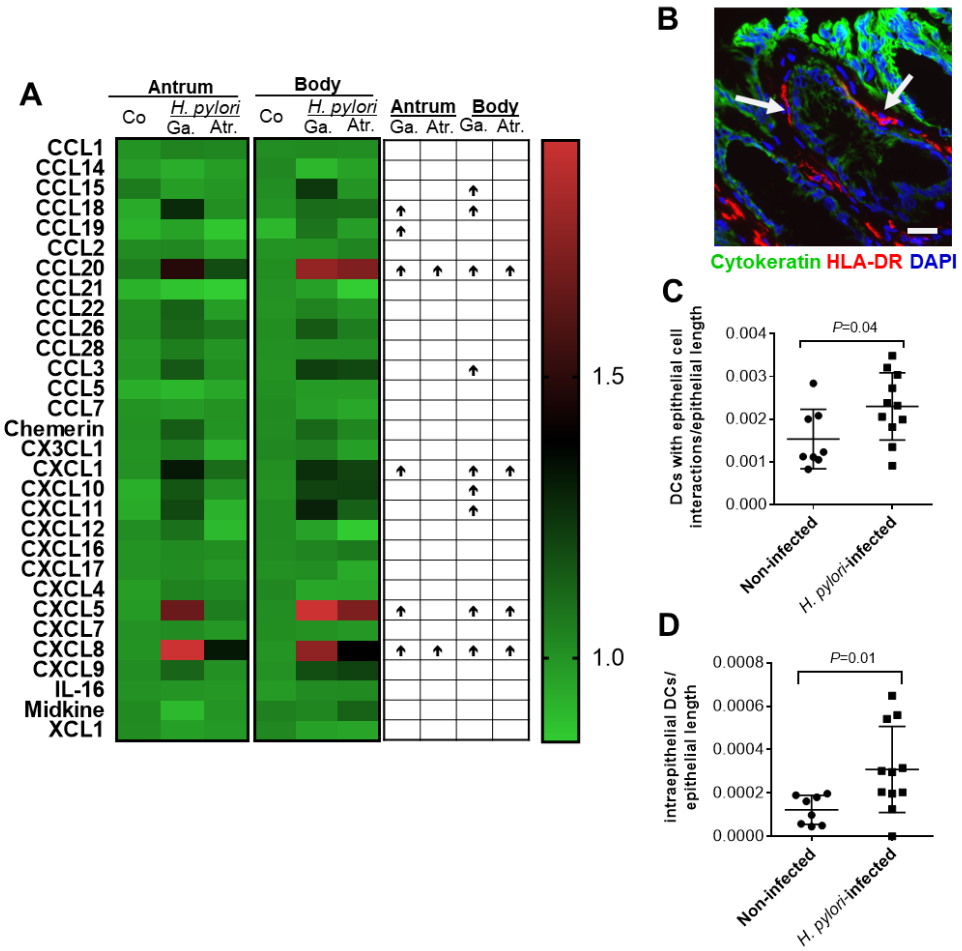

Figure 5.6. *H. pylori* infection induces increased chemokine expression in gastric tissues and enhances the recruitment of DC to the gastric epithelium. (A) Heatmap displaying relative chemokine gene expression in human gastric antrum and body from non-infected (Co.) and *H. pylori* infected donors without atrophy (gastritis, Ga.) and with gastric atrophy (Atr.; n=3 each); data extracted from Gene Expression Omnibus data set records GDS5338 (antrum) and GDS5411 (body). Arrow (↑) indicates significant upregulation (ANOVA with Dunnett's multiple comparisons test, $P \leq 0.05$). (B, C, D) Gastric biopsy samples from *H. pylori*-infected (n=11) and non-infected (n=8) human donors were immuno-labeled for HLA-DR (Cy3, red) and epithelial cytokeratin (type 7/8; FITC, green). Cell nuclei were labeled with DAPI (blue). Images were acquired on a Nikon Eclipse T2000-U fluorescent microscope equipped with a CoolSnap ES digital camera and NIS Elements BR2.30 software with a 20 x objective. (B) Representative image of non-*H. pylori*-infected mucosa. Arrows indicate examples of DCs in direct contact with epithelial cells. Bar: 20 µm. (C) The number of HLA-DR^{high} DCs in direct contact with the basal side of the gastric epithelium was counted and normalized to epithelial length. Data from individual subjects, mean ± are shown. Data were analyzed by Student's *t* test. (D) The number of intraepithelial DCs was determined using the approach described for (C).

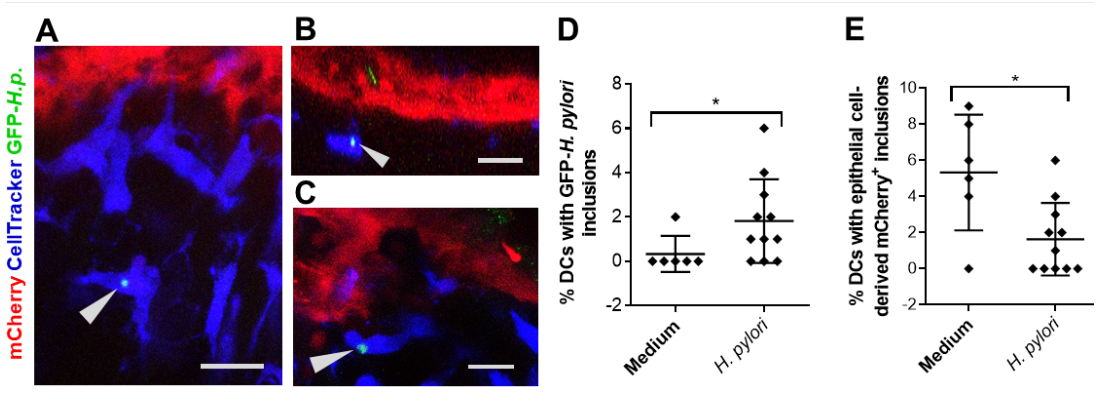

Figure 5.7. MoDCs co-cultured with *H. pylori*-infected human gastric spheroids phagocytose *H. pylori* bacteria. (A-C) Confocal image analysis of gastric epithelial spheroid-MoDC co-cultures reveals internalized GFP-positive material in a subset of MoDCs (arrowheads). mCherry-expressing spheroids (red) were infected with GFP-*H. pylori* (green), and CellTracker™-labeled MoDCs (blue) were added for 48 h. Representative images of 3 independent co-culture experiments; bar = 20 µm. (D, E) Percentage of MoDCs with (D) green fluorescent (GFP^+) inclusions and (E) red fluorescent ($mCherry^+$) inclusions (see Fig. 3E, pink in merged images) after 48 h of co-culture with non-infected versus GFP-*H. pylori* infected gastric spheroids. Co-cultures were imaged on a Leica SP5 Confocal Scanning Laser Microscope using a 63x objective. Data from one out of three representative experiments; individual data points, mean and SD are shown. *$P \leq 0.05$, Mann-Whitney U Test.

SUPPLEMENTAL INFORMATION

Supplemental Video 1: MoDCs spontaneously migrate towards the epithelium of a gastric spheroid. MoDCs labeled with CellTracker™ Green were added to a gastric spheroid culture and imaged for 48 h on an EVOS FL Auto system with a 10 x objective, with cells imaged every 10 min. Movie shows merge of phase contrast and green fluorescent image. Video shown corresponds to 3 h 55 min. Video is representative of three independent cultures with five or more spheroids each.

LITERATURE CITED

1. Delahay RM & Rugge M (2012) Pathogenesis of Helicobacter pylori infection. *Helicobacter* 17 Suppl 1:9-15.

2. Cover TL & Blaser MJ (2009) Helicobacter pylori in health and disease. *Gastroenterology* 136(6):1863-1873.

3. Shiu J & Blanchard TG (2013) Dendritic cell function in the host response to Helicobacter pylori infection of the gastric mucosa. *Pathog Dis* 67(1):46-53.

4. Bimczok D, *et al.* (2010) Human primary gastric dendritic cells induce a Th1 response to H. pylori. *Mucosal Immunol* 3(3):260-269.

5. Kao JY, *et al.* (2010) Helicobacter pylori immune escape is mediated by dendritic cell-induced Treg skewing and Th17 suppression in mice. *Gastroenterology* 138(3):1046-1054.

6. Bimczok D, *et al.* (2015) Human gastric epithelial cells contribute to gastric immune regulation by providing retinoic acid to dendritic cells. *Mucosal Immunol* 8(3):533-544.

7. Bimczok D, *et al.* (2013) Helicobacter pylori infection inhibits phagocyte clearance of apoptotic gastric epithelial cells. *J Immunol* 190(12):6626-6634.

8. McDonald KG, *et al.* (2017) CCR6 Promotes Steady State Intestinal Mononuclear Phagocyte Association with the Intestinal Epithelium, Imprinting, and Immune Surveillance. *Immunology*.

9. Rescigno M, *et al.* (2001) Dendritic cells express tight junction proteins and penetrate gut epithelial monolayers to sample bacteria. *Nat Immunol* 2(4):361-367.

10. Butler M, *et al.* (2006) Modulation of dendritic cell phenotype and function in an in vitro model of the intestinal epithelium. *Eur J Immunol* 36(4):864-874.

11. Bermudez-Brito M, *et al.* (2015) Lactobacillus paracasei CNCM I-4034 and its culture supernatant modulate Salmonella-induced inflammation in a novel transwell co-culture of human intestinal-like dendritic and Caco-2 cells. *BMC Microbiol* 15(1):79.

12. Zeuthen LH, Fink LN, & Frokiaer H (2008) Epithelial cells prime the immune response to an array of gut-derived commensals towards a tolerogenic phenotype

through distinct actions of thymic stromal lymphopoietin and transforming growth factor-beta. *Immunology* 123(2):197-208.

13. Emami CN, Mittal R, Wang L, Ford HR, & Prasadarao NV (2011) Recruitment of dendritic cells is responsible for intestinal epithelial damage in the pathogenesis of necrotizing enterocolitis by Cronobacter sakazakii. *J Immunol* 186(12):7067-7079.

14. Leonard F, Collnot EM, & Lehr CM (2010) A three-dimensional coculture of enterocytes, monocytes and dendritic cells to model inflamed intestinal mucosa in vitro. *Mol Pharm* 7(6):2103-2119.

15. Noel G, *et al.* (2017) A primary human macrophage-enteroid co-culture model to investigate mucosal gut physiology and host-pathogen interactions. *Sci Rep* 7:45270.

16. Nozaki K, *et al.* (2016) Co-culture with intestinal epithelial organoids allows efficient expansion and motility analysis of intraepithelial lymphocytes. *J Gastroenterol* 51(3):206-213.

17. Necchi V, Manca R, Ricci V, & Solcia E (2009) Evidence for transepithelial dendritic cells in human H. pylori active gastritis. *Helicobacter.* 14(3):208-222.

18. Niess JH, *et al.* (2005) CX3CR1-mediated dendritic cell access to the intestinal lumen and bacterial clearance. *Science* 307(5707):254-258.

19. Hill DR, *et al.* (2017) Bacterial colonization stimulates a complex physiological response in the immature human intestinal epithelium. *Elife* 6.

20. Tummuru MK, Cover TL, & Blaser MJ (1994) Mutation of the cytotoxin-associated cagA gene does not affect the vacuolating cytotoxin activity of Helicobacter pylori. *Infect.Immun.* 62(6):2609-2613.

21. Bartfeld S, *et al.* (2015) In vitro expansion of human gastric epithelial stem cells and their responses to bacterial infection. *Gastroenterology* 148(1):126-136.

22. Schlaermann P, *et al.* (2016) A novel human gastric primary cell culture system for modelling Helicobacter pylori infection in vitro. *Gut* 65(2):202-213.

23. Arnold IC, *et al.* (2017) NLRP3 Controls the Development of Gastrointestinal CD11b(+) Dendritic Cells in the Steady State and during Chronic Bacterial Infection. *Cell Rep* 21(13):3860-3872.

24. Iliev ID, Mileti E, Matteoli G, Chieppa M, & Rescigno M (2009) Intestinal epithelial cells promote colitis-protective regulatory T-cell differentiation through dendritic cell conditioning. *Mucosal Immunol* 2(4):340-350.

25. Iliev ID, *et al.* (2009) Human intestinal epithelial cells promote the differentiation of tolerogenic dendritic cells. *Gut* 58(11):1481-1489.

26. Adhikary S, Kocieda VP, Yen JH, Tuma RF, & Ganea D (2012) Signaling through cannabinoid receptor 2 suppresses murine dendritic cell migration by inhibiting matrix metalloproteinase 9 expression. *Blood* 120(18):3741-3749.

27. Hammarfjord O & Wallin RP (2010) Dendritic cell function at low physiological temperature. *J Leukoc Biol* 88(4):747-756.

28. Chieppa M, Rescigno M, Huang AY, & Germain RN (2006) Dynamic imaging of dendritic cell extension into the small bowel lumen in response to epithelial cell TLR engagement. *J Exp.Med.* 203(13):2841-2852.

29. Merad M & Manz MG (2009) Dendritic cell homeostasis. *Blood* 113(15):3418-3427.

30. Hardbower DM, *et al.* (2017) Ornithine decarboxylase regulates M1 macrophage activation and mucosal inflammation via histone modifications. *Proc Natl Acad Sci U S A* 114(5):E751-E760.

31. Drakes ML, Czinn SJ, & Blanchard TG (2006) Regulation of murine dendritic cell immune responses by Helicobacter felis antigen. *Infect.Immun.* 74(8):4624-4633.

32. Lamb A, *et al.* (2009) Helicobacter pylori CagA activates NF-kappaB by targeting TAK1 for TRAF6-mediated Lys 63 ubiquitination. *EMBO Rep* 10(11):1242-1249.

33. Lamb A & Chen LF (2010) The many roads traveled by Helicobacter pylori to NFkappaB activation. *Gut Microbes* 1(2):109-113.

34. Tran CT, Garcia M, Garnier M, Burucoa C, & Bodet C (2017) Inflammatory signaling pathways induced by Helicobacter pylori in primary human gastric epithelial cells. *Innate Immun* 23(2):165-174.

35. Mustapha P, *et al.* (2014) Chemokines and antimicrobial peptides have a cag-dependent early response to Helicobacter pylori infection in primary human gastric epithelial cells. *Infect Immun* 82(7):2881-2889.

36. Vanbervliet B, *et al.* (2002) Sequential involvement of CCR2 and CCR6 ligands for immature dendritic cell recruitment: possible role at inflamed epithelial surfaces. *Eur J Immunol* 32(1):231-242.

37. Dieu MC, *et al.* (1998) Selective recruitment of immature and mature dendritic cells by distinct chemokines expressed in different anatomic sites. *J Exp Med* 188(2):373-386.

38. Abernethy NJ, Hay JB, Kimpton WG, Washington E, & Cahill RN (1991) Lymphocyte subset-specific and tissue-specific lymphocyte-endothelial cell recognition mechanisms independently direct the recirculation of lymphocytes from blood to lymph in sheep. *Immunology* 72(2):239-245.

39. Rieder G, *et al.* (2001) Comparison of CXC chemokines ENA-78 and interleukin-8 expression in Helicobacter pylori-associated gastritis. *Infect Immun* 69(1):81-88.

40. Veinotte L, Gebremeskel S, & Johnston B (2016) CXCL16-positive dendritic cells enhance invariant natural killer T cell-dependent IFNgamma production and tumor control. *Oncoimmunology* 5(6):e1160979.

41. Binti Mohd Amir NAS, *et al.* (2018) Evidence for the Existence of a CXCL17 Receptor Distinct from GPR35. *J Immunol* 201(2):714-724.

42. Cavarelli M, Foglieni C, Rescigno M, & Scarlatti G (2013) R5 HIV-1 envelope attracts dendritic cells to cross the human intestinal epithelium and sample luminal virions via engagement of the CCR5. *EMBO Mol Med* 5(5):776-794.

43. Yin Y, *et al.* (2015) CpG DNA assists the whole inactivated H9N2 influenza virus in crossing the intestinal epithelial barriers via transepithelial uptake of dendritic cell dendrites. *Mucosal Immunol* 8(4):799-814.

44. Martin-Latil S, *et al.* (2012) Transcytosis of HTLV-1 across a tight human epithelial barrier and infection of subepithelial dendritic cells. *Blood* 120(3):572-580.

45. Sebrell TA, *et al.* (2018) Live imaging analysis of human gastric epithelial spheroids reveals spontaneous rupture, rotation and fusion events. *Cell Tissue Res* 371(2):293-307.

46. Bimczok D, *et al.* (2011) Stromal regulation of human gastric dendritic cells restricts the Th1 response to Helicobacter pylori. *Gastroenterology* 141(3):929-938.

47. Tummuru MK, Cover TL, & Blaser MJ (1994) Mutation of the cytotoxin-associated cagA gene does not affect the vacuolating cytotoxin activity of Helicobacter pylori. *Infect Immun* 62(6):2609-2613.

48. Roe MM, *et al.* (2017) Differential regulation of CD103 (alphaE integrin) expression in human dendritic cells by retinoic acid and Toll-like receptor ligands. *J Leukoc Biol* 101(5):1169-1180.

49. Schneider CA, Rasband WS, & Eliceiri KW (2012) NIH Image to ImageJ: 25 years of image analysis. *Nat Methods* 9(7):671-675.

50. Nookaew I, *et al.* (2013) Transcriptome signatures in Helicobacter pylori-infected mucosa identifies acidic mammalian chitinase loss as a corpus atrophy marker. *BMC Med Genomics* 6:41.

CHAPTER 6

CD103 (αE INTEGRIN) UNDERGOES ENDOSOMAL TRAFFICKING IN HUMAN DENDRITIC CELLS BUT DOES NOT MEDIATE EPITHELIAL ADHESION

Contribution of Authors and Co-Authors

Manuscript in Chapter 6

Author: Steve Swain

Contributions: Planned and oversaw the experiments, performed the experiments, analyzed the data, wrote the manuscript.

Author: Mandi Roe

Contributions: Performed the experiments, analyzed the data, wrote the manuscript.

Co-Author: Thomas A. Sebrell

Contributions: Performed the experiments.

Co-Author: Barkan Sidar

Contributions: Performed the experiments.

Co-Author: Jennifer Dankoff

Contributions: Performed the experiments.

Co-Author: Rachel VanAusdol

Contributions: Performed the experiments.

Co-Author: Lesley E. Smythies

Contributions: Initiated the project, critically discussed the data and obtained funding.

Co-Author: Phillip D. Smith

Contributions: Initiated the project, critically discussed the data and obtained funding.

Co-Author: Diane Bimczok

Contributions: Planned and oversaw the experiments, performed the experiments, initiated the project, critically discussed the data and obtained funding, analyzed the data, wrote the manuscript.

Manuscript Information

Steve Swain, Mandi Roe, Thomas A. Sebrell, Barkan Sidar, Jennifer Dankoff, Rachel VanAusdol, Lesley E. Smythies, Phillip D. Smith, Diane Bimczok

Frontiers in Immunology

Status of Manuscript:
____ Prepared for submission to a peer-reviewed journal
____ Officially submitted to a peer-reviewed journal
____ Accepted by a peer-reviewed journal
__X_ Published in a peer-reviewed journal

Published by Frontiers in Immunology
In Volume 9, Article 2989 (2018)

DOI: 10.3389/fimmu.2018.02989

Keywords: gastrointestinal epithelium, integrin alpha E, antigen-presenting cell, cell adhesion, endosome.

ABSTRACT

Dendritic cell (DC) expression of CD103, the α subunit of αEβ7 integrin, is thought to enable DC interactions with E-cadherin-expressing gastrointestinal epithelia for improved mucosal immunosurveillance. In the stomach, efficient DC surveillance of the epithelial barrier is crucial for the induction of immune responses to *H. pylori*, the causative agent of peptic ulcers and gastric cancer. However, gastric DCs express only low levels of surface CD103, as we previously showed. We here tested the hypothesis that intracellular pools of CD103 in human gastric DCs can be redistributed to the cell surface for engagement of epithelial cell-expressed E-cadherin to promote DC-epithelial cell adhesion. In support of our hypothesis, immunofluorescence analysis of tissue sections showed that $CD103^+$ gastric DCs were preferentially localized within the gastric epithelial layer. Flow cytometry and imaging cytometry revealed that human gastric DCs expressed intracellular CD103, corroborating our previous findings in monocyte-derived DCs (MoDCs). Using confocal microscopy, we show that CD103 was present in endosomal compartments, where CD103 partially co-localized with clathrin, early endosome antigen-1 and Rab11, suggesting that CD103 undergoes endosomal trafficking similar to β1 integrins. Dynamic expression of CD103 on human MoDCs was confirmed by internalization assay. To analyze whether DC-expressed CD103 promotes adhesion to E-cadherin, we performed adhesion and spreading assays on E-cadherin-coated glass slides. In MoDCs generated in the presence of retinoic acid, which express increased CD103, intracellular CD103 significantly redistributed towards the E-cadherin-coated glass surface. However, DCs spreading and adhesion did not differ between E-cadherin-coated slides and slides coated with serum alone. In adhesion assays using E-cadherin-positive HT-29 cells, DC binding was significantly improved by addition of Mn^{2+} and decreased in the presence of EGTA, consistent with the dependence of integrin-based interactions on divalent cations. However, retinoic acid failed to increase DC adhesion, and a CD103 neutralizing antibody was unable to inhibit DC binding to the E-cadherin positive cells. In contrast, a blocking antibody to DC-expressed E-cadherin significantly reduced DC binding to the epithelium. Overall, these data indicate that CD103 engages in DC-epithelial cell interactions upon contact with epithelial E-cadherin, but is not a major driver of DC adhesion to gastrointestinal epithelia.

INTRODUCTION

Dendritic cells (DCs) frequently interact with the epithelial layer of the gastric mucosa, as shown in previous studies (1-3). As professional antigen-presenting cells, DCs control the immune response to *Helicobacter pylori* (*H. pylori*) (4), a bacterial pathogen that causes chronic gastritis, peptic ulcer disease and gastric cancer (5-7). Specifically, the type of T cell response induced by the DCs largely determines whether *H. pylori* infection causes only mild inflammation or leads to severe inflammatory pathologies including ulcers or cancer (8-10). For those DCs that are located immediately beneath or within the gastric epithelium, their spatial interactions with the epithelial cells have important functional implications for the immune response to *H. pylori*. First, DCs that reside within the epithelial layer or extend transepithelial dendrites have direct access to the gastric lumen for *H. pylori* antigen sampling (1-3, 11). Second, positioning of gastric DCs immediately below the epithelium increases the probability for pathogen capture upon epithelial barrier breach, and third, the close proximity of DCs to epithelial cells likely enhances the paracrine effects of epithelial-derived mediators that regulate DC function (12-14). In spite of the importance of DC-epithelial interactions for gastrointestinal immune responses, the molecular mechanisms of these interactions are not well defined.

Binding of DC-expressed CD103 (αEß7 integrin) to epithelial E-cadherin was proposed as a potential mechanism for DC adhesion to epithelial cells (15-17). CD103, the α subunit of αEß7 integrin, is widely recognized as an important DC subset and lineage marker in humans and mice (18-20). Specifically, CD103 identifies a DC subset

termed conventional DC1 that is able to cross-present exogenous antigens to CD8 T cells and that induces mucosal tolerance to commensals and dietary antigens (19, 21). The functional role of CD103 has been extensively studied in transfected cells lines, where the A-domain of the αE (CD103) integrin subunit was shown to interact with the top surface of E-cadherin domain 1, and in intestinal intraepithelial lymphocytes (IELs), where CD103 anchors the IELs within the epithelial layer (22-24). In spite of its frequent use as a DC marker, the function of CD103 in primary human DCs has received little investigative attention. Therefore, the goal of our study was to determine whether CD103 enables DCs in the human stomach to interact with the epithelium through E-cadherin engagement.

Notably, previous studies from our laboratory and others have shown that surface CD103 expression of gastric DCs is low compared to CD103 expression on DCs in other tissue compartments such as the small intestine (14, 25-27). This low surface CD103 expression was unexpected, since gastric DCs have a tolerogenic capacity similar to that of human intestinal DCs (14, 28) and also are efficient producers of retinoic acid (RA), properties generally associated with intestinal $CD103^+$ DC subsets (14, 29, 30). However, we also showed that human monocyte-derived DCs express considerable amounts of CD103 in intracellular compartments (25). Other integrins including α5β1, α6β4 and αMβ2 are expressed in endosomal compartments and recirculate through the membrane to enable dynamic and tightly regulated interactions with their respective ligands (31-33). Therefore, we hypothesized that intracellular pools of αE integrin/CD103 present in human gastric DCs can be redistributed to the cell surface for

engagement of epithelial cell-expressed E-cadherin in the stomach to promote DC-epithelial cell adhesion. Interestingly, our experiments revealed that CD103 undergoes endosomal trafficking in human DCs and is engaged upon DC contact with epithelial E-cadherin but is not the major adhesion factor that mediates epithelial cell binding.

MATERIALS AND METHODS

Human Blood and Tissue Samples

Heparinized blood samples were obtained with local IRB approval from healthy adult volunteers in Birmingham, AL (IRB# X120806005), or Bozeman, MT (IRB #DB082817 and #DB092614). Gastric tissue specimens were obtained with Institutional Review Board (IRB) approval and informed consent from non-*H. pylori*-infected adult subjects undergoing elective gastric bypass surgery or sleeve gastrectomy for treatment of obesity at the University of Alabama at Birmingham (IRB# F120815005) or were provided as exempt specimens by the National Disease Research Interchange (Philadelphia, PA; IRB# DB062615-EX).

Antibodies

The following mouse anti-human monoclonal antibodies were used for flow cytometry, imaging cytometry and confocal analysis of MoDCs: HLA-DR (clone L243), CD11c (B-ly6), CD103/αE (B-Ly7,) CD3 (HIT3a), CD19 (SJ25C1), CD45 (2D1), CD56 (MY31), E-cadherin (67A4), CD49d (9F10) purchased from eBioscience, Biolegend, or Tonbo, all San Diego, CA. Endosomal compartments were labelled with rabbit anti-human clathrin (D3C6, Cell Signaling, Danvers, MA), rabbit anti-human EEA-1

(polyclonal), mouse anti-human Rab7a (Rab7-117) and rabbit anti-human Rab11 (polyclonal), all from Abcam, Cambridge, MA. The following monoclonal antibodies were used for staining of paraffin-embedded tissue sections: anti-human HLA-DR (LN-3) and anti-human CD103 (EPR4166(2)), both Abcam, Cambridge, MA. The following antibodies were used in neutralization assays: anti-human CD103 (2G5) (Beckman Coulter, France) and anti-human E-cadherin (SHE78-7) (Thermo Fisher Scientific, Waltham, MA). Appropriate isotype-matched control antibodies were used in all experiments.

Dendritic Cells

To obtain human gastric DCs, mucosal tissue was subjected to three rounds of EDTA treatment and then digested with collagenase solution to obtain lamina propria mononuclear cells, as described previously (14, 25). Gastric DCs were then enriched using MACS sorting for HLA-DR$^+$ cells (Miltenyi Biotec, Auburn, CA).

To generate monocyte-derived DCs (MoDCs), PBMCs were isolated using Ficoll density gradient centrifugation, and MoDCs were differentiated from MACS-isolated CD14$^+$ blood monocytes by culturing 2x10^6 monocytes per well in 24-well plates in complete medium (DMEM, 10% heat-inactivated human AB serum and antibiotics) or serum-free medium (X-Vivo 10, with HEPES and L-Glutamine) supplemented with recombinant human GM-CSF (25 ng/mL) and IL-4 (17 ng/mL), both from R&D Systems, Minneapolis, MN (25, 28). To enhance DC CD103 expression, 100 nM retinoic acid (RA, Sigma, St. Louis, MO) was added to some MoDC cultures, as described

previously (25). Cytokines and RA were replenished after 3 days, and after 5 – 6 days, non-adherent cells were harvested as MoDCs by vigorous pipetting.

Immunofluorescent Labeling of Tissues and Cells for Microscopy

We used 4 μm paraffin-embedded sections to analyze CD103 expression by human gastric DCs *in situ.* Sections were de-paraffinized and then incubated in a vegetable steamer for 30 min in pre-heated Unmasking Solution (Vector Laboratories, Burlingame, CA) for antigen retrieval. Sections were then blocked in normal goat serum and incubated in the presence of primary antibodies overnight. Species specific secondary antibodies labelled with Alexa 488 or Alexa 555 (SouthernBiotech, Birmingham, AL) were added for 30 min. Finally, nuclei were stained with DAPI, and sections were mounted in Fluoroshield (Sigma-Aldrich) and sealed with nail varnish. For microscopic analysis of MoDCs, cells were stained either directly on glass-bottom plates or chamber slides (CD103 distribution and spreading assays) or were stained in suspension and then spotted onto glass slides (endosomal markers). For intracellular labeling, DCs were permeabilized with Cytofix/Cytoperm solution (Becton Dickinson) for 20 min at 4˚C, washed with PermWash buffer (Becton Dickinson) and then were incubated with antibodies for 30 min at 4˚C. Nuclei were labeled with DRAQ5 or DAPI.

Microscopy and Image Analysis

Immunofluorescence analysis of slides was performed on an Olympus BX60 upright fluorescence microscope equipped with a DS-Ri1 digital camera and with NIS Elements software (Nikon, Melville, NY) or on an EVOS FL Cell Imaging system

(Thermo Fisher Scientific). Confocal microscopy images were acquired using a Zeiss LSM 510 META system, with a 63x objective and a step size of 0.5 μm, or an inverted Leica SP5 Confocal Scanning Laser Microscope (Leica, Wetzlar, Germany) with a 20x objective or a 63x water immersion objective with Immersol (W 2010, Zeiss, Oberkochen, Germany). Digital image analysis was performed using ImageJ 1.48v software (Schneider et al. 2012). The distribution of $CD103^+$ DCs in relation to the epithelium in gastric tissue sections was determined by manual counting on digital images, using NIS Elements software. Three-dimensional co-localization of red (endosomal markers) and green (CD103) voxels in confocal stacks was determined using the JaCOP plugin to calculate Mander's co-localization coefficient (34). Part of this procedure involved screening 16 algorithms for optimal exclusion of background staining; the Bernsen method of auto-thresholding was chosen and applied objectively to all images (35). In tissue sections, regions of interest were set to exclude surface and glandular epithelial cells.

FACS Analysis

For Flow cytometry, cells were labeled with pre-determined optimum concentrations of antibodies at 4°C for 15 min, followed by washing in FACS Stain Buffer (BD Biosciences). For intracellular staining, cells were fixed and permeabilized with Cytofix/Cytoperm (BD Bioscience), and antibodies we added in the presence of BD PermWash buffer. Dead cells were labelled with LIVE/DEAD® yellow dye (Life Technologies, Carlsbad, CA). A BD LSR or LSRII was used for flow cytometry; and data were analyzed using FlowJo V10 software (Treestar, Ashland, OR). Gastric DCs

were gated as live $CD45^{pos}$/$lineage^{neg}$/$HLA\text{-}DR^{high}$ cells. The lineage cocktail contained antibodies to CD3, CD19, and CD56.

Imaging Cytometry

Imaging cytometry was performed using an ImageStreamX Mark II (Amnis Corp., Seattle, WA). Cells were prepared as described for FACS analysis, with 7-AAD or DAPI used to label nuclei in fixed cells. Data were analyzed with IDEAS software v6.1 (Amnis Corp.). The following channels were recorded: Ch 1 – brightfield, Ch 2 – CD103 FITC, channel 3 – CD11c PE, and channel 5 – 7-AAD or channel 7 – DAPI. DCs were gated as focused cells based on Gradient RMS Ch 1, single cells based on Aspect Ratio and Area Ch1, and Intensity of CD11c PE in Ch 3.

Internalization Assay

Relative rates of internalization of CD103 were determined in MoDCs using a variation of the method from Chen, Luo, Jian and Randazzo (36). Briefly, aliquots of MoDCs generated in the presence of retinoic acid (100 nM) were chilled to 4˚C, then incubated with FITC labeled mouse anti-human CD103 for 30 minutes. Unbound antibody was then removed by washing in ice cold media. Time zero samples were left on ice, and internalization was initiated in the remaining samples by resuspending the samples in 37˚C media and incubating them at that temperature for the indicated times. At each time point, samples were quickly washed in ice cold FACS buffer and left on ice to inhibit further internalization. After washing, cells were incubated for 30 minutes with anti-mouse IgG eFluor660 to label remaining cell surface anti-CD103 antibodies. Cells

were then washed again in cold FACS buffer and analyzed with a BD LSR flow cytometer. Mean fluorescent intensities were normalized to the highest value of that fluorophore in each experiment.

Adhesion and Spreading Assays

For adhesion and spreading assays with recombinant E-cadherin, glass bottom 24-well or 96-well plates were coated with goat anti-human IgG at 5 μg/mL and incubated overnight at 4ºC. Non-adherent IgG was washed off with PBS + Ca^{2+}, and Fc-tagged recombinant human E-cadherin (Acro Biosystems, Newark, DE) at 2 μg/mL or an equal volume human serum was added to wells and incubated at room temperature for 1 hour. Alternatively, wells were coated directly with 0.2 μg/mL recombinant human E-cadherin (R&D systems, Minneapolis, MN) for 1 hour. After coating, wells were washed, blocked with human serum and washed again. MoDCs were incubated for 30 minutes with an anti-human CD103 neutralizing antibody (20 μg/mL), an appropriate isotype control antibody or were left untreated and then were added to the plates at $5x10^5$/mL. After incubation for 40 min at 37˚C, non-adherent cells were gently washed off and cells were fixed with Cytofix/Cytoperm (BD biosciences, San Jose, CA). MoDCs were blocked with 10% goat serum and stained with HLA-DR FITC, a secondary IgG2a FITC to enhance signal, and DAPI to label cell nuclei. Wells were then imaged on an EVOS FL Cell imaging system and analyzed using ImageJ.

To quantify DC adhesion to gastrointestinal epithelial cells, HT-29 cells were cultured on 48 well plates for 3 days at a starting concentration of $3x10^5$ per well to obtain a 100% confluency for co-culture. MoDCs generated in medium alone or in the

presence of RA were harvested and pre-treated with DC culture medium containing one of the following for 30 minutes at 37ºC: 2 mM Mn^{2+}; 1 mM EGTA; 2 mM Mn^{2+} and 1 mM EGTA; anti-human CD103 (2 – 20 μg/mL); or anti-human E-cadherin (5 μg/mL). MoDCs were next plated with the HT-29 monolayers at $2x10^5$ cells per well and incubated for 2 hours at 37ºC, with antibodies or other additives remaining in the culture media. Following incubation, non-adherent cells were gently washed off with media, and adherent MoDCs and HT-29 cells were harvested using 0.25% trypsin/1mM EDTA (Millipore, Darmstadt, Germany). Cells were then stained with HLA-DR FITC antibody, counting beads were added, and recovered MoDCs were quantified by flow cytometry. Experiments with <5% DC adhesion were excluded from the analyses, because it was difficult to interpret minor changes in adhesion when overall adhesion levels were extremely low. Experiments with low overall adhesion correlated neither with low DC CD103 or E-cadherin expression levels nor with a specific passage number or reduced E-cadherin expression of the HT-29 cells.

To quantify CD103 expression following MoDC HT-29 co-culture, a subset of MoDCs were incubated without HT-29 cells and subjected to the same 0.25% trypsin/1mM EDTA treatment. MoDCs incubated alone and those co-cultured with HT-29 cells were then stained for CD103 expression and analyzed by flow cytometry.

Statistical analysis

Data were analysed using GraphPad Prism 6.05. Results are presented as mean ±SEM. Differences between values were analyzed for statistical significance by the two-

tailed Student's *t*-test or one- or two-way ANOVA with appropriate post hoc analysis as indicated. Differences were considered significant at $P<0.05$.

RESULTS

Gastric Intraepithelial DCs Contain a Significant CD103-Expressing DC Subset

Flow cytometric analyses of gastric DCs have shown that $CD103^+$ DCs are rare in both human and murine stomach (14, 25-27). Here, we used immunofluorescence analysis of human gastric tissue sections to analyze CD103 expression by gastric mononuclear phagocytes in more detail. Mucosal DCs, and possibly some macrophages, were identified based on high expression of HLA-DR in conjunction with an irregular cell morphology. Notably, our previous studies showed that gastric $HLA\text{-}DR^{high}$ cells are $CD45^+$ leukocytes that express the DC-specific transcription factor zDC, but not the intestinal macrophage marker CD13 and that do not include B cells, T cells, mast cells or NK cells (1, 14). Our immunofluorescence analyses confirmed that CD103 expression by $HLA\text{-}DR^{high}$ cells in the gastric mucosa relatively rare (**Fig. 1a**). Likewise, the majority of $CD103^+$ cells, likely T lymphocytes, were negative for HLA-DR expression (**Fig. 1a**). However, individual $CD103^+$ $HLA\text{-}DR^+$ DCs were detected in close association with the gastric glandular epithelium, either at intraepithelial sites or directly below the epithelium (**Fig. 1b,c**). We next performed a quantitative analysis of the distribution of $CD103^-$ and $CD103^+$ DC subsets in relationship to the gastric epithelium by counting DCs at intraepithelial, subepithelial (with epithelial contact), and lamina propria sites (no epithelial contact) (**Fig. 1d,e**). Although intraepithelial $HLA\text{-}DR^+$ DCs

represented <2% of all gastric mucosal DCs, a proportion ($P \leq 0.05$) of these cells expressed CD103. Specifically, 46.1% of intraepithelial gastric HLA-DR^+ cells were positive for CD103 compared to only 10.7% and 6.9% of $CD103^+$ DCs at subepithelial and lamina propria sites, respectively (**Fig. 1e**). These observations suggest that, in spite of an overall low expression of CD103 by human gastric DCs, CD103 might still contribute to DC interactions with the gastric epithelium in those DCs that are integrated into the epithelial cell layer.

Intracellular Expression of CD103 (αE integrin) in Human Monocyte-Derived and Gastric DCs

Human monocyte-derived DCs (MoDCs) contain intracellular as well as surface-expressed CD103 (25). Having shown that gastric DCs express low levels of surface CD103 overall (14, 25), but that surface CD103 expression is more frequent on gastric intraepithelial DCs (**Fig. 1b,e**), we hypothesized that intracellular CD103 pools may be recruited to the cell membrane to mediate binding to epithelial E-cadherin. Therefore, we next analyzed whether primary human gastric DCs also express intracellular CD103. As shown in **Fig. 2a,c,** significant levels of CD103 were detected in both gastric DCs and MoDCs when cells were permeabilized prior to immunolabeling, consistent with intracellular expression. In addition, intracellular CD103 expression was confirmed by imaging flow cytometry (**Fig. 2d,e**). In contrast, we did not observe significant intracellular expression of α4 integrin, in spite of high surface expression (**Fig. 2b**).

Using confocal microscopy, we detected CD103 in vesicular inclusions with a typical endosomal morphology in immature MoDCs with and without concurrent surface

CD103 expression (**Fig. 3a**). A similar vesicular staining pattern for CD103 was also seen in DCs isolated from human gastric lamina propria (**Fig. 3b**). Thus, CD103 expression in endosomal compartments appears to be a common feature of human DCs.

CD103 Partially Co-Localizes with Clathrin and Early, Recycling, and Late Endosomal Markers

Previous studies have shown that integrins may undergo endosomal trafficking to allow dynamic interactions with their ligands and facilitate cell migration (32, 37, 38). To characterize the endosomal expression of CD103 in human DCs in more detail, we analyzed co-localization of CD103 with markers for endocytic uptake (clathrin), early endosomes (early endosomal antigen-1, EEA-1), recycling endosomes (Rab11), and late endosomes (Rab7a) in MoDCs (**Fig.4**). In untreated MoDCs, 23.2 ± 1.2% of CD103 was co-localized with clathrin, corresponding to a Manders' co-localization coefficient of 0.232. Lower coefficients were detected for CD103 co-localization with Rab11 (16.7 ± 1.6%) and the late endosomal marker Rab7a (16.2 ± 1.2%), which targets endosomal cargo for lysosomal degradation (39). Only 6.6 ± 0.7% of CD103 co-localized with the early endosomal marker EEA-1. In control slides without primary antibodies, a co-localization co-efficient of 0.71 ± 0.69% was measured (data not shown). Interestingly, MoDCs treated with retinoic acid (RA) showed increased co-localization with clathrin (29.6 ± 1.3%; $P \leq 0.01$), but lower co-localization with Rab11 (12.6 ±1.1%; $P \leq 0.05$). The partial co-localization of CD103 with endosomal markers suggests that CD103 undergoes some endosomal trafficking in human DCs.

CD103 in Human MoDCs Undergoes Continuous Trafficking through the Cell Membrane

To functionally analyze whether DC CD103 undergoes endosomal recycling, we performed an internalization assay, as previously described by Chen, Luo, Jian and Randazzo (36). RA-treated MoDCs were used to achieve a high initial expression of CD103 on the DCs. DCs were then incubated for up to 40 min at 37˚C and were kept on ice at all other times to inhibit endosomal trafficking until all cells were collected, with the 0 min sample incubated on ice for the entire 40 min of the assay. As shown in **Fig. 5**, the level of CD103 on the cell surface as detected with the secondary reagent decreased significantly with prolonged incubation at 37˚C ($P \leq 0.01$), whereas total CD103 expression detected with the primary antibody remained constant. These observations are consistent with internalization of surface expressed CD103 and indicate that CD103 undergoes endosomal recycling, as previously shown for α5β1 and α2β1 integrins (36, 37). Thus, CD103 may be involved in dynamic binding of DCs to the epithelial layer in spite of low surface expression.

Intracellular CD103 Engages in E-cadherin Binding, but does not Mediate DC Adhesion to Epithelial Cells

Having shown that human DCs contain dynamic pools of intracellular CD103, we next asked whether intracellular CD103 may be recruited to the DC surface for E-cadherin binding. RA-treated or untreated DCs were incubated on glass-bottom plates coated with recombinant E-cadherin (**Supplemental Fig. 1**). The RA-treated DCs expressed increased levels of surface CD103 (**Supplemental Fig. 2**). We hypothesized that engagement of E-cadherin by DC CD103 would lead to an accumulation of CD103

staining close to the E-cadherin-coated glass surface (**Fig. 6a**). Our analysis of CD103 distribution across the vertical axis of the DCs showed a small, but significant shift in the proportion of CD103 close to the glass surface in RA-treated MoDCs in wells that were coated with E-cadherin compared to serum alone (**Fig. 6b**, $P \leq 0.05$). However, this trend was not observed in MoDCs generated in the absence of RA.

On hard surfaces such as glass slides, adhesion complexes including integrin-dependent interactions influence cell spreading by enabling cells to extend actin-based lamellipodia (40). A previous study had shown that K562 cells transfected with αE(CD103)β7 formed epithelial protrusions and migrated on E-cadherin-coated surfaces (41). To determine whether CD103 promotes spreading and adhesion of human DCs on E-cadherin-positive surfaces, we used RA-treated and untreated MoDCs that were blocked with a CD103 neutralizing antibody or an isotype control antibody. As shown in **Fig. 6c**, RA-treated DCs showed a trend ($P=0.05$) for increased spreading on E-cadherin. However, DC spreading was not influenced by blocking CD103 on the DCs with a neutralizing antibody. The total number of adhered DCs also did not differ between treatments (data not shown). These results indicate that CD103 may relocate to the cell surface to engage in E-cadherin binding, but that overall DC adhesion to E-cadherin is largely independent of CD103.

Bivalent Cations Promote DC Adhesion to E-cadherin-Expressing Gastrointestinal Epithelial Cells

To analyze the interactions between MoDCs and cell-expressed E-cadherin, we performed MoDC adhesion assays with HT-29 cells, a colonic epithelial cell line strongly

positive for E-cadherin. Importantly, HT-29 cells have an atypical E-cadherin distribution that involves E-cadherin expression on the apical cell surface (**Fig. 7a, b**), but do not have any mutations in the E-cadherin gene *CDH1* (42, 43). DCs were incubated on top of HT-29 monolayers, and adherent cells were recovered by trypsinization after 2 h (**Fig. 7c**). On average, 14.4 ± 3.7% of MoDCs were recovered from the cultures as adherent cells (**Fig. 7d**). To determine whether integrins including αE integrin (CD103) are involved in DC adhesion to the HT-29 cells, we added 1 mM manganese (Mn^{2+}), a strong activator of integrins that promotes ligand binding (44, 45). Both in RA-treated and untreated MoDCs, addition of Mn^{2+} significantly increased adhesion to HT-29 cells ($P \leq 0.001$ and $P \leq 0.05$, respectively). We also added EGTA, which inactivates bivalent cations such as Ca^{2+}, Mg^{2+} and Mn^{2+} that are involved in integrin- and E-cadherin-dependent interactions. EGTA significantly decreased the number of both and RA-treated and untreated DCs that were recovered from the co-cultures ($P \leq 0.05$ and $P \leq 0.01$, respectively). Although there was a trend for increased adhesion in RA-treated MoDCs, RA had no significant effect on DC binding to HT-29 cells, similar to our observations from the spreading analysis (**Fig. 6**). Interestingly, co-culture with the HT-29 slightly increased surface expression of CD103 on the MoDCs (**Fig. 7e,** $P = 0.056$).

<u>Neutralization of DC CD103 does not Inhibit Adhesion to E-cadherin Expressing Epithelial Cells</u>

To specifically assess the involvement of CD103 in the interactions between DCs and epithelial cells, RA-treated MoDCs were blocked with a CD103 neutralizing antibody prior to adding the cells to the HT-29 monolayer in the presence of Mn^{2+}. To

avoid loss of blocking activity due to CD103 internalization, excess antibody was left in the cell culture medium during the adhesion assays. However, no decrease in DC adhesion to the HT-29 cells was seen with a wide range of antibody concentrations (**Fig. 7f**).

Homotypic E-cadherin Interactions may be Involved in DC Binding to E-cadherin on Gastrointestinal Epithelial Cells

To form adherens junctions, E-cadherin undergoes homotypic interactions with E-cadherin expressed on other cells (46), and DCs have been shown to express E-cadherin in previous studies (47-49). Our FACS analysis revealed that subsets of both human gastric DCs and MoDCs expressed E-cadherin (**Fig. 7g,h**), independent of RA treatment (**Supplemental Fig. 2**). Thus, E-cadherin-E-cadherin interactions may contribute to DC-epithelial cell interactions. Indeed, pre-treatment of the MoDCs with an E-cadherin neutralizing antibody significantly decreased DC adhesion to HT-29 monolayers (**Fig. 7i**). However, when we compared MoDC adhesion to HT-29 cells with adhesion to AGS cells, which lack E-cadherin expression, we found that a significantly higher number of DCs adhered to the AGS cells than the HT-29 cells (**Supplemental Fig. 3**, $P \leq 0.01$). Interestingly, binding to AGS cells decreased when DCs were generated in the presence of RA. Overall, these data suggest that both E-cadherin-dependent and integrin-dependent mechanisms contribute to DC binding to the gastrointestinal epithelium, but that CD103-E-cadherin interactions are only minor contributors.

DISCUSSION

CD103 (αE integrin) is widely used as a maker for DC subsets in humans and mice (30), but the functional role of CD103 for the DCs has attracted little investigative attention. We here sought to elucidate whether CD103 could mediate DC-epithelial cell interactions in the human gastric mucosa. A number of previous reports had speculated that CD103 might mediate adhesion of gastrointestinal DCs to E-cadherin expressed in the epithelial layer (15-17), similar to the mechanism shown for the retention of intraepithelial lymphocytes within the epithelial compartment (23, 50). Studies from our laboratory have shown that DCs in the gastric mucosa are exposed to RA generated by gastric epithelial cells, and that RA induces CD103 expression in human MoDCs (14, 25). Our results from the present study suggest that CD103 is engaged upon binding of primary DCs to gastrointestinal epithelium, but is not a major mediator of adhesion.

One specific consideration when investigating CD103 in human gastric DCs was that less than 10% of the DCs expressed CD103 on their surface, as we have previously shown (14, 25). However, based on the detection of intracellular CD103 (αE integrin), we hypothesized that these intracellular pools could be recruited to the cell surface for dynamic interactions with their ligands. Thus, integrins α5β1, α6β4, αMβ1 and α4β1 are continuously recycled through endosomal pathways during cell migration (33). However, not all integrins participate in the endocytotic cycle, and some integrins are recycled at only low rates (31). Indeed, we here confirmed that α4 integrin, which, like αE integrin, pairs with β7 integrin, was not expressed intracellularly. Our report is the first to demonstrate that CD103 in human DCs is expressed in endosomal compartments

and recirculates through the cell membrane, suggesting that αE integrin recycling occurs in human DCs. It has been proposed that motile cells, such as DCs performing immunosurveillance functions, may require more trafficking of integrins and therefore contain a higher intracellular proportion (51). We demonstrated that 40% of surface CD103 was internalized in less than 1 hour. Moreover, 23 – 30% of CD103 co-localized with clathrin, consistent with the established role of clathrin in the endocytic recycling of integrin-mediated adhesions (52). A lower percentage of CD103 co-localized with the early endosome antigen 1 (EEA-1, 7%) and Rab11 (17%), a marker for long-loop endosomal recycling. Notably, previous publications have similarly reported co-localization co-efficients between 5% and 30% for integrins and endosomal markers in cells that were not specifically treated to enhance endosomal trafficking. Thus, Ezratty et al. (52) reported that 20 – 25% of β1 integrin co-localized with Rab5. In a publication by the Goldenring group, a Manders' co-localization co-efficient of >0.2 (>20%) for co-localization of Rab25 with β1 and α5 integrins was considered high (53). Gu et al. (54) from the Brenner lab analyzed co-localization of β3 integrin with endosomal markers and found between 2 – 8 % of co-localization with EEA-1, Rab4, 5 and 11 at baseline, with increased co-localization upon PDGF-stimulated micropinocytosis. Khandelwal (55) used a functional endocytosis assay with fluorescently labeled cargo and detected co-localization co-efficients of 10% and 20% for the endosomal cargo with EEA-1 and Rab11, respectively, and Karjalainen (56) analyzed co-localization of α2 integrin with caveolin and detected 5 – 10% of co-localization at baseline. Therefore, we consider our observed co-localization of CD103 with the endosomal markers to be biologically

relevant. Co-localization of CD103/ integrin αE with clathrin, EEA1, and Rab11 suggests that integrin αE undergoes canonical trafficking similar to α5β1 integrin (57). However, the fact that CD103 also was co-localized with the late endosomal marker Rab7a may indicate that a proportion of intracellular CD103 is targeted for lysosomal degradation rather than recycling to the cell surface. Notably, when added together, less than 60% of all CD103 co-localized with any endosomal marker, suggesting that a significant proportion of CD103 is present at sites that are not endosomal compartments. These might represent newly synthesized CD103 molecules in the endoplasmic reticulum or in the Golgi apparatus. Interestingly, RA treatment of the MoDCs led to increased co-localization with clathrin and EEA-1, but decreased co-localization with Rab11 and Rab7a. Thus, RA seems to both upregulate CD103 expression (25, 58) and alter its trafficking. Overall, our results suggest that, even on cells with low surface CD103 expression, CD103 may be recruited from endosomal pools for dynamic binding to epithelial E-cadherin or other ligands.

In support of a role for CD103 in human DC-epithelial interactions, we here showed significantly increased expression of CD103 on human HLA-DR$^+$ DCs that were integrated into the gastric epithelial layer. Moreover, Z-stack analysis of MoDCs bound to E-cadherin-coated glass slides showed significant re-distribution of DC-expressed CD103 to the E-cadherin positive interface, albeit only in RA-treated cells. In addition, *in vitro* adhesion assays to E-cadherin-expressing HT-29 cells revealed a dependence on bivalent cations including manganese, consistent with an integrin-dependent mechanism (45). Conversely, when MoDCs were treated with a CD103 neutralizing antibody,

adhesion to E-cadherin-positive HT-29 cells or to E-cadherin-coated glass slides was unaffected, arguing against a major role of CD103 in mediating DC binding to the gastrointestinal epithelium. Notably, while internalization of CD103 with bound blocking antibody may have decreased the efficiency of the neutralization, this would not be expected to completely abrogate functional activity of the blocking antibody, especially since a high antibody concentration (5μg/mL) was used and additional antibody was present in the culture medium during the assay. Also, RA treatment, which increases MoDC CD103 expression, did not significantly influence MoDC binding to E-cadherin-expressing HT-29 cells or spreading on E-cadherin-coated glass surface, corroborating the results from the antibody neutralization experiments. Thus, adhesion of human DCs to gastrointestinal epithelia does not appear to be driven by CD103-E-cadherin interactions. Notably, we used high expression of HLA-DR to detect DCs in human gastric tissue sections, since no other more specific general DC marker has been identified for human stomach (1, 28). In the murine gastric mucosa, CX_3CR1^+ $CD103^-$ macrophages and $CD103^-$ DCs were able to sample *H. pylori* bacteria, whereas bacterial uptake by $CD103^+$ DCs could not be detected (27), which also does not support our original hypothesis that CD103 positions gastric mononuclear cells at the epithelial interface for luminal *H. pylori* uptake. Along the same lines, an earlier report that investigated intraepithelial DCs in murine small intestine, the spatial relationship of murine intestinal DCs with the epithelium was not altered in CD103 knockout mice (59), whereas the number of IELs was significantly reduced in these animals (60). Together,

these observations indicate that there are functional differences between T cell and DC-expressed CD103.

Our adhesion experiments did show that antibody inhibition of DC-expressed E-cadherin significantly suppressed DC binding to HT-29 cells, suggesting a role for homotypic E-cadherin-E-cadherin interactions. Thus, our results corroborate previous studies that showed Langerhans cells and other DCs of the skin and female genital tract interact with the epithelium through E-cadherin-E-cadherin binding (49, 61, 62). Notably, although homotypic E-cadherin interactions are calcium dependent, it appears that calcium can be replaced by the bivalent transitional elements manganese (Mn^{2+}) and cadmium (Cd^{2+}) (63), which would explain the observed increase in adhesion in the presence of Mn^{2+}. The significant decrease in MoDC HT-29 adhesion in the presence of EGTA is consistent with either homotypic E-cadherin-E-cadherin interactions, which are calcium-dependent (64), or heterotypic E-cadherin interactions with αE integrin, which is activated by manganese (Mn^{2+}) (65). Since E-cadherin is widely expressed on mucosal epithelial cells, it is a likely candidate for mediating the retention of motile immune cells at the epithelial barrier, and additional heterotypic E-cadherin ligands with expression on DCs including killer cell lectin-like receptor G1 (KLRG1) have been identified (23, 47, 66, 67). Surprisingly, MoDC adhesion to E-cadherin negative AGS cells was significantly higher than adhesion to HT-29 cells. These results suggest that DC adhesion to the gastrointestinal epithelium may involve additional molecular interactions independent of CD103 or E-cadherin, such as tight junction proteins (11, 68) and other integrins. Notably, all myeloid cells including DCs express β2 integrin (CD18). CD18

forms heterodimers with CD11a, CD11b, and CD11c (69) and contributes to cell-cell contact formation by binding to intracellular adhesion molecules (ICAMs), which may be expressed on gastric and intestinal epithelial cells (70, 71). Notably, adhesion of DCs to epithelial cells via β2 integrins would be consistent with our experimental observations that showed increased binding in the presence of Mn^{2+} and decreased binding in the presence of EGTA. Whether β2 integrins are major mediators of DC adhesion to the human gastric epithelium will be a subject of future studies.

If the interactions between DC-expressed CD103 and epithelial cells that we observed in human gastric tissue section do not result in strong adhesion, one might question the relevance of these interactions. However, engagement of CD103 by epithelial E-cadherin may lead to outside-in signaling through the cytoplasmic portion of the integrin (72). Previous studies have shown that in cytotoxic T cells, engagement of E-cadherin by CD103 triggers the phosphorylation of PLCγ1 and ERK1/2 (73), and engagement of CD103 by an anti-CD103 antibody can enhance T cell proliferation (74). Therefore, interactions between DC CD103 and epithelial E-cadherin could regulate certain DC functional characteristics through the activation of intracellular signaling cascades.

In summary, our study has provided novel insights in the regulation and function of CD103 (E integrin) in human DCs. We show that, like other integrins in motile cells, CD103 undergoes endosomal trafficking, which likely enables dynamic interactions between CD103 and its ligands. Our results also corroborate previous reports (59) that CD103 is not essential for the retention of DCs at gastrointestinal epithelial sites. The

mechanisms by which CD103 on DCs in the human gastrointestinal tract interact with epithelial cells may be more subtle than simple adhesive interactions and requires further experimental exploration.

ACKNOWLEDGEMENTS

Funding for our study was provided by the National Institutes of Health grants K01 DK097144 (DB); R03 DK107960 (DB) and startup funding from Montana State University. We greatly appreciate support from the National Institutes of Health IDeA Program grant GM110732, and equipment grants from the M.J. Murdock Charitable Trust (2016028:MNL:8/25/2016) and the Montana State University Agricultural Experimental Station for the Flow Cytometry Core Facility at Montana State University. Dr. Smythies received funding from the Broad Medical Foundation and the Crohn's and Colitis Foundation of America, and Dr. Smith also received funding from the Crohn's and Colitis Foundation of America that supported this study. We greatly acknowledge Dr. Heini Miettinen-Granger's input on experimental design and her comments on our final manuscript. Dr. Agnieszka Rynda-Apple's critical feedback on our manuscript is likewise greatly appreciated. We would also like to thank all our human volunteers for donating blood samples for this study.

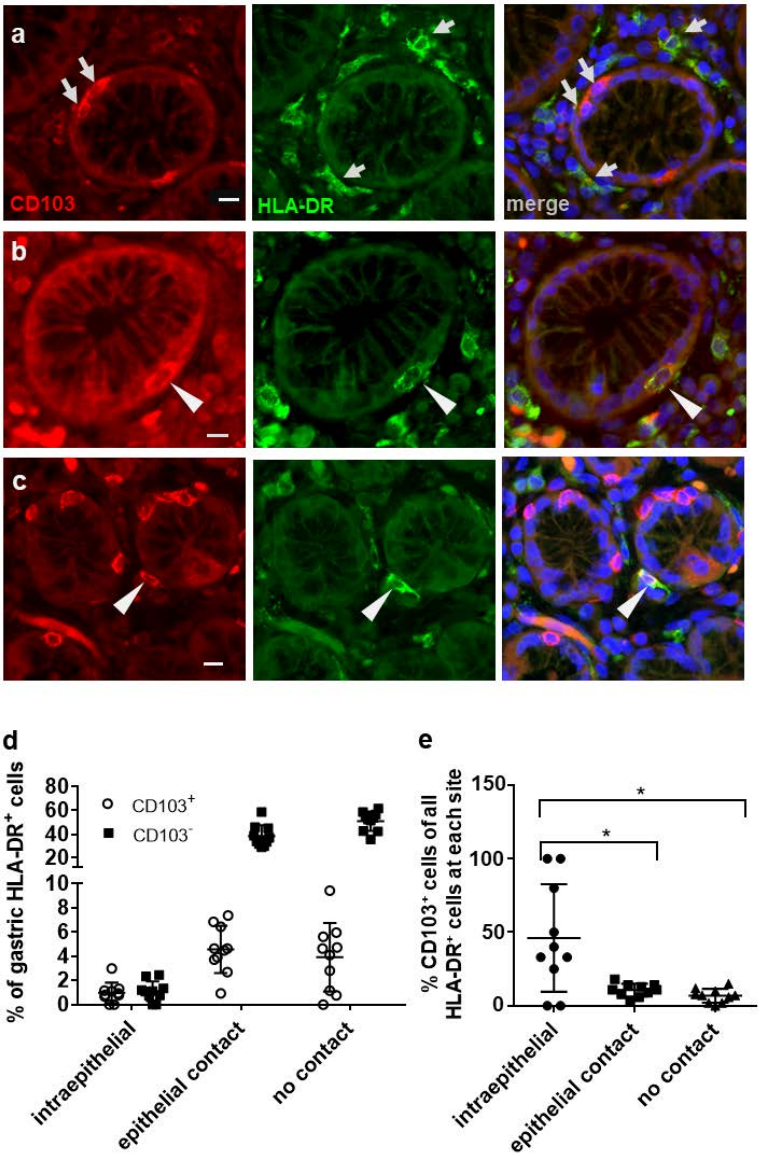

Figure 6.1. Distribution of CD103$^+$ DCs in human gastric mucosa. Paraffin-embedded tissue sections from the gastric mucosa of non-*H. pylori*-infected human subjects was immunofluorescently labelled for HLA-DR (Alexa 488, green) and CD103 (Alexa 555, red). Nuclei were stained with DAPI. (a) High magnification single color and merged images of gastric mucosa with multiple cells positive for either CD103 or HLA-DR (arrows). (b) Occasional intraepithelial HLA-DR$^+$ DCs and (c) subepithelial DCs with epithelial contact show staining for CD103. Arrowheads point out HLA-DR$^+$ DCs that co-express CD103. Bar = 20 μm. (d,e) Quantitative analysis of HLA-DR$^+$ DCs with and without CD103 expression at intraepithelial, subepithelial (with epithelial contact), and lamina propria sites (no epithelial contact). Tissue sections from 10 human subjects were analyzed. *$P \leq 0.05$, ANOVA with Tukey's post hoc test.

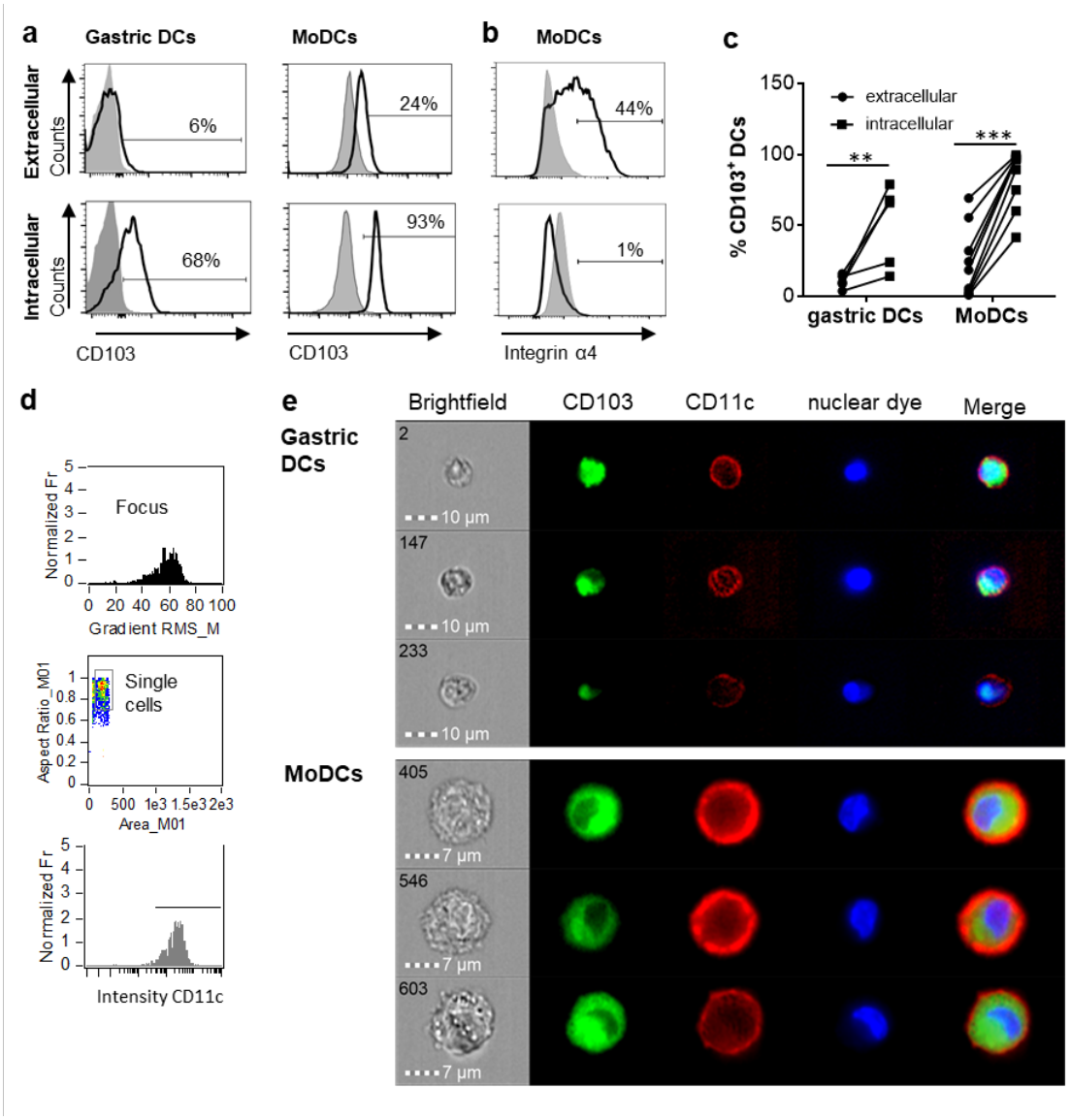

Figure 6.2. Human gastric and MoDCs contain intracellular CD103 pools. Human gastric DCs gated as live/ HLA-DR^{high}/CD45^{pos}/lineage^{neg} cells or MoDCs were labelled with (a) an anti-CD103 antibody or (b) an anti-α4 integrin antibody using extracellular or intracellular staining protocols. (a, b) representative histograms. and (b) individual values from 4 (gastric DCs) or 9 (MoDCs) independent experiments. $^{**}P \leq 0.01$, $^{***}P \leq 0.001$, ANOVA with Tukey's post hoc test. (c) Gating strategy for ImageStream imaging cytometry to select for focused, single cells with high CD11c expression. (d) Representative images from 3 independent imaging cytometry experiments show intracellular CD103 in CD11c^{+} gastric DCs and MoDCs, 40x objective. BF, bright field; nuclear dye, 7-AAD.

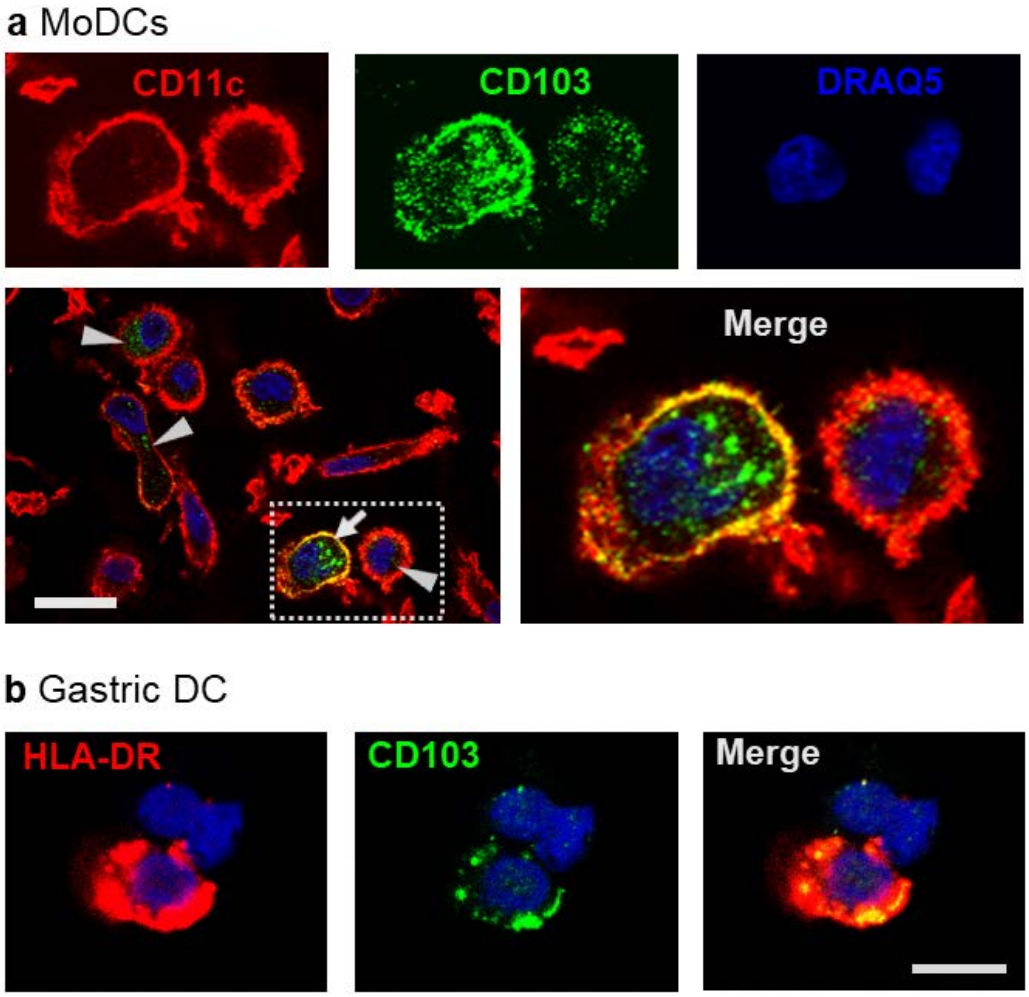

Figure 6.3. Confocal microscopy analysis shows endosomal expression pattern of CD103 in human monocyte-derived DCs. (a) Confocal images of human MoDCs that were permeabilized and labeled with antibodies to CD103 (Alexa488) and CD11c (Alexa555) Nuclei were labeled with DRAQ5. Arrowheads point to intracellular $CD103^+$ vesicles in DCs without surface CD103 expression, arrow indicates a DC with both surface and intracellular CD103 expression. Representative images from one of three similar experiments are shown. Bar: 20 μm. (b) Gastric lamina propria cells were permeabilized and labeled with antibodies to CD103 (Alexa488) and HLA-DR (Alexa555). Image shows a gastric HLA-DR^+ DC. Bar: 10 μm.

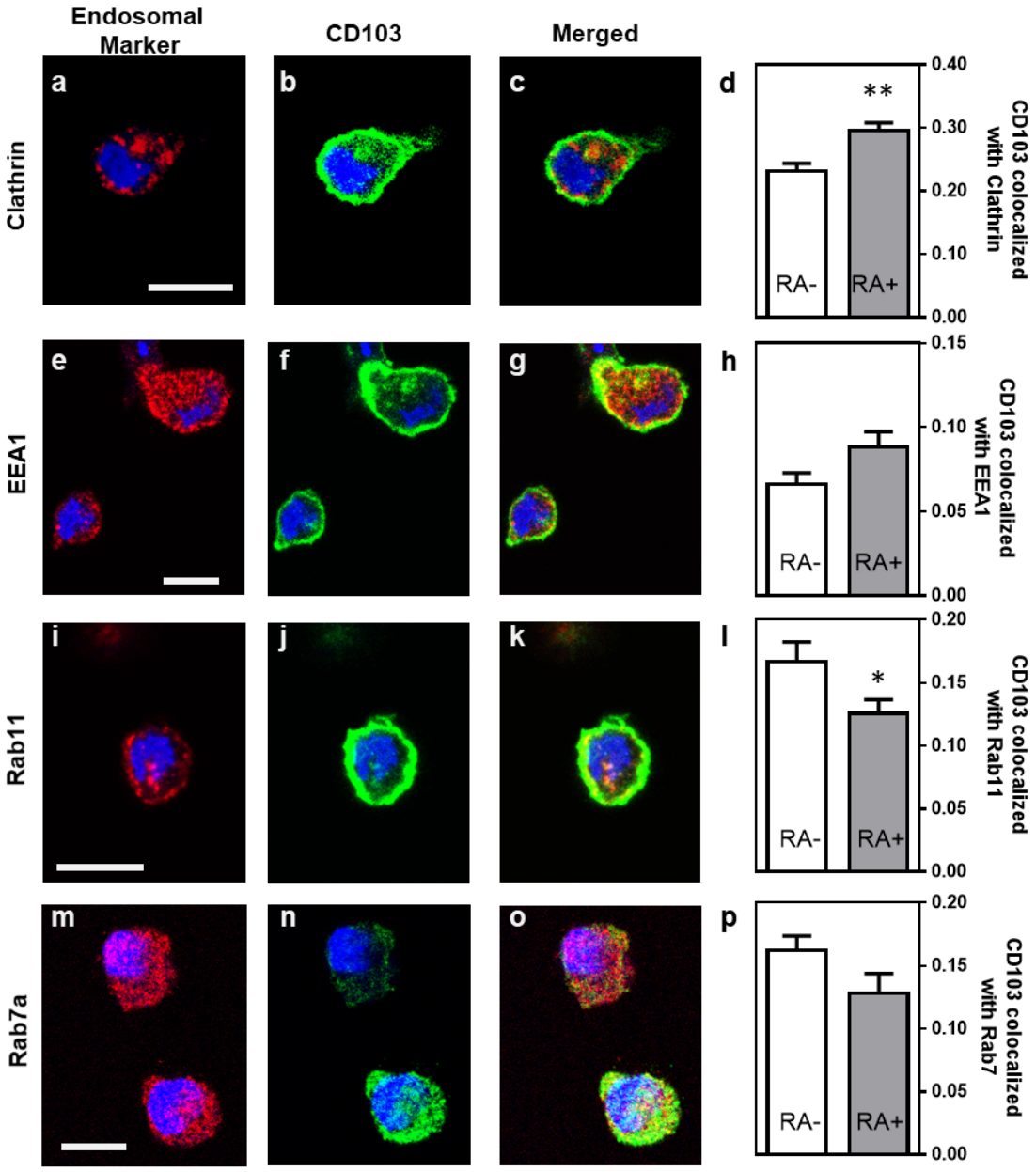

Figure 6.4. Partial co-localization of CD103 with endosomal markers in human MoDCs. MoDCs generated in medium alone or in the presence of retinoic acid (RA, 100 nM) were permeabilized and stained with antibodies to CD103 (green) and the following endosomal markers (red): (a-c) clathrin, (e-g) EEA-1, (i-k) Rab11, and (m-o) Rab7a. Images were obtained by confocal microscopy. Co-localization of CD103 with (d) clathrin, (h) EEA-1, (l) Rab11 and (p) Rab7a was calculated as the Manders' colocalization coefficient (M2) using ImageJ. Mean ± SEM of 10 – 17 confocal images obtained from 2 independent experiments. Bar = 20 μm, *$P \leq 0.05$; **$P \leq 0.01$; unpaired Student's T-test.

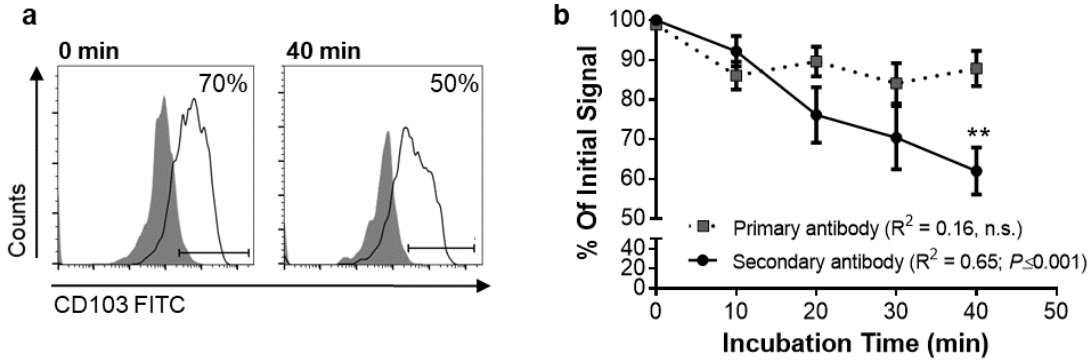

Figure 6.5. Internalization of surface-expressed CD103 in human MoDCs. Human MoDCs were labeled with an anti-CD103 FITC (mouse IgG1), washed, and chilled with ice-cold buffer. Time zero samples were left on ice, and internalization was initiated in the remaining samples by resuspending the samples in 37˚C media and incubating them at that temperature for the indicated times. Following incubation, cells were harvested with cold buffer and then left on ice until all samples were collected. Anti-CD103 antibody remaining on the surface of the DCs was detected with a secondary anti-mouse IgG1 antibody. (a) Representative FACS plots and (b) pooled data from 4 independent experiments show a significant decrease in surface CD103 after 40 min. 2-way ANOVA with Sidak's multiple comparisons.

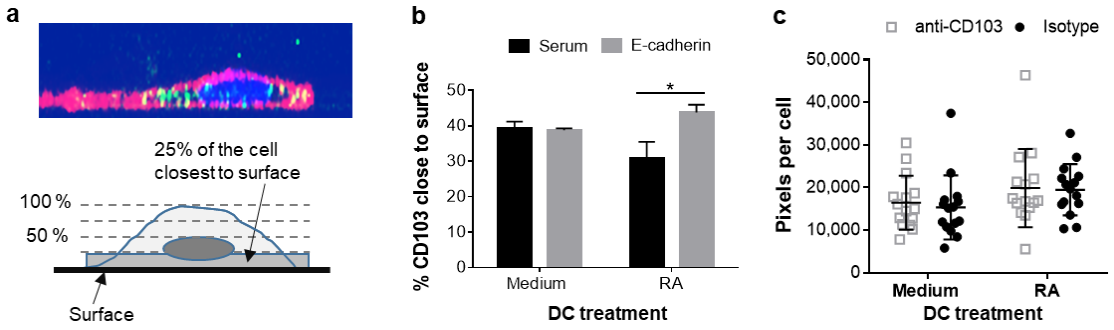

Figure 6.6. Adhesion of RA-treated MoDCs to E-cadherin-coated surfaces alters distribution of CD103. DC interactions with E-cadherin were analyzed by performing adhesion and spreading assays on glass slides coated with recombinant human E-cadherin. (a, b) RA-treated and untreated MoDCs were added to E-cadherin-coated slides and were incubated at 37˚C for 40 min. Cells were then fixed, permeabilized and stained for CD103 expression. Z-stack images (0.5 μm step size) of adherent MoDCs were collected by confocal microscopy and analyzed for the distribution of CD103 in relation to the glass surface. (a) Top panel: Orthogonal representation of an immunofluorescently labeled MoDC adhered to a glass surface and analyzed by z-stack confocal imaging. CD11c: red, CD103: green, DAPI nuclear stain: blue. Bottom panel: Graphical representation of the image analysis approach. (b) Summarized data from 3 independent experiments were analyzed. *$P \leq 0.05$, 1-way ANOVA with Tukey's post hoc test. (c) Spreading analysis of DCs on E-cadherin-coated glass slides. Glass slides were first coated with anti-human IgG antibodies and then with recombinant human E-cadherin-Fc. MoDCs generated in the presence of medium alone or 100 nM RA were pre-treated with a CD103 neutralizing antibody or an isotype control antibody for 30 min at 4˚C. Cells were then added to the slides in the presence of 2 mM Mn^{2+} and incubated at 37˚C for 40 min. Cell spreading was analyzed by fluorescence microscopy based on HLA-DR^{+} pixels per nucleus. Individual data points (n=15 areas), mean and SEM from one representative out of 3 independent experiments are shown.

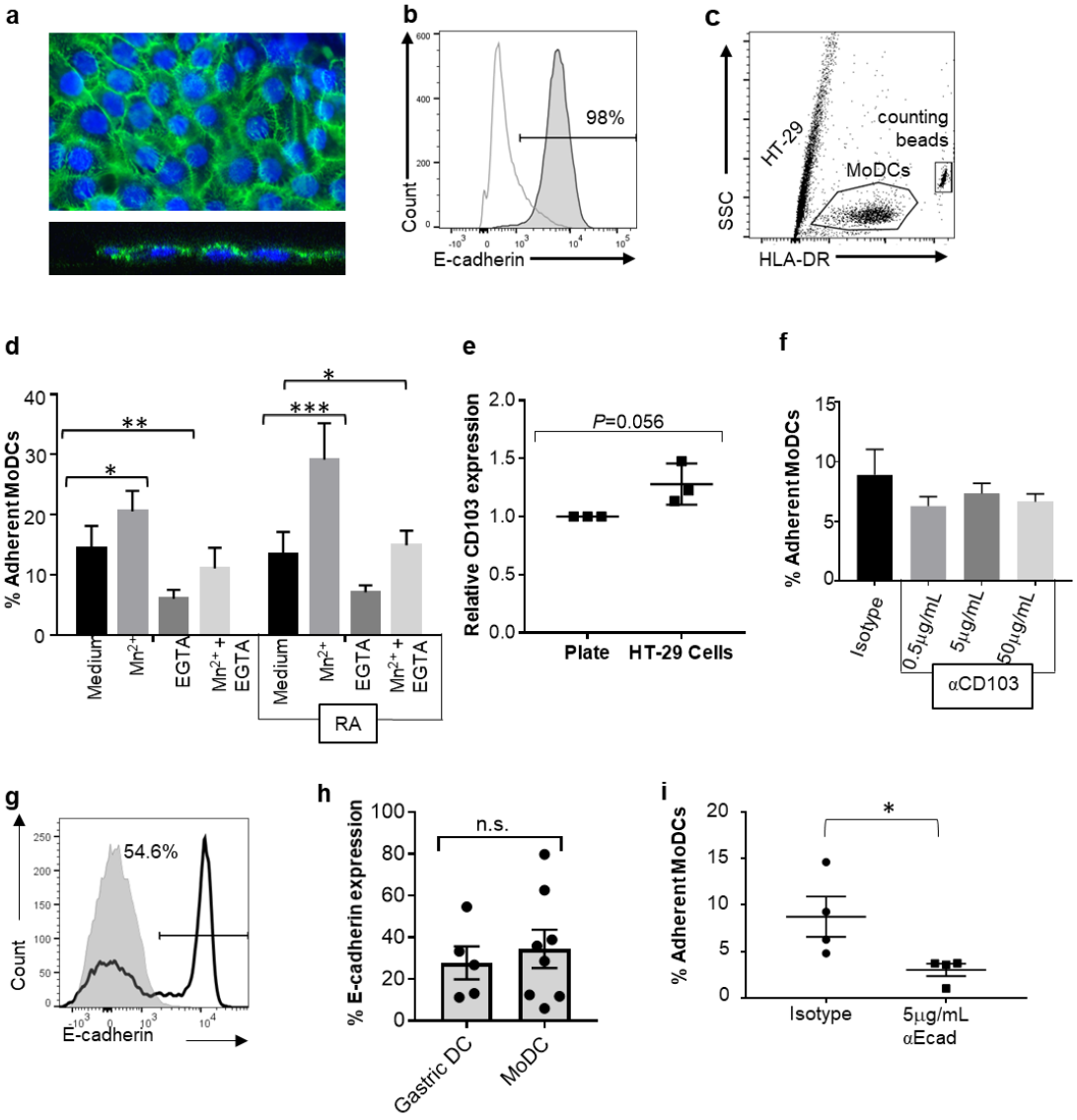

Figure 6.7. CD103 is not a major mediator of DC adhesion to E-cadherin-expressing epithelial cells. To analyze MoDC binding to E-cadherin expressed by epithelial cells, MoDCs were added to confluent monolayers of HT-29 cells for 2 h. Non-adherent cells were then removed by gentle washing, the remaining cells were collected by trypsinization, and the number of adherent DCs was determined using counting beads and HLA-DR-labeling of the DCs. (a) Confocal analysis of an HT-29 monolayer shows E-cadherin expression on the luminal surface. Top panel: maximum Z-projection; bottom panel: orthogonal view. Nuclei are labeled with DRAQ5 (blue). (b) Representative FACS histogram of E-cadherin expression on HT-29 cells. Grey line: isotype control; dark grey filled: anti-E-cadherin. (c) Gating strategy for counting adherent MoDCs following co-culture with HT-29 cells. (d) Percentage of MoDCs adherent to HT-29 cells in the presence of Mn^{2+}, EGTA, or Mn^{2+} + EGTA (n=6). RA indicates that cells were

derived in the presence of 100 nM RA. *$P \leq 0.05$, **$P \leq 0.01$, ***$P \leq 0.001$; 2-way ANOVA with Dunnett's multiple comparisons. (e)_Normalized CD103 expression on MoDCs after recovery from HT-29 co-cultures (with Mn^{2+}). Data from 3 independent experiments, paired, one-tailed Student's *t* test. (f) MoDCs were incubated with an isotype control antibody or the indicated concentrations of anti-CD103 antibody before and during co-culture with HT-29 cells, and the number of adherent DCs was determined. N=3, *$P \leq 0.05$; unpaired, two-tailed T-test. (g, h) Representative histogram and pooled data for E-cadherin expression on human gastric (n=5) and MoDCs (n=8). (i) MoDCs were treated with anti-E-cadherin antibody before and during co-culture with HT-29 cells, and the number of adherent DCs was determined. N=4, *$P \leq 0.05$; unpaired, two-tailed Student's *t* test.

SUPPLEMENTAL INFORMATION

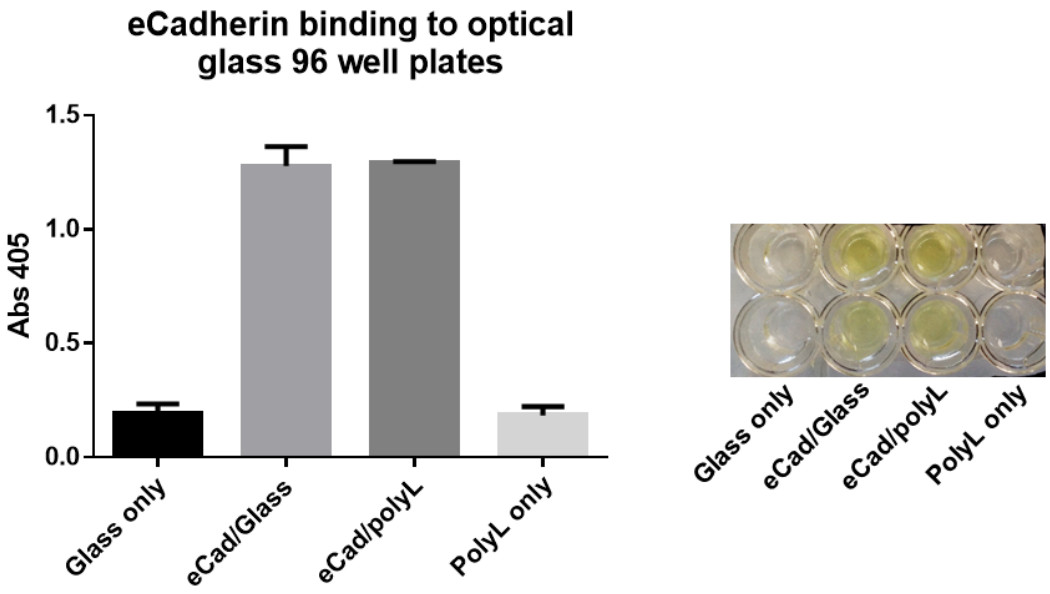

Supplemental Figure 1: Coating of glass surfaces with rh E-cadherin. Untreated or poly-L lysine-coated wells of a glass bottom 96 well plate were incubated with recombinant human E-cadherin (1 μg/mL) in PBS for 60 min. Following a blocking step with 10 % human serum, and several washes, E-cadherin bound to the plate was detected using an anti-E-cadherin antibody and visualized using an alkaline phosphatase detection system. Left panel: Mean absorption (405 nm) ± SEM of duplicate wells. Right panel: Plate image.

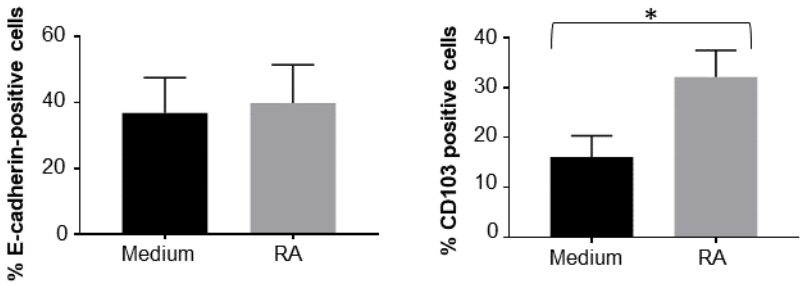

Supplemental Figure 2: Retinoic acid significantly increases expression of CD103, but not E-cadherin in human MoDCs. MoDCs were treated with 100nM RA and surface expression of E-cadherin (left panel, n=12) and CD103 (right panel, n=13) were analyzed with flow cytometry. *$P \leq 0.05$; unpaired, two-tailed T-test.

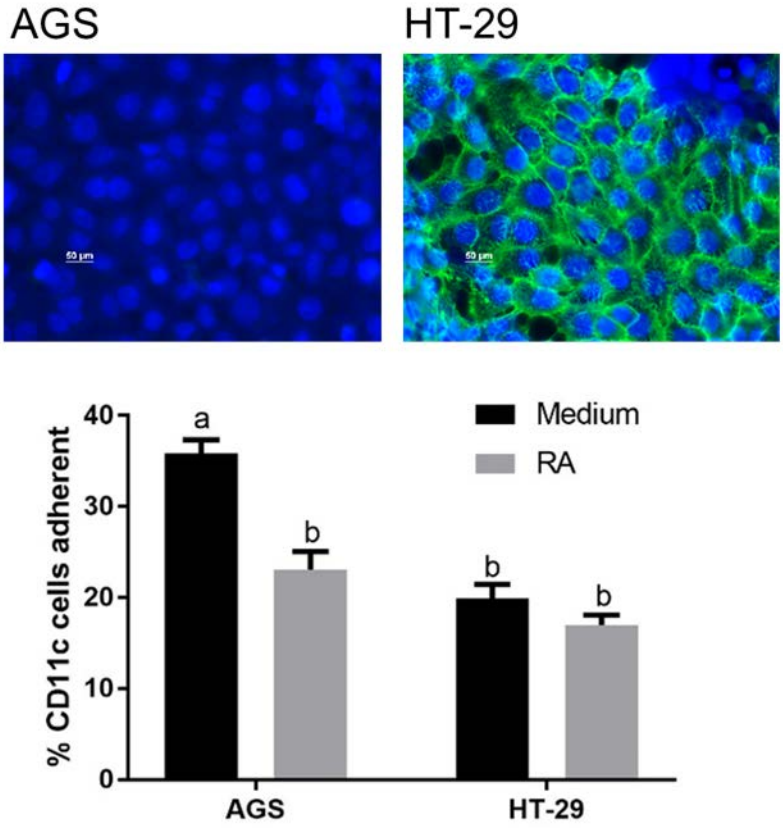

Supplemental Figure 3: Strong adhesion of MoDCs to E-cadherin negative AGS cells. Top panel: Confocal analysis of an AGS and an HT-29 monolayer shows surface E-cadherin expression (green) by the HT-29, but not by AGS cells. Bottom panel: RA-treated or untreated MoDCs were added to confluent monolayers of AGS or HT-29 cells for 2 h. Non-adherent cells were then removed by gentle washing, the remaining cells were collected by trypsinization, and the number of adherent DCs was determined using counting beads and CD11c-labeling of the DCs. Mean ± SEM of 3 independent experiments. Data were analyzed by ANOVA with Tukey's post hoc test. a, b: different letters indicate significantly different values ($P \leq 0.05$).

LITERATURE CITED

1. Bimczok D, *et al.* (2010) Human primary gastric dendritic cells induce a Th1 response to H. pylori. *Mucosal Immunol* 3(3):260-269.

2. Kao JY, *et al.* (2010) Helicobacter pylori immune escape is mediated by dendritic cell-induced Treg skewing and Th17 suppression in mice. *Gastroenterology* 138(3):1046-1054.

3. Necchi V, Manca R, Ricci V, & Solcia E (2009) Evidence for transepithelial dendritic cells in human H. pylori active gastritis. *Helicobacter* 14(3):208-222.

4. Shiu J & Blanchard TG (2013) Dendritic cell function in the host response to Helicobacter pylori infection of the gastric mucosa. *Pathog Dis* 67(1):46-53.

5. Moss SF & Malfertheiner P (2007) Helicobacter and gastric malignancies. *Helicobacter.* 12 Suppl 1:23-30.

6. Amieva M & Peek RM, Jr. (2016) Pathobiology of Helicobacter pylori-Induced Gastric Cancer. *Gastroenterology* 150(1):64-78.

7. Hitzler I, Oertli M, Becher B, Agger EM, & Muller A (2011) Dendritic cells prevent rather than promote immunity conferred by a helicobacter vaccine using a mycobacterial adjuvant. *Gastroenterology* 141(1):186-196, 196 e181.

8. Harris PR, *et al.* (2008) Helicobacter pylori gastritis in children is associated with a regulatory T-cell response. *Gastroenterology* 134(2):491-499.

9. Serrano C, *et al.* (2013) Downregulated Th17 responses are associated with reduced gastritis in Helicobacter pylori-infected children. *Mucosal Immunol*.

10. Robinson K, *et al.* (2008) Helicobacter pylori-induced peptic ulcer disease is associated with inadequate regulatory T cell responses. *Gut* 57(10):1375-1385.

11. Rescigno M, *et al.* (2001) Dendritic cells express tight junction proteins and penetrate gut epithelial monolayers to sample bacteria. *Nat Immunol* 2(4):361-367.

12. Iliev ID, Mileti E, Matteoli G, Chieppa M, & Rescigno M (2009) Intestinal epithelial cells promote colitis-protective regulatory T-cell differentiation through dendritic cell conditioning. *Mucosal Immunol* 2(4):340-350.

13. Iliev ID, *et al.* (2009) Human intestinal epithelial cells promote the differentiation of tolerogenic dendritic cells. *Gut* 58(11):1481-1489.

14. Bimczok D, *et al.* (2015) Human gastric epithelial cells contribute to gastric immune regulation by providing retinoic acid to dendritic cells. *Mucosal Immunol* 8(3):533-544.

15. Hadley GA & Higgins JM (2014) Integrin alphaEbeta7: molecular features and functional significance in the immune system. *Adv Exp Med Biol* 819:97-110.

16. Watchmaker PB, *et al.* (2014) Comparative transcriptional and functional profiling defines conserved programs of intestinal DC differentiation in humans and mice. *Nat Immunol* 15(1):98-108.

17. Habtezion A, Nguyen LP, Hadeiba H, & Butcher EC (2016) Leukocyte Trafficking to the Small Intestine and Colon. *Gastroenterology* 150(2):340-354.

18. Guilliams M, *et al.* (2014) Dendritic cells, monocytes and macrophages: a unified nomenclature based on ontogeny. *Nat Rev Immunol* 14(8):571-578.

19. Haniffa M, Collin M, & Ginhoux F (2013) Ontogeny and functional specialization of dendritic cells in human and mouse. *Adv Immunol* 120:1-49.

20. Segura E (2016) Review of Mouse and Human Dendritic Cell Subsets. *Methods Mol Biol* 1423:3-15.

21. Scott CL, Aumeunier AM, & Mowat AM (2011) Intestinal CD103+ dendritic cells: master regulators of tolerance? *Trends Immunol* 32(9):412-419.

22. Corps E, *et al.* (2001) Recognition of E-cadherin by integrin alpha(E)beta(7): requirement for cadherin dimerization and implications for cadherin and integrin function. *J Biol Chem* 276(33):30862-30870.

23. Cepek KL, *et al.* (1994) Adhesion between epithelial cells and T lymphocytes mediated by E-cadherin and the alpha E beta 7 integrin. *Nature* 372(6502):190-193.

24. Higgins JM, *et al.* (2000) The role of alpha and beta chains in ligand recognition by beta 7 integrins. *J Biol Chem* 275(33):25652-25664.

25. Roe MM, *et al.* (2017) Differential regulation of CD103 (alphaE integrin) expression in human dendritic cells by retinoic acid and Toll-like receptor ligands. *J Leukoc Biol* 101(5):1169-1180.

26. Viladomiu M, *et al.* (2017) Cooperation of Gastric Mononuclear Phagocytes with Helicobacter pylori during Colonization. *J Immunol* 198(8):3195-3204.

27. Arnold IC, *et al.* (2017) NLRP3 Controls the Development of Gastrointestinal CD11b(+) Dendritic Cells in the Steady State and during Chronic Bacterial Infection. *Cell Rep* 21(13):3860-3872.

28. Bimczok D, *et al.* (2011) Stromal regulation of human gastric dendritic cells restricts the Th1 response to Helicobacter pylori. *Gastroenterology* 141(3):929-938.

29. Agace WW & Persson EK (2012) How vitamin A metabolizing dendritic cells are generated in the gut mucosa. *Trends Immunol* 33(1):42-48.

30. del Rio ML, Bernhardt G, Rodriguez-Barbosa JI, & Forster R (2010) Development and functional specialization of CD103+ dendritic cells. *Immunol Rev* 234(1):268-281.

31. Bretscher MS (1992) Circulating integrins: alpha 5 beta 1, alpha 6 beta 4 and Mac-1, but not alpha 3 beta 1, alpha 4 beta 1 or LFA-1. *EMBO J* 11(2):405-410.

32. Bridgewater RE, Norman JC, & Caswell PT (2012) Integrin trafficking at a glance. *J Cell Sci* 125(Pt 16):3695-3701.

33. Paul NR, Jacquemet G, & Caswell PT (2015) Endocytic Trafficking of Integrins in Cell Migration. *Curr Biol* 25(22):R1092-1105.

34. Bolte S & Cordelieres FP (2006) A guided tour into subcellular colocalization analysis in light microscopy. *J Microsc.* 224(Pt 3):213-232.

35. Dunn KW, Kamocka MM, & McDonald JH (2011) A practical guide to evaluating colocalization in biological microscopy. *Am J Physiol Cell Physiol* 300(4):C723-742.

36. Chen PW, Luo R, Jian X, & Randazzo PA (2014) The Arf6 GTPase-activating proteins ARAP2 and ACAP1 define distinct endosomal compartments that regulate integrin alpha5beta1 traffic. *J Biol Chem* 289(44):30237-30248.

37. Rainero E & Norman JC (2013) Late endosomal and lysosomal trafficking during integrin-mediated cell migration and invasion: cell matrix receptors are trafficked through the late endosomal pathway in a way that dictates how cells migrate. *Bioessays* 35(6):523-532.

38. Maritzen T, Schachtner H, & Legler DF (2015) On the move: endocytic trafficking in cell migration. *Cell Mol Life Sci*.

39. Guerra F & Bucci C (2016) Multiple Roles of the Small GTPase Rab7. *Cells* 5(3):E34.

40. Vernerey FJ & Farsad M (2014) A mathematical model of the coupled mechanisms of cell adhesion, contraction and spreading. *J Math Biol* 68(4):989-1022.

41. Schlickum S, *et al.* (2008) Integrin alpha E(CD103)beta 7 influences cellular shape and motility in a ligand-dependent fashion. *Blood* 112(3):619-625.

42. Gout S, *et al.* (2004) Early enterocytic differentiation of HT-29 cells: biochemical changes and strength increases of adherens junctions. *Exp Cell Res* 299(2):498-510.

43. Efstathiou JA, *et al.* (1999) Mutated epithelial cadherin is associated with increased tumorigenicity and loss of adhesion and of responsiveness to the motogenic trefoil factor 2 in colon carcinoma cells. *Proc Natl Acad Sci U S A* 96(5):2316-2321.

44. Ye F, Kim C, & Ginsberg MH (2012) Reconstruction of integrin activation. *Blood* 119(1):26-33.

45. Zhang K & Chen J (2012) The regulation of integrin function by divalent cations. *Cell Adh Migr* 6(1):20-29.

46. van Roy F & Berx G (2008) The cell-cell adhesion molecule E-cadherin. *Cell Mol Life Sci* 65(23):3756-3788.

47. Van den Bossche J, Malissen B, Mantovani A, De Baetselier P, & Van Ginderachter JA (2012) Regulation and function of the E-cadherin/catenin complex in cells of the monocyte-macrophage lineage and DCs. *Blood* 119(7):1623-1633.

48. Riedl E, *et al.* (2000) Functional involvement of E-cadherin in TGF-beta 1-induced cell cluster formation of in vitro developing human Langerhans-type dendritic cells. *J Immunol* 165(3):1381-1386.

49. Jakob T, Brown MJ, & Udey MC (1999) Characterization of E-cadherin-containing junctions involving skin-derived dendritic cells. *J Invest Dermatol* 112(1):102-108.

50. Schon MP, *et al.* (1999) Mucosal T lymphocyte numbers are selectively reduced in integrin alpha E (CD103)-deficient mice. *J Immunol* 162(11):6641-6649.

51. Lobert VH, *et al.* (2010) Ubiquitination of alpha 5 beta 1 integrin controls fibroblast migration through lysosomal degradation of fibronectin-integrin complexes. *Dev Cell* 19(1):148-159.

52. Ezratty EJ, Bertaux C, Marcantonio EE, & Gundersen GG (2009) Clathrin mediates integrin endocytosis for focal adhesion disassembly in migrating cells. *J Cell Biol* 187(5):733-747.

53. Krishnan M, Lapierre LA, Knowles BC, & Goldenring JR (2013) Rab25 regulates integrin expression in polarized colonic epithelial cells. *Mol Biol Cell* 24(6):818-831.

54. Gu Z, Noss EH, Hsu VW, & Brenner MB (2011) Integrins traffic rapidly via circular dorsal ruffles and macropinocytosis during stimulated cell migration. *J Cell Biol* 193(1):61-70.

55. Khandelwal P, Ruiz WG, & Apodaca G (2010) Compensatory endocytosis in bladder umbrella cells occurs through an integrin-regulated and RhoA- and dynamin-dependent pathway. *EMBO J* 29(12):1961-1975.

56. Karjalainen M, *et al.* (2008) A Raft-derived, Pak1-regulated entry participates in alpha2beta1 integrin-dependent sorting to caveosomes. *Mol Biol Cell* 19(7):2857-2869.

57. De Franceschi N, Hamidi H, Alanko J, Sahgal P, & Ivaska J (2015) Integrin traffic - the update. *J Cell Sci* 128(5):839-852.

58. den Hartog G, van Altena C, Savelkoul HF, & van Neerven RJ (2013) The mucosal factors retinoic acid and TGF-beta1 induce phenotypically and functionally distinct dendritic cell types. *Int Arch Allergy Immunol* 162(3):225-236.

59. Farache J, *et al.* (2013) Luminal bacteria recruit CD103+ dendritic cells into the intestinal epithelium to sample bacterial antigens for presentation. *Immunity* 38(3):581-595.

60. Taraszka KS, *et al.* (2000) Molecular basis for leukocyte integrin alpha(E)beta(7) adhesion to epithelial (E)-cadherin. *J Exp Med* 191(9):1555-1567.

61. Hubert P, *et al.* (2005) E-cadherin-dependent adhesion of dendritic and Langerhans cells to keratinocytes is defective in cervical human papillomavirus-associated (pre)neoplastic lesions. *J Pathol* 206(3):346-355.

62. Tang A, Amagai M, Granger LG, Stanley JR, & Udey MC (1993) Adhesion of epidermal Langerhans cells to keratinocytes mediated by E-cadherin. *Nature* 361(6407):82-85.

63. Lacaz-Vieira F (1997) Calcium site specificity. Early Ca2+-related tight junction events. *J Gen Physiol* 110(6):727-740.

64. Nagafuchi A & Takeichi M (1988) Cell binding function of E-cadherin is regulated by the cytoplasmic domain. *EMBO J* 7(12):3679-3684.

65. Ni H, Li A, Simonsen N, & Wilkins JA (1998) Integrin activation by dithiothreitol or Mn2+ induces a ligand-occupied conformation and exposure of a novel NH2-terminal regulatory site on the beta1 integrin chain. *J Biol Chem* 273(14):7981-7987.

66. Banh C, Fugere C, & Brossay L (2009) Immunoregulatory functions of KLRG1 cadherin interactions are dependent on forward and reverse signaling. *Blood* 114(26):5299-5306.

67. Ito M, *et al.* (2006) Killer cell lectin-like receptor G1 binds three members of the classical cadherin family to inhibit NK cell cytotoxicity. *J Exp Med* 203(2):289-295.

68. Cavarelli M, Foglieni C, Rescigno M, & Scarlatti G (2013) R5 HIV-1 envelope attracts dendritic cells to cross the human intestinal epithelium and sample luminal virions via engagement of the CCR5. *EMBO Mol Med* 5(5):776-794.

69. Schittenhelm L, Hilkens CM, & Morrison VL (2017) beta2 Integrins As Regulators of Dendritic Cell, Monocyte, and Macrophage Function. *Front Immunol* 8:1866.

70. Crowe SE, *et al.* (1995) Expression of interleukin 8 and CD54 by human gastric epithelium after Helicobacter pylori infection in vitro. *Gastroenterology* 108(1):65-74.

71. Mane V & Muro S (2012) Biodistribution and endocytosis of ICAM-1-targeting antibodies versus nanocarriers in the gastrointestinal tract in mice. *Int J Nanomedicine* 7:4223-4237.

72. Shen B, Delaney MK, & Du X (2012) Inside-out, outside-in, and inside-outside-in: G protein signaling in integrin-mediated cell adhesion, spreading, and retraction. *Curr Opin Cell Biol* 24(5):600-606.

73. Le Floc'h A, *et al.* (2011) Minimal engagement of CD103 on cytotoxic T lymphocytes with an E-cadherin-Fc molecule triggers lytic granule polarization via a phospholipase Cgamma-dependent pathway. *Cancer Res* 71(2):328-338.

74. Russell GJ, *et al.* (1994) Distinct structural and functional epitopes of the alpha E beta 7 integrin. *Eur J Immunol* 24(11):2832-2841.

CHAPTER 7

CONCLUSION

In Chapter 2, we described unexpected phenomena exhibited by human gastric organoids (HGOs). These include HGO coalescence, rotational motion, and periodic, spontaneous rupture events. HGO coalescence is rare, but fundamentally interesting, and may have applications in bioengineering approaches for assembling larger HGO-based structures or may offer insight into therapeutic uses for HGOs; for example, transplanted gastric and colonic organoids have been shown to improve the healing of defective epithelia in murine GI tract and colon respectively. HGO rotation is likely due to pseudopodia, which are generally associated with the cellular movement. These dynamics may be influenced by the specific characteristics of the Matrigel matrix, which differs from normal basement membrane and extracellular matrix in composition and structure or may be due to basal pseudopod formation. Further experimentation into the effect of Matrigel stiffness on gastric organoid growth and dynamics is warranted. HGO rupturing is perhaps the most common of the observed phenomena, occurring for more than 40% of spheroids imaged, but the probability of rupture varied widely for HGOs derived from different human donors.

In Chapter 3, we presented a simple pressure balance to provide a framework for understanding rupture events. Various osmotic stress conditions showed that moderate osmotic perturbations ($\leq$ 50 mOsm) caused HGOs to shrink and swell proportionally rather quickly due to the diffusion of water. Even though the shell elasticity was negligible at smaller perturbations, at very dilute media concentrations, osmotic swelling

caused strain-dependent shell elasticity to become a significant factor in the structural integrity of the organoid. In contrast with the osmotic perturbations applied, organoids swell in their growth media over hours and even days. Thus, the rupture events are an indirect result of osmotic swelling carried out by the diffusion of water due to osmolyte concentration regulation by the epithelial shell, consistent with the suppressed rupture events through drug treatment that inhibits proton pumps.

In Chapter 4, we describe an engineering-based approach to overcome the transport limitations imposed by the closed shell of gut organoids, which suppresses advection. To accomplish this, we engineer a millifluidic device to establish liquid flow through the lumen of a gastrointestinal organoid. This approach opens the field for broader applications of HIO models in biomedical research such as the controlled injection of bacteria for microbiome and pathogeneses studies. Also, this platform could be integrated with microfluidic systems for advanced real-time screening for drug development as well as metabolomics studies. The limits of HIO culturing and experimentation have not been fully explored, but this prototype chip we call the Gut Organoid Flow Chip (GOFlowChip) provides a significant advancement by mimicking a critically important parameter of the human gut: luminal flow.

In Chapter 5, we developed and evaluated a novel co-culture model by using HGOs derived from primary human cells which enabled functional studies of the interactions between the gastric epithelium, DCs, and luminal *H. pylori* bacteria. By contrast to work in previous chapters, here, the enclosed structure of an HGO allows for the investigation of immunological mechanisms within the mucosal environment in the

human stomach. HGOs enable direct access of immune cells to the basolateral side of the epithelium and support active *H. pylori* infection over several days and are, therefore, suitable for studying gastric DC-epithelial cell crosstalk *in vitro*. With this model, we demonstrated human DCs showing chemotactic activity for epithelial-derived factors and forming close interactions with the epithelium. In conclusion, the gastric epithelium promoted accelerated recruitment of DCs to the epithelial cell interface upon *H. pylori* infection through a chemokine-dependent mechanism. Furthermore, we anticipate that the DC-epithelial cell co-culture model described here can be easily adapted for studying other mucosal sites, immune cells and pathogens. However, consistent with our previous studies, organoids may occasionally rupture, releasing luminal material including infectious agents, apoptotic epithelial cell material and mucus in an uncontrolled manner; this must be considered throughout such co-culture model systems.

In Chapter 6, we addressed the question of whether the attachment protein CD103 on dendritic cells is the chief mediator of DC-epithelial cell adhesion. To test this hypothesis, we performed confocal microscopy to image CD103 presence in endosomal compartments, where CD103 partially co-localized with intracellular transport and signaling proteins such as clathrin, early endosome antigen-1, and Rab11, indicating that CD103 undergoes endosomal trafficking like b1 integrins. In conclusion, we found that CD103 does not mediate the DC adhesion to gastrointestinal epithelia, though it engages in DC-epithelial cell interactions. While this study provided novel insights into the regulation and function of CD103 in human DCs, the mechanisms by which CD103 on

DCs in the human gastrointestinal tract interact with epithelial cells require further experimental exploration.

CUMULATIVE LITERATURE CITED

Abernethy, N. J., J. B. Hay, W. G. Kimpton, E. Washington, and R. N. Cahill. "Lymphocyte Subset-Specific and Tissue-Specific Lymphocyte-Endothelial Cell Recognition Mechanisms Independently Direct the Recirculation of Lymphocytes from Blood to Lymph in Sheep." *Immunology* 72, no. 2 (1991): 239-45.

Adhikary, S., V. P. Kocieda, J. H. Yen, R. F. Tuma, and D. Ganea. "Signaling through Cannabinoid Receptor 2 Suppresses Murine Dendritic Cell Migration by Inhibiting Matrix Metalloproteinase 9 Expression." *Blood* 120, no. 18 (2012): 3741-9.

Agace, W. W. and E. K. Persson. "How Vitamin a Metabolizing Dendritic Cells Are Generated in the Gut Mucosa." *Trends Immunol* 33, no. 1 (2012): 42-8.

Agarwal, A., J. A. Goss, A. Cho, M. L. McCain, and K. K. Parker. "Microfluidic Heart on a Chip for Higher Throughput Pharmacological Studies." *Lab on a Chip* 13, no. 18 (2013): 3599-608.

Akkerman, N. and L. H. K. Defize. "Dawn of the Organoid Era: 3d Tissue and Organ Cultures Revolutionize the Study of Development, Disease, and Regeneration." *Bioessays* 39, no. 4 (2017).

Alberts B, Johnson A, Lewis J et al. *Principles of Membrane Transport*. 4th ed. Molecular Biology of the Cell. New York: Garland Science, 2002.

Allen, J. W. and S. N. Bhatia. "Formation of Steady-State Oxygen Gradients in Vitro - Application to Liver Zonation." *Biotechnology and Bioengineering* 82, no. 3 (2003): 253-62.

Amieva, M. and R. M. Peek, Jr. "Pathobiology of Helicobacter Pylori-Induced Gastric Cancer." *Gastroenterology* 150, no. 1 (2016): 64-78.

Arnold, I. C., X. Zhang, S. Urban, M. Artola-Boran, M. G. Manz, K. M. Ottemann, and A. Muller. "Nlrp3 Controls the Development of Gastrointestinal Cd11b(+) Dendritic Cells in the Steady State and During Chronic Bacterial Infection." *Cell Rep* 21, no. 13 (2017): 3860-72.

Aurora, M. and J. R. Spence. "Hpsc-Derived Lung and Intestinal Organoids as Models of Human Fetal Tissue." *Developmental Biology* 420, no. 2 (2016): 230-38.

Banh, C., C. Fugere, and L. Brossay. "Immunoregulatory Functions of Klrg1 Cadherin Interactions Are Dependent on Forward and Reverse Signaling." *Blood* 114, no. 26 (2009): 5299-306.

Baraki, Y. M., P. Traverso, H. A. Elariny, and Y. Fang. "Preoperative Prediction of Stomach Weight to Be Removed in Laparoscopic Sleeve Gastrectomy Procedure." *Surg Technol Int* 20 (2010): 167-71.

Barker, N., M. Huch, P. Kujala, M. van de Wetering, H. J. Snippert, J. H. van Es, T. Sato, D. E. Stange, H. Begthel, M. van den Born, E. Danenberg, S. van den Brink, J. Korving, A. Abo, P. J. Peters, N. Wright, R. Poulsom, and H. Clevers. "Lgr5(+Ve) Stem Cells Drive Self-Renewal in the Stomach and Build Long-Lived Gastric Units in Vitro." *Cell Stem Cell* 6, no. 1 (2010): 25-36.

Barker, N., J. H. van Es, J. Kuipers, P. Kujala, M. van den Born, M. Cozijnsen, A. Haegebarth, J. Korving, H. Begthel, P. J. Peters, and H. Clevers. "Identification of Stem Cells in Small Intestine and Colon by Marker Gene Lgr5." *Nature* 449, no. 7165 (2007): 1003-U1.

Bartfeld, S., T. Bayram, M. van de Wetering, M. Huch, H. Begthel, P. Kujala, R. Vries, P. J. Peters, and H. Clevers. "In Vitro Expansion of Human Gastric Epithelial Stem Cells and Their Responses to Bacterial Infection." *Gastroenterology* 148, no. 1 (2015): 126-36.

Baudoin, R., L. Griscom, M. Monge, C. Legallais, and E. Leclerc. "Development of a Renal Microchip for in Vitro Distal Tubule Models." *Biotechnology Progress* 23, no. 5 (2007): 1245-53.

Benton, G., J. George, H. K. Kleinman, and I. P. Arnaoutova. "Advancing Science and Technology Via 3d Culture on Basement Membrane Matrix." *J Cell Physiol* 221, no. 1 (2009): 18-25.

Bermudez-Brito, M., S. Munoz-Quezada, C. Gomez-Llorente, E. Matencio, F. Romero, and A. Gil. "Lactobacillus Paracasei Cncm I-4034 and Its Culture Supernatant Modulate Salmonella-Induced Inflammation in a Novel Transwell Co-Culture of Human Intestinal-Like Dendritic and Caco-2 Cells." *BMC Microbiol* 15, no. 1 (2015): 79.

Bertaux-Skeirik, N., R. Feng, M. A. Schumacher, J. Li, M. M. Mahe, A. C. Engevik, J. E. Javier, R. M. Peek, Jr., K. Ottemann, V. Orian-Rousseau, G. P. Boivin, M. A. Helmrath, and Y. Zavros. "Cd44 Plays a Functional Role in Helicobacter Pylori-Induced Epithelial Cell Proliferation." *PLoS Pathog* 11, no. 2 (2015): e1004663.

Bimczok, D., R. H. Clements, K. B. Waites, L. Novak, D. E. Eckhoff, P. J. Mannon, P. D. Smith, and L. E. Smythies. "Human Primary Gastric Dendritic Cells Induce a Th1 Response to H. Pylori." *Mucosal Immunol* 3, no. 3 (2010): 260-9.

Bimczok, D., J. M. Grams, R. D. Stahl, K. B. Waites, L. E. Smythies, and P. D. Smith. "Stromal Regulation of Human Gastric Dendritic Cells Restricts the Th1 Response to Helicobacter Pylori." *Gastroenterology* 141, no. 3 (2011): 929-38.

Bimczok, D., J. Y. Kao, M. Zhang, S. Cochrun, P. Mannon, S. Peter, C. M. Wilcox, K. E. Monkemuller, P. R. Harris, J. M. Grams, R. D. Stahl, P. D. Smith, and L. E. Smythies. "Human Gastric Epithelial Cells Contribute to Gastric Immune Regulation by Providing Retinoic Acid to Dendritic Cells." *Mucosal Immunol* 8, no. 3 (2015): 533-44.

Bimczok, D., L. E. Smythies, K. B. Waites, J. M. Grams, R. D. Stahl, P. J. Mannon, S. Peter, C. M. Wilcox, P. R. Harris, S. Das, P. B. Ernst, and P. D. Smith. "Helicobacter Pylori Infection Inhibits Phagocyte Clearance of Apoptotic Gastric Epithelial Cells." *J Immunol* 190, no. 12 (2013): 6626-34.

Binti Mohd Amir, N. A. S., A. E. Mackenzie, L. Jenkins, K. Boustani, M. C. Hillier, T. Tsuchiya, G. Milligan, and J. E. Pease. "Evidence for the Existence of a Cxcl17 Receptor Distinct from Gpr35." *J Immunol* 201, no. 2 (2018): 714-24.

Bohorquez, D. V., R. Chandra, L. A. Samsa, S. R. Vigna, and R. A. Liddle. "Characterization of Basal Pseudopod-Like Processes in Ileal and Colonic Pyy Cells." *J Mol Histol* 42, no. 1 (2011): 3-13.

Bolte, S. and F. P. Cordelieres. "A Guided Tour into Subcellular Colocalization Analysis in Light Microscopy." *J Microsc.* 224, no. Pt 3 (2006): 213-32.

Booth, R. and H. Kim. "Characterization of a Microfluidic in Vitro Model of the Blood-Brain Barrier (Mu Bbb)." *Lab on a Chip* 12, no. 10 (2012): 1784-92.

Bradford, E. M., S. H. Ryu, A. P. Singh, G. Lee, T. Goretsky, P. Sinh, D. B. Williams, A. L. Cloud, E. Gounaris, V. Patel, O. F. Lamping, E. B. Lynch, M. P. Moyer, I. G. De Plaen, D. J. Shealy, G. Y. Yang, and T. A. Barrett. "Epithelial Tnf Receptor Signaling Promotes Mucosal Repair in Inflammatory Bowel Disease." *J Immunol* 199, no. 5 (2017): 1886-97.

Bretscher, M. S. "Circulating Integrins: Alpha 5 Beta 1, Alpha 6 Beta 4 and Mac-1, but Not Alpha 3 Beta 1, Alpha 4 Beta 1 or Lfa-1." *EMBO J* 11, no. 2 (1992): 405-10.

Bridgewater, R. E., J. C. Norman, and P. T. Caswell. "Integrin Trafficking at a Glance." *J Cell Sci* 125, no. Pt 16 (2012): 3695-701.

Brumfield, S. K., A. C. Ortmann, V. Ruigrok, P. Suci, T. Douglas, and M. J. Young. "Particle Assembly and Ultrastructural Features Associated with Replication of the Lytic Archaeal Virus Sulfolobus Turreted Icosahedral Virus." *J Virol* 83, no. 12 (2009): 5964-70.

Buckley, A. and J. R. Turner. "Cell Biology of Tight Junction Barrier Regulation and Mucosal Disease." *Cold Spring Harbor Perspectives in Biology* 10, no. 1 (2018).

Burgess, D. R. "Structure of the Epithelial - Mesenchymal Interface During Early Morphogenesis of the Chick Duodenum." *Tissue Cell* 8, no. 1 (1976): 147-58.

Butler, M., C. Y. Ng, D. A. van Heel, G. Lombardi, R. Lechler, R. J. Playford, and S. Ghosh. "Modulation of Dendritic Cell Phenotype and Function in an in Vitro Model of the Intestinal Epithelium." *Eur J Immunol* 36, no. 4 (2006): 864-74.

Capeling, Meghan M., Michael Czerwinski, Sha Huang, Yu-Hwai Tsai, Angeline Wu, Melinda S. Nagy, Benjamin Juliar, Nambirajan Sundaram, Yang Song, Woojin M. Han, Shuichi Takayama, Eben Alsberg, Andres J. Garcia, Michael Helmrath, Andrew J. Putnam, and Jason R. Spence. "Nonadhesive Alginate Hydrogels Support Growth of Pluripotent Stem Cell-Derived Intestinal Organoids." *Stem Cell Reports* 12, no. 2 (2019): 381-94.

Carraro, A., W. M. Hsu, K. M. Kulig, W. S. Cheung, M. L. Miller, E. J. Weinberg, E. F. Swart, M. Kaazempur-Mofrad, J. T. Borenstein, J. P. Vacanti, and C. Neville. "In Vitro Analysis of a Hepatic Device with Intrinsic Microvascular-Based Channels." *Biomedical Microdevices* 10, no. 6 (2008): 795-805.

Cavarelli, M., C. Foglieni, M. Rescigno, and G. Scarlatti. "R5 Hiv-1 Envelope Attracts Dendritic Cells to Cross the Human Intestinal Epithelium and Sample Luminal Virions Via Engagement of the Ccr5." *EMBO Mol Med* 5, no. 5 (2013): 776-94.

Cepek, K. L., S. K. Shaw, C. M. Parker, G. J. Russell, J. S. Morrow, D. L. Rimm, and M. B. Brenner. "Adhesion between Epithelial Cells and T Lymphocytes Mediated by E-Cadherin and the Alpha E Beta 7 Integrin." *Nature* 372, no. 6502 (1994): 190-3.

Chao, P., T. Maguire, E. Novik, K. C. Cheng, and M. L. Yarmush. "Evaluation of a Microfluidic Based Cell Culture Platform with Primary Human Hepatocytes for the Prediction of Hepatic Clearance in Human." *Biochemical Pharmacology* 78, no. 6 (2009): 625-32.

Chen, P. W., R. Luo, X. Jian, and P. A. Randazzo. "The Arf6 Gtpase-Activating Proteins Arap2 and Acap1 Define Distinct Endosomal Compartments That Regulate Integrin Alpha5beta1 Traffic." *J Biol Chem* 289, no. 44 (2014): 30237-48.

Chen, W. L. K., C. Edington, E. Suter, J. J. Yu, J. J. Velazquez, J. G. Velazquez, M. Shockley, E. M. Large, R. Venkataramanan, D. J. Hughes, C. L. Stokes, D. L. Trumper, R. L. Carrier, M. Cirit, L. G. Griffith, and D. A. Lauffenburger. "Integrated Gut/Liver Microphysiological Systems Elucidates Inflammatory Inter-Tissue Crosstalk." *Biotechnology and Bioengineering* 114, no. 11 (2017): 2648-59.

Cheng, S., J. M. Prot, E. Leclerc, and F. Y. Bois. "Zonation Related Function and Ubiquitination Regulation in Human Hepatocellular Carcinoma Cells in Dynamic Vs. Static Culture Conditions." *Bmc Genomics* 13 (2012).

Cheng, W., N. Klauke, H. Sedgwick, G. L. Smith, and J. M. Cooper. "Metabolic Monitoring of the Electrically Stimulated Single Heart Cell within a Microfluidic Platform." *Lab on a Chip* 6, no. 11 (2006): 1424-31.

Chieppa, M., M. Rescigno, A. Y. Huang, and R. N. Germain. "Dynamic Imaging of Dendritic Cell Extension into the Small Bowel Lumen in Response to Epithelial Cell Tlr Engagement." *J Exp.Med.* 203, no. 13 (2006): 2841-52.

Chou, C. C. "Contribution of Splanchnic Circulation to Overall Cardiovascular and Metabolic Homeostasis - Introduction." *Federation Proceedings* 42, no. 6 (1983): 1656-57.

Clayman, C. B. "Evaluation of Cimetidine (Tagamet). An Antagonist of Hydrochloric Acid Secretion." *JAMA* 238, no. 12 (1977): 1289-90.

Corpron, R. E. "The Ultrastructure of the Gastric Mucosa in Normal and Hypophysectomized Rats." *Am J Anat* 118, no. 1 (1966): 53-90.

Corps, E., C. Carter, P. Karecla, T. Ahrens, P. Evans, and P. Kilshaw. "Recognition of E-Cadherin by Integrin Alpha(E)Beta(7): Requirement for Cadherin Dimerization and Implications for Cadherin and Integrin Function." *J Biol Chem* 276, no. 33 (2001): 30862-70.

Cover, T. L. and M. J. Blaser. "Helicobacter Pylori in Health and Disease." *Gastroenterology* 136, no. 6 (2009): 1863-73.

Creamer, B., R. G. Shorter, and J. Bamforth. "The Turnover and Shedding of Epithelial Cells. I. The Turnover in the Gastro-Intestinal Tract." *Gut* 2 (1961): 110-8.

Crowe, S. E., L. Alvarez, M. Dytoc, R. H. Hunt, M. Muller, P. Sherman, J. Patel, Y. Jin, and P. B. Ernst. "Expression of Interleukin 8 and Cd54 by Human Gastric Epithelium after Helicobacter Pylori Infection in Vitro." *Gastroenterology* 108, no. 1 (1995): 65-74.

Cruz-Acuña, Ricardo, Miguel Quirós, Attila E. Farkas, Priya H. Dedhia, Sha Huang, Dorothée Siuda, Vicky García-Hernández, Alyssa J. Miller, Jason R. Spence, Asma Nusrat, and Andrés J. García. "Synthetic Hydrogels for Human Intestinal Organoid Generation and Colonic Wound Repair." *Nature Cell Biology* 19 (2017): 1326.

Cruz-Acuña, Ricardo, Miguel Quirós, Sha Huang, Dorothée Siuda, Jason R. Spence, Asma Nusrat, and Andrés J. García. "Peg-4mal Hydrogels for Human Organoid Generation, Culture, and in Vivo Delivery." *Nat Protoc* 13, no. 9 (2018): 2102-19.

Davies, Jamie and Melanie Lawrence. *Organs and Organoids*. San Diego, Oxford: Academic Press Imprint, Elsevier Science & Technology Books, 2018.

Day, R. E., P. Kitchen, D. S. Owen, C. Bland, L. Marshall, A. C. Conner, R. M. Bill, and M. T. Conner. "Human Aquaporins: Regulators of Transcellular Water Flow." *Biochimica Et Biophysica Acta-General Subjects* 1840, no. 5 (2014): 1492-506.

De Franceschi, N., H. Hamidi, J. Alanko, P. Sahgal, and J. Ivaska. "Integrin Traffic - the Update." *J Cell Sci* 128, no. 5 (2015): 839-52.

Dedhia, P. H., N. Bertaux-Skeirik, Y. Zavros, and J. R. Spence. "Organoid Models of Human Gastrointestinal Development and Disease." *Gastroenterology* 150, no. 5 (2016): 1098-112.

Dekkers, J. F., C. L. Wiegerinck, H. R. de Jonge, I. Bronsveld, H. M. Janssens, K. M. de Winter-de Groot, A. M. Brandsma, N. W. de Jong, M. J. Bijvelds, B. J. Scholte, E. E. Nieuwenhuis, S. van den Brink, H. Clevers, C. K. van der Ent, S. Middendorp, and J. M. Beekman. "A Functional Cftr Assay Using Primary Cystic Fibrosis Intestinal Organoids." *Nat Med* 19, no. 7 (2013): 939-45.

del Rio, M. L., G. Bernhardt, J. I. Rodriguez-Barbosa, and R. Forster. "Development and Functional Specialization of Cd103+ Dendritic Cells." *Immunol Rev* 234, no. 1 (2010): 268-81.

Delahay, R. M. and M. Rugge. "Pathogenesis of Helicobacter Pylori Infection." *Helicobacter* 17 Suppl 1 (2012): 9-15.

deMello, A. J. "Control and Detection of Chemical Reactions in Microfluidic Systems." *Nature* 442, no. 7101 (2006): 394-402.

Demitrack, E. S., G. B. Gifford, T. M. Keeley, A. J. Carulli, K. L. VanDussen, D. Thomas, T. J. Giordano, Z. Liu, R. Kopan, and L. C. Samuelson. "Notch Signaling Regulates Gastric Antral Lgr5 Stem Cell Function." *EMBO J* 34, no. 20 (2015): 2522-36.

Demitrack, E. S., G. B. Gifford, T. M. Keeley, N. Horita, A. Todisco, D. K. Turgeon, C. W. Siebel, and L. C. Samuelson. "Notch1 and Notch2 Regulate Epithelial Cell Proliferation in Mouse and Human Gastric Corpus." *Am J Physiol Gastrointest Liver Physiol* 312, no. 2 (2017): G133-G44.

den Hartog, G., R. Chattopadhyay, A. Ablack, E. H. Hall, L. D. Butcher, A. Bhattacharyya, L. Eckmann, P. R. Harris, S. Das, P. B. Ernst, and S. E. Crowe. "Regulation of Rac1 and Reactive Oxygen Species Production in Response to Infection of Gastrointestinal Epithelia." *PLoS Pathog* 12, no. 1 (2016): e1005382.

den Hartog, G., C. van Altena, H. F. Savelkoul, and R. J. van Neerven. "The Mucosal Factors Retinoic Acid and Tgf-Beta1 Induce Phenotypically and Functionally Distinct Dendritic Cell Types." *Int Arch Allergy Immunol* 162, no. 3 (2013): 225-36.

Diamond, J. M. and J. M. Tormey. "Role of Long Extracellular Channels in Fluid Transport across Epithelia." *Nature* 210, no. 5038 (1966): 817-20.

Dieu, M. C., B. Vanbervliet, A. Vicari, J. M. Bridon, E. Oldham, S. Ait-Yahia, F. Briere, A. Zlotnik, S. Lebecque, and C. Caux. "Selective Recruitment of Immature and Mature Dendritic Cells by Distinct Chemokines Expressed in Different Anatomic Sites." *J Exp Med* 188, no. 2 (1998): 373-86.

Drakes, M. L., S. J. Czinn, and T. G. Blanchard. "Regulation of Murine Dendritic Cell Immune Responses by Helicobacter Felis Antigen." *Infect.Immun.* 74, no. 8 (2006): 4624-33.

Dunn, K. W., M. M. Kamocka, and J. H. McDonald. "A Practical Guide to Evaluating Colocalization in Biological Microscopy." *Am J Physiol Cell Physiol* 300, no. 4 (2011): C723-42.

Efstathiou, J. A., D. Liu, J. M. Wheeler, H. C. Kim, N. E. Beck, M. Ilyas, A. J. Karayiannakis, N. J. Mortensen, W. Kmiot, R. J. Playford, M. Pignatelli, and W. F. Bodmer. "Mutated Epithelial Cadherin Is Associated with Increased Tumorigenicity and Loss of Adhesion and of Responsiveness to the Motogenic Trefoil Factor 2 in Colon Carcinoma Cells." *Proc Natl Acad Sci U S A* 96, no. 5 (1999): 2316-21.

El-Ali, J., P. K. Sorger, and K. F. Jensen. "Cells on Chips." *Nature* 442, no. 7101 (2006): 403-11.

Emami, C. N., R. Mittal, L. Wang, H. R. Ford, and N. V. Prasadarao. "Recruitment of Dendritic Cells Is Responsible for Intestinal Epithelial Damage in the Pathogenesis of Necrotizing Enterocolitis by Cronobacter Sakazakii." *J Immunol* 186, no. 12 (2011): 7067-79.

Engevik, A. C., R. Feng, E. Choi, S. White, N. Bertaux-Skeirik, J. Li, M. M. Mahe, E. Aihara, L. Yang, B. DiPasquale, S. Oh, K. A. Engevik, A. S. Giraud, M. H. Montrose, M. Medvedovic, M. A. Helmrath, J. R. Goldenring, and Y. Zavros. "The Development of Spasmolytic Polypeptide/Tff2-Expressing Metaplasia (Spem) During Gastric Repair Is Absent in the Aged Stomach." *Cell Mol Gastroenterol Hepatol* 2, no. 5 (2016): 605-24.

Engevik, M. A., M. B. Yacyshyn, K. A. Engevik, J. Wang, B. Darien, D. J. Hassett, B. R. Yacyshyn, and R. T. Worrell. "Human Clostridium Difficile Infection: Altered Mucus Production and Composition." *American Journal of Physiology-Gastrointestinal and Liver Physiology* 308, no. 6 (2015): G510-G24.

Esch, M. B., J. M. Prot, Y. I. Wang, P. Miller, J. R. Llamas-Vidales, B. A. Naughton, D. R. Applegate, and M. L. Shuler. "Multi-Cellular 3d Human Primary Liver Cell Culture Elevates Metabolic Activity under Fluidic Flow." *Lab on a Chip* 15, no. 10 (2015): 2269-77.

Esch, M. B., J. H. Sung, J. Yang, C. H. Yu, J. J. Yu, J. C. March, and M. L. Shuler. "On Chip Porous Polymer Membranes for Integration of Gastrointestinal Tract Epithelium with Microfluidic 'Body-on-a-Chip' Devices." *Biomedical Microdevices* 14, no. 5 (2012): 895-906.

Ezratty, E. J., C. Bertaux, E. E. Marcantonio, and G. G. Gundersen. "Clathrin Mediates Integrin Endocytosis for Focal Adhesion Disassembly in Migrating Cells." *J Cell Biol* 187, no. 5 (2009): 733-47.

Farache, J., I. Koren, I. Milo, I. Gurevich, K. W. Kim, E. Zigmond, G. C. Furtado, S. A. Lira, and G. Shakhar. "Luminal Bacteria Recruit Cd103+ Dendritic Cells into the Intestinal Epithelium to Sample Bacterial Antigens for Presentation." *Immunity* 38, no. 3 (2013): 581-95.

Finkbeiner, S. R., X. L. Zeng, B. Utama, R. L. Atmar, N. F. Shroyer, and M. K. Estes. "Stem Cell-Derived Human Intestinal Organoids as an Infection Model for Rotaviruses." *Mbio* 3, no. 4 (2012).

Finkbeiner, Stacy R, David R Hill, Christopher H Altheim, Priya H Dedhia, Matthew J Taylor, Yu-Hwai Tsai, Alana M Chin, Maxime M Mahe, Carey L Watson, Jennifer J Freeman, Roy Nattiv, Matthew Thomson, Ophir D Klein, Noah F Shroyer, Michael A Helmrath, Daniel H Teitelbaum, Peter J Dempsey, and Jason R Spence. "Transcriptome-Wide Analysis Reveals Hallmarks of Human Intestine Development and Maturation In vitro and In vivo." *Stem Cell Reports* 4, no. 6 (2015): 1140-55.

Forbester, J. L., D. Goulding, L. Vallier, N. Hannan, C. Hale, D. Pickard, S. Mukhopadhyay, and G. Dougan. "Interaction of Salmonella Enterica Serovar Typhimurium with Intestinal Organoids Derived from Human Induced Pluripotent Stem Cells." *Infection and Immunity* 83, no. 7 (2015): 2926-34.

Fritsche, C. S., O. Simsch, E. J. Weinberg, B. Orrick, C. Stamm, M. R. Kaazempur-Mofrad, J. T. Borenstein, R. Hetzer, and J. P. Vacanti. "Pulmonary Tissue Engineering Using Dual-Compartment Polymer Scaffolds with Integrated Vascular Tree." *International Journal of Artificial Organs* 32, no. 10 (2009): 701-10.

Fung, K. Y. Y., G. D. Fairn, and W. L. Lee. "Transcellular Vesicular Transport in Epithelial and Endothelial Cells: Challenges and Opportunities." *Traffic* 19, no. 1 (2018): 5-18.

Gifford, G. B., E. S. Demitrack, T. M. Keeley, A. Tam, N. La Cunza, P. H. Dedhia, J. R. Spence, D. M. Simeone, I. Saotome, A. Louvi, C. W. Siebel, and L. C. Samuelson. "Notch1 and Notch2 Receptors Regulate Mouse and Human Gastric Antral Epithelial Cell Homoeostasis." *Gut* 66, no. 6 (2017): 1001-11.

Girabawe, C. and S. Fraden. "An Image-Driven Drop-on-Demand System." *Sensors and Actuators B-Chemical* 238 (2017): 532-39.

Giridharan, G. A., M. D. Nguyen, R. Estrada, V. Parichehreh, T. Hamid, M. A. Ismahil, S. D. Prabhu, and P. Sethu. "Microfluidic Cardiac Cell Culture Model (Mu Cccm)." *Analytical Chemistry* 82, no. 18 (2010): 7581-87.

Gout, S., C. Marie, M. Laine, G. Tavernier, M. R. Block, and M. Jacquier-Sarlin. "Early Enterocytic Differentiation of Ht-29 Cells: Biochemical Changes and Strength Increases of Adherens Junctions." *Exp Cell Res* 299, no. 2 (2004): 498-510.

Gray, Henry and Susan Standring. *Gray's Anatomy: The Anatomical Basis of Clinical Practice*. Churchill Livingstone, 2008.

Grosberg, A., P. W. Alford, M. L. McCain, and K. K. Parker. "Ensembles of Engineered Cardiac Tissues for Physiological and Pharmacological Study: Heart on a Chip." *Lab on a Chip* 11, no. 24 (2011): 4165-73.

Grosberg, A., A. P. Nesmith, J. A. Goss, M. D. Brigham, M. L. McCain, and K. K. Parker. "Muscle on a Chip: In Vitro Contractility Assays for Smooth and Striated Muscle." *Journal of Pharmacological and Toxicological Methods* 65, no. 3 (2012): 126-35.

Gu, Z., E. H. Noss, V. W. Hsu, and M. B. Brenner. "Integrins Traffic Rapidly Via Circular Dorsal Ruffles and Macropinocytosis During Stimulated Cell Migration." *J Cell Biol* 193, no. 1 (2011): 61-70.

Guerra, F. and C. Bucci. "Multiple Roles of the Small Gtpase Rab7." *Cells* 5, no. 3 (2016): E34.

Guilliams, M., F. Ginhoux, C. Jakubzick, S. H. Naik, N. Onai, B. U. Schraml, E. Segura, R. Tussiwand, and S. Yona. "Dendritic Cells, Monocytes and Macrophages: A Unified Nomenclature Based on Ontogeny." *Nat Rev Immunol* 14, no. 8 (2014): 571-8.

Habtezion, A., L. P. Nguyen, H. Hadeiba, and E. C. Butcher. "Leukocyte Trafficking to the Small Intestine and Colon." *Gastroenterology* 150, no. 2 (2016): 340-54.

Hadley, G. A. and J. M. Higgins. "Integrin Alphaebeta7: Molecular Features and Functional Significance in the Immune System." *Adv Exp Med Biol* 819 (2014): 97-110.

Hammarfjord, O. and R. P. Wallin. "Dendritic Cell Function at Low Physiological Temperature." *J Leukoc Biol* 88, no. 4 (2010): 747-56.

Haniffa, M., M. Collin, and F. Ginhoux. "Ontogeny and Functional Specialization of Dendritic Cells in Human and Mouse." *Adv Immunol* 120 (2013): 1-49.

Hardbower, D. M., M. Asim, P. B. Luis, K. Singh, D. P. Barry, C. Yang, M. A. Steeves, J. L. Cleveland, C. Schneider, M. B. Piazuelo, A. P. Gobert, and K. T. Wilson. "Ornithine Decarboxylase Regulates M1 Macrophage Activation and Mucosal Inflammation Via Histone Modifications." *Proc Natl Acad Sci U S A* 114, no. 5 (2017): E751-E60.

Harris, P. R., S. W. Wright, C. Serrano, F. Riera, I. Duarte, J. Torres, A. Pena, A. Rollan, P. Viviani, E. Guiraldes, J. M. Schmitz, R. G. Lorenz, L. Novak, L. E. Smythies, and P. D. Smith. "Helicobacter Pylori Gastritis in Children Is Associated with a Regulatory T-Cell Response." *Gastroenterology* 134, no. 2 (2008): 491-9.

Heath, J. P. "Epithelial Cell Migration in the Intestine." *Cell Biol Int* 20, no. 2 (1996): 139-46.

Henry, O. Y. F., R. Villenave, M. J. Cronce, W. D. Leineweber, M. A. Benz, and D. E. Ingber. "Organs-on-Chips with Integrated Electrodes for Trans-Epithelial Electrical Resistance (Teer) Measurements of Human Epithelial Barrier Function." *Lab on a Chip* 17, no. 13 (2017): 2264-71.

Heo, I., D. Dutta, D. A. Schaefer, N. Iakobachvili, B. Artegiani, N. Sachs, K. E. Boonekamp, G. Bowden, A. P. A. Hendrickx, R. J. L. Willems, P. J. Peters, M. W. Riggs, R. O'Connor, and H. Clevers. "Modelling Cryptosporidium Infection in Human Small Intestinal and Lung Organoids." *Nature Microbiology* 3, no. 7 (2018): 814-+.

Higgins, J. M., M. Cernadas, K. Tan, A. Irie, J. Wang, Y. Takada, and M. B. Brenner. "The Role of Alpha and Beta Chains in Ligand Recognition by Beta 7 Integrins." *J Biol Chem* 275, no. 33 (2000): 25652-64.

Hill, D. R., S. Huang, M. S. Nagy, V. K. Yadagiri, C. Fields, D. Mukherjee, B. Bons, P. H. Dedhia, A. M. Chin, Y. H. Tsai, S. Thodla, T. M. Schmidt, S. Walk, V. B. Young, and J. R. Spence. "Bacterial Colonization Stimulates a Complex Physiological Response in the Immature Human Intestinal Epithelium." *Elife* 6 (2017).

Hill, D. R., S. Huang, Y. H. Tsai, J. R. Spence, and V. B. Young. "Real-Time Measurement of Epithelial Barrier Permeability in Human Intestinal Organoids." *J Vis Exp*, no. 130 (2017).

Hill, D. R. and J. R. Spence. "Gastrointestinal Organoids: Understanding the Molecular Basis of the Host-Microbe Interface." *Cellular and Molecular Gastroenterology and Hepatology* 3, no. 2 (2017): 138-49.

Hitzler, I., M. Oertli, B. Becher, E. M. Agger, and A. Muller. "Dendritic Cells Prevent Rather Than Promote Immunity Conferred by a Helicobacter Vaccine Using a Mycobacterial Adjuvant." *Gastroenterology* 141, no. 1 (2011): 186-96, 96 e1.

Howitt, M. R., S. Lavoie, M. Michaud, A. M. Blum, S. V. Tran, J. V. Weinstock, C. A. Gallini, K. Redding, R. F. Margolskee, L. C. Osborne, D. Artis, and W. S. Garrett. "Tuft Cells, Taste-Chemosensory Cells, Orchestrate Parasite Type 2 Immunity in the Gut." *Science* 351, no. 6279 (2016): 1329-33.

Hubert, P., J. H. Caberg, C. Gilles, L. Bousarghin, E. Franzen-Detrooz, J. Boniver, and P. Delvenne. "E-Cadherin-Dependent Adhesion of Dendritic and Langerhans Cells to Keratinocytes Is Defective in Cervical Human Papillomavirus-Associated (Pre)Neoplastic Lesions." *J Pathol* 206, no. 3 (2005): 346-55.

Huh, D., H. Fujioka, Y. C. Tung, N. Futai, R. Paine, J. B. Grotberg, and S. Takayama. "Acoustically Detectable Cellular-Level Lung Injury Induced by Fluid Mechanical Stresses in Microfluidic Airway Systems." *Proceedings of the National Academy of Sciences of the United States of America* 104, no. 48 (2007): 18886-91.

Huh, D., D. C. Leslie, B. D. Matthews, J. P. Fraser, S. Jurek, G. A. Hamilton, K. S. Thorneloe, M. A. McAlexander, and D. E. Ingber. "A Human Disease Model of Drug Toxicity-Induced Pulmonary Edema in a Lung-on-a-Chip Microdevice." *Science Translational Medicine* 4, no. 159 (2012).

Huh, D., B. D. Matthews, A. Mammoto, M. Montoya-Zavala, H. Y. Hsin, and D. E. Ingber. "Reconstituting Organ-Level Lung Functions on a Chip." *Science* 328, no. 5986 (2010): 1662-68.

Hynds, R. E. and A. Giangreco. "Concise Review: The Relevance of Human Stem Cell-Derived Organoid Models for Epithelial Translational Medicine." *Stem Cells* 31, no. 3 (2013): 417-22.

Iizuka, M. and S. Konno. "Wound Healing of Intestinal Epithelial Cells." *World J Gastroenterol* 17, no. 17 (2011): 2161-71.

Iliev, I. D., E. Mileti, G. Matteoli, M. Chieppa, and M. Rescigno. "Intestinal Epithelial Cells Promote Colitis-Protective Regulatory T-Cell Differentiation through Dendritic Cell Conditioning." *Mucosal Immunol* 2, no. 4 (2009): 340-50.

Iliev, I. D., I. Spadoni, E. Mileti, G. Matteoli, A. Sonzogni, G. M. Sampietro, D. Foschi, F. Caprioli, G. Viale, and M. Rescigno. "Human Intestinal Epithelial Cells Promote the Differentiation of Tolerogenic Dendritic Cells." *Gut* 58, no. 11 (2009): 1481-9.

Ito, M., T. Maruyama, N. Saito, S. Koganei, K. Yamamoto, and N. Matsumoto. "Killer Cell Lectin-Like Receptor G1 Binds Three Members of the Classical Cadherin Family to Inhibit Nk Cell Cytotoxicity." *J Exp Med* 203, no. 2 (2006): 289-95.

Jakob, T., M. J. Brown, and M. C. Udey. "Characterization of E-Cadherin-Containing Junctions Involving Skin-Derived Dendritic Cells." *J Invest Dermatol* 112, no. 1 (1999): 102-8.

Jang, K. J., A. P. Mehr, G. A. Hamilton, L. A. McPartlin, S. Y. Chung, K. Y. Suh, and D. E. Ingber. "Human Kidney Proximal Tubule-on-a-Chip for Drug Transport and Nephrotoxicity Assessment." *Integrative Biology* 5, no. 9 (2013): 1119-29.

Jang, K. J. and K. Y. Suh. "A Multi-Layer Microfluidic Device for Efficient Culture and Analysis of Renal Tubular Cells." *Lab on a Chip* 10, no. 1 (2010): 36-42.

John W. Calvert, David J. Lefer. "Overview of Cardiac Muscle Physiology." In *Muscle*, edited by Eric N. Olson Joseph A. Hill, vol 1, 57-66: Academic Press, 2012.

Kane, B. J., M. J. Zinner, M. L. Yarmush, and M. Toner. "Liver-Specific Functional Studies in a Microfluidic Array of Primary Mammalian Hepatocytes." *Analytical Chemistry* 78, no. 13 (2006): 4291-98.

Kao, J. Y., M. Zhang, M. J. Miller, J. C. Mills, B. Wang, M. Liu, K. A. Eaton, W. Zou, B. E. Berndt, T. S. Cole, T. Takeuchi, S. Y. Owyang, and J. Luther. "Helicobacter Pylori Immune Escape Is Mediated by Dendritic Cell-Induced Treg Skewing and Th17 Suppression in Mice." *Gastroenterology* 138, no. 3 (2010): 1046-54.

Karam, S. M., Q. Li, and J. I. Gordon. "Gastric Epithelial Morphogenesis in Normal and Transgenic Mice." *Am J Physiol* 272, no. 5 Pt 1 (1997): G1209-20.

Karjalainen, M., E. Kakkonen, P. Upla, H. Paloranta, P. Kankaanpaa, P. Liberali, G. H. Renkema, T. Hyypia, J. Heino, and V. Marjomaki. "A Raft-Derived, Pak1-Regulated Entry Participates in Alpha2beta1 Integrin-Dependent Sorting to Caveosomes." *Mol Biol Cell* 19, no. 7 (2008): 2857-69.

Khanal, G., K. Chung, X. Solis-Wever, B. Johnson, and D. Pappas. "Ischemia/Reperfusion Injury of Primary Porcine Cardiomyocytes in a Low-Shear Microfluidic Culture and Analysis Device." *Analyst* 136, no. 17 (2011): 3519-26.

Khandelwal, P., W. G. Ruiz, and G. Apodaca. "Compensatory Endocytosis in Bladder Umbrella Cells Occurs through an Integrin-Regulated and Rhoa- and Dynamin-Dependent Pathway." *EMBO J* 29, no. 12 (2010): 1961-75.

Kim, H. J., D. Huh, G. Hamilton, and D. E. Ingber. "Human Gut-on-a-Chip Inhabited by Microbial Flora That Experiences Intestinal Peristalsis-Like Motions and Flow." *Lab on a Chip* 12, no. 12 (2012): 2165-74.

Kim, H. J. and D. E. Ingber. "Gut-on-a-Chip Microenvironment Induces Human Intestinal Cells to Undergo Villus Differentiation." *Integrative Biology* 5, no. 9 (2013): 1130-40.

Krishnan, M., L. A. Lapierre, B. C. Knowles, and J. R. Goldenring. "Rab25 Regulates Integrin Expression in Polarized Colonic Epithelial Cells." *Mol Biol Cell* 24, no. 6 (2013): 818-31.

Lacaz-Vieira, F. "Calcium Site Specificity. Early Ca2+-Related Tight Junction Events." *J Gen Physiol* 110, no. 6 (1997): 727-40.

Lamb, A. and L. F. Chen. "The Many Roads Traveled by Helicobacter Pylori to Nfkappab Activation." *Gut Microbes* 1, no. 2 (2010): 109-13.

Lamb, A., X. D. Yang, Y. H. Tsang, J. D. Li, H. Higashi, M. Hatakeyama, R. M. Peek, S. R. Blanke, and L. F. Chen. "Helicobacter Pylori Caga Activates Nf-Kappab by Targeting Tak1 for Traf6-Mediated Lys 63 Ubiquitination." *EMBO Rep* 10, no. 11 (2009): 1242-9.

Lancaster, M. A. and J. A. Knoblich. "Organogenesis in a Dish: Modeling Development and Disease Using Organoid Technologies." *Science* 345, no. 6194 (2014).

Lancaster, M. A., M. Renner, C. A. Martin, D. Wenzel, L. S. Bicknell, M. E. Hurles, T. Homfray, J. M. Penninger, A. P. Jackson, and J. A. Knoblich. "Cerebral Organoids Model Human Brain Development and Microcephaly." *Nature* 501, no. 7467 (2013): 373-+.

Larsen, E. H., N. J. Willumsen, N. Mobjerg, and J. N. Sorensen. "The Lateral Intercellular Space as Osmotic Coupling Compartment in Isotonic Transport." *Acta Physiol (Oxf)* 195, no. 1 (2009): 171-86.

Le Floc'h, A., A. Jalil, K. Franciszkiewicz, P. Validire, I. Vergnon, and F. Mami-Chouaib. "Minimal Engagement of Cd103 on Cytotoxic T Lymphocytes with an E-Cadherin-Fc Molecule Triggers Lytic Granule Polarization Via a Phospholipase Cgamma-Dependent Pathway." *Cancer Res* 71, no. 2 (2011): 328-38.

Lee, D. W., S. K. Ha, I. Choi, and J. H. Sung. "3d Gut-Liver Chip with a Pk Model for Prediction of First-Pass Metabolism." *Biomedical Microdevices* 19, no. 4 (2017).

Lee, P. J., P. J. Hung, and L. P. Lee. "An Artificial Liver Sinusoid with a Microfluidic Endothelial-Like Barrier for Primary Hepatocyte Culture." *Biotechnology and Bioengineering* 97, no. 5 (2007): 1340-46.

Legendre, A., R. Baudoin, G. Alberto, P. Paullier, M. Naudot, T. Bricks, J. Brocheton, S. Jacques, J. Cotton, and E. Leclerc. "Metabolic Characterization of Primary Rat Hepatocytes Cultivated in Parallel Microfluidic Biochips." *Journal of Pharmaceutical Sciences* 102, no. 9 (2013): 3264-76.

Leonard, F., E. M. Collnot, and C. M. Lehr. "A Three-Dimensional Coculture of Enterocytes, Monocytes and Dendritic Cells to Model Inflamed Intestinal Mucosa in Vitro." *Mol Pharm* 7, no. 6 (2010): 2103-19.

Leslie, J. L., S. Huang, J. S. Opp, M. S. Nagy, M. Kobayashi, V. B. Young, and J. R. Spence. "Persistence and Toxin Production by Clostridium Difficile within Human Intestinal Organoids Result in Disruption of Epithelial Paracellular Barrier Function." *Infection and Immunity* 83, no. 1 (2015): 138-45.

Leushacke, M. and N. Barker. "Ex Vivo Culture of the Intestinal Epithelium: Strategies and Applications." *Gut* 63, no. 8 (2014): 1345-54.

Lindemans, C. A., M. Calafiore, A. M. Mertelsmann, M. H. O'Connor, J. A. Dudakov, R. R. Jenq, E. Velardi, L. F. Young, O. M. Smith, G. Lawrence, J. A. Ivanov, Y. Y. Fu, S. Takashima, G. Q. Hua, M. L. Martin, K. P. O'Rourke, Y. H. Lo, M. Mokry, M. Romera-Hernandez, T. Cupedo, L. E. Dow, E. E. Nieuwenhuis, N. F. Shroyer, C. Liu, R. Kolesnick, M. R. M. van den Brink, and A. M. Hanash. "Interleukin-22 Promotes Intestinal-Stem-Cell-Mediated Epithelial Regeneration." *Nature* 528, no. 7583 (2015): 560-+.

Lipkin, M. "Cell Replication in the Gastrointestinal Tract of Man." *Gastroenterology* 48 (1965): 616-24.

Liu, M. C., H. C. Shih, J. G. Wu, T. W. Weng, C. Y. Wu, J. C. Lu, and Y. C. Tung. "Electrofluidic Pressure Sensor Embedded Microfluidic Device: A Study of Endothelial Cells under Hydrostatic Pressure and Shear Stress Combinations." *Lab on a Chip* 13, no. 9 (2013): 1743-53.

Lobert, V. H., A. Brech, N. M. Pedersen, J. Wesche, A. Oppelt, L. Malerod, and H. Stenmark. "Ubiquitination of Alpha 5 Beta 1 Integrin Controls Fibroblast Migration through Lysosomal Degradation of Fibronectin-Integrin Complexes." *Dev Cell* 19, no. 1 (2010): 148-59.

Lodish H, Berk A, Zipursky SL, et al. *Transport across Epithelia*. Molecular Cell Biology. New York: W. H. Freeman, 2000.

Lowrey, Lawson G. "Prenatal Growth of the Pigs." *The American Journal of Anatomy* 12 (1911): 131.

Lukovac, S., C. Belzer, L. Pellis, B. J. Keijser, W. M. de Vos, R. C. Montijn, and G. Roeselers. "Differential Modulation by Akkermansia Muciniphila and Faecalibacterium Prausnitzii of Host Peripheral Lipid Metabolism and Histone Acetylation in Mouse Gut Organoids." *Mbio* 5, no. 4 (2014).

Ma, T. H. and A. S. Verkman. "Aquaporin Water Channels in Gastrointestinal Physiology." *Journal of Physiology-London* 517, no. 2 (1999): 317-26.

Mahe, M. M., E. Aihara, M. A. Schumacher, Y. Zavros, M. H. Montrose, M. A. Helmrath, T. Sato, and N. F. Shroyer. "Establishment of Gastrointestinal Epithelial Organoids." *Curr Protoc Mouse Biol* 3, no. 4 (2013): 217-40.

Mahler, G. J., M. B. Esch, R. P. Glahn, and M. L. Shuler. "Characterization of a Gastrointestinal Tract Microscale Cell Culture Analog Used to Predict Drug Toxicity." *Biotechnology and Bioengineering* 104, no. 1 (2009): 193-205.

Mane, V. and S. Muro. "Biodistribution and Endocytosis of Icam-1-Targeting Antibodies Versus Nanocarriers in the Gastrointestinal Tract in Mice." *Int J Nanomedicine* 7 (2012): 4223-37.

Maritzen, T., H. Schachtner, and D. F. Legler. "On the Move: Endocytic Trafficking in Cell Migration." *Cell Mol Life Sci* (2015).

Marshall, L. E., R. Koomullil, A. R. Frost, and J. L. Berry. "Computational and Experimental Analysis of Fluid Transport through Three-Dimensional Collagen-Matrigel Hydrogels." *Annals of Biomedical Engineering* 45, no. 4 (2017): 1027-38.

Martin-Latil, S., N. F. Gnadig, A. Mallet, M. Desdouits, F. Guivel-Benhassine, P. Jeannin, M. C. Prevost, O. Schwartz, A. Gessain, S. Ozden, and P. E. Ceccaldi. "Transcytosis of Htlv-1 across a Tight Human Epithelial Barrier and Infection of Subepithelial Dendritic Cells." *Blood* 120, no. 3 (2012): 572-80.

Martinez-Guryn, K., N. Hubert, K. Frazier, S. Urlass, M. W. Musch, P. Ojeda, J. F. Pierre, J. Miyoshi, T. J. Sontag, C. M. Cham, C. A. Reardon, V. Leone, and E. B. Chang. "Small Intestine Microbiota Regulate Host Digestive and Absorptive Adaptive Responses to Dietary Lipids." *Cell Host & Microbe* 23, no. 4 (2018): 458-+.

Maschmeyer, I., A. K. Lorenz, K. Schimek, T. Hasenberg, A. P. Ramme, J. Hubner, M. Lindner, C. Drewell, S. Bauer, A. Thomas, N. S. Sambo, F. Sonntag, R. Lauster, and U. Marx. "A Four-Organ-Chip for Interconnected Long-Term Co-Culture of Human Intestine, Liver, Skin and Kidney Equivalents." *Lab on a Chip* 15, no. 12 (2015): 2688-99.

Mathew, B., S. Munoz-Descalzo, E. Corujo-Simon, C. Schroter, E. H. K. Stelzer, and S. C. Fischer. "Mouse Icm Organoids Reveal Three-Dimensional Cell Fate Clustering." *Biophysical Journal* 116, no. 1 (2019): 127-41.

McCracken, K. W., E. M. Cata, C. M. Crawford, K. L. Sinagoga, M. Schumacher, B. E. Rockich, Y. H. Tsai, C. N. Mayhew, J. R. Spence, Y. Zavros, and J. M. Wells. "Modelling Human Development and Disease in Pluripotent Stem-Cell-Derived Gastric Organoids." *Nature* 516, no. 7531 (2014): 400-+.

McCracken, K. W., J. C. Howell, J. M. Wells, and J. R. Spence. "Generating Human Intestinal Tissue from Pluripotent Stem Cells in Vitro." *Nat Protoc* 6, no. 12 (2011): 1920-8.

McDonald, K. G., L. W. Wheeler, J. R. McDole, S. Joerger, J. K. Gustafsson, D. H. Kulkarni, K. A. Knoop, I. R. Williams, M. J. Miller, and R. D. Newberry. "Ccr6 Promotes Steady State Intestinal Mononuclear Phagocyte Association with the Intestinal Epithelium, Imprinting, and Immune Surveillance." *Immunology* (2017).

McNiven, M. A. "Breaking Away: Matrix Remodeling from the Leading Edge." *Trends Cell Biol* 23, no. 1 (2013): 16-21.

Meng, Z. J., W. Wang, X. Liang, W. C. Zheng, N. N. Deng, R. Xie, X. J. Ju, Z. Liu, and L. Y. Chu. "Plug-N-Play Microfluidic Systems from Flexible Assembly of Glass-Based Flow-Control Modules." *Lab on a Chip* 15, no. 8 (2015): 1869-78.

Merad, M. and M. G. Manz. "Dendritic Cell Homeostasis." *Blood* 113, no. 15 (2009): 3418-27.

Miura, T. and R. Tanaka. "In Vitro Vasculogenesis Models Revisited Measurement of Vegf Diffusion in Matrigel." *Mathematical Modelling of Natural Phenomena* 4, no. 4 (2009): 118-30.

Miyoshi, H. "Wnt-Expressing Cells in the Intestines: Guides for Tissue Remodeling." *J Biochem* 161, no. 1 (2017): 19-25.

Miyoshi, H., R. Ajima, C. T. Luo, T. P. Yamaguchi, and T. S. Stappenbeck. "Wnt5a Potentiates Tgf-Beta Signaling to Promote Colonic Crypt Regeneration after Tissue Injury." *Science* 338, no. 6103 (2012): 108-13.

Miyoshi, H. and T. S. Stappenbeck. "In Vitro Expansion and Genetic Modification of Gastrointestinal Stem Cells in Spheroid Culture." *Nature Protocols* 8, no. 12 (2013): 2471-82.

Mollazade, Kaveh, Mahmoud Omid, Fardin Akhlaghian Tab, and Sayed Saeid Mohtasebi. "Principles and Applications of Light Backscattering Imaging in Quality Evaluation of Agro-Food Products: A Review." *Food Bioprocess Tech* 5, no. 5 (2012): 1465-85.

Morizane, R., A. Q. Lam, B. S. Freedman, S. Kishi, M. T. Valerius, and J. V. Bonventre. "Nephron Organoids Derived from Human Pluripotent Stem Cells Model Kidney Development and Injury." *Nature Biotechnology* 33, no. 11 (2015): 1193-U127.

Moss, S. F. and P. Malfertheiner. "Helicobacter and Gastric Malignancies." *Helicobacter.* 12 Suppl 1 (2007): 23-30.

Mustapha, P., I. Paris, M. Garcia, C. T. Tran, J. Cremniter, M. Garnier, J. P. Faure, T. Barthes, I. G. Boneca, F. Morel, J. C. Lecron, C. Burucoa, and C. Bodet. "Chemokines and Antimicrobial Peptides Have a Cag-Dependent Early Response to Helicobacter Pylori Infection in Primary Human Gastric Epithelial Cells." *Infect Immun* 82, no. 7 (2014): 2881-9.

Nagafuchi, A. and M. Takeichi. "Cell Binding Function of E-Cadherin Is Regulated by the Cytoplasmic Domain." *EMBO J* 7, no. 12 (1988): 3679-84.

Nakajo, A., S. Yoshimura, H. Togawa, M. Kunii, T. Iwano, A. Izumi, Y. Noguchi, A. Watanabe, A. Goto, T. Sato, and A. Harada. "Ehbp1l1 Coordinates Rab8 and Bin1 to Regulate Apical-Directed Transport in Polarized Epithelial Cells." *Journal of Cell Biology* 212, no. 3 (2016): 297-306.

Necchi, V., R. Manca, V. Ricci, and E. Solcia. "Evidence for Transepithelial Dendritic Cells in Human H. Pylori Active Gastritis." *Helicobacter.* 14, no. 3 (2009): 208-22.

Nguyen, M. D., J. P. Tinney, F. Ye, A. A. Elnakib, F. P. Yuan, A. El-Baz, P. Sethu, B. B. Keller, and G. A. Giridharan. "Effects of Physiologic Mechanical Stimulation on Embryonic Chick Cardiomyocytes Using a Microfluidic Cardiac Cell Culture Model." *Analytical Chemistry* 87, no. 4 (2015): 2107-13.

Ni, H., A. Li, N. Simonsen, and J. A. Wilkins. "Integrin Activation by Dithiothreitol or Mn2+ Induces a Ligand-Occupied Conformation and Exposure of a Novel Nh2-Terminal Regulatory Site on the Beta1 Integrin Chain." *J Biol Chem* 273, no. 14 (1998): 7981-7.

Nie, Y. Z., Y. W. Zheng, M. Ogawa, E. Miyagi, and H. Taniguchi. "Human Liver Organoids Generated with Single Donor-Derived Multiple Cells Rescue Mice from Acute Liver Failure." *Stem Cell Research & Therapy* 9 (2018).

Niess, J. H., S. Brand, X. Gu, L. Landsman, S. Jung, B. A. McCormick, J. M. Vyas, M. Boes, H. L. Ploegh, J. G. Fox, D. R. Littman, and H. C. Reinecker. "Cx3cr1-Mediated Dendritic Cell Access to the Intestinal Lumen and Bacterial Clearance." *Science* 307, no. 5707 (2005): 254-8.

Nigro, G., R. Rossi, P. H. Commere, P. Jay, and P. J. Sansonetti. "The Cytosolic Bacterial Peptidoglycan Sensor Nod2 Affords Stem Cell Protection and Links Microbes to Gut Epithelial Regeneration." *Cell Host & Microbe* 15, no. 6 (2014): 792-98.

Noel, G., N. W. Baetz, J. F. Staab, M. Donowitz, O. Kovbasnjuk, M. F. Pasetti, and N. C. Zachos. "A Primary Human Macrophage-Enteroid Co-Culture Model to Investigate Mucosal Gut Physiology and Host-Pathogen Interactions." *Sci Rep* 7 (2017): 45270.

Noguchi, T. K., N. Ninomiya, M. Sekine, S. Komazaki, P. C. Wang, M. Asashima, and A. Kurisaki. "Generation of Stomach Tissue from Mouse Embryonic Stem Cells." *Nature Cell Biology* 17, no. 8 (2015): 984-U62.

Nookaew, I., K. Thorell, K. Worah, S. Wang, M. L. Hibberd, H. Sjovall, S. Pettersson, J. Nielsen, and S. B. Lundin. "Transcriptome Signatures in Helicobacter Pylori-Infected Mucosa Identifies Acidic Mammalian Chitinase Loss as a Corpus Atrophy Marker." *BMC Med Genomics* 6 (2013): 41.

Novik, E., T. J. Maguire, P. Y. Chao, K. C. Cheng, and M. L. Yarmush. "A Microfluidic Hepatic Coculture Platform for Cell-Based Drug Metabolism Studies." *Biochemical Pharmacology* 79, no. 7 (2010): 1036-44.

Nozaki, K., W. Mochizuki, Y. Matsumoto, T. Matsumoto, M. Fukuda, T. Mizutani, M. Watanabe, and T. Nakamura. "Co-Culture with Intestinal Epithelial Organoids Allows Efficient Expansion and Motility Analysis of Intraepithelial Lymphocytes." *J Gastroenterol* 51, no. 3 (2016): 206-13.

Ootani, A., X. Li, E. Sangiorgi, Q. T. Ho, H. Ueno, S. Toda, H. Sugihara, K. Fujimoto, I. L. Weissman, M. R. Capecchi, and C. J. Kuo. "Sustained in Vitro Intestinal Epithelial Culture within a Wnt-Dependent Stem Cell Niche." *Nat Med* 15, no. 6 (2009): 701-6.

Park, H. S., S. Liu, J. McDonald, N. Thakor, and I. H. Yang. "Neuromuscular Junction in a Microfluidic Device." *2013 35th Annual International Conference of the Ieee Engineering in Medicine and Biology Society (Embc)* (2013): 2833-35.

Park, S. H., W. Y. Sim, B. H. Min, S. S. Yang, A. Khademhosseini, and D. L. Kaplan. "Chip-Based Comparison of the Osteogenesis of Human Bone Marrow- and Adipose Tissue-Derived Mesenchymal Stem Cells under Mechanical Stimulation." *Plos One* 7, no. 9 (2012).

Paul, N. R., G. Jacquemet, and P. T. Caswell. "Endocytic Trafficking of Integrins in Cell Migration." *Curr Biol* 25, no. 22 (2015): R1092-105.

Pechhold, K., T. Pohl, and D. Kabelitz. "Rapid Quantification of Lymphocyte Subsets in Heterogeneous Cell Populations by Flow Cytometry." *Cytometry* 16, no. 2 (1994): 152-9.

Powell, R. H. and M. S. Behnke. "Wrn Conditioned Media Is Sufficient for in Vitro Propagation of Intestinal Organoids from Large Farm and Small Companion Animals." *Biol Open* 6, no. 5 (2017): 698-705.

Puleo, C. M., W. M. Ambrose, T. Takezawa, J. Elisseeff, and T. H. Wang. "Integration and Application of Vitrified Collagen in Multilayered Microfluidic Devices for Corneal Microtissue Culture." *Lab on a Chip* 9, no. 22 (2009): 3221-27.

Rainero, E. and J. C. Norman. "Late Endosomal and Lysosomal Trafficking During Integrin-Mediated Cell Migration and Invasion: Cell Matrix Receptors Are Trafficked through the Late Endosomal Pathway in a Way That Dictates How Cells Migrate." *Bioessays* 35, no. 6 (2013): 523-32.

Rescigno, M., M. Urbano, B. Valzasina, M. Francolini, G. Rotta, R. Bonasio, F. Granucci, J. P. Kraehenbuhl, and P. Ricciardi-Castagnoli. "Dendritic Cells Express Tight Junction Proteins and Penetrate Gut Epithelial Monolayers to Sample Bacteria." *Nat Immunol* 2, no. 4 (2001): 361-7.

Reuss, L., *Encyclopedia of Life Sciences.* Chichester: John Wiley & Sons, Ltd, 2009.

Rieder, G., W. Einsiedl, R. A. Hatz, M. Stolte, G. A. Enders, and A. Walz. "Comparison of Cxc Chemokines Ena-78 and Interleukin-8 Expression in Helicobacter Pylori-Associated Gastritis." *Infect Immun* 69, no. 1 (2001): 81-8.

Riedl, E., J. Stockl, O. Majdic, C. Scheinecker, K. Rappersberger, W. Knapp, and H. Strobl. "Functional Involvement of E-Cadherin in Tgf-Beta 1-Induced Cell Cluster Formation of in Vitro Developing Human Langerhans-Type Dendritic Cells." *J Immunol* 165, no. 3 (2000): 1381-6.

Riehl, T. E., S. Santhanam, L. Foster, M. Ciorba, and W. F. Stenson. "Cd44 and Tlr4 Mediate Hyaluronic Acid Regulation of Lgr5+ Stem Cell Proliferation, Crypt Fission, and Intestinal Growth in Postnatal and Adult Mice." *Am J Physiol Gastrointest Liver Physiol* 309, no. 11 (2015): G874-87.

Robinson, K., R. Kenefeck, E. L. Pidgeon, S. Shakib, S. Patel, R. J. Polson, A. M. Zaitoun, and J. C. Atherton. "Helicobacter Pylori-Induced Peptic Ulcer Disease Is Associated with Inadequate Regulatory T Cell Responses." *Gut* 57, no. 10 (2008): 1375-85.

Roe, M. M., S. Swain, T. A. Sebrell, M. A. Sewell, M. M. Collins, B. A. Perrino, P. D. Smith, L. E. Smythies, and D. Bimczok. "Differential Regulation of Cd103 (Alphae Integrin) Expression in Human Dendritic Cells by Retinoic Acid and Toll-Like Receptor Ligands." *J Leukoc Biol* 101, no. 5 (2017): 1169-80.

Rohrer, G. V., J. R. Scott, W. Joel, and S. Wolf. "The Fine Structure of Human Gastric Parietal Cells." *Am J Dig Dis* 10 (1965): 13-21.

Rosenthal, R., S. Milatz, S. M. Krug, B. Oelrich, J. D. Schulzke, S. Amasheh, D. Gunzel, and M. Fromm. "Claudin-2, a Component of the Tight Junction, Forms a Paracellular Water Channel." *Journal of Cell Science* 123, no. 11 (2010): 1913-21.

Russell, G. J., C. M. Parker, K. L. Cepek, D. A. Mandelbrot, A. Sood, E. Mizoguchi, E. C. Ebert, M. B. Brenner, and A. K. Bhan. "Distinct Structural and Functional Epitopes of the Alpha E Beta 7 Integrin." *Eur J Immunol* 24, no. 11 (1994): 2832-41.

Sachs, N., J. de Ligt, O. Kopper, E. Gogola, G. Bounova, F. Weeber, A. V. Balgobind, K. Wind, A. Gracanin, H. Begthel, J. Korving, R. van Boxtel, A. A. Duarte, D. Lelieveld, A. van Hoeck, R. F. Ernst, F. Blokzijl, I. J. Nijman, M. Hoogstraat, M. van de Ven, D. A. Egan, V. Zinzalla, J. Moll, S. F. Boj, E. E. Voest, L. Wessels, P. J. van Diest, S. Rottenberg, R. G. J. Vries, E. Cuppen, and H. Clevers. "A Living Biobank of Breast Cancer Organoids Captures Disease Heterogeneity." *Cell* 172, no. 1-2 (2018): 373-+.

Sancak, Y., T. R. Peterson, Y. D. Shaul, R. A. Lindquist, C. C. Thoreen, L. Bar-Peled, and D. M. Sabatini. "The Rag Gtpases Bind Raptor and Mediate Amino Acid Signaling to Mtorc1." *Science* 320, no. 5882 (2008): 1496-501.

Sandbichler, A. M., M. Egg, T. Schwerte, and B. Pelster. "Claudin 28b and F-Actin Are Involved in Rainbow Trout Gill Pavement Cell Tight Junction Remodeling under Osmotic Stress." *Journal of Experimental Biology* 214, no. 9 (2011): 1473-87.

Sato, T. and H. Clevers. "Snapshot: Growing Organoids from Stem Cells." *Cell* 161, no. 7 (2015): 1700-00 e1.

Sato, T., D. E. Stange, M. Ferrante, R. G. J. Vries, J. H. van Es, S. van den Brink, W. J. van Houdt, A. Pronk, J. van Gorp, P. D. Siersema, and H. Clevers. "Long-Term Expansion of Epithelial Organoids from Human Colon, Adenoma, Adenocarcinoma, and Barrett's Epithelium." *Gastroenterology* 141, no. 5 (2011): 1762-72.

Sato, T., R. G. Vries, H. J. Snippert, M. van de Wetering, N. Barker, D. E. Stange, J. H. van Es, A. Abo, P. Kujala, P. J. Peters, and H. Clevers. "Single Lgr5 Stem Cells Build Crypt-Villus Structures in Vitro without a Mesenchymal Niche." *Nature* 459, no. 7244 (2009): 262-U147.

Schittenhelm, L., C. M. Hilkens, and V. L. Morrison. "Beta2 Integrins as Regulators of Dendritic Cell, Monocyte, and Macrophage Function." *Front Immunol* 8 (2017): 1866.

Schlaermann, P., B. Toelle, H. Berger, S. C. Schmidt, M. Glanemann, J. Ordemann, S. Bartfeld, H. J. Mollenkopf, and T. F. Meyer. "A Novel Human Gastric Primary Cell Culture System for Modelling Helicobacter Pylori Infection in Vitro." *Gut* 65, no. 2 (2016): 202-13.

Schlickum, S., H. Sennefelder, M. Friedrich, G. Harms, M. J. Lohse, P. Kilshaw, and M. P. Schon. "Integrin Alpha E(Cd103)Beta 7 Influences Cellular Shape and Motility in a Ligand-Dependent Fashion." *Blood* 112, no. 3 (2008): 619-25.

Schneider, C. A., W. S. Rasband, and K. W. Eliceiri. "Nih Image to Imagej: 25 Years of Image Analysis." *Nat Methods* 9, no. 7 (2012): 671-5.

Schon, M. P., A. Arya, E. A. Murphy, C. M. Adams, U. G. Strauch, W. W. Agace, J. Marsal, J. P. Donohue, H. Her, D. R. Beier, S. Olson, L. Lefrancois, M. B. Brenner, M. J. Grusby, and C. M. Parker. "Mucosal T Lymphocyte Numbers Are Selectively Reduced in Integrin Alpha E (Cd103)-Deficient Mice." *J Immunol* 162, no. 11 (1999): 6641-9.

Schumacher, M. A., E. Aihara, R. Feng, A. Engevik, N. F. Shroyer, K. M. Ottemann, R. T. Worrell, M. H. Montrose, R. A. Shivdasani, and Y. Zavros. "The Use of Murine-Derived Fundic Organoids in Studies of Gastric Physiology." *J Physiol* 593, no. 8 (2015): 1809-27.

Schwank, G., A. Andersson-Rolf, B. K. Koo, N. Sasaki, and H. Clevers. "Generation of Bac Transgenic Epithelial Organoids." *PLoS One* 8, no. 10 (2013): e76871.

Schweinlin, M., S. Wilhelm, I. Schwedhelm, J. Hansmann, R. Rietscher, C. Jurowich, H. Walles, and M. Metzger. "Development of an Advanced Primary Human in Vitro Model of the Small Intestine." *Tissue Engineering Part C-Methods* 22, no. 9 (2016): 873-83.

Scott, C. L., A. M. Aumeunier, and A. M. Mowat. "Intestinal Cd103+ Dendritic Cells: Master Regulators of Tolerance?" *Trends Immunol* 32, no. 9 (2011): 412-9.

Sebrell, T. A., B. Sidar, R. Bruns, R. A. Wilkinson, B. Wiedenheft, P. J. Taylor, B. A. Perrino, L. C. Samuelson, J. N. Wilking, and D. Bimczok. "Live Imaging Analysis of Human Gastric Epithelial Spheroids Reveals Spontaneous Rupture, Rotation and Fusion Events." *Cell Tissue Res* 371, no. 2 (2018): 293-307.

Sebrell, Thomas A., Marziah Hashimi, Barkan Sidar, Royce Wilkinson, Liliya Kirpotina, Mark T. Quinn, Zeynep Malkoç, Paul J. Taylor, James N. Wilking, and Diane Bimczok. "A Novel Gastric Spheroid Co-Culture Model Reveals Chemokine-Dependent Recruitment of Human Dendritic Cells to the Gastric Epithelium." *Cellular and Molecular Gastroenterology and Hepatology* (2019).

Segura, E. "Review of Mouse and Human Dendritic Cell Subsets." *Methods Mol Biol* 1423 (2016): 3-15.

Serrano, C., S. W. Wright, D. Bimczok, C. L. Shaffer, T. L. Cover, A. Venegas, M. G. Salazar, L. E. Smythies, P. R. Harris, and P. D. Smith. "Downregulated Th17 Responses Are Associated with Reduced Gastritis in Helicobacter Pylori-Infected Children." *Mucosal Immunol* (2013).

Shah, Pranjul, Joëlle V. Fritz, Enrico Glaab, Mahesh S. Desai, Kacy Greenhalgh, Audrey Frachet, Magdalena Niegowska, Matthew Estes, Christian Jäger, Carole Seguin-Devaux, Frederic Zenhausern, and Paul Wilmes. "A Microfluidics-Based in Vitro Model of the Gastrointestinal Human–Microbe Interface." *Nature Communications* 7 (2016): 11535.

Shen, B., M. K. Delaney, and X. Du. "Inside-out, Outside-in, and inside-Outside-In: G Protein Signaling in Integrin-Mediated Cell Adhesion, Spreading, and Retraction." *Curr Opin Cell Biol* 24, no. 5 (2012): 600-6.

Shi, M. J., D. Majumdar, Y. D. Gao, B. M. Brewer, C. R. Goodwin, J. A. McLean, D. Lib, and D. J. Webb. "Glia Co-Culture with Neurons in Microfluidic Platforms Promotes the Formation and Stabilization of Synaptic Contacts." *Lab on a Chip* 13, no. 15 (2013): 3008-21.

Shin, M., K. Matsuda, O. Ishii, H. Terai, M. Kaazempur-Mofrad, J. Borenstein, M. Detmar, and J. P. Vacanti. "Endothelialized Networks with a Vascular Geometry in Microfabricated Poly(Dimethyl Siloxane)." *Biomedical Microdevices* 6, no. 4 (2004): 269-78.

Shiu, J. and T. G. Blanchard. "Dendritic Cell Function in the Host Response to Helicobacter Pylori Infection of the Gastric Mucosa." *Pathog Dis* 67, no. 1 (2013): 46-53.

Silen, W. and S. Ito. "Mechanisms for Rapid Re-Epithelialization of the Gastric Mucosal Surface." *Annu Rev Physiol* 47 (1985): 217-29.

Simunovic, M. and A. H. Brivanlou. "Embryoids, Organoids and Gastruloids: New Approaches to Understanding Embryogenesis." *Development* 144, no. 6 (2017): 976-85.

Sin, A., K. C. Chin, M. F. Jamil, Y. Kostov, G. Rao, and M. L. Shuler. "The Design and Fabrication of Three-Chamber Microscale Cell Culture Analog Devices with Integrated Dissolved Oxygen Sensors." *Biotechnology Progress* 20, no. 1 (2004): 338-45.

Sinagoga, K. L. and J. M. Wells. "Generating Human Intestinal Tissues from Pluripotent Stem Cells to Study Development and Disease." *Embo Journal* 34, no. 9 (2015): 1149-63.

Sivaraman, A., J. K. Leach, S. Townsend, T. Iida, B. J. Hogan, D. B. Stolz, R. Fry, L. D. Samson, S. R. Tannenbaum, and L. G. Griffith. "A Microscale in Vitro Physiological Model of the Liver: Predictive Screens for Drug Metabolism and Enzyme Induction." *Current Drug Metabolism* 6, no. 6 (2005): 569-91.

Skardal, A., S. V. Murphy, M. Devarasetty, I. Mead, H. W. Kang, Y. J. Seol, Y. S. Zhang, S. R. Shin, L. Zhao, J. Aleman, A. R. Hall, T. D. Shupe, A. Kleensang, M. R. Dokmeci, S. J. Lee, J. D. Jackson, J. J. Yoo, T. Hartung, A. Khademhosseini, S. Soker, C. E. Bishop, and A. Atala. "Multi-Tissue Interactions in an Integrated Three-Tissue Organ-on-a-Chip Platform." *Scientific Reports* 7 (2017).

Smith, J. M., P. A. Johanesen, M. K. Wendt, D. G. Binion, and M. B. Dwinell. "Cxcl12 Activation of Cxcr4 Regulates Mucosal Host Defense through Stimulation of Epithelial Cell Migration and Promotion of Intestinal Barrier Integrity." *Am J Physiol Gastrointest Liver Physiol* 288, no. 2 (2005): G316-26.

Snouber, L. C., F. Letourneur, P. Chafey, C. Broussard, M. Monge, C. Legallais, and E. Leclerc. "Analysis of Transcriptomic and Proteomic Profiles Demonstrates Improved Madin-Darby Canine Kidney Cell Function in a Renal Microfluidic Biochip." *Biotechnology Progress* 28, no. 2 (2012): 474-84.

Spence, J. R., C. N. Mayhew, S. A. Rankin, M. F. Kuhar, J. E. Vallance, K. Tolle, E. E. Hoskins, V. V. Kalinichenko, S. I. Wells, A. M. Zorn, N. F. Shroyer, and J. M. Wells. "Directed Differentiation of Human Pluripotent Stem Cells into Intestinal Tissue in Vitro." *Nature* 470, no. 7332 (2011): 105-9.

Stelzner, M., M. Helmrath, J. C. Dunn, S. J. Henning, C. W. Houchen, C. Kuo, J. Lynch, L. Li, S. T. Magness, M. G. Martin, M. H. Wong, J. Yu, and N. I. H. Intestinal Stem Cell Consortium. "A Nomenclature for Intestinal in Vitro Cultures." *Am J Physiol Gastrointest Liver Physiol* 302, no. 12 (2012): G1359-63.

Stevens, C. E. and Ian D. Hume. *Comparative Physiology of the Vertebrate Digestive System*. 2nd ed. Cambridge ; New York: Cambridge University Press, 1995.

Stewart, S. A., D. M. Dykxhoorn, D. Palliser, H. Mizuno, E. Y. Yu, D. S. An, D. M. Sabatini, I. S. Chen, W. C. Hahn, P. A. Sharp, R. A. Weinberg, and C. D. Novina. "Lentivirus-Delivered Stable Gene Silencing by Rnai in Primary Cells." *RNA* 9, no. 4 (2003): 493-501.

Takahashi, T. "Organoids for Drug Discovery and Personalized Medicine." *Annual Review of Pharmacology and Toxicology, Vol 59* 59 (2019): 447-62.

Takasato, M., P. X. Er, H. S. Chiu, B. Maier, G. J. Baillie, C. Ferguson, R. G. Parton, E. J. Wolvetang, M. S. Roost, S. M. C. D. Lopes, and M. H. Little. "Kidney Organoids from Human Ips Cells Contain Multiple Lineages and Model Human Nephrogenesis." *Nature* 526, no. 7574 (2015): 564-U238.

Tang, A., M. Amagai, L. G. Granger, J. R. Stanley, and M. C. Udey. "Adhesion of Epidermal Langerhans Cells to Keratinocytes Mediated by E-Cadherin." *Nature* 361, no. 6407 (1993): 82-5.

Taraszka, K. S., J. M. Higgins, K. Tan, D. A. Mandelbrot, J. H. Wang, and M. B. Brenner. "Molecular Basis for Leukocyte Integrin Alpha(E)Beta(7) Adhesion to Epithelial (E)-Cadherin." *J Exp Med* 191, no. 9 (2000): 1555-67.

Tavana, H., P. Zamankhan, P. J. Christensen, J. B. Grotberg, and S. Takayama. "Epithelium Damage and Protection During Reopening of Occluded Airways in a Physiologic Microfluidic Pulmonary Airway Model." *Biomedical Microdevices* 13, no. 4 (2011): 731-42.

Toh, Y. C., T. C. Lim, D. Tai, G. F. Xiao, D. van Noort, and H. R. Yu. "A Microfluidic 3d Hepatocyte Chip for Drug Toxicity Testing." *Lab on a Chip* 9, no. 14 (2009): 2026-35.

Torisawa, Y. S., C. S. Spina, T. Mammoto, A. Mammoto, J. C. Weaver, T. Tat, J. J. Collins, and D. E. Ingber. "Bone Marrow-on-a-Chip Replicates Hematopoietic Niche Physiology in Vitro." *Nature Methods* 11, no. 6 (2014): 663-+.

Tran, C. T., M. Garcia, M. Garnier, C. Burucoa, and C. Bodet. "Inflammatory Signaling Pathways Induced by Helicobacter Pylori in Primary Human Gastric Epithelial Cells." *Innate Immun* 23, no. 2 (2017): 165-74.

Tsantoulas, C., C. Farmer, P. Machado, K. Baba, S. B. McMahon, and R. Raouf. "Probing Functional Properties of Nociceptive Axons Using a Microfluidic Culture System." *Plos One* 8, no. 11 (2013).

Tummuru, M. K., T. L. Cover, and M. J. Blaser. "Mutation of the Cytotoxin-Associated Caga Gene Does Not Affect the Vacuolating Cytotoxin Activity of Helicobacter Pylori." *Infect Immun* 62, no. 6 (1994): 2609-13.

Tummuru, M. K., T. L. Cover, and M. J. Blaser. "Mutation of the Cytotoxin-Associated Caga Gene Does Not Affect the Vacuolating Cytotoxin Activity of Helicobacter Pylori." *Infect.Immun.* 62, no. 6 (1994): 2609-13.

Unbekandt, M. and J. A. Davies. "Dissociation of Embryonic Kidneys Followed by Reaggregation Allows the Formation of Renal Tissues." *Kidney International* 77, no. 5 (2010): 407-16.

van de Wetering, M., M. Oosterwegel, D. Dooijes, and H. Clevers. "Identification and Cloning of Tcf-1, a T Lymphocyte-Specific Transcription Factor Containing a Sequence-Specific Hmg Box." *EMBO J* 10, no. 1 (1991): 123-32.

van de Wijdeven, R., O. H. Ramstad, U. S. Bauer, O. Halaas, A. Sandvig, and I. Sandvig. "Structuring a Multi-Nodal Neural Network in Vitro within a Novel Design Microfluidic Chip." *Biomedical Microdevices* 20, no. 1 (2018).

Van den Bossche, J., B. Malissen, A. Mantovani, P. De Baetselier, and J. A. Van Ginderachter. "Regulation and Function of the E-Cadherin/Catenin Complex in Cells of the Monocyte-Macrophage Lineage and Dcs." *Blood* 119, no. 7 (2012): 1623-33.

van Roy, F. and G. Berx. "The Cell-Cell Adhesion Molecule E-Cadherin." *Cell Mol Life Sci* 65, no. 23 (2008): 3756-88.

Vanbervliet, B., B. Homey, I. Durand, C. Massacrier, S. Ait-Yahia, O. de Bouteiller, A. Vicari, and C. Caux. "Sequential Involvement of Ccr2 and Ccr6 Ligands for Immature Dendritic Cell Recruitment: Possible Role at Inflamed Epithelial Surfaces." *Eur J Immunol* 32, no. 1 (2002): 231-42.

VanDussen, K. L., J. M. Marinshaw, N. Shaikh, H. Miyoshi, C. Moon, P. I. Tarr, M. A. Ciorba, and T. S. Stappenbeck. "Development of an Enhanced Human Gastrointestinal Epithelial Culture System to Facilitate Patient-Based Assays." *Gut* 64, no. 6 (2015): 911-20.

Veinotte, L., S. Gebremeskel, and B. Johnston. "Cxcl16-Positive Dendritic Cells Enhance Invariant Natural Killer T Cell-Dependent Ifngamma Production and Tumor Control." *Oncoimmunology* 5, no. 6 (2016): e1160979.

Vernerey, F. J. and M. Farsad. "A Mathematical Model of the Coupled Mechanisms of Cell Adhesion, Contraction and Spreading." *J Math Biol* 68, no. 4 (2014): 989-1022.

Viladomiu, M., J. Bassaganya-Riera, N. Tubau-Juni, B. Kronsteiner, A. Leber, C. W. Philipson, V. Zoccoli-Rodriguez, and R. Hontecillas. "Cooperation of Gastric Mononuclear Phagocytes with Helicobacter Pylori During Colonization." *J Immunol* 198, no. 8 (2017): 3195-204.

Viravaidya, K. and M. L. Shuler. "Incorporation of 3t3-L1 Cells to Mimic Bioaccumulation in a Microscale Cell Culture Analog Device for Toxicity Studies." *Biotechnology Progress* 20, no. 2 (2004): 590-97.

Wang, Y. Q., L. Wang, Y. Q. Guo, Y. J. Zhu, and J. H. Qin. "Engineering Stem Cell-Derived 3d Brain Organoids in a Perfusable Organ-on-a-Chip System." *Rsc Advances* 8, no. 3 (2018): 1677-85.

Wang, Y. T., S. D. Mohammed, A. D. Farmer, D. Wang, N. Zarate, A. R. Hobson, P. M. Hellstrom, J. R. Semler, B. Kuo, S. S. Rao, W. L. Hasler, M. Camilleri, and S. M. Scott. "Regional Gastrointestinal Transit and Ph Studied in 215 Healthy Volunteers Using the Wireless Motility Capsule: Influence of Age, Gender, Study Country and Testing Protocol." *Alimentary Pharmacology & Therapeutics* 42, no. 6 (2015): 761-72.

Watchmaker, P. B., K. Lahl, M. Lee, D. Baumjohann, J. Morton, S. J. Kim, R. Zeng, A. Dent, K. M. Ansel, B. Diamond, H. Hadeiba, and E. C. Butcher. "Comparative Transcriptional and Functional Profiling Defines Conserved Programs of Intestinal Dc Differentiation in Humans and Mice." *Nat Immunol* 15, no. 1 (2014): 98-108.

Watson, C. J., M. Rowland, and G. Warhurst. "Functional Modeling of Tight Junctions in Intestinal Cell Monolayers Using Polyethylene Glycol Oligomers." *American Journal of Physiology-Cell Physiology* 281, no. 2 (2001): C388-C97.

Wells, J. M. and J. R. Spence. "How to Make an Intestine." *Development* 141, no. 4 (2014): 752-60.

Williams, J. M., C. A. Duckworth, M. D. Burkitt, A. J. Watson, B. J. Campbell, and D. M. Pritchard. "Epithelial Cell Shedding and Barrier Function: A Matter of Life and Death at the Small Intestinal Villus Tip." *Vet Pathol* 52, no. 3 (2015): 445-55.

Willyard, C. "The Boom in Mini Stomachs, Brains, Breasts, Kidneys and More." *Nature* 523, no. 7562 (2015): 520-22.

Workman, Michael J., John P. Gleeson, Elissa J. Troisi, Hannah Q. Estrada, S. Jordan Kerns, Christopher D. Hinojosa, Geraldine A. Hamilton, Stephan R. Targan, Clive N. Svendsen, and Robert J. Barrett. "Enhanced Utilization of Induced Pluripotent Stem Cell–Derived Human Intestinal Organoids Using Microengineered Chips." *Cellular and Molecular Gastroenterology and Hepatology* 5, no. 4 (2018): 669-77.e2.

Xiao, R. R., W. J. Zeng, Y. T. Li, W. Zou, L. Wang, X. F. Pei, M. Xie, and W. H. Huang. "Simultaneous Generation of Gradients with Gradually Changed Slope in a Microfluidic Device for Quantifying Axon Response." *Analytical Chemistry* 85, no. 16 (2013): 7842-50.

Ye, F., C. Kim, and M. H. Ginsberg. "Reconstruction of Integrin Activation." *Blood* 119, no. 1 (2012): 26-33.

Yin, Y., T. Qin, X. Wang, J. Lin, Q. Yu, and Q. Yang. "Cpg DNA Assists the Whole Inactivated H9n2 Influenza Virus in Crossing the Intestinal Epithelial Barriers Via Transepithelial Uptake of Dendritic Cell Dendrites." *Mucosal Immunol* 8, no. 4 (2015): 799-814.

Yui, S., T. Nakamura, T. Sato, Y. Nemoto, T. Mizutani, X. Zheng, S. Ichinose, T. Nagaishi, R. Okamoto, K. Tsuchiya, H. Clevers, and M. Watanabe. "Functional Engraftment of Colon Epithelium Expanded in Vitro from a Single Adult Lgr5(+) Stem Cell." *Nat Med* 18, no. 4 (2012): 618-23.

Zachos, N. C., O. Kovbasnjuk, J. Foulke-Abel, J. In, S. E. Blutt, H. R. de Jonge, M. K. Estes, and M. Donowitz. "Human Enteroids/Colonoids and Intestinal Organoids Functionally Recapitulate Normal Intestinal Physiology and Pathophysiology." *Journal of Biological Chemistry* 291, no. 8 (2016): 3759-66.

Zeitoun, P. and A. Lambling. "Ultrastructure of the Gastric Mucosa in Human Hemochromatosis." *Scand J Gastroenterol* 2, no. 3 (1967): 222-34.

Zeuthen, L. H., L. N. Fink, and H. Frokiaer. "Epithelial Cells Prime the Immune Response to an Array of Gut-Derived Commensals Towards a Tolerogenic Phenotype through Distinct Actions of Thymic Stromal Lymphopoietin and Transforming Growth Factor-Beta." *Immunology* 123, no. 2 (2008): 197-208.

Zhang, K. and J. Chen. "The Regulation of Integrin Function by Divalent Cations." *Cell Adh Migr* 6, no. 1 (2012): 20-9.

Zhang, W. T., W. Y. Lee, D. S. Siegel, P. Tolias, and J. Zilberberg. "Patient-Specific 3d Microfluidic Tissue Model for Multiple Myeloma." *Tissue Engineering Part C-Methods* 20, no. 8 (2014): 663-70.

Zhang, Y., Z. Gazit, G. Pelled, D. Gazit, and G. Vunjak-Novakovic. "Patterning Osteogenesis by Inducible Gene Expression in Microfluidic Culture Systems." *Integrative Biology* 3, no. 1 (2011): 39-47.

Zhang, Y. S., J. Aleman, S. R. Shin, T. Kilic, D. Kim, S. A. M. Shaegh, S. Massa, R. Riahi, S. Chae, N. Hu, H. Avci, W. Zhang, A. Silvestri, A. S. Nezhad, A. Manbohi, F. De Ferrari, A. Polini, G. Calzone, N. Shaikh, P. Alerasool, E. Budina, J. Kang, N. Bhise, J. Ribas, A. Pourmand, A. Skardal, T. Shupe, C. E. Bishop, M. R. Dokmeci, A. Atala, and A. Khademhosseini. "Multisensor-Integrated Organs-on-Chips Platform for Automated and Continual in Situ Monitoring of Organoid Behaviors." *Proceedings of the National Academy of Sciences of the United States of America* 114, no. 12 (2017): E2293-E302.

Ziegler, L., S. Grigoryan, I. H. Yang, N. V. Thakor, and R. S. Goldstein. "Efficient Generation of Schwann Cells from Human Embryonic Stem Cell-Derived Neurospheres." *Stem Cell Reviews and Reports* 7, no. 2 (2011): 394-403.